UNIVERSITY OF CALIFORNIA

IRVINE

Ligand Exploration in the Synthesis and Reactivity of +2 Ion Rare-Earth Metal Complexes

DISSERTATION

submitted in partial satisfaction of the requirements for the degree of

DOCTOR OF PHILOSOPHY

in Chemistry

by

David H. Woen

Dissertation Committee:
Distinguished Professor William J. Evans, Chair
Professor A. S. Borovik
Assistant Professor Jenny Y. Yang

2017

DEDICATION

This dissertation is dedicated to my parents, Bambang and Sioengo,

and to my sisters, Christine, Veronica, and Vicky,

in recognition of their love, support, and inspiration.

TABLE OF CONTENTS

LIST OF FIGURES

LIST OF TABLES

ACKNOWLEDGEMENTS

To my advisor, Professor Bill Evans, I would like to express my deepest appreciation and admiration. Thank you for allowing me to join your research group and to learn so much through the unique group dynamics that you have established. I appreciate your tolerance of all my imperfections and mistakes. You always bring out the best of me and you continue to motivate me to move forward. Your excitement about chemistry is contagious and your friendliness, despite your reputable success and distinctions, is very inspiring to me. I feel very fortunate and honored to have pursued my graduate career under your guidance.

To Professor Andy Borovik, thank you for providing me with helpful suggestions and encouragements. I appreciate you taking interest in my work during our discussions. I also want to thank you for making me feel welcome through your humor as well as your personal outlook on graduate school and careers in science.

To Professor Jenny Yang, I appreciate that you are always willing to listen and care about my progress and developments in graduate school. You have provided me with valuable advice and support. I also would like to thank you for organizing the Inorganic graduate student programs, which I am glad to have been a part of.

To everyone mentioned above as well as Professors Alan Heyduk, Filipp Furche, Shane Ardo, Mike Green, and Claudia Czimczik, thank you for serving on my committee during my second year report or candidacy exam. I appreciate your time and feedbacks.

To Professor Filipp Furche and Guo Chen, thank you for providing all the computational work described in this dissertation, as well as your helpful ideas and suggestions. I have enjoyed our discussions together. To Dr. Tim Boyle from Sandia National Laboratories, thank you providing the idea and starting material for the scandium reduction project described in this dissertation.

To Dr. Joe Ziller, as well as the previous and current X-ray facility assistants, Dr. Jordan Corbey, Dr. Jason Jones, and Mikey Wojnar, I appreciate your patience, knowledge, and assistance with X-ray crystallography. To Dr. Ethan Hill and Victoria Oswald, thank you for helping me with EPR spectroscopy, especially with running my helium EPR samples. To Dr. Phil Dennison and Dr. Dima Fishman, thank you for your all your help at the spectroscopy facilities at UCI.

To Dr. Jordan Corbey, thank you for being my mentor when I joined the Evans lab, for your patience in showing me the lab protocols, and for all your advices throughout the years. I would also like to thank Dr. Megan Fieser, Prof. Chris Kotyk, Dr. Ryan Langeslay, Dr. Cory Windorff, and Dr. Chad Palumbo, who have provided so much help in many different ways. To all the previous and current Evans group members, including those mentioned above as well as Dr. Doug

Kindra, Dr. Conrad Goodwin, Casey Johnson, Avery Fordham, Mitch Nascimento, Dr. Nick Rightmire, Monica Boshart, Megan Dumas, Sam Moehring, Austin Ryan, Dan Huh, Tener Jenkins, and Mary Angadol, I will remember all the favors you have done for me and all the enjoyable moments I have had with each of you.

To everyone in the Lavallo research group at UC Riverside, especially Professor Vince Lavallo, Dr. Allen Chan, Javier Fajardo, Jr., and Uday Chauhan, thank you for making my undergraduate chemistry research experience a blast and for inspiring me to pursue graduate school. I also appreciate your continued friendship and support throughout my graduate career.

To my sisters, Christine, Veronica, and Vicky, thank you for being great and caring friends, for listening to my stories and sharing yours, and for cooking and allowing me to eat your delicious meals and snacks. To my cousin Ali, uncle Jin, and uncle Kie, thank you for taking care of me in the absence of my parents since I was little. You continue to provide me with valuable guidance and support even until now.

Last but not least, to my parents, Bambang and Sioengo, thank you for raising me to be the person that I am today. I really admire both of you considering all the struggles that you have had to go through. You inspire me to keep going.

CURRICULUM VITAE

David Hartono Woen

Email: dwoen@uci.edu

Citizenship: United States of America

EDUCATION

2013–2017 **University of California, Irvine**
Ph.D. Inorganic Chemistry with Prof. William J. Evans
Dissertation: Ligand Exploration in the Synthesis and Reactivity of +2 Ion Rare-Earth Metal Complexes

2011–2013 **University of California, Riverside**
B.S. Chemistry with Prof. Vincent Lavallo
Undergraduate Research: Synthesis of Carboranyl-Substituted Ligands for Transition Metal Complexes

WORK EXPERIENCE

2013–2017 **University of California, Irvine**
Research Assistant
Teaching Assistant
General/Organic Chemistry Laboratory
General Chemistry Discussion

AWARDS AND FELLOWSHIPS

2012−2013 UC Riverside Dean's Honor List
2013 UC Riverside Undergraduate Research and Creative Activity Mini-Grant
2017 DOE Office of Science Graduated Student Research (SCGSR) Award − *declined*
2017 UC Irvine Regents' Dissertation Fellowship

OUTREACH

2012−2013 Outreach Coordinator of Chemistry Club at UC Riverside
2012−2013 Adopt-A-Street − Keep Riverside Clean & Beautiful volunteer
2013 Chemistry and math tutor volunteer at John W. North High School, Riverside, CA

2014−2017 Provided laboratory tours to non-chemistry major undergraduate honors students

PUBLICATIONS

1. Estrada, J.; Woen, D. H.; Tham, F. S.; Miyake, G. M.; Lavallo V. "Synthesis and Reactivity of a Zwitterionic Palladium Allyl Complex Supported by a Perchlorinated Carboranyl Phosphine" *Inorganic Chemistry* **2015**, 54, 5142−5144. DOI: 10.1021/acs.inorgchem.5b00576

2. Corbey, J. F.; Woen, D. H.; Palumbo, C. T.; Fieser, M. E.; Ziller, J. W.; Furche, F.; and Evans W. J. "Ligand Effects in the Synthesis of Ln^{2+} Complexes by Reduction of Tris(cyclopentadienyl) Precursors Including C–H Bond Activation of an Indenyl Anion" *Organometallics* **2015**, 34, 3909−3921. DOI: 10.1021/acs.organomet.5b00500

3. Corbey, J. F.; Woen, D. H.; Ziller, J. W.; Evans W. J. "Synthesis and Structure of Nitrile-Solvated Rare Earth Metallocene Cations $[Cp_2Ln(NCR)_3][BPh_4]$ (Cp = C_5Me_5, $C_5H_4SiMe_3$; R = Me, ^{t}Bu, Ph)" *Polyhedron* **2016**, 103, 44−50. DOI: 10.1016/j.poly.2015.09.002

4. Fieser, M. E.; Woen, D. H.; Corbey, J. F.; Mueller, T. J.; Ziller, J. W; Evans, W. J. "Raman spectroscopy of the N–N bond in rare earth dinitrogen complexes" *Dalton Transactions* **2016**, 45, 14634−14644. DOI: 10.1039/C5DT04547A

5. Woen, D. H.; Evans, W. J. "Expanding the + 2 Oxidation State of the Rare-Earth Metals, Uranium, and Thorium in Molecular Complexes" in: Bünzli, J, -C. G.; Pecharsky, V. K. (Eds.) *Handbook on the Physics and Chemistry of Rare Earths*, Vol 50, Elsevier Science, Amsterdam, **2016** (Ch 293). DOI: 10.1016/bs.hpcre.2016.08.002

6. Woen, D. H.; Chen, G. P.; Ziller, J. W.; Boyle, T. J.; Furche, F.; Evans, W. J. "Solution Synthesis, Structure, and CO_2 Reduction Reactivity of a Scandium(II) Complex, $\{Sc[N(SiMe_3)_2]_3\}^-$" *Angewandte Chemie, International Edition* **2017**, 56, 2050−2053; *Angewandte Chemie* **2017**, 129, 2082–2085. Designated VIP. DOI: 10.1002/ange.201611758

7. Fieser, M. E; Ferrier, M. G; Su, J.; Batista, E.; Cary, S. K.; Engle, J. W.; Evans, W. J.; Lezama Pacheco, J. S.; Kozimor, S. A.; Olson, A. C.; Ryan, A. J.; Stein, B. W.; Wagner, G. L.; Woen, D. H.; Vitova, T.; Yang, P. "Evaluating the Electronic Structure of Formal Ln^{II} Ions in $Ln^{II}(C_5H_4SiMe_3)_3^{1-}$ Complexes Using XANES Spectroscopy and DFT Calculations" *Chemical Science* **2017**, 8, 6076−6091. DOI: 10.1039/C7SC00825B

8. Woen, D. H.; Kotyk C. M.; Mueller, T. J.; Ziller, J. W.; Evans, W. J. "Tris(pentamethylcyclopentadienyl) Complexes of the Late Lanthanides, Tb, Dy, Ho, and Er: Solution and Mechanochemical Syntheses and Structural Comparisons" *Organometallics* **2017**, *in press*. ACS Editors' Choice. DOI: 10.1021/acs.organomet.7b00385

9. Woen, D. H.; Chen, G. P.; Ziller, J. W.; Boyle, T. J.; Furche, F.; Evans, W. J. "End-on Bridging Dinitrogen Complex of Scandium" *Journal of American Chemical Society* **2017**, *139*, 14861–14864. DOI: 10.1021/jacs.7b08456

10. Demir, S; Boshart, M. D.; Corbey, J. F.; Woen, D. H.; Gonzalez, M. I.; Ziller, J. W.; Meihaus, K. R.; Long, J. R.; Evans, W. J. "Slow Magnetic Relaxation in a Dysprosium Ammonia Metallocene Complex" *Inorganic Chemistry* **2017** *in press*. DOI: 10.1021/acs.inorgchem.7b02390

PUBLICATIONS IN PREPARATION

1. Woen, D. H.; Ziller, J. W.; Evans, W. J. "Reactivity and Decomposition Studies of Transient Ln^{2+} Species, $[(C_5H_4Me)_3Ln]^{1-}$" *in preparation*.

2. Jenkins, T. F.; Woen, D. H.; Ziller, J. W.; Evans, W. J. "Synthesis, Structure, and Reactivity of New Ln^{2+} complexes, [K(2.2.2-cryptand)][$(C_5Me_4H)_3Ln$]" *in preparation*

3. Fleischauer, V. E.; Woen, D. H.; Evans, W. J.; Neidig, M. L. "MCD spectroscopy of the Ln^{2+} complexes, [K(2.2.2-cryptand)][$(C_5H_4SiMe_3)_3Ln$]" *in preparation*.

4. Ariciu, A. -M.; Woen, D. H.; Kostopoulos, A. K.; Goodwin, C. A. P.; McInnes, E. J. L.; Winpenny, R. E. P.; Evans, W. J.;Tuna, F. "s-Block Radicals as Molecular Electron Spin Qubits" *in preparation*

PRESENTATIONS

1. Woen, David H.; Ziller, Joseph W.; Evans, William J. "Methylcyclopentadienide as a supporting ligand for a reduced dinitrogen complex of yttrium" *249th ACS National Meeting & Exposition* Denver, CO, United States, **2015**.

2. Woen, D. H.; Chen, G. P.; Ziller, J. W.; Boyle, T. J.; Furche, F.; Evans, W. J. "Solution Synthesis and CO_2 Reduction Reactivity of a Rare Sc^{2+} Complex $[Sc(NR_2)_3]^{1-}$ (R = $SiMe_3$)" *SoCal Organometallics Meeting* UCLA, Los Angeles, CA, **2016**.

3. Woen, D. H. "Synthesis, Structure, and Reactivity of a Sc(II) Complex" *Inorganic Chemistry Department Graduate Student Seminar* UCI, Irvine, CA, **2017**.

4. Woen, D. H.; Chen, G. P.; Ziller, J. W.; Boyle, T. J.; Furche, F.; Evans, W. J. "Solution Synthesis and CO_2 Reduction Reactivity of a Rare Sc^{2+} Complex $[Sc(NR_2)_3]^{1-}$ (R = $SiMe_3$)" *253rd ACS National Meeting & Exposition* San Francisco, CA, United States, **2017**.

5. Woen, D. H. "Synthesis, Structure, and Reactivity of a Scandium(II) Complex, $\{Sc[N(SiMe_3)_2]_3\}^-$" *Invited talk at Los Alamos National Laboratory*, **2017**.

PUBLICATIONS CONTAINING ACKNOWLEDGED CONTRIBUTIONS

1. Tanifuji, K.; Sickerman, N. S.; Lee, C. C.; Nagasawa, T.; Miyaksaki, K.; Ohki, Y.; Tatsumi, K.; Ribbe, M. W. "Structure and Reactivity of an Asymmetric Synthetic Mimic of Nitrogenase Cofactor" *Angew. Chem., Int. Ed. Engl.* **2016**, 55, 15633−15636. DOI: 10.1002/anie.201608806

2. Sickerman, N. S.; Tanifuji, K.; Lee, L. L.; Ohki, Y.; Tatsumi, K.; Ribbe, M. W.; Hu, Y. "Reduction of C1 substrates to hydrocarbons by the homometallic precursor and synthetic mimic of the nitrogenase cofactor" *J. Am. Chem. Soc.* **2017**, 139, 603−606. DOI: 10.1021/jacs.6b11633

ABSTRACT OF THE DISSERTATION

Ligand Exploration in the Synthesis and Reactivity

of +2 Ion Rare-Earth Metal Complexes

By

David H. Woen

Doctor of Philosophy in Chemistry

University of California, Irvine, 2017

Professor William J. Evans, Chair

This dissertation focuses on efforts to expand upon the discovery that the +2 oxidation state is available in molecular forms for all the rare-earth metals, i.e. Sc, Y, and the lanthanides. In addition to the previously isolated +2 ion complexes of La, Ce, Nd, Sm, Eu, Dy, Tm, Yb, and Sc, the first complexes containing +2 ions of Y, Pr, Gd, Tb, Ho, Er, and Lu had been prepared under strongly reducing conditions with the $(C_5H_4SiMe_3)_3^{3-}$ ligand set. This dissertation describes efforts to broaden the ligand sets available to isolate new +2 rare-earth metal ions and to study their reactivity and physical properties. Chapter 1 describes the use of $(C_5H_5)_3^{3-}$ and $(C_5H_4Me)_3^{3-}$ ligand sets to isolate more examples of Y^{2+} complexes, and compares their stability and properties with those of other ligand sets. For $(C_5H_4Me)_3^{3-}$, reduction reactions with other rare-earth metals as well as some reactivity studies are also described. Chapter 2 describes the dinitrogen reactivity of the Y^{2+} species generated from the reductions of $(C_5H_5)_3Y$ and $(C_5H_4Me)_3Y$. Chapter 3 describes the synthesis and reactivity of +2 ion complexes from the reduction of $(C_5Me_4H)_3Ln$ complexes. Chapter 4 describes the synthesis of the first crystallographically characterizable Sc^{2+}

complex, $\{Sc[N(SiMe_3)_2]_3\}^-$ including physical characterization by EPR and UV-vis spectroscopy. Chapter 5 describes the reactivity of the Sc^{2+} complex, $[Sc[N(SiMe_3)_2]_3\}^-$, with dinitrogen to generate the first end-on bridging dinitrogen complex of a rare-earth metal, $\{[Sc[N(SiMe_3)_2]_3]_2(\mu\text{-}\eta^2\text{:}\eta^2\text{-}N_2)\}^{2-}$. Chapter 6 describes additional reactivity studies of $[Sc[N(SiMe_3)_2]_3\}^-$ with carbon monoxide, carbon dioxide, and acetonitrile. Chapter 7 describes the mechanochemical synthesis of the sterically crowded complexes, $(C_5Me_5)_3Ln$ (Ln = Tb, Dy, Ho, Er).

INTRODUCTION

Redox reactions are among the two most common types of reactions in chemistry with the other being acid/base reactions. One of the most fundamental aspects of a metal that governs its ability to participate in redox reactions is the number of oxidation states that it can exhibit. For many years for most of the rare-earth metals, the +3 oxidation state was the only accessible oxidation state in molecular form. The +4 oxidation state is rare and only available with Ce, and although the +2 oxidation state is more common, it was only accessible for almost a century (1906-1997) with only Sm, Eu and Yb.[1-5] For three more rare-earth metals, Nd, Dy, and Tm, the +2 ions were finally discovered in molecular forms for the first time between 1997-2001.[6-7] These were isolated as the diiodides, $LnI_2(solvent)_x$ (Ln = Tm, Dy, Nd; solvent = DME or THF, x = 3 or 5). Based on extensive solid state studies[8-9] and the calculated reduction potentials,[10] Table 0.1, it was assumed that Sm^{2+}, Eu^{2+}, Yb^{2+}, Nd^{2+}, Dy^{2+}, and Tm^{2+} were the only elements that could form stable molecular complexes; the others were too reducing to isolate. These six ions have been termed the "traditional" divalent ions.

TABLE 0.1. Estimated Ln^{3+}/Ln^{2+} Reduction Potentials (±0.2 V vs SHE) of Yttrium and the Lanthanides Based on Experimental and Spectroscopic Data.[10]

Ln	Potential	Ln	Potential
Eu	−0.35	**Pr**	−2.7
Yb	−1.15	**Y**	−2.8
Sm	−1.55	**Ho**	−2.9
Tm	−2.3	**Er**	−3.1
Dy	−2.5	**La**	−3.1
Nd	−2.6	**Ce**	−3.2
Pm	−2.6	**Tb**	−3.7
Lu	−2.72	**Gd**	−3.9

Although the other rare-earth metals could not be isolated as the +2 ions, some +2 ion-like reactivity was observed through the alkali metal reduction of the +3 ion complexes, LnA_3 or LnA_2A' (Ln = rare-earth metal; A or A' = anionic ligand), in the presence of a substrate.[11-16] One such reaction that was widely explored was the reduction of dinitrogen to form bridging $(N=N)^{2-}$ bimetallic complexes, eq 0.1. For example, the reduction of $Ln(NR_2)_3$ (R = $SiMe_3$)

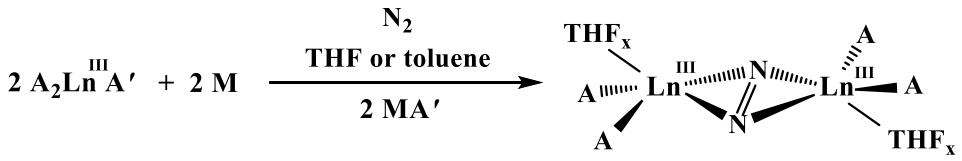

(0.1)

Ln = Sc, Y, La, Ce, Pr, Nd, Gd, Tb, Dy, Ho, Er, Tm, Lu
A = $N(SiMe_3)_2$, $OC_6H_3{}^tBu_2$-2,6, C_5Me_5, C_5Me_4H, $C_5H_2{}^tBu_3$
A′ = A or BPh_4
M = K, KC_8, Na; x = 0-1

under dinitrogen readily formed $[(R_2N)_2Ln(THF)]_2[\mu\text{-}\eta^2\text{:}\eta^2\text{-}N_2]$.[17-19] In the case of Tm, Dy, and Nd, the $(N=N)^{2-}$ complexes could also be generated from the reaction of the +2 ion diiodides with KNR_2 under dinitrogen, eq 0.2.[13,20-22] This suggested that the LnA_3 reductions under dinitrogen that form the $(N=N)^{2-}$ complexes in eq 0.1 could possibly proceed through a transient +2 ion intermediate.

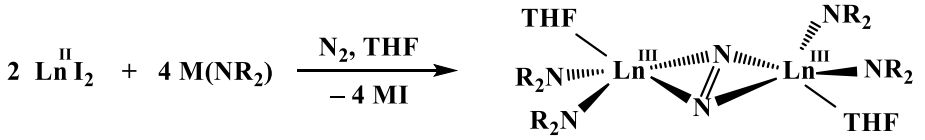

(0.2)

Ln = Tm, Dy, Nd
R = $SiMe_3$
M = K, Na

The possibility that the +2 oxidation state of the other rare-earth metals might be accessible in solution was also supported by EPR spectroscopy. For scandium, the first reports supporting the formation of molecular complexes containing Sc^{2+} were published in the 1990s by Cloke and

coworkers.[23-24] The Sc^{2+} complexes were generated from a reaction process involving the vaporization of Sc^0 starting material using an electron beam gun and subsequent condensation into the reaction vessel. Just two Sc^{2+} complexes were successfully identified by EPR spectroscopy, both showing a complicated multi-line hyperfine pattern that was attributed to the interactions between an unpaired electron with the I = 7/2 nuclear spin of ^{45}Sc as well as other nuclei on the ligands. Unfortunately, the difficulty of preparing and handling these complexes prevented structural characterization by X-ray crystallography.

Additional EPR evidence of a +2 ion rare-earth metal complex was reported by Lappert and coworkers in 1997 with La from the reduction of Cp''_3La [$Cp'' = C_5H_3(SiMe_3)_2$] using K smear in dimethoxyethane, which gave an eight-line hyperfine pattern consistent with I = 7/2 of ^{138}La.[25] This La^{2+} species could not be isolated and definitively characterized since it further reacted with dimethoxyethane to form the bridging methoxide complex, $(Cp''_2La)_2(\mu\text{-OMe})_2$.[25] It took more than a decade later before it was found that the use of a different solvent, THF, and the addition of a chelate, such as 2.2.2-cryptand (crypt) or 18-crown-6 (crown), provided the stability which allowed the first isolation and crystallographic identification of "non-traditional divalent" ion complexes, [K(chelate)][Cp''_3La], eq 0.3.[26] A similar reaction was performed with Ce and gave a crystal structure containing a mixture of the Ce^{3+}/Ce^{2+} complexes, Cp''_3Ce/[K(chelate)][Cp''_3Ce], eq 0.3.[26]

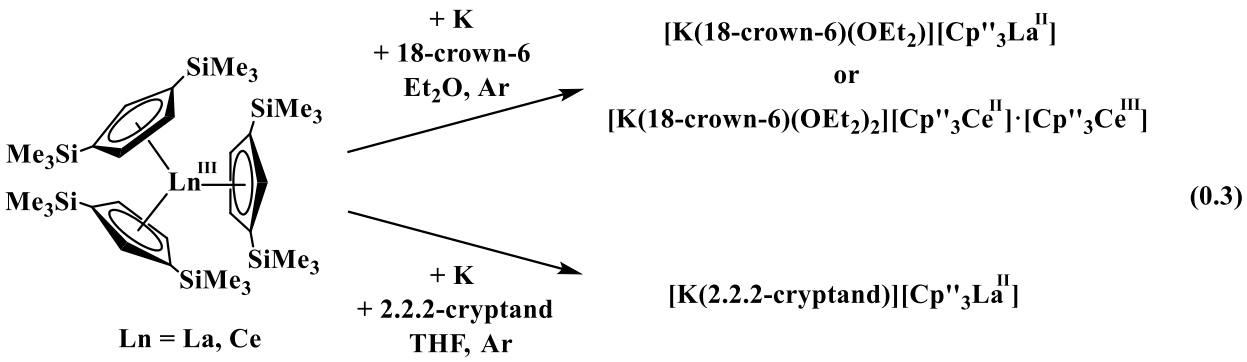

(0.3)

For yttrium, EPR evidence for the formation of a complex containing the +2 ion was reported by the Evans group in 2011 from the reduction of $Y(NR_2)_3$ using KC_8 at low temperature.[27] The EPR spectrum contained a two-line hyperfine pattern, which is consistent with an unpaired electron interacting with the I = ½ of ^{89}Y. This Y^{2+} complex was highly unstable even when a chelating agent was added. It was also very reactive; it reacted with dinitrogen to form the previously isolated $(N=N)^{2-}$ complex, $[(R_2N)_2Y(THF)]_2[\mu\text{-}\eta^2\text{:}\eta^2\text{-}N_2]$,[27] which further supports the postulation that the formation of the $(N=N)^{2-}$ complexes via eq 0.1 likely goes through +2 ion intermediates. Shortly thereafter, another Y^{2+} complex was synthesized from the reduction of Cp'_3Y ($Cp' = C_5H_4SiMe_3$) using KC_8 in the presence of crown, as identified by EPR spectroscopy. In this case however, the Y^{2+} complex did not readily react with dinitrogen to produce the expected $(N=N)^{2-}$ complex, $[Cp'_2Y(THF)]_2[\mu\text{-}\eta^2\text{:}\eta^2\text{-}N_2]$; it was actually stable enough to crystallize and was analyzed by X-ray crystallography to give the first crystal structure of an Y^{2+} complex, [K(crown)][Cp'_3Y], eq 0.4.

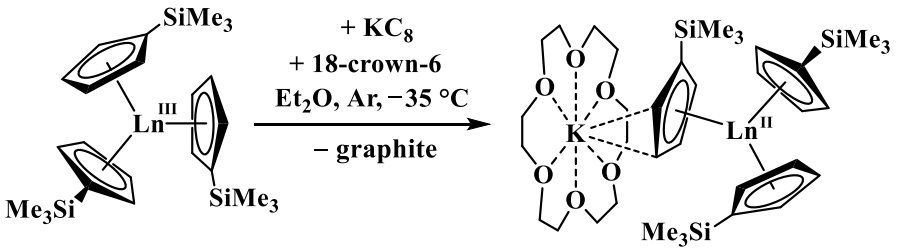

Ln = Y, Ho, Er **(0.4)**

The reduction of Cp'_3Ln using KC_8 in the presence of crown was extended to the lanthanide metals with Ln = Er and Ho, which gave the first crystallographic identification of Er^{2+} and Ho^{2+} in [K(crown)][Cp'_3Ln], eq 0.4. It was later found that the use of crypt rather than crown gave more stable +2 ion metal complexes, and the chemistry was expanded to the remainder of the rare-earth metals, Pr, Gd, Tb, Dy, Lu, with the complexes [K(crypt)][Cp'_3Ln], eq 0.5. This reduction system was successfully used to form +2 ion complexes of yttrium and all of the other lanthanide metals

as well, allowing comparison studies of the "traditional" vs "non-traditional" divalent ions in the same ligand environment.

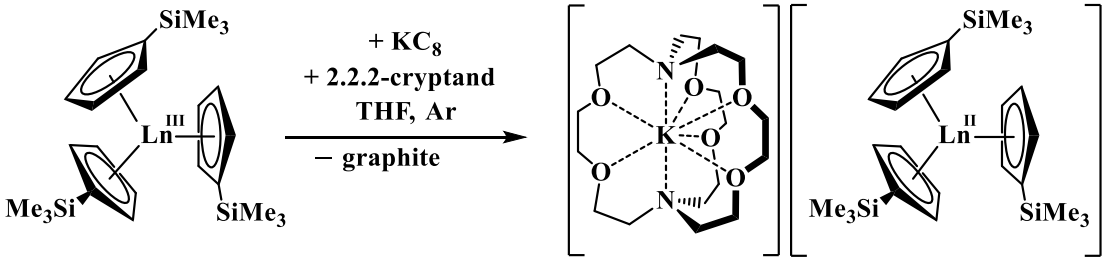

(0.5)

Ln = Y, lanthanides except Pm

Structural comparison between the divalent complexes, [K(crypt)][Cp′$_3$Ln], and their trivalent precursors, Cp′$_3$Ln, revealed that the average metal−ring centroid distances are always longer in the reduced species. For complexes of the "traditional" +2 ions of Eu, Yb, Sm, Tm, Dy, and Nd, an increase of 0.1-0.2 Å was previously observed upon reduction. Surprisingly, for all of the "non-traditional" divalent ion complexes, the observed increase was much smaller (0.027-0.031 Å). Furthermore, in the [K(crypt)][Cp′$_3$Ln] series, only four out of the six "traditional" divalent ion complexes with Ln = Sm, Eu, Tm, Yb, showed large increases (0.123-0.156 Å), whereas the other two with Ln = Nd and Dy only showed small increases (0.030 Å and 0.036 Å, respectively). UV−visible measurements in conjunction with TD-DFT calculations revealed that the "non-traditional" divalent ions have $4f^n5d^1$ ($3d^1$ for Y) electron configurations, whereas the "non-traditional" divalent ions have $4f^{n+1}$ electron configurations, except for those with Ln = Nd and Dy, which surprisingly have $4f^n5d^1$ electron configurations. This indicated that Nd and Dy can adopt either the $4f^n5d^1$ or the $4f^{n+1}$ electron configurations depending on the ligand systems, and they have been termed "configurational crossover" ions.

Dissertation Outline. The research presented in this dissertation focuses on the exploration of other ligand systems and reaction conditions in efforts to isolate more examples of rare-earth metals ions in the +2 oxidation state and to study their reactivity and physical properties.

Chapter 1 describes the synthesis of new Y^{2+} species using the $(Cp_3)^{3-}$ (Cp = C_5H_5) and $(Cp^{Me}_3)^{3-}$ (C_5H_4Me) ligand systems. These species were highly unstable, but could be identified using EPR spectroscopy. Their EPR spectra are compared to those of other Y^{2+} species to give some insights into the electron donor ability of the ligands. Reactivity studies with $PhSiH_3$ to derivatize the unstable Y^{2+} species, as well as reduction with other rare-earth metals and their decomposition studies are also described. Chapter 2 describes the dinitrogen reactivity studies of the Y^{2+} species generated from the reductions of Cp_3Y and Cp^{Me}_3Y. These studies compare the addition of dinitrogen to the freshly generated Y^{2+} species vs the reduction of the Y^{3+} precursors under dinitrogen. For Cp^{Me}_3Y, an $(N=N)^{2-}$ complex, $[Cp^{Me}_2Y(THF)]_2(\mu\text{-}\eta^2\text{:}\eta^2\text{-}N_2)$, and a radical byproduct were identified. Analogous products were obtained using Dy as the metal center. These products were also studied using Raman and EPR spectroscopies. Chapter 3 describes the reduction of rare-earth metal ion complexes with the tetraalkyl-substituted cyclopentadienyl ligand environment, $(Cp^{tet}_3)^{3-}$ (Cp^{tet} = C_5Me_4H), for comparison with the monoalkyl-substituted cyclopentadienyl ligand environment, $(Cp^{Me}_3)^{3-}$, described in Chapter 1. Similarly the reduction of $(Cp^{tet}_3)Y$ did not give a stable Y^{2+} complex, but the reduction of $(Cp^{tet}_3)Ln$ with the larger rare-earth metals, praseodymium and neodymium gave stable Ln^{2+} complexes. Reactivity studies of these Ln^{2+} complexes with dinitrogen and $PhSiH_3$ are also described. Chapter 4 describes the use of an amide ligand system, $(NR_2)_3^{3-}$ (R = $SiMe_3$), to synthesize the first crystallographically-authenticated Sc^{2+} complex, $[Sc(NR_2)_3]^{1-}$. The spectroscopic properties as well as the stability of this complex are discussed. Chapter 5 describes the reactivity of $[Sc(NR_2)_3]^{1-}$ with dinitrogen to form the first $(N=N)^{2-}$ complex of a rare-earth metal with an end-on bridging motif. This complex shows many differences compared to the previous dinitrogen-bridged rare-earth metal complexes. Chapter 6 describes the reactivity of the $[Sc(NR_2)_3]^{1-}$ complex with carbon monoxide, carbon

dioxide, and acetonitrile. This complex displays reversible binding of carbon monoxide at low temperature. In contrast, it irreversibly reacts with acetonitrile and carbon dioxide to form bridging bimetallic complexes, $\{[(R_2N)_3Sc]_2(\mu\text{-}C_2O_4\text{-}\kappa^1O\text{:}\kappa^1O'')\}^{1-}$ and $\{[(R_2N)_3Sc]_2[\mu\text{-}N(Me)CC(Me)N]\}^{1-}$, respectively, by two electron coupling reactions. The carbon dioxide reaction also yielded an extended polymer containing a rare $(CO_2)^{1-}$ moiety, $[(R_2N)_3Sc(\mu\text{-}OCO\text{-}\kappa^1O\text{:}\kappa^1O')K(crown)]_n$. Chapter 7 describes the synthesis of new members of another class of tris(cyclopentadienyl) complexes which have pentaalkyl-substituted cyclopentadienyl ligands. These sterically crowded $(C_5Me_5)_3Ln$ complexes were previously not available for Ln = Ho and Er because they react with solvents such as THF and arenes. The synthesis of these complexes by solvent-free mechanochemistry is described.

References

(1) Matignon, C.; Cazes, E. C. *Ann. Chim. Phys.* **1906**, *8*, 417-426.

(2) Klemm, W.; Schuth, W. *Z. Anorg. Allg. Chem.* **1929**, *184*, 352-358.

(3) Jantsch, G.; Grubitsch, H.; Hoffmann, F. *Z. Anorg. Allg. Chem.* **1929**, *185*, 49-64.

(4) Bochkarev, M. N.; Fedushkin, I. L.; Fagin, A. A.; Petrovskaya, T. V.; Ziller, J. W.; Broomhall-Dillard, R. N. R.; Evans, W. J. *Angew. Chem., Int. Ed.* **1997**, *36*, 133-135.

(5) Bochkarev, M. N.; Fedushkin, I. L.; Dechert, S.; Fagin, A. A.; Schumann, H. *Angew. Chem., Int. Ed.* **2001**, *40*, 3176-3178.

(6) Evans, W. J.; Allen, N. T.; Ziller, J. W. *j. Am. Chem. Soc.* **2000**, *122*, 11749-11750.

(7) Bochkarev, M. N.; Fagin, A. A. *Chem. Eur. J.* **1999**, *5*, 2990-2992.

(8) Meyer, G. *Chem. Rev.* **1988**, *88*, 93-107.

(9) Meyer, G.; Meyer, H.-J. *Chem. Mater.* **1992**, *4*, 1157-1168.

(10) Morss, L. R. *Chem. Rev.* **1976**, *76*, 827-841.

(11) Evans, W. J.; Lee, D. S.; Johnston, M. A.; Ziller, J. W. *Organometallics* **2005**, *24*, 6393-6397.

(12) Evans, W. J.; Rego, D. B.; Ziller, J. W. *Inorg. Chem.* **2006**, *45*, 10790-10798.

(13) Evans, W. J.; Fang, M.; Zucchi, G.; Furche, F.; Ziller, J. W.; Hoekstra, R. M.; Zink, J. I. *J. Am. Chem. Soc.* **2009**, *131*, 11195–11202.

(14) Lorenz, S. E.; Schmiege, B. M.; Lee, D. S.; Ziller, J. W.; Evans, W. J. *Inorg. Chem.* **2010**, *49*, 6655-6663.

(15) Schmiege, B. M.; Ziller, J. W.; Evans, W. J. *Inorg. Chem.* **2010**, *49*, 10506-10511.

(16) Demir, S.; Lorenz, S. E.; Fang, M.; Furche, F.; Meyer, G.; Ziller, J. W.; Evans, W. J. *J. Am. Chem. Soc.* **2010**, *132*, 11151-11158.

(17) Bochkarev, M. N.; Fedushkin, I. L.; Fagin, A. A.; Petrovskaya, T. V.; Ziller, J. W.; Broomhall-Dillard, R. N. R.; J., E. W. *Angew. Chem. Int. Ed.* **1997**, *36*, 133-135.

(18) Bochkarev, M. N.; Fedushkin, I. L.; Dechert, S.; Fagin, A. A.; Schumann, H. *Angew. Chem. Int. Ed.* **2001**, *40*, 3176-3178.

(19) Bochkarev, M. N.; Fagin, A. A. *Chem. Eur. J.* **1999**, *5*, 2990-2992.

(20) Evans, W. J.; Allen, N. T.; Ziller, J. W. *J. Am. Chem. Soc.* **2001**, *123*, 7927-7928.

(21) Evans, W. J.; Allen, N. T.; Ziller, J. W. *Angew. Chem., Int. Ed.* **2002**, *41*, 359-361.

(22) Evans, W. J.; Zucchi, G.; Ziller, J. W. *J. Am. Chem. Soc.* **2003**, *125*, 10-11.

(23) Cloke, F. G. N.; Khan, K.; Perutz, R. N. *J. Chem. Soc., Chem. Commun.* **1991**, 1372-1373.

(24) Polly L. Arnold; Cloke, F. G. N.; Nixon, J. F. *Chem. Commun.* **1998**, 797-798.

(25) Cassani, M. C.; Lappert, M. F.; Laschi, F. *Chem. Commun.* **1997**, 1563-1564.

(26) Hitchcock, P. B.; Lappert, M. F.; Maron, L.; Protchenko, A. V. *Angew. Chem., Int. Ed.* **2008**, *47*, 1488-1491.

(27) Fang, M.; Lee, D. S.; Ziller, J. W.; Doedens, R. J.; Bates, J. E.; Furche, F.; Evans, W. J. *J. Am. Chem. Soc.* **2011**, *133*, 3784-3787.

CHAPTER 1

Synthesis and Reactivity of +2 Ion Rare-Earth Metal Complexes with $(C_5H_5)^{1-}$ and $(C_5H_4Me)^{1-}$ as Ligands

Introduction*

As described in the Introduction section of this dissertation, it was previously believed that the +2 oxidation states of the lanthanide metals were limited to the six "traditional" divalent metals, Eu, Yb, Sm, Tm, Dy, and Nd, based on extensive solid state studies[1-2] and the calculated $4f^n/4f^{n+1}$ reduction potentials.[3] This belief was overturned in 2008 when Lappert et. al. reported that the tris(silylcyclopentadienyl) ligand system, $(Cp''_3)^{3-}$ [Cp″ = $C_5H_3(SiMe_3)_2$], allowed the isolation and structural characterization of molecular complexes containing lanthanum in the +2 oxidation state, [K(crypt)][Cp″$_3$La] (crypt = 2.2.2-cryptand], eq 1.1.[4] Later, it was found by the

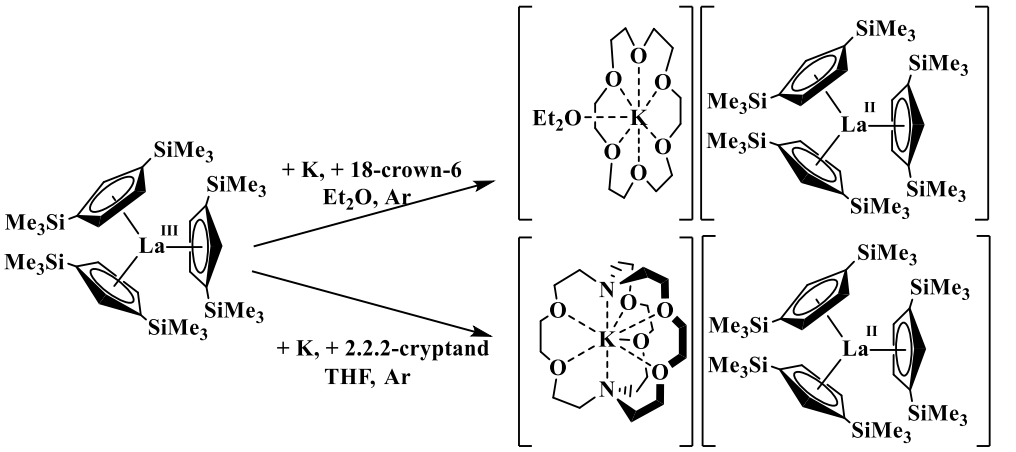

(1.1)

Evans group that the use of another tris(silylcyclopentadienyl) ligand system, $(Cp'_3)^{3-}$ (Cp′ = $C_5H_4SiMe_3$), allowed the isolation and structural characterization of the +2 ions of all the

* Portions of this chapter have been published: Corbey, J. F.; Woen, D. H.; Palumbo, C. T.; Fieser, M. E.; Ziller, J. W.; Furche, F.; and Evans W. J. *Organometallics* **2015**, 34, 3909−3921. DOI: 10.1021/acs.organomet.5b00500

lanthanides (except the radioactive promethium), as well as the rare-earth metal, yttrium, in [K(crypt)][Cp'$_3$Ln] (Ln = Y and lanthanides except Pm), **1-Ln**, eq 1.2.[5-8] These reports were unprecedented because they included the first isolation and characterization of the +2 ions of La, Ce, Pr, Gd, Tb, Ho, Er, Lu and Y, which have since been termed "non-traditional" divalent ions.

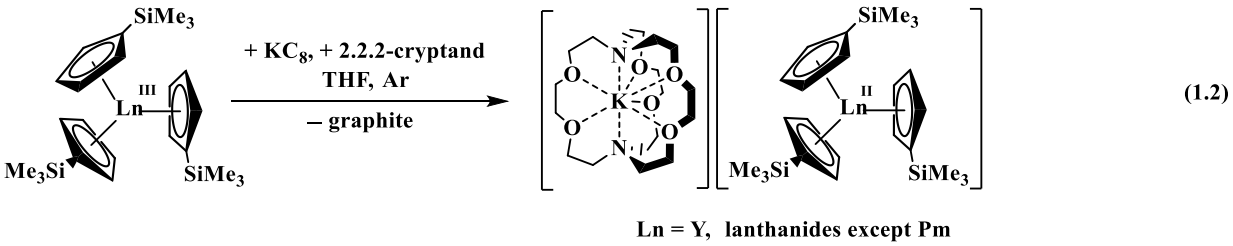

(1.2)

It is apparent that in all these complexes, the cyclopentadienyl ligands are silyl-substituted. Hence, it became of interest to determine whether the use of silyl substituents was necessary for isolating the +2 ions with the "non-traditional" divalent metals. This Chapter describes initial efforts to probe this by exploring the use of other cyclopentadienyl substituents in isolating new examples of +2 rare-earth metal ion complexes. More specifically, the use of the tris(cyclopentadienyl) and tris(methylcyclopentadienyl) ligand systems, $(Cp_3)^{3-}$ ($Cp = C_5H_5$) and $(Cp^{Me}{}_3)^{3-}$ ($Cp^{Me} = C_5H_4Me$), respectively, is discussed.

Yttrium was initially used as the primary metal to start this investigation because (1) although it is not a lanthanide, it displays lanthanide-like properties and has a similar size to that of the mid-late lanthanide, holmium,[9] (2) its +2 ion can be easily identified using EPR spectroscopy, shown as a two-line hyperfine pattern due to the I = ½ of the 100% naturally abundant ^{89}Y isotope,[5,7,10] and (3) its diamagnetic property in the +3 oxidation state allows less complicated characterization using NMR spectroscopy. In the case of the $(Cp^{Me}{}_3)^{3-}$ ligand set, the exploration was further expanded to other lanthanide metals as well as to reactivity studies.

Results and Discussion

Syntheses $Cp_3Y(THF)$ and $Cp^{Me}{}_3Ln(THF)$ (Ln = La, Pr, Gd, Y). The syntheses of the +3 ion rare-earth metal complexes used as precursors in this Chapter follow an adaptation of previously reported procedures in the literature. $Cp_3Y(THF)$ (Cp = C_5H_5) was prepared from the reaction of three equiv of KCp with YCl_3 in THF. The $Cp^{Me}{}_3Ln(THF)$ (Cp^{Me} = C_5H_4Me) complexes were prepared from the reaction of three equiv of either KCp^{Me} or $NaCp^{Me}$ with $LnCl_3$ in THF. For $Cp^{Me}{}_3Y(THF)$, X-ray crystallographic structure was obtained, Figure 1.1., since this structure had not been reported in the literature and it could be useful for comparison with complexes in +2 oxidation states.

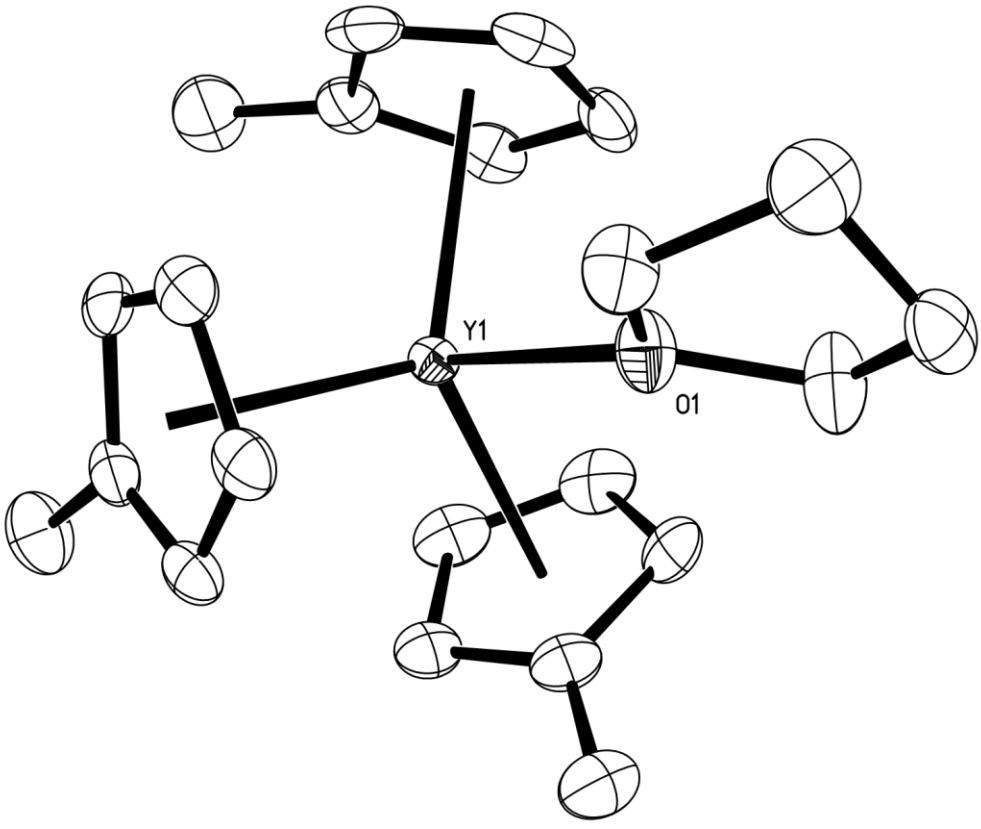

Figure 1.1. Thermal ellipsoid plot of $Cp^{Me}{}_3Y(THF)$ drawn at 50% probability level. Hydrogen atoms are omitted for clarity.

Reductions of $Cp_3Y(THF)$ and $Cp^{Me}_3Y(THF)$. The reductions of $Cp_3Y(THF)$ and $Cp^{Me}_3Y(THF)$ using KC_8 in the presence of 2.2.2-cryptand (crypt) at −35 °C yielded dark-colored solutions, **2-Y** and **3-Y**, respectively. EPR spectra of each dark solution were collected, Figure 1.2 and 1.3. The room temperature spectrum of each solution showed the expected isotropic two-line pattern for Y^{2+} based on previous reports.[5,7,10] For **2-Y**, the EPR spectrum is observed at g_{iso} = 1.991 with A = 42.9 G, whereas for **3-Y**, the spectrum is found at g_{iso} = 1.991 with A = 47.0 G. Frozen solutions at 77 K generated more complex EPR spectra due to the anisotropy of the complexes. An axial signal with $g_{\parallel}$ = 2.003 and $g_{\perp}$ = 1.986 was obtained for **2-Y**, which was expected for a system with a C_3-based symmetry. For **3-Y**, however, simulation and exact determination of the g-values were hindered by the fact that there appears to be an added feature in the spectrum in the form of an extra high intensity signal (singlet) at around g = 2.001. This feature is attributed to the presence of an electride species. In order to support this assignment, the electride species was independently prepared from the reaction of crypt and KC_8 in THF. The EPR spectrum of that product gave a signal at g = 2.001, Figure 1.4.

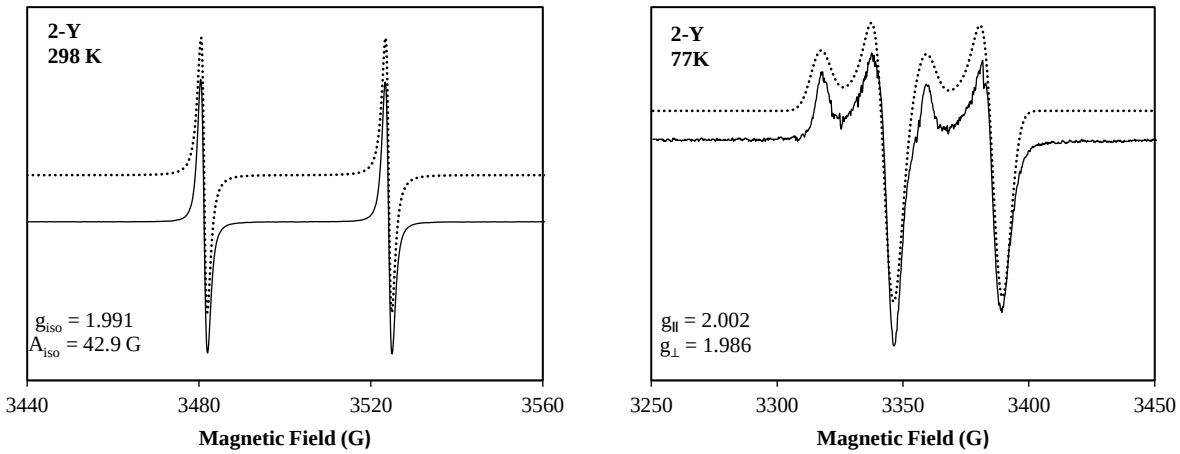

Figure 1.2. X-band EPR spectra of the reduction product of $Cp_3Y(THF)$, **2-Y**, collected at 298 K (left) and 77 K (right). Simulated spectra are shown as dotted lines.

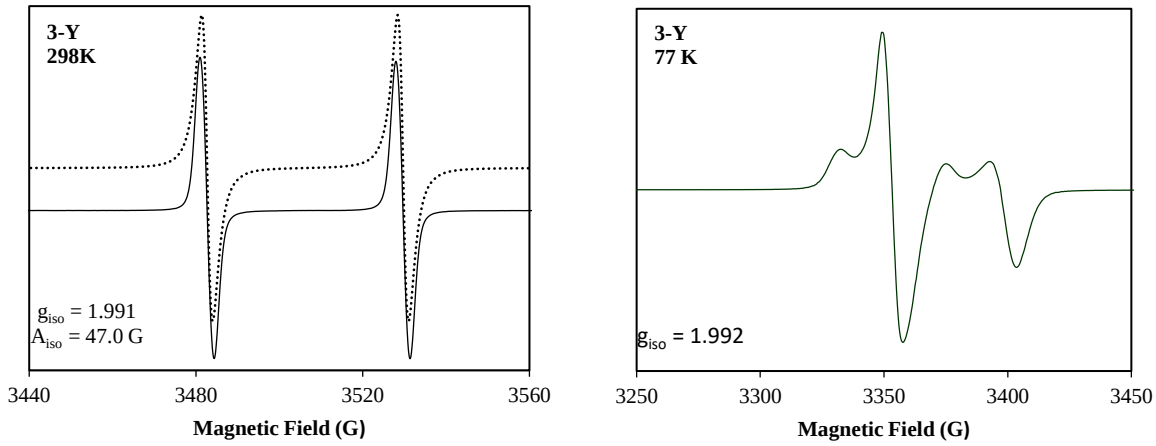

Figure 1.3. X-band EPR spectra of the reduction product of $Cp^{Me}{}_3Y(THF)$, **3-Y**, collected at 298 K (left) and 77 K (right). Simulated spectra are shown as dotted lines.

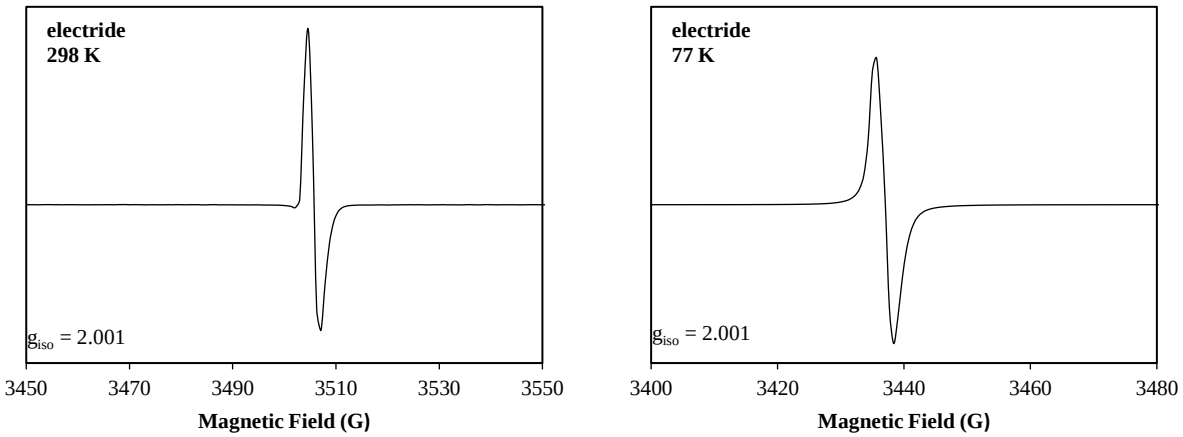

Figure 1.4. X-band EPR spectrum of an electride species formed from the reaction of crypt and KC_8 in THF collected at 298 K (left) and 77 K (right).

Both **2-Y** and **3-Y** were highly unstable and decomposed at −35 °C over time to form pale-colored solutions. In comparison, the previously reported Y^{2+} complex, [K(crypt)][Cp'$_3$Y], **1-Y**, was stable at −35 °C and could even be structurally characterized. These results suggested that the use of hydrogen and methyl cyclopentadienyl substituents do not lead to stable Y^{2+} species as observed with the use of silyl substituents.

At this point, the available data indicated that the use of silyl substituents was important in the stabilization and isolation of Y^{2+}, and this could be attributed to either electronic effects or steric effects, or both. In order to first analyze the electronic effects of the substituents, the EPR hyperfine coupling constants of the three Y^{2+} species were compared. The previously reported coupling constant of **1-Y** was 36.6 G,[5,7] which is smaller than the 42.9 G coupling constant of **2-Y** and the 47.0 G of **3-Y**, Table 1.1. Since hyperfine coupling constant can be attributed to the degree of interaction between an electron and the metal center, it was possible that lower coupling constant observed in **1-Y** compared to **2-Y** and **3-Y** was caused by the reduction in electron density on the metal by having silyl substitutents on the cyclopentadienyl ligands. This is consistent with

previous reports by Bercaw and Lappert indicating that silyl-substitution on cyclopentadienyl ligands lowers the reduction potential of the corresponding metal complex, while alkyl-substitution has the opposite effect.[19,32]

Another set of data consistent with this trend was obtained by another graduate student in the Evans group, Dr. Chad T. Palumbo, with the isolation and analysis by EPR spectroscopy of three new Y^{2+} species from the reductions of Cp''_2YCp^{Me}, Cp''_3Y, and Cp''_2YCp [$Cp'' = C_5H_3(SiMe_3)_2$] to give spectra with A = 36.4, 36.1, and 34.6, respectively, Table 1.1. All these complexes have at least two cyclopentadienyl ligands with two silyl substituents, and their coupling constants are all lower than that of **1-Y**. Therefore, more silyl substituents appear to correspond to lower coupling constants, which is consistent with the decrease of electron donor ability of the cyclopentadienyl ligands, Figure 1.5.

Table 1.1. Room temperature EPR spectra data of Y^{2+} complexes from the reduction of Y^{3+} complexes with varying ancillary ligands.

Y^{3+} Precursors	**g_{iso}**	**A (G)**
a) Cp''_2YCp	1.9904	34.6
b) Cp''_3Y	1.9908	36.1
c) Cp''_2YCp^{Me}	1.9904	36.4
d) Cp'_3Y	1.991	36.6
e) $Cp_3Y(THF)$	1.9905	42.8
f) $Cp^{Me}_3Y(THF)$	1.9903	46.9

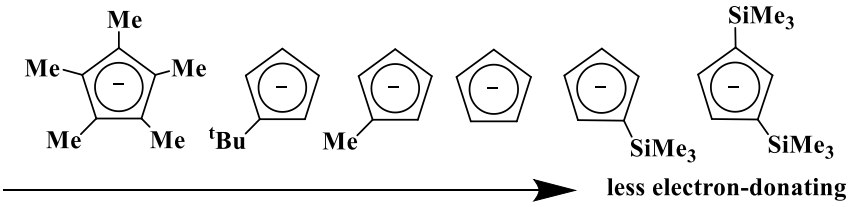

Figure 1.5. Expected trend in ligand electron donorability based on substituent.[19,32]

Since less electron donor ability of the ligands should provide more stability for metal ions with low oxidation states, it was expected that the use of the disilylcyclopentadienyl ligands would provide more stable Y^{2+} complexes than **1-Y**. However, it was found that all of the Y^{2+} complexes with disilylcyclopentadienyl ligands were also less stable than **1-Y**. In fact, the Y^{2+} complex produced from the reduction of the complex with all three ligands being disilylcyclopentadienyl, Cp''_3Y, was found to be less stable than those generated from the complexes with the mixed ligand systems, Cp''_2YCp^{Me} and Cp''_2YCp, both of which were still less stable than **1-Y**. These results were attributed the idea that having at least two silyl groups on the cyclopentadienyl ligand might cause steric over-saturation which could lead to lower stability.

Reactivity with $PhSiH_3$. Since both **2-Y** and **3-Y** were too unstable and could not be characterized by X-ray crystallography, it became of interest to perform in situ reactivity studies in order to derivatize these highly reactive species. Reactivity studies with $PhSiH_3$ were attractive since $PhSiH_3$ has been shown to react with rare-earth and actinide complexes to make isolable hydride products.[11-17] This was previously demonstrated by another Evans group member, Dr. Cory Windorff, with the reaction of a U^{2+} species, [K(2.2.2-cryptand)][Cp'_3U] and $PhSiH_3$ to produce the U^{3+} hydride species, [K(2.2.2-cryptand)][Cp'_3UH], eq. 1.3.[18] In this case, the U^{2+} complex had previously been characterized.[18] For the rare-earth metals, there are several hydride complexes known that retain three cyclopentadienyl ligands as found in the uranium complex

above, even though these complexes are bimetallic: $[K(THF)_6][(Cp_3Lu)_2(\mu\text{-}H)]$[19] and {K(18-crown-6)(toluene)$_2$}{[$(C_5H_4Si^tBuMe_2)_3Ln]_2(\mu$-H)} (Ln = La, Ce).[20] If all three of the cyclopentadienyl ligands from **2-Y** and **3-Y** could be retained in the derivatization products, it would be a good indication that the they were retained in the Y^{2+} species.

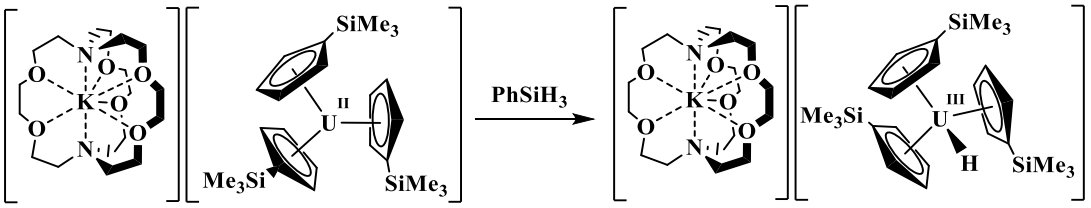

(1.3)

The reaction of freshly generated **2-Y** with $PhSiH_3$ in THF at −35 °C immediately generated a faint yellow solution. However, no crystalline solids were obtained and the products could not be identified. The reaction of freshly generated **3-Y** with $PhSiH_3$ in THF at −35 °C also generated an immediate color change to faint yellow, but in this case, crystalline solids were successfully grown from THF by layer diffusion with Et_2O. Surprisingly, X-ray crystallographic analysis of the colorless crystalline product revealed an yttrium-silyl complex [K(2.2.2-cryptand)][$Cp^{Me}_3Y(SiH_2Ph)$], **4**, Figure 1.6. The Y−Si bond length of this ten-coordinate complex was determined to be 2.954 Å, which is similar to the 2.979(3) and 2.961(2) Å bond lengths observed in the six-coordinate complexes, $(R_3Si)YI_2(THF)_3$ and $[(Et)R_2Si]YI_2(THF)$ (R = $SiMe_3$), respectively. However, the Y−Si bond length of **4** is significantly shorter than the 3.038 Å in the ten-coordinate complex, $Cp_3Y\{Si[N(CH_2{}^tBu)]_2(C_6H_4\text{-}1,2)\}$,[21] possibly due to the silicon-based ligand being a neutral donor silylene ligand. Although transition metal–SiH_2Ph complexes are known,[26-33] there has never been a report on any rare-earth–SiH_2Ph complexes in the literature.

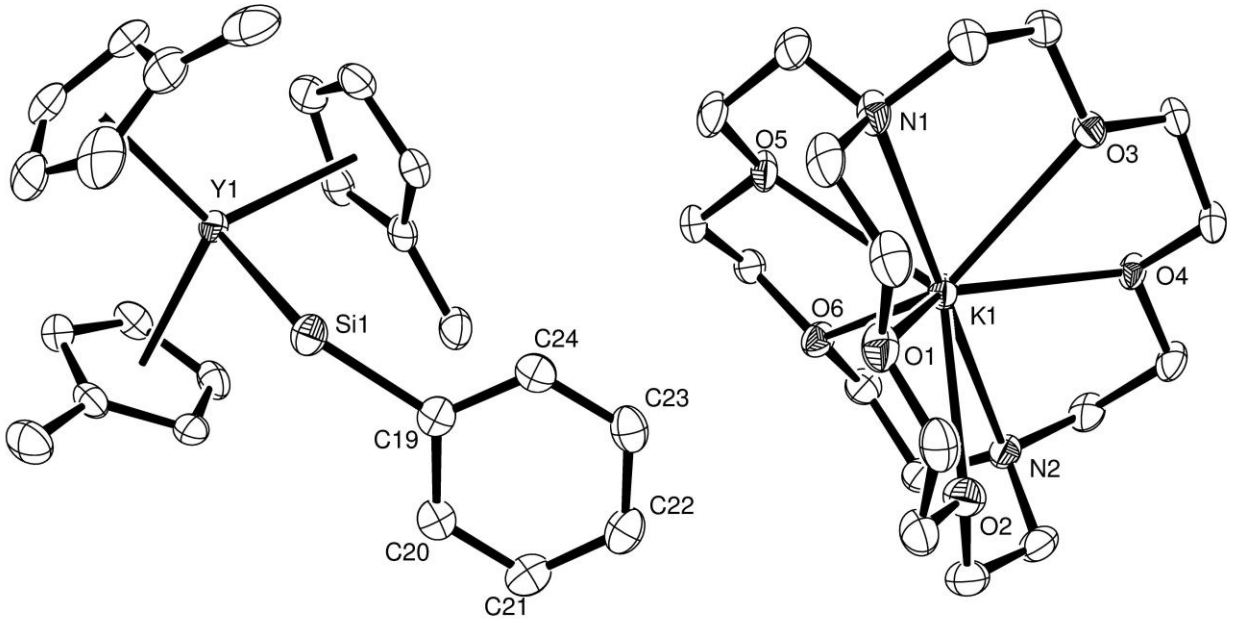

Figure 1.6. Thermal ellipsoid plot of [K(2.2.2-cryptand)][$Cp^{Me}_3Y(SiH_2Ph)$], **4**. Hydrogen atoms are omitted for clarity.

The reaction was repeated using an excess of $PhSiH_3$ and colorless crystals with a different morphology than those of **4** were obtained. This product was characterized by X-ray crystallography as a bimetallic yttrium complex, **5**, Figure 1.7. ^{1}H NMR spectroscopy shows a triplet at δ −0.33 ppm with a coupling constant of 34.3 Hz. This coupling is within the $^1J_{YH}$ = 27.2-34.6 Hz range found in previous reports of bimetallic yttrium bridging dihydride complexes[34-37] and the negative hydride shift is fairly close to the δ −1.03 ppm of the anionic tetrahydride complex, $\{Li(THF)_4\}\{[Cp_2Y(\mu\text{-}H)_3](\mu_3\text{-}H)\}$.[38] The crystal data of **5** were not of high enough quality to allow the identification of the seventh anionic ligand beyond the six cyclopentadienyl groups. However, the Y–Y distance was determined to be ~4.3 Å, and each metal is located ~0.4 Å out of the plane of its three Cp-ring centroids towards the other metal. Since anionic bridging

mono-hydride complexes $[K(THF)_6][(Cp_3Lu)_2(\mu\text{-}H)]$[19] and {K(18-crown-6)(toluene)$_2$}{$[(C_5H_4Si^tBuMe_2)_3Ln]_2(\mu\text{-}H)$} (Ln = La, Ce)[20] are known, it is likely that **5** adopts a similar identity to those complexes, namely $[K(2.2.2\text{-cryptand})][(Cp^{Me}{}_3Y)_2(\mu\text{-}H)]$. The ~4.3 Å Y–Y distance of **5** is within the 4.18 (Lu–Lu), 4.513 (Ce–Ce), and 4.523 (La–La) Å distances of those previously reported bridging mono-hydride complexes.[19-20] This is reasonable considering that the ionic radius of Y is similar to Dy and Ho, which are in the middle of the lanthanide series.

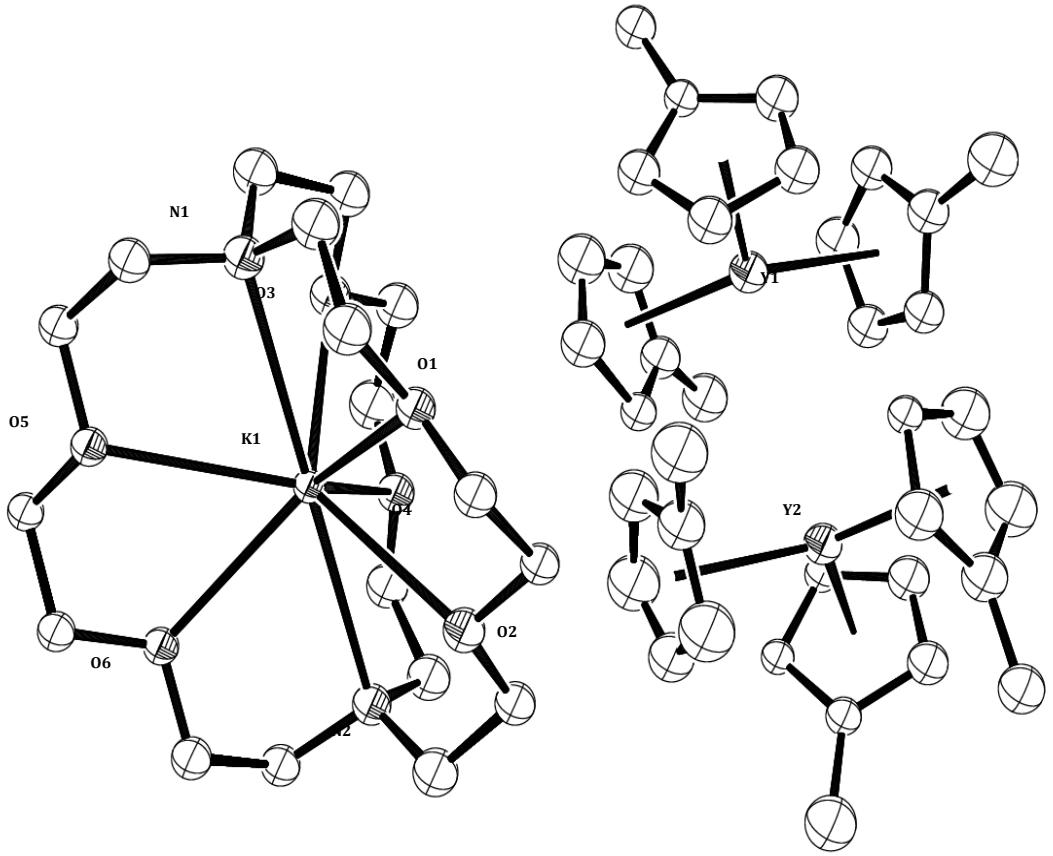

Figure 1.7. Thermal ellipsoid plot of $[K(2.2.2\text{-cryptand})][(Cp^{Me}{}_3Y)_2(\mu\text{-}H)]$, **5**, drawn at 50% probability level. No bridging moiety could be located. Hydrogen atoms are omitted for clarity.

Reductions of $Cp^{Me}_3Ln(THF)$ (Ln = La, Pr, Gd). The reduction studies using the $(Cp^{Me}_3)^{3-}$ ligand system were extended to other lanthanide metals, La, Pr, and Gd. Reductions of $Cp^{Me}_3Ln(THF)$ (Ln = La, Pr, Gd) using KC_8 in the presence of crypt at −35 °C generated deep dark brown solutions, **3-La**, **3-Pr**, and **3-Gd**, respectively, that decomposed within several minutes at −35 °C to faint yellow. For lanthanum and gadolinium, EPR spectroscopic measurements were performed on the fresh reduction products, Figure 1.8 and Figure 1.9, since the previously reported La^{2+} complex, $[Cp''_3La]^{1-}$, generated an EPR spectrum with an eight-line hyperfine pattern consistent with $I = 7/2$ of ^{139}La, whereas the Gd^{2+} complex, $[Cp'_3Gd]^{1-}$, **1-Gd**, generated a broad singlet. Consistent with these previous reports, the room temperature EPR spectrum of **3-La** displays an eight-line hyperfine pattern at g = 1.971 with A = 196 G. The frozen solution at 77 K generated an EPR spectrum with complicated feature that still shows an eight-line hyperfine pattern with an estimated g-value of 1.970. The room temperature EPR spectrum of **3-Gd** displays a broad singlet at g = 1.988 and the frozen solution at 77 K gave a broad singlet at g = 1.977. Both EPR signals of **3-Gd** are noticeably broader than those of the previously characterized [K(crypt)][Cp'_3Gd] **1-Gd**. A possible reason is the higher concentration of the sample, which could amplify the normally negligible contributions from the seven unpaired electrons in the 4f orbitals as well as the $I = 3/2$ of the combined 30.5% naturally abundant ^{155}Gd and ^{157}Gd isotopes. In addition, there might have been a significant amount of decomposition product containing other Gd^{2+} ions, as well as decomposition products containing Gd^{3+} ions, which at high concentrations, have been reported to show a broad shallow signal.[7] The broad signals do not appear to be that of an organic free radical since the latter is typically displayed at approximately $g_{iso} = 2.002$.

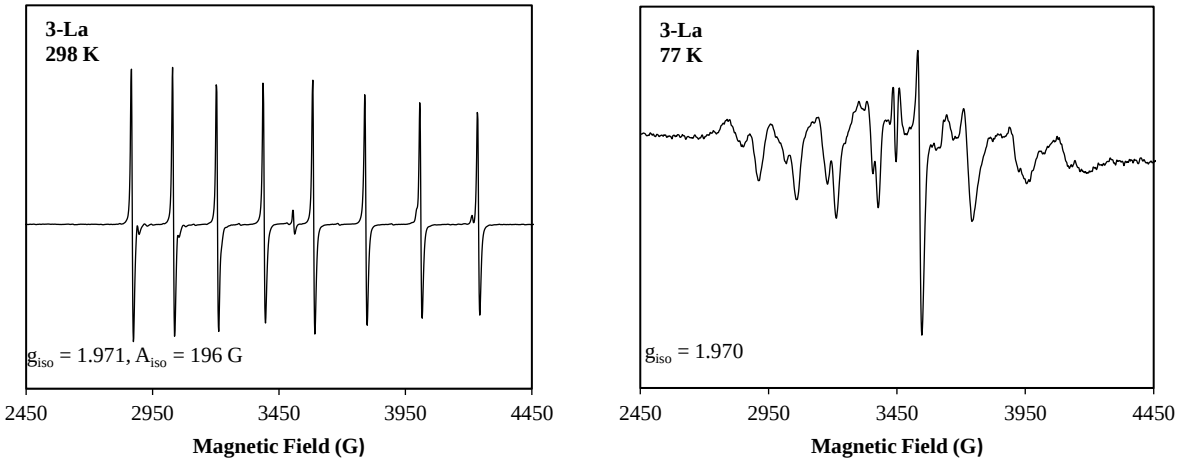

Figure 1.8. X-band EPR spectra of the reduction product of $Cp^{Me}_3La(THF)$, **3-La**, collected at 298 K (left) and 77 K (right). Simulated spectra are shown as dotted lines if available.

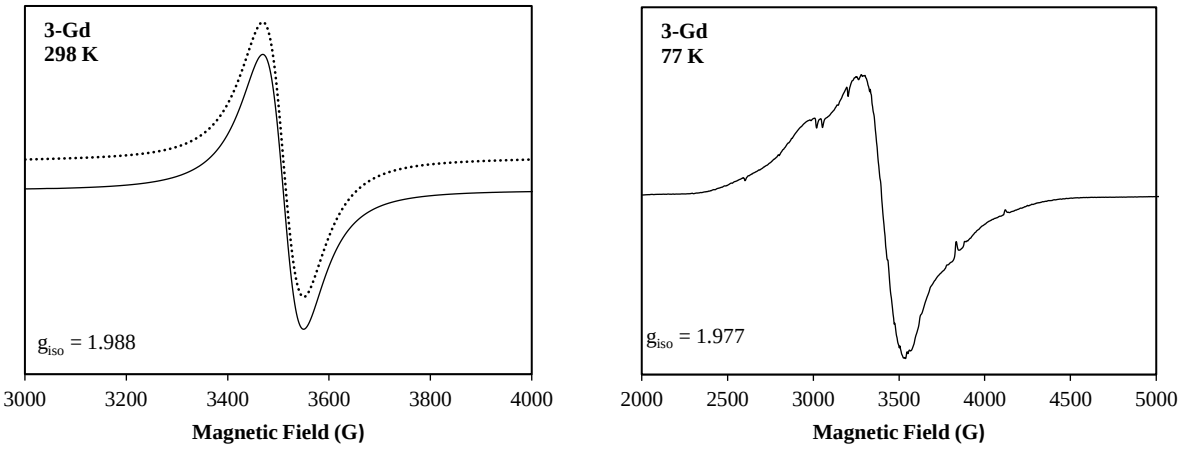

Figure 1.9. X-band EPR spectra of the reduction product of $Cp^{Me}_3Gd(THF)$, **3-Gd**, collected at 298 K (left) and 77 K (right). Simulated spectra are shown as dotted lines if available.

For **3-La** and **3-Pr**, pale colored decomposition products were successfully identified by X-ray crystallography as the bridging ring-opened THF products, $[K(crypt)]_2[(Cp^{Me}_3Ln)_2(\mu\text{-}OCH_2CH_2CH_2CH_2)]$ [Ln = La (**6-La**), Pr (**6-Pr**)], Figure 1.10. These complexes crystallize in the

monoclinic space group $P2_1/c$ and their crystal structures are isomorphous. They crystallize as bimetallic species with inversion centers so that there is just one Cp^{Me}_3Ln unit and one K(crypt) moiety in each unit cell. Refinement of the structures was complicated by the fact that the dianionic bridging ligand is non-symmetrical. This led to disorder in the bridging ligands, since the bridging ligand could be oriented as $(\mu\text{-}OCH_2CH_2CH_2CH_2)^{2-}$ or $(\mu\text{-}CH_2CH_2CH_2CH_2O)^{2-}$. This situation with the inversion symmetry initially gave a refinement in which the bridge appeared to have six atoms that could be modeled by $(\mu\text{-}CH_2CH_2CH_2CH_2CH_2CH_2)^{2-}$! In addition, there is disorder in the orientation of one of the Cp^{Me} rings for each metal, in which the Me substituent points toward or away from the bridges. Both disorders are shown in Figure 1.11.

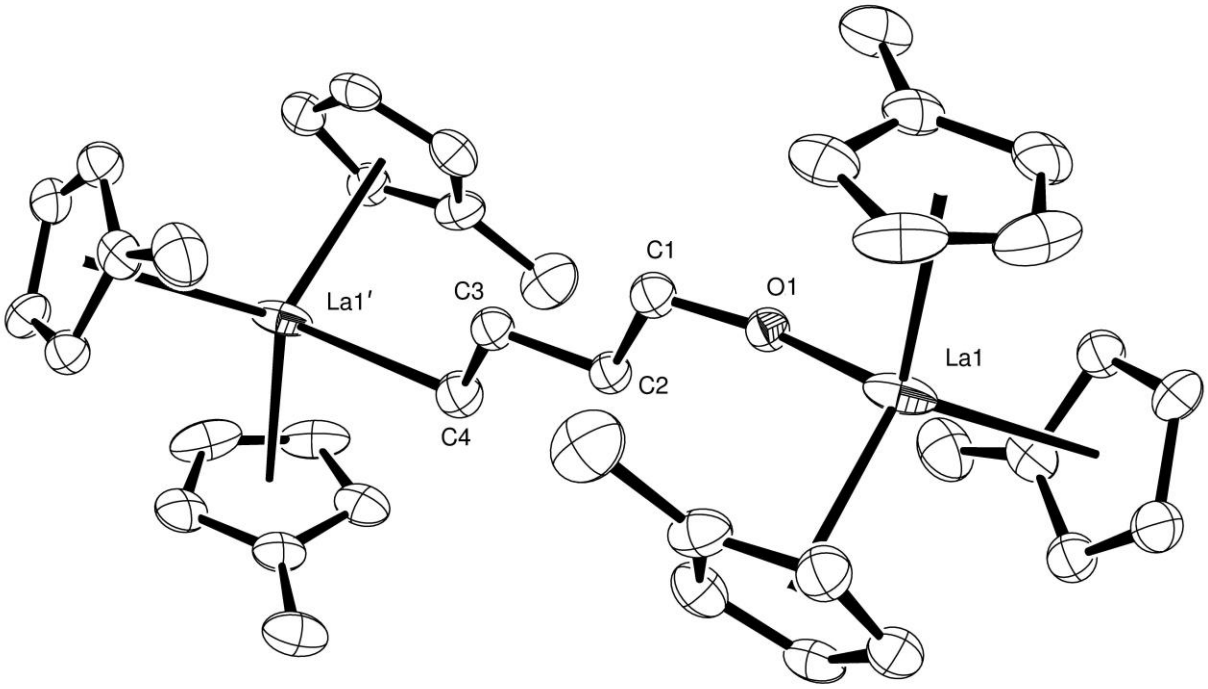

Figure 1.10. Thermal ellipsoid plot of one bimetallic anion of **6-La** drawn at 50% probability level. Disorder, hydrogen atoms, two THF molecules, and two $[K(crypt)]^+$ countercations are omitted for clarity. **6-Pr** is isomorphous.

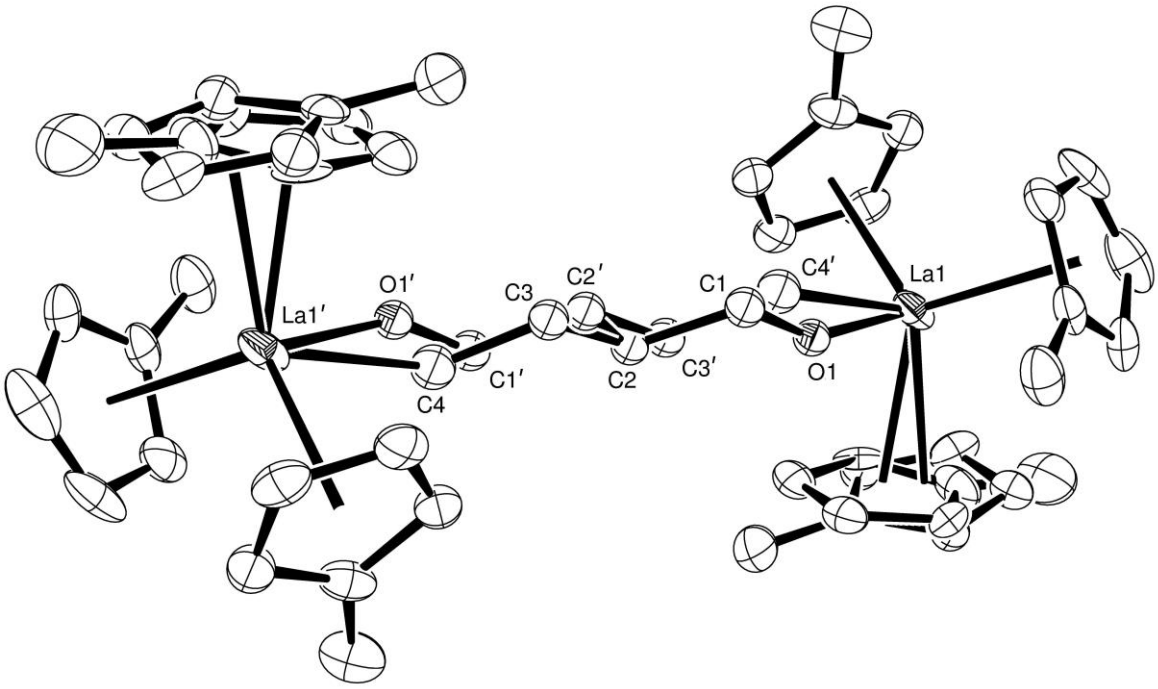

Figure 1.11. Thermal ellipsoid plot of one bimetallic anion of **6-La** drawn at 50% probability level with disorder shown. Hydrogen atoms, two THF molecules, and two $[K(crypt)]^+$ countercations are omitted for clarity.

The ^{1}H NMR spectrum of the product of the decomposition of **3-La** shows resonances consistent with the X-ray crystallographic data of **6-La**. Two sets of Cp^{Me} resonances with equal integrations are observed: one at δ 5.58 (*m*, 6H, C_5H_4Me), 5.56 (*m*, 6H, C_5H_4Me), and 2.16 (*m*, 9H, C_5H_4*Me*) ppm, and another one at δ 5.48 (*m*, 6H, C_5H_4Me), 5.45 (*m*, 6H, C_5H_4Me), and 2.13 (*m*, 9H, C_5H_4*Me*) ppm. This is consistent with the differing proton environments in one $Cp^{Me}{}_3$La moiety compared to the other. Additionally, a set of resonances consistent with the bridging ring-opened THF was also observed: δ 3.81 (*t*, 2H, OC*H*$_2$CH$_2$CH$_2$CH$_2$), 1.55 (*q*, 2H, OCH$_2$C*H*$_2$CH$_2$CH$_2$), 1.39 (*q*, 2H, OCH$_2$CH$_2$C*H*$_2$CH$_2$), and −0.22 (*q*, 2H, OCH$_2$CH$_2$CH$_2$C*H*$_2$) ppm.

Similar to **4-Y** and **5-Y**, each metal center in **6-Ln** retains all three of the anionic cyclopentadienyl ligands. This suggests that, similar to the reduction of Cp^{Me}_3Y, the reductions of Cp^{Me}_3La and Cp^{Me}_3Pr likely generated Ln^{2+} complexes that still have all three cyclopentadienyl ligands retained. The results from both reactivity studies support the assignment that **3-Y**, **3-La** and **3-Pr** could be $[Cp^{Me}_3Y]^{1-}$, $[Cp^{Me}_3La]^{1-}$, and $[Cp^{Me}_3Pr]^{1-}$, respectively.

The fact that the Ln^{2+} complexes with the $(Cp^{Me}_3)^{3-}$ ligand system are significantly less stable and more reactive than those with the $(Cp'_3)^{3-}$ could be attributed to the smaller steric bulk of the methyl substituent compared to the trimethylsilyl substituent. The reduced steric bulk leads to steric under-saturation that provides an open coordination site for the metal to interact and react with a substrate, e.g. either $PhSiH_3$ or THF. These data again support that steric effects play a role in the stabilization of the +2 ions of the "non-traditional" divalent metals.

Conclusion

Reduction studies of rare-earth metals using the $(Cp_3)^{3-}$ and $(Cp^{Me}_3)^{3-}$ ligand systems did not provide more stable Ln^{2+} complexes, which indicates that $(Cp'_3)^{3-}$ is still the best ligand system to isolate these Ln^{2+} ions. EPR spectroscopy studies provided hyperfine coupling constant data in concordance with previous reports that alkyl substituents cause cyclopentadienyl ligands to be more electron donating whereas silyl substituents cause them to be less electron donating. This could be an electronic explanation as to why the $(Cp'_3)^{3-}$ allows the isolation of the "non-traditional" divalent ions that were previously thought to be too reducing to isolate.

In addition to electronic factors, it appears that steric effects also play a role in the isolation of Ln^{2+} ions since the bulkier silyl cyclopentadienyl ligand system, $(Cp''_3)^{3-}$, did not provide more stable Y^{2+}, presumably because of steric oversaturation. In the case with the $(Cp^{Me}_3)^{3-}$ ligand

system, steric under-saturation seems to be the reason that the Ln^{2+} complexes are significantly less stable and highly reactive. The steric under-saturation and the consequently more open coordination environment provide the basis for these Ln^{2+} complexes to readily react with $PhSiH_3$ or THF to form the Ln^{3+} products, [K(2.2.2-cryptand)][$Cp^{Me}_3Y(SiH_2Ph)$], **4**, and [K(crypt)]$_2$[$(Cp^{Me}_3Ln)_2(\mu$-$OC_3H_6CH_2)$] [Ln = La (**4-La**), Pr (**4-Pr**)]. In all these products, each metal retains all three of the anionic cyclopentadienyl ligands. This suggests that the highly unstable Ln^{2+} products generated from the reduction of Cp^{Me}_3Ln still possess three anionic ligands and could be assigned as $[Cp^{Me}_3Ln]^{1-}$ (Ln = La, Pr, Y).

Experimental

All manipulations and syntheses described below were conducted with rigorous exclusion of air and water using standard Schlenk line and glovebox techniques under an argon or dinitrogen atmosphere. Solvents were sparged with UHP argon and dried by passage through columns containing Q-5 and molecular sieves prior to use. Deuterated NMR solvents were dried over NaK alloy, degassed by three freeze-pump-thaw cycles, and vacuum transferred before use. Methylcyclopentadiene were dried over molecular sieves and degassed by three freeze-pump-thaw cycles. 2.2.2-Cryptand (crypt) was purchased from Merck and dried under reduced pressure before use. KC_5H_5 and NaC_5H_4Me were synthesized via an adaptation of a literature procedure[39] in which the organic dimer is cracked and distilled onto a toluene solution of $KN(SiMe_3)_2$ or $NaN(SiMe_3)_2$, respectively. The resulting white precipitate was then washed with hexane and dried. KC_8,[40] anhydrous $LnCl_3$ (Ln = Y, La, Pr, Gd),[41] and $Cp_3Y(THF)$[42] were prepared according to the literature. ^{1}H NMR spectra were recorded on Bruker GN500 or CRYO500 MHz spectrometers (^{13}C NMR at 125 MHz) at 298 K unless otherwise stated and referenced internally to residual

protio-solvent resonances. Electron paramagnetic resonance spectra were collected using a Bruker EMX spectrometer equipped with an ER041XG microwave bridge in THF at 298 K and 77 K unless otherwise specified. EPR simulations were performed using P.E.S.T. WinSim developed by the National Institutes of Environmental Health Sciences or EasySpin.[43] IR samples were prepared as KBr pellets on a Varian 1000 FT-IR system or Jasco 4700 FTIR. Elemental analyses were conducted on a Perkin-Elmer 2400 Series II CHNS elemental analyzer.

$Cp^{Me}_3Y(THF)$. Analogous to a previously published procedure for the unsolvated La analog,[24] a pale yellow THF (5 mL) solution of $NaCp^{Me}$ (293 mg, 2.87 mmol) was added to a THF (5 mL) slurry of YCl_3 (175 mg, 0.896 mmol) and the cloudy yellow mixture was allowed to stir overnight. Pale yellow insoluble material was removed by centrifugation, and the yellow supernatant was filtered, dried under reduced pressure, and extracted using toluene. The extract was filtered and the solvent was removed under reduced pressure to yield $Cp^{Me}_3Y(THF)$ (279 mg, 78.2%) as a pale yellow powder. Colorless crystals suitable for X-ray diffraction were grown from toluene/hexane at −35 °C. ^{1}H NMR (C_6D_6): δ 5.94 (m, C_5H_4Me, 6H), 5.76 (m, C_5H_4Me, 6H), 3.36 (m, C_4H_8O, 4H), 2.22 (s, C_5H_4Me, 9H), 1.15 (m, C_4H_8O, 4H). ^{13}C NMR (C_6D_6): δ 118.35 (C_5H_4Me), 115.17 (C_5H_4Me), 108.43 (C_5H_4Me), 73.09 (C_4H_8O), 25.48 (C_4H_8O), 15.49 (C_5H_4Me). IR: 3084m, 2924w, 2861w, 2731s, 1613w, 1492s, 1455m, 1379s, 1339s, 1239s, 1169s, 1036m, 1013s, 930s, 832m, 766m, 616s cm^{-1}. Anal. Calcd for $C_{22}H_{29}OY$: C, 66.33; H, 7.34. Found: C, 66.14; H, 7.50.

$Cp^{Me}_3La(THF)$. Following the procedure for $Cp^{Me}_3Y(THF)$ above, a pale yellow THF (7 mL) solution of $NaCp^{Me}$ (244 mg, 2.39 mmol) was added to a THF (2 mL) slurry of $LaCl_3$ (196 mg, 79.7 mmol) to yield $Cp^{Me}_3La(THF)$ (147 mg, 49.2%) as a pale yellow powder after workup. Colorless crystals were grown from toluene/hexane at −35 °C. ^{1}H NMR (C_6D_6): δ 6.00 (m,

C_5H_4Me, 6H), 5.89 (m, C_5H_4Me, 6H), 3.35 (m, C_4H_8O, 4H), 2.25 (s, C_5H_4Me, 9H), 1.16 (m, C_4H_8O, 4H).

$Cp^{Me}{}_3Pr$ (THF). Following the procedure for $Cp^{Me}{}_3Y(THF)$ above, a pale yellow THF (7 mL) solution of KCp^{Me} (67 mg, 0.27 mmol) was added to a THF (2 mL) slurry of $PrCl_3$ (96 mg, 0.81 mmol) to yield $Cp^{Me}{}_3Pr(THF)$ (60 mg, 49%) as green solids after workup. Colorless crystals were grown from toluene/hexane at −35 °C.

$Cp^{Me}{}_3Gd(THF)$. Following the procedure for $Cp^{Me}{}_3Y(THF)$ above, a pale yellow THF (5 mL) solution of $NaCp^{Me}$ (370 mg, 3.62 mmol) was added to a THF (5 mL) slurry of $GdCl_3$ (318 mg, 1.21 mmol) to yield $Cp^{Me}{}_3Gd(THF)$ (327 mg, 58.1%) as a pale yellow powder after workup. Colorless crystals were grown from toluene/hexane at −35 °C with a NdFeB magnet attached to the outside. IR: 3089m, 2925w, 2861w, 2733s, 1619w, 1491s, 1454m, 1380s, 1340s, 1239s, 1167s, 1045s, 1012s, 935s, 830s, 775m, 613s cm^{-1}. Anal. Calcd for $C_{22}H_{29}OGd$: C, 56.62; H, 6.26. Found: C, 56.30; H, 6.07.

Reduction of $Cp_3Y(THF)$ for EPR analysis of 2-Y. In an argon-filled glovebox, crypt (79 mg, 0.21 mmol) and $Cp_3Y(THF)$ (60 mg, 0.21 mmol) were dissolved in THF (5 mL) and left in the freezer for a few hours upon which excess KC_8 was added and the solution was filtered into a pre-chilled scintillation vial to yield a black solution **3-Y**. A small amount of the solution was transferred to a pre-chilled EPR tube and kept cold until it could be inserted into the EPR Spectrometer.

Reduction of $Cp^{Me}{}_3Y(THF)$ for EPR analysis of 3-Y. In an argon-filled glovebox, crypt (115 mg, 0.305 mmol) and $Cp^{Me}{}_3Y(THF)$ (100 mg, 0.251 mmol) were dissolved in THF (5 mL) and placed in the freezer for a few hours. Using a pre-chilled pipette, the cold solution was run through a pre-chilled filter pipette packed with KC_8 into a pre-chilled scintillation vial to obtain a

deep brown solution **3-Y**. A small amount of the solution was transferred to a pre-chilled EPR tube and kept cold until it could be inserted into the EPR spectrometer.

Reduction of $Cp^{Me}_3La(THF)$ for EPR analysis of 3-La. Following the procedure for **3-Y**, crypt (8 mg, 0.022 mmol) and $Cp^{Me}_3La(THF)$ (10 mg, 0.022 mmol) were dissolved in THF (0.5 mL) and placed in the freezer for a few hours. The cold solution was run through a pre-chilled filter pipette packed with KC_8 into a pre-chilled scintillation vial to obtain a deep brown solution **3-La**. A small amount of the solution was transferred to a pre-chilled EPR tube and kept cold until it could be inserted into the EPR spectrometer.

Reduction of $Cp^{Me}_3Gd(THF)$ for EPR analysis of 3-Gd. Following the procedure for **3-Y**, crypt (99 mg, 0.26 mmol) and $Cp^{Me}_3Gd(THF)$ (114 mg, 0.244 mmol) were dissolved in THF (5 mL) and placed in the freezer for a few hours. The cold solution was run through a pre-chilled filter pipette packed with KC_8 into a pre-chilled scintillation vial to obtain a deep red solution **3-Gd**. A small amount of the solution was transferred to a pre-chilled EPR tube and kept cold until it could be inserted into the EPR spectrometer.

[K(2.2.2-cryptand)] [$Cp^{Me}_3Y(SiH_2Ph)$], 4. In an argon-filled glovebox, a THF (5 mL) solution of $Cp^{Me}_3Y(THF)$ (71 mg, 0.22 mmol) and crypt (82 mg, 0.22 mmol) was prechilled at −35 °C before it was pushed through a pre-chilled filter pipette packed with KC_8 onto a stirring pre-chilled THF (5 mL) solution containing $PhSiH_3$ (30 mg, 0.28 mmol). The resulting dark solution quickly turned pale yellow, which was then concentrated to ~3 mL, layered with Et_2O, and left at −35 °C. Colorless crystals of **9** suitable for X-ray diffraction were obtained after several days.

[K(2.2.2-cryptand)][($Cp^{Me}_3Y)_2(\mu$-H)], 5. In an argon-filled glovebox, a THF (2 mL) solution of $Cp^{Me}_3Y(THF)$ (71 mg, 0.22 mmol) and crypt (82 mg, 0.22 mmol) was prechilled at −35 °C before it was pushed through a pre-chilled filter pipette packed with KC_8 onto a stirring pre-

chilled THF (1 mL) solution containing $PhSiH_3$ (50 mg, 0.46 mmol). The resulting dark solution quickly turned pale yellow. The solution was transferred to the bottom of a prechilled Et_2O (15 mL) solution and was left at −35 °C. Colorless crystals of **10** suitable for X-ray diffraction were obtained after several days. ^{1}H NMR (THF-d_8): δ 5.74 (m, C_5H_4Me), 5.62 (m, C_5H_4Me), 3.54 (s, OC_2H_4Ot), 3.49 (t, NCH_2CH_2O, $^3J_{HH}$ = 5.0 Hz), 2.51 (t, NCH_2CH_2O, $^3J_{HH}$ = 5.0 Hz), 2.28 (s, C_5H_4Me), −0.33 (t, μ-H, $^1J_{YH}$ = 34.3 Hz). Anal. Calcd for $C_{54}H_{79}N_2O_6Y_2K$: C, 60.66; H, 7.45; N, 2.62. Found: C, 59.38; H, 7.51; N, 2.61. The ^{1}H NMR integrations were complicated by the presence of some impurity, possibly some analogous species to **10** except with one or more Cp ligands in place of the six Cp^{Me} ligands. This is evident in the distinctive hydride signal at δ −0.44 (t, $^1J_{YH}$ = 34.3 Hz).

$[K(crypt)]_2[(Cp^{Me}{}_3La)_2(\mu\text{-}OC_3H_6CH_2)]$, 6-La. In an argon-filled glovebox, crypt (25 mg, 0.066 mmol) and $Cp^{Me}{}_3La(THF)$ (25 mg, 0.066 mmol) were dissolved in THF (1 mL) and placed cooled to −35 °C for a few hours. KC_8 was added to the solution to generate a black mixture. The mixture was quickly filtered to give a dark brown solution and transferred to the bottom of a pre-chilled hexane (5 mL) solution for layer diffusion. Before the set up was transferred back into the glovebox freezer, it was observed that the dark color was already fading. After 24 h, off-white crystalline solids of were obtained. The solids were washed with room temperature Et_2O (3X) and dried (21 mg, 36%). Single crystals of $[K(crypt)]_2[(Cp^{Me}{}_3La)_2(\mu\text{-}OC_3H_6CH_2)]$, **6-La** suitable for X-ray diffraction were grown from THF/hexane layer diffusion at −35 °C. ^{1}H NMR (THF-d_8): δ 5.58 (*m*, 6H, C_5H_4Me), 5.56 (*m*, 6H, C_5H_4Me), 5.48 (*m*, 6H, C_5H_4Me), 5.45 (*m*, 6H, C_5H_4Me), 3.81 (*t*, 2H, $OCH_2CH_2CH_2CH_2$), 3.57 (crypt), 3.53 (*t*, 24H, crypt), 2.54 (*t*, 24H, crypt), 2.16 (*m*, 9H, C_5H_4Me), 2.13 (*m*, 9H, C_5H_4Me), 1.55 (*q*, 2H, $OCH_2CH_2CH_2CH_2$), 1.39 (*q*, 2H, $OCH_2CH_2CH_2CH_2$), and −0.22 (*q*, 2H, $OCH_2CH_2CH_2CH_2$) ppm.

IR: 3074w, 2959m, 2884s, 2816m, 2762m, 2660w, 1956w, 1476m, 1459m, 1444m, 1412w, 1353s, 1295m, 1200m, 1134s, 1103vs, 1078s, 1029m, 952s, 932m, 806m, 731s, 621w cm^{-1}.

[K(crypt)]$_2$[(Cp$^{Me}{}_3$Pr)$_2$(μ-OC$_3$H$_6$CH$_2$)], 6-Pr. Following the procedure for **6-La**, a 1 mL THF solution of crypt (16 mg, 0.042 mmol) and Cp$^{Me}{}_3$Pr(THF) (16 mg, 0.036 mmol) was reacted with KC_8 to give an off-white crystalline solid (10 mg, 27%). Single crystals of [K(crypt)]$_2$[(Cp$^{Me}{}_3$Pr)$_2$(μ-OC$_3$H$_6$CH$_2$)], **6-Pr**, suitable for X-ray diffraction were grown from THF/hexane layer diffusion at −35 °C. IR: 3075w, 2959m, 2886s, 2812m, 2760m, 2627w, 2670w, 1958w, 1476m, 1459m, 1444m, 1410w, 1356s, 1298m, 1266m, 1237w, 1172w, 1133s, 1105vs, 1079s, 1043w, 1029m, 950s, 931m, 803m, 733s, 619w cm^{-1}.

X-ray Data Collection, Structure Solution and Refinement for Cp$^{Me}{}_3$Y(THF). A colorless crystal of approximate dimensions 0.194 x 0.171 x 0.091 mm was mounted on a glass fiber and transferred to a Bruker SMART APEX II diffractometer. The APEX2[44] program package was used to determine the unit-cell parameters and for data collection (90 sec/frame scan time for a sphere of diffraction data). The raw frame data was processed using SAINT[45] and SADABS[46] to yield the reflection data file. Subsequent calculations were carried out using the SHELXTL[47] program. The diffraction symmetry was *mmm* and the systematic absences were consistent with the orthorhombic space group $P2_12_12_1$ that was later determined to be correct. The structure was solved by direct methods and refined on F^2 by full-matrix least-squares techniques. The analytical scattering factors[48] for neutral atoms were used throughout the analysis. Hydrogen atoms were included using a riding model. At convergence, wR2 = 0.0921 and Goof = 1.056 for 221 variables refined against 4540 data (0.74 Å), R1 = 0.0363 for those 3782 data with $I > 2.0\sigma(I)$. The structure was refined as a 2-component inversion twin.

X-ray Data Collection, Structure Solution and Refinement for 4. A colorless crystal of approximate dimensions 0.210 x 0.272 x 0.437 mm was mounted on a glass fiber and transferred to a Bruker SMART APEX II diffractometer. The APEX2[44] program package was used to determine the unit-cell parameters and for data collection (25 sec/frame scan time for a sphere of diffraction data). The raw frame data was processed using SAINT[45] and SADABS[46] to yield the reflection data file. Subsequent calculations were carried out using the SHELXTL[47] program. The diffraction symmetry was 2/*m* and the systematic absences were consistent with the monoclinic space group $P2_1/n$ that was later determined to be correct. The structure was solved by dual space methods and refined on F^2 by full-matrix least-squares techniques. The analytical scattering factors[48] for neutral atoms were used throughout the analysis. H(1) and H(2) were located from a difference-Fourier map and refined (x,y,z and U_{iso}). H(13)A was refined with d(C-H) = 0.95 Å. The remaining hydrogen atoms were included using a riding model. C(18) was disordered and included using multiple components with partial site-occupancy-factors. Least-squares analysis yielded wR2 = 0.0930 and Goof = 1.035 for 502 variables refined against 9546 data (0.78 Å), R1 = 0.0387 for those 8224 data with $I > 2.0\sigma(I)$.

X-ray Data Collection, Structure Solution and Refinement for 6-La. A colorless crystal of approximate dimensions 0.095 x 0.126 x 0.270 mm was mounted in a cryoloop and transferred to a Bruker SMART APEX II diffractometer. The APEX2[44] program package was used to determine the unit-cell parameters and for data collection (40 sec/frame scan time for a sphere of diffraction data). The raw frame data was processed using SAINT[45] and SADABS[46] to yield the reflection data file. Subsequent calculations were carried out using the SHELXTL[47] program. The diffraction symmetry was 2/*m* and the systematic absences were consistent with the monoclinic space group $P2_1/c$ that was later determined to be correct. The structure was solved

by dual space methods and refined on F^2 by full-matrix least-squares techniques. The analytical scattering factors[48] for neutral atoms were used throughout the analysis. Hydrogen atoms were included using a riding model. The molecule was located about an inversion center. The bridging tetrahydrofuran ligand was disordered about the inversion center. There were two molecules of tetrahydrofuran solvent present. Several atoms were disordered and included using multiple components with partial site-occupancy-factors. Least-squares analysis yielded wR2 = 0.1183 and Goof = 1.057or 441 variables refined against 7562 data (0.85 Å), R1 = 0.0516 for those 5628 data with $I > 2.0\sigma(I)$.

X-ray Data Collection, Structure Solution and Refinement for 6-Pr. A colorless crystal of approximate dimensions 0.095 x 0.126 x 0.270 mm was mounted in a cryoloop and transferred to a Bruker SMART APEX II diffractometer. The APEX2[44] program package was used to determine the unit-cell parameters and for data collection (40 sec/frame scan time for a sphere of diffraction data). The raw frame data was processed using SAINT[45] and SADABS[46] to yield the reflection data file. Subsequent calculations were carried out using the SHELXTL[47] program. The diffraction symmetry was 2/*m* and the systematic absences were consistent with the monoclinic space group $P2_1/c$ that was later determined to be correct. The structure was solved by dual space methods and refined on F^2 by full-matrix least-squares techniques. The analytical scattering factors[48] for neutral atoms were used throughout the analysis. Hydrogen atoms were included using a riding model. The molecule was located about an inversion center. The bridging tetrahydrofuran ligand was disordered about the inversion center. There were two molecules of tetrahydrofuran solvent present. Several atoms were disordered and included using multiple components with partial site-occupancy-factors. Least-squares analysis yielded wR2 = 0.1183 and

Goof = 1.057or 441 variables refined against 7562 data (0.85 Å), R1 = 0.0516 for those 5628 data with I > 2.0σ(I).

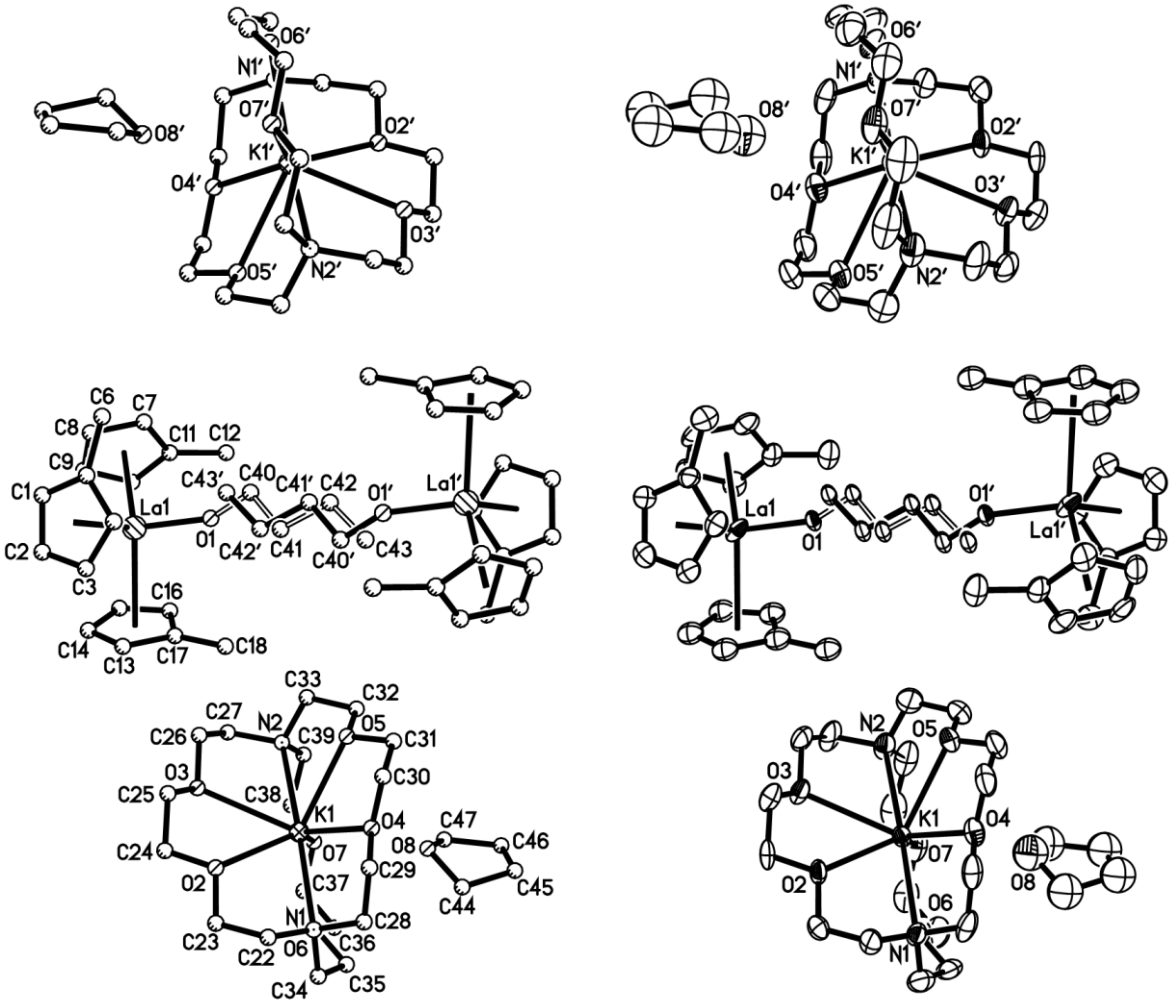

Figure 1.12. Thermal ellipsoid plots of **6-La** (left) and **6-Pr** (right) drawn at 50% probability level. Hydrogen atoms, disorder about one of the Cp^{Me} rings per metal and the THF molecules in the lattice are omitted for clarity.

References

(1) Meyer, G. *Chem. Rev.* **1988**, *88*, 93-107.

(2) Meyer, G.; Meyer, H.-J. *Chem. Mater.* **1992**, *4*, 1157-1168.

(3) Morss, L. R. *Chem. Rev.* **1976**, *76*, 827-841.

(4) Hitchcock, P. B.; Lappert, M. F.; Maron, L.; Protchenko, A. V. *Angew. Chem., Int. Ed.* **2008**, *47*, 1488-1491.

(5) MacDonald, M. R.; Ziller, J. W.; Evans, W. J. *J. Am. Chem. Soc.* **2011**, *133*, 15914-15917.

(6) MacDonald, M. R.; Bates, J. E.; Fieser, M. E.; Ziller, J. W.; Furche, F.; Evans, W. J. *J. Am. Chem. Soc.* **2012**, *134*, 8420-8423.

(7) MacDonald, M. R.; Bates, J. E.; Ziller, J. W.; Furche, F.; Evans, W. J. *J. Am. Chem. Soc.* **2013**, *135*, 9857-9868.

(8) Fieser, M. E.; MacDonald, M. R.; Krull, B. T.; Bates, J. E.; Ziller, J. W.; Furche, F.; Evans, W. J. *J. Am. Chem. Soc.* **2015**, *137*, 369-382.

(9) Daane, A. H. **1968**, *"Yttrium". In Hampel, Clifford A. THe Encyclopedia of the Chemical Elements. New York: Reinhold Book Corporation*
810-821.

(10) Fang, M.; Lee, D. S.; Ziller, J. W.; Doedens, R. J.; Bates, J. E.; Furche, F.; Evans, W. J. *J. Am. Chem. Soc.* **2011**, *133*, 3784-3787.

(11) Pagano, J. K.; Dorhout, J. M.; Waterman, R.; Czerwinskic, K. R.; Kiplinger, J. L. *Chem. Commun.* **2015**, *51*, 17379-17381.

(12) MarcinKonkol; JunOkuda *Coord. Chem. Rev.* **2008**, *252*, 1577-1591.

(13) Zeimentz, P. M.; Arndt, S.; Elvidge, B. R.; Okuda, J. *Chem. Rev.* **2006**, *106*, 2404-2433.

(14) Venugopal, A.; Fegler, W.; Spaniol, T. P.; Maron, L.; Okuda, J. *J. Am. Chem. Soc.* **2011**, *133*, 17574-17577.

(15) Fegler, W.; Venugopal, A.; Kramer, M.; Okuda, J. *Angew. Chem. Int. Ed.* **2014**, *54*, 1724-1736.

(16) Okuda, J. *Coord. Chem. Rev.* **2017**, *340*, 2-9.

(17) Paparo, A.; Silvia, J. S.; Kefalidis, C. E.; Spaniol, T. P.; Maron, L.; Okuda, J.; Cummins, C. C. *Angew. Chem. Int. Ed.* **2015**, *54*, 9115-9119.

(18) Windorff, C. J.; MacDonald, M. R.; Meihaus, K. R.; Ziller, J. W.; Long, J. R.; Evans, W. J. *Chem. Eur. J.* **2016**, *22*, 772-782.

(19) Schumann, H.; Genthe, W.; Hahn, E. *J. Organomet. Chem.* **1986**, *299*, 67-84.

(20) Gun'ko, Y. K.; Hitchcock, P. B.; Lappert, M. F. *Organometallics* **2000**, *19*, 2832-2834.

(21) Cai, X.; Gehrhus, B.; Hitchcock, P. B.; Lappert, M. F. *Can. J. Chem.* **2000**, *78*, 1484-1490.

(22) William J. Evans, T. J. B. a. J. W. Z. *J. Organomet. Chem.* **1993**, *462*, 141-148.

(23) Herrmann, W. A.; Eppinger, J. r.; Spiegler, M.; Runte, O.; Anwander, R. *Organometallics* **1997**, *16*, 1813-1815.

(24) Eppinger, J. r.; Spiegler, M.; Hieringer, W.; Herrmann, W. A.; Anwander, R. *J. Am. Chem. Soc.* **2000**, *122*, 3080-3096.

(25) Klimpel, M. G.; Gorlitzer, H. W.; Tafipolsky, M.; Spiegler, M.; Scherer, W.; Anwander, R. *J. Organomet. Chem.* **2002**, *647*, 236-244.

(26) Hao, J.; Vabre, B.; Zargarian, D. *J. Am. Chem. Soc.* **2015**, *137*, 15287-15298.

(27) Heiden, Z. M.; Zampella, G.; Gioia, L. D.; Rauchfuss, T. B. *Angew. Chem. Int. Ed.* **2008**, *47*, 9756-9759.

(28) Mork, B. V.; Tilley, T. D.; Schultz, A. J.; Cowan, J. A. *J. Am. Chem. Soc.* **2004**, *126*, 10428-10440.

(29) Scheuermann, M. L.; Semproni, S. P.; Pappas, I.; Chirik, P. J. *J. Am. Chem. Soc.* **2014**, *53*, 9463-9465.

(30) Britten, J.; Mu, Y.; Harrod, J. F.; Polowin, J.; Baird, M. C.; Samuel, E. *Organometallics* **1993**, *12*, 2672-2676.

(31) Zuzek, A. A.; Parkin, G. *J. Am. Chem. Soc.* **2014**, *136*, 8177-8180.

(32) Heyn, R. H.; Tilley, T. D. *J. Am. Chem. Soc.* **1992**, *114*, 1917-1919.

(33) Liu, H.-J.; Raynaud, C.; Eisenstein, O.; Tilley, T. D. *J. Am. Chem. Soc.* **2014**, *136*, 11473-11482.

(34) Cui, D.; Nishiura, M.; Tardif, O.; Hou, Z. *Organometallics* **2008**, *27*, 2428-2435.

(35) Booij, M.; Deelman, B.-J.; Duchateau, R.; Postma, D. S.; Meetsma, A.; Teuben, J. H. *Organometallics* **1993**, *12*, 3531-3540.

(36) Zhang, J.; Yi, W.; Zhang, Z.; Chen, Z.; Zhou, X. *Organometallics* **2011**, *30*, 4320-4324.

(37) Evans, W. J.; Meadows, J. H.; Wayda, A. L.; Hunter, W. E.; Atwood, J. L. *J. Am. Chem. Soc.* **1982**, *104*, 2008-2014.

(38) Evans, W. J.; Meadows, J. H.; Hanusa, T. P. *J. Am. Chem. Soc.* **1984**, *106*, 4454-4460.

(39) Reynolds, L. T.; Wilkinson, G. *J. Inorg. Nucl. Chem.* **1959**, *9*, 86-92.

(40) Bergbreiter, D. E.; Killough, J. M. *J. Am. Chem. Soc.* **1978**, *100*, 2126-2134.

(41) Meyer, G.; Ax, P. *Mater. Res. Bull.* **1982**, *17*, 1447-1455.

(42) Rogers, R. D.; Atwood, J. L.; Emad, A.; Sikora, D. J.; Rausch, M. D. *J. Organomet. Chem.* **1981**, *216*, 382-392.

(43) Stoll, S.; Schweiger, A. J. *Magn. Reson.* **2006**, *178*, 42.

(44) Bruker AXS, Inc., APEX2 Version 2014.11-0, Madison, WI, **2014**.

(45) Bruker AXS, Inc., SAINT Version 8.34a, Madison, WI, **2013**.

(46) Sheldrick, G. M.; SADABS, Version 2014/5, Bruker AXS, Inc., Madison, WI, **2014**.

(47) Sheldrick, G. M.; SHELXTL, Version 2014/7, Bruker AXS, Inc., Madison, WI, **2014**.

(48) *International Tables for Crystallography, Vol. C*, Kluwer Academic Publishers, Dordrecht, **1992**.

CHAPTER 2

Dinitrogen Reduction Reactivity of Rare-Earth Metal Complexes with $(C_5H_4Me)^{1-}$ as Ligands

Introduction*

As previously described in the Introduction section of this dissertation, the formation of $[A_2Ln(THF)]_2[\mu\text{-}\eta^2\text{:}\eta^2\text{-}N_2]$ (A = anionic ligands, Ln = yttrium and lanthanides) complexes from the reduction of LnA_2A' precursors under dinitrogen is believed to proceed through transient Ln^{2+} intermediates.[1-7] This was previously considered as an indication that the rare-earth metals could display Ln^{2+}-like reactivity even when their Ln^{2+} ions had never been isolated before. It was later found that the +2 ions could indeed be isolated based on the reports of the Ln^{2+} complexes, $[K(crypt)][Cp'_3Ln]$ (crypt = 2.2.2-cryptand, $Cp' = C_5H_4SiMe_3$, Ln = Y, lanthanides except Pr).[8-11] However, it was found that these complexes do not readily react with dinitrogen to form dinitrogen complexes. In addition, reduction of the Ln^{3+} precursors, Cp'_3Ln, under dinitrogen without any chelating agents such as crypt or 18-crown-6 did not give the expected $[Cp'_2Ln(THF)]_2[\mu\text{-}\eta^2\text{:}\eta^2\text{-}N_2]$. For yttrium, the reduced dinitrogen complex, $[Cp'_2Y(THF)]_2[\mu\text{-}\eta^2\text{:}\eta^2\text{-}N_2]$, could be generated, but from the reduction of a precursor with a heteroleptic ligand system, $[Cp'_2Y(THF)_2][BPh_4]$.[11] This result could be rationalized since the metal interaction with the anionic $(BPh_4)^{1-}$ is weak. Hence, if reduction formed a $\{[Cp'_2Y(THF)_2][BPh_4]\}^{1-}$ complex, it could readily lose the borate anion to form a highly unstable Y^{2+} species that is very reactive towards dinitrogen reduction.

*Portions of this chapter have been published: Fieser, M. E.; Woen, D. H.; Corbey, J. F.; Mueller, T. J.; Ziller, J. W; Evans, W. J. *Dalton Trans.* **2016**, 45, 14634−14644. DOI: 10.1039/C5DT04547A

A generalization that could be derived from these findings is that systems that could form stable Ln^{2+} complexes do not reduce dinitrogen, whereas systems that do not form stable Ln^{2+} complexes do. Since the reduction of $Cp_3Y(THF)$ (Cp = C_5H_5) and $Cp^{Me}{}_3Y(THF)$ (Cp^{Me} = C_5H_4Me) described in Chapter 1 generated highly unstable Y^{2+} species,[12] it became of interest to determine whether reduced dinitrogen complexes could be obtained from the reduction of these complexes under dinitrogen.

This Chapter describes efforts to obtain new data to evaluate the generalization stated above through the exploration of dinitrogen reduction reactivity with $Cp_3Y(THF)$ and $Cp^{Me}{}_3Y(THF)$. Comparisons of Raman spectroscopic data as well as identification of dinitrogen-based radical species are also described.

Results and Discussion

Reduction under Dinitrogen. The reduction of $Cp^{Me}{}_3Y(THF)$, **1-Y**, using KC_8 in THF under dinitrogen produced a brown-green solution. Removal of the solvent and subsequent removal of a brown material by extraction using toluene gave pale blue colored species that could be crystallized from the toluene solution at −35 °C. X-ray crystallographic analysis of the pale blue crystals revealed that they are the reduced dinitrogen complex, $[Cp^{Me}{}_2Y(THF)]_2(\mu\text{-}\eta^2\text{:}\eta^2\text{-}N_2)$, **2-Y**, Figure 2.1, eq 2.1. This complex crystallizes in the monoclinic space group $P2_1/n$. The complex is a bimetallic complex bridged by an $(N{=}N)^{2-}$ ligand and forms as a neutral species with two cyclopentadienyl ligands and one coordinated THF per metal. The measured N−N distance of 1.250(2) Å is consistent with those of other $(N{=}N)^{2-}$ rare-earth metal dinitrogen complexes that range from 1.088(12)-1.305(6) Å.[5,7]

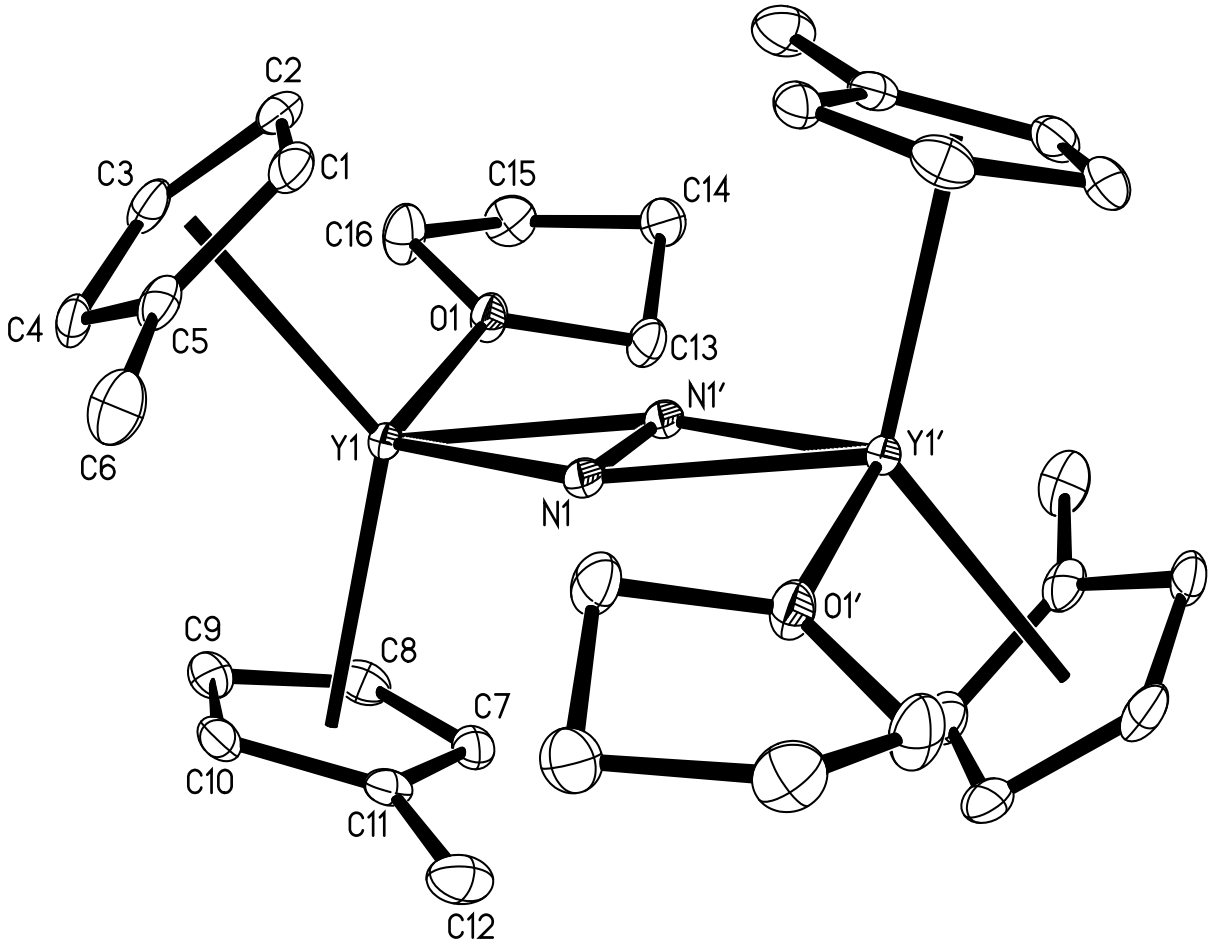

Figure 2.1. Thermal ellipsoid plot of $[Cp^{Me}{}_2Y(THF)]_2(\mu\text{-}\eta^2\text{:}\eta^2\text{-}N_2)$, **2-Y**, drawn at the 50% probability level. Hydrogen atoms are omitted for clarity.

The formation of **2-Y** from the reduction of **1-Y** supports the hypothesis that the use of a system that does not provide stable Ln^{2+} complexes could lead to dinitrogen reduction reactivity. However, no such data could be obtained by studying the $(Cp_3)^{3-}$ ligand system. The reduction of $Cp_3Y(THF)$ under dinitrogen produced a pale-yellow product, but it could not be identified. The lack of characterizable reduced dinitrogen product from this reaction does not necessarily eliminate the formation of a reduced dinitrogen species, but it cannot be used as a valid data to support the formation of a such species either.

Raman Spectroscopy. The use of Raman spectroscopy to probe the degree of activation of diatomic molecules in metal complexes has been widely applied in transition metal chemistry[13-21] since it is a reliable alternative to X-ray crystallography when disorder and vibrational motion prevent accurate determination of bond distances.[16,20] However, application of this technique in dinitrogen rare-earth chemistry[22-26] has been limited due to the high air sensitivity of the reduced dinitrogen complexes. In light of this, a previous Evans group member, Dr. Megan E. Fieser, developed a procedure for collecting Raman data on single crystals of highly air-sensitive rare-earth metal complexes by using a custom-built quartz sample holder fitted with a greaseless high vacuum stopcock that allows the crystals to lay flat in the beam of a Renishaw inVia confocal Raman microscope.[27-28]

Using this technique, Raman spectroscopy was successfully performed to further probe the dinitrogen activation in **2-Y**. The Raman spectrum shows an absorption at 1454 cm^{-1}, Figure 2.2, Table 1.1 (entry 1). The isotopologue, obtained from the reduction of **1-Y** under 1 atm of $^{15}N_2$, provided a new spectrum with a peak at 1404 cm^{-1}, Figure 2.2, which exactly matches the calculated isotopic value. These data confirm that the Raman shift indeed arose from the bridging $(N=N)^{2-}$ moiety and that the $(N=N)^{2-}$ moiety is an activated product from the dinitrogen atmosphere.

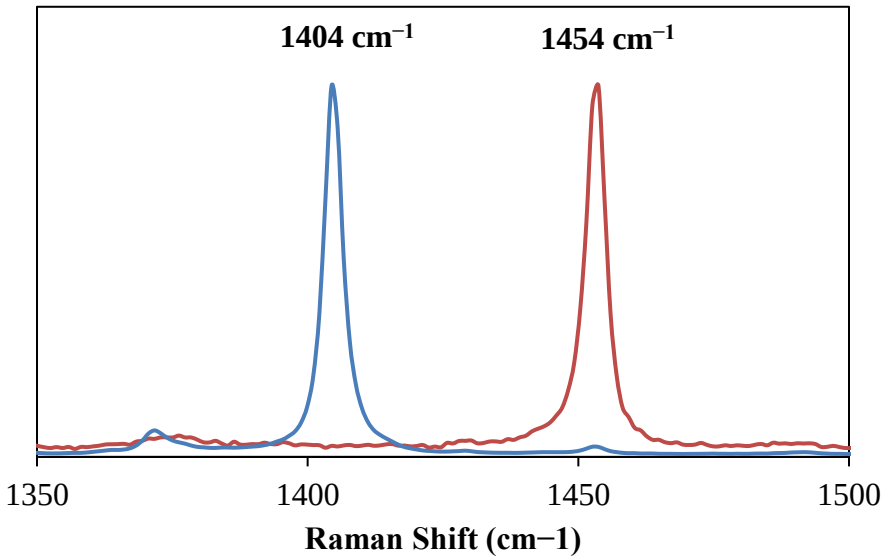

Figure 2.2. Raman spectra of $[Cp^{Me}_2Y(THF)]_2(\mu\text{-}\eta^2\text{:}\eta^2\text{-}N_2)$, **2-Y**, and its ^{15}N isotopologue with $(N{=}N)^{2-}$ Raman shifts at 1454 cm^{-1} and 1404 cm^{-1}, respectively. Peak intensities are normalized to allow clearer comparison.

The 1454 cm^{-1} Raman shift of **2-Y** is higher in energy than that observed from the reduced dinitrogen complex of yttrium with $(C_5Me_5)^{1-}$ as ancillary ligands, $[(C_5Me_5)_2Y]_2(\mu\text{-}\eta^2\text{:}\eta^2\text{-}N_2)$, **3-Y**,[29-30] independently synthesized and analyzed by Dr. Megan E. Fieser, which generates a peak at 1428 cm^{-1}, Table 2.1 (entry 2). This indicates a slightly lower degree of activation in the $(N{=}N)^{2-}$ bridge of **2-Y** compared to that of the latter. This difference could have arisen from the fact that each metal center in **2-Y** is solvated by THF. Another yttrium complex with THF solvation is the reduced dinitrogen complex with $[NR_2]^{1-}$ (R = $SiMe_3$) as ancillary ligands, $[(R_2N)_2Y(THF)]_2(\mu\text{-}\eta^2\text{:}\eta^2\text{-}N_2)$, **4-Y**,[7] which was synthesized by Dr. Jordan F. Corbey and analyzed by Dr. Megan E. Fieser to give a Raman shift of 1422 cm^{-1}, Table 2.1 (entry 3). Again, this indicates a slightly lower degree of activation in the $(N{=}N)^{2-}$ bridge of **2-Y** compared to that of the latter. Since both

complexes are THF solvated, it is possible that the higher degree of activation in the latter is caused by higher donor ability of the $[N(SiMe_3)]^{1-}$ compared to $(Cp^{Me})^{1-}$.

Table 2.1. Crystal structure N–N bond lengths and N–N Raman shifts for $[A_2Y(THF)_x]_2(\mu\text{-}\eta^2\text{:}\eta^2\text{-}N_2)$ (A = Cp^{Me}, C_5Me_5, NR_2; x = 0, 1).

	N–N Raman shift (cm^{-1})	N–N bond length (Å)
1. $[Cp^{Me}_2Y(THF)]_2(\mu\text{-}\eta^2\text{:}\eta^2\text{-}N_2)$, 2-Y	1454	1.250(2)
2. $[(C_5Me_5)_2Y]_2(\mu\text{-}\eta^2\text{:}\eta^2\text{-}N_2)$, 3-Y	1428	1.172(6)[29-30]
3. $[(R_2N)_2Y(THF)]_2(\mu\text{-}\eta^2\text{:}\eta^2\text{-}N_2)$, 4-Y	1422	1.268(3)[7]

The crystal structure N–N bond length of **3-Y** was previously reported to be 1.172(6) Å,[29-30] Table 2.1 (entry 2), which is shorter than the 1.250(2) Å of **2-Y**. This contradicts the deduction based on Raman data that the degree of dinitrogen activation in **3-Y** is higher than that in **2-Y**. Comparison of Raman data obtained by Dr. Megan E. Fieser and the N–N bond lengths of other $[(C_5Me_5)_2Ln]_2(\mu\text{-}\eta^2\text{:}\eta^2\text{-}N_2)$, **3-Ln**, complexes, Table 2.2, can be used to investigate this discrepancy. The 1.2386(5) and 1.238(4) Å N–N bond lengths of **3-Gd** and **3-Tb**, respectively, are noticeably longer than the 1.172(6) Å of **3-Y**, indicating lower activation in the latter. However, the 1432 and 1433 cm^{-1} Raman shifts of **3-Gd** and **3-Tb**, respectively, are higher in energy than the 1428 cm^{-1} of **3-Y**, indicating a contradicting higher activation in the latter. The N–N bond length of **3-Lu** from four different crystal structures varies between 1.111(5)-1.242(11) Å, whereas its Raman data reliably displays a peak at 1406 cm^{-1}. Lastly, the 1.088(12) Å N–N bond length of **3-Sm** is shorter than the 1.098 Å of free inactivated dinitrogen,[31] but the Raman data reliably displays a peak at 1416 cm^{-1}, which is consistent with that of a doubly reduced

dinitrogen. These data of **3-Ln** provide a good example of a scenario where the use of X-ray crystallography fails to generate reliable data that can rather be obtained through Raman spectroscopy. This also explains the discrepancy observed in the comparison between **2-Y** and **3-Y**.

Table 2.2. Crystal structure N–N bond lengths and N–N Raman shifts for $[(C_5Me_5)_2Ln]_2(\mu\text{-}\eta^2\text{:}\eta^2\text{-}N_2)$ (Ln = Y, Sm, Gd, Tb, Lu).

	N–N Raman shift (cm^{-1})	**N–N bond length (Å)**
1. $[(C_5Me_5)_2Y]_2(\mu\text{-}\eta^2\text{:}\eta^2\text{-}N_2)$, 3-Y	1428	1.172(6)
2. $[(C_5Me_5)_2Gd]_2(\mu\text{-}\eta^2\text{:}\eta^2\text{-}N_2)$, 3-Gd	1432	1.236(5)[28]
3. $[(C_5Me_5)_2Tb]_2(\mu\text{-}\eta^2\text{:}\eta^2\text{-}N_2)$, 3-Tb	1433	1.238(4)[28]
4. $[(C_5Me_5)_2Lu]_2(\mu\text{-}\eta^2\text{:}\eta^2\text{-}N_2)$, 3-Lu	1406	1.111(5)-1.242(11)[28]
5. $[(C_5Me_5)_2Sm]_2(\mu\text{-}\eta^2\text{:}\eta^2\text{-}N_2)$, 3-Sm	1416	1.088(12)[31]

Dinitrogen Radical Species. The brown material generated from the reduction of $Cp^{Me}_3Y(THF)$, **1-Y**, using KC_8 in THF under dinitrogen was also analyzed using EPR spectroscopy to reveal a paramagnetic species, **5**, whose EPR spectroscopy data are shown in Figure 2.3. No crystalline solid suitable for X-ray diffraction studies of this species was obtained and interpretation of the multi-line pattern EPR signal was difficult due to peak overlap. Isotope study using $^{15}N_2$ provided a less complex EPR spectrum as shown in Figure 2.3. This spectrum shows a twelve-line pattern, which, based on the simulation of the spectrum, could originate from a radical interacting with three $I = ½$ ^{89}Y nuclei and two $I = ½$ ^{15}N nuclei. Comparable parameters were subsequently used to successfully simulate the spectrum of the ^{14}N isotopologue.

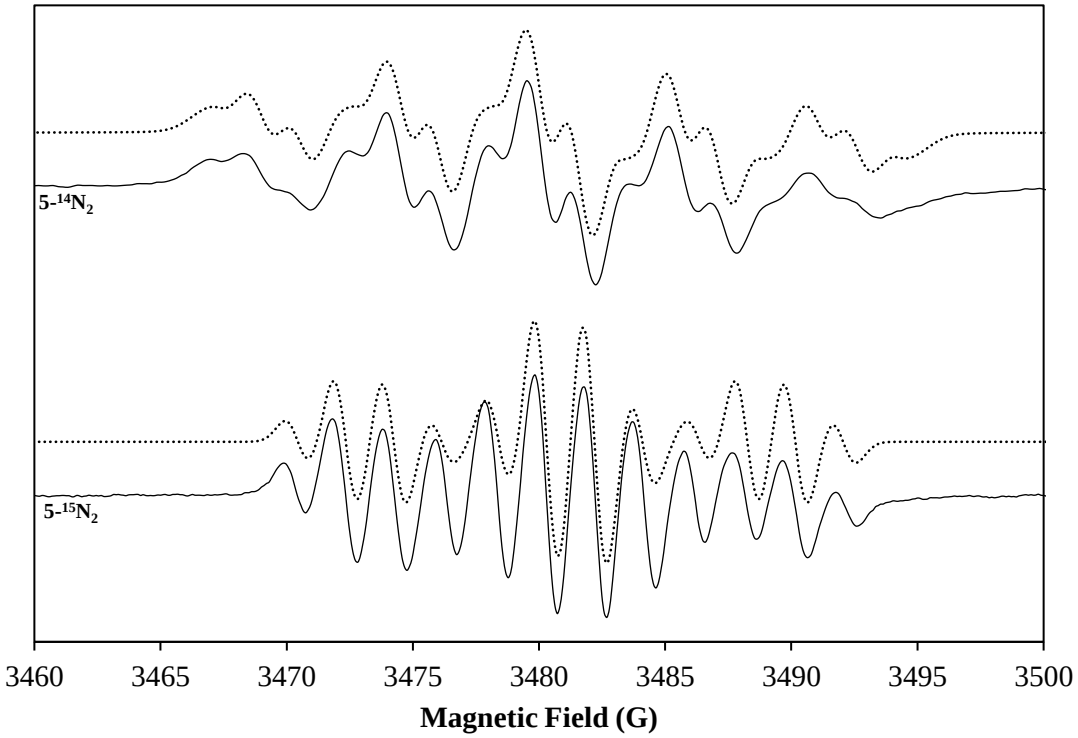

Figure 2.3. X-band EPR spectra of **5-$^{14}N_2$** (top) and **5-$^{15}N_2$** (bottom) collected at 298 K. Simulated spectra are shown as dotted lines. Simulated parameters: g_{iso} = 2.005, $A_{iso}(^{14}N)$ = 5.5 G, $A_{iso}(^{15}N)$ = 8.0 G, $A_{iso}(^{89}Y)$ = 1.7 G (**5-$^{14}N_2$**) and 1.9 G **(5-$^{15}N_2$)**.

The g-values and the simulated hyperfine coupling constants of both spectra are very similar to those of the previously reported and crystallographically-characterized $\{K(THF)_6\}\{[(R_2N)_2Y(THF)]_2(\mu\text{-}\eta^2\text{:}\eta^2\text{-}N_2)\}$, **6-K(THF)$_6$**,[32-33] and $\{[(R_2N)_2Y(THF)]_2(\mu\text{-}\eta^2\text{:}\eta^2\text{-}N_2)\}$, **6-K**, Figure 2.4.[22] The comparisons of their simulated parameters are summarized in Table 1.3. The simulated $A_{iso}(^{89}Y)$ = 1.7-1.9 G of **5** is slightly smaller than the $A_{iso}(^{89}Y)$ = 3.1 of **6-K(THF)$_6$**, but this is reasonable considering that the predicted radical interaction in **5** is shared between three yttrium centers rather than two as in **6-K(THF)$_6$**. Consistently, the simulated $A_{iso}(^{15}N)$ = 8.0 G and $A_{iso}(^{14}N)$ = 5.5 G of **6-K(THF)$_6$** are slightly smaller than the $A_{iso}(^{15}N)$ = 8.2

G and $A_{iso}(^{14}N)$ = 5.8 G of **6-K(THF)$_6$**, and this can be reasoned by the fact that the predicted radical in **4-Y** is delocalized around a five-atom core instead of a four-atom core as in **6-K(THF)$_6$**.

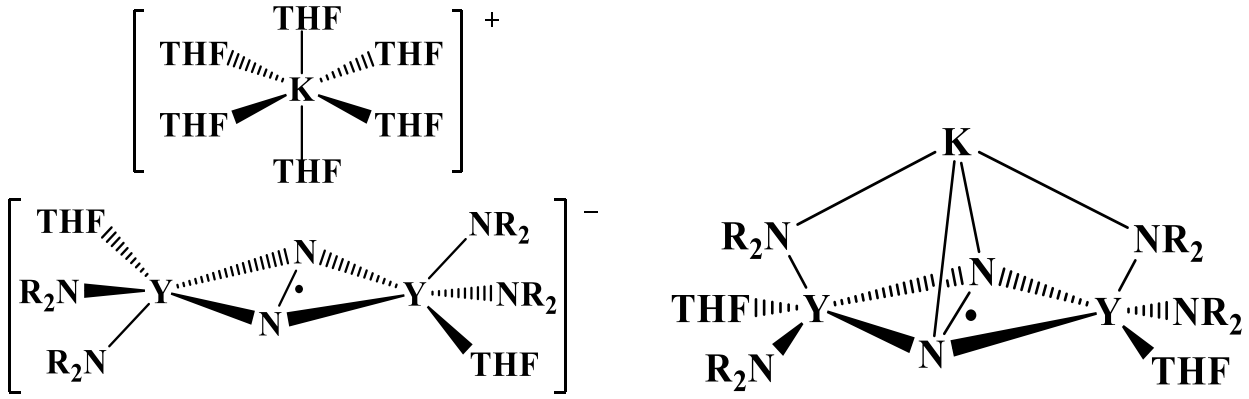

Figure 2.4. Diagram representations of the previously crystallographically-characterized complexes, $\{K(THF)_6\}\{[(R_2N)_2Y(THF)]_2(\mu\text{-}\eta^2\text{:}\eta^2\text{-}N_2)\}$, **6-K(THF)$_6$**, (left) and $\{[(R_2N)_2Y(THF)]_2(\mu\text{-}\eta^2\text{:}\eta^2\text{-}N_2)\}$, **6-K** (right).[22]

Table 1.3. Simulated EPR parameters of **5**, **6-K(THF)$_6$**, and **6-K**.[22,32-33]

	5	**6-K(THF)$_6$**	**6-K**
g_{iso}	2.005	2.0038	2.0038
$A_{iso}(^{14}N)$	5.5 G	5.8 G	5.8 G
$A_{iso}(^{15}N)$	8.0 G	8.2 G	8.2 G
$A_{iso}(^{89}Y)$	1.9-1.7 G	3.1 G	3.1 G
$A_{iso}(^{39}K)$	n/a	n/a	0.44 G
Radical core	"Y_3N_2" (predicted)	Y_2N_2 (confirmed)	Y_2N_2K (confirmed)

Based on the data above, it is possible that the paramagnetic species, **5**, is a "Y_3N_2" radical species with a formula of $\{(Cp^{Me}{}_2Y)_3(\mu\text{-}\eta^3\text{:}\eta^3\text{-}N_2)\}$, Figure 2.5. This proposed species is not unreasonable considering that radical delocalization over a five-atom core is also observed in the crystallographically characterized $\{[(R_2N)_2Y(THF)]_2(\mu\text{-}\eta^2\text{:}\eta^2\text{-}N_2)\}$, **6-K**, Figure 2.4.[22] One can imagine that if the potassium atom in **6-K** is replaced by an yttrium atom, the resulting structure would display a "Y_3N_2" core resembling the proposed five-atom core for **5**. Another similar example was reported by Chirik et. al. from the reduction of $(C_5H_3Me_2)TiI$ using KC_8 under dinitrogen, which although not reproducible, formed a trimetallic titanium complex with a reduced dinitrogen center, shown in Figure 2.5.[34] In this case, the dinitrogen bridge is bound side-on to one metal center and end-on to the other two metal centers. This could also be the case for **5**.

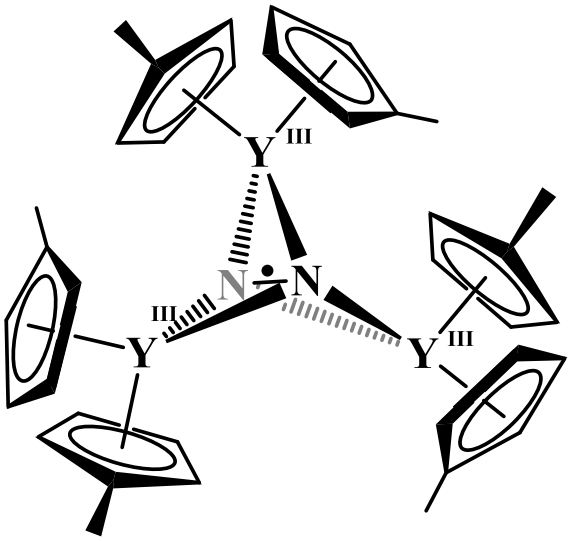

Figure 2.5. Diagram representation of the postulated structure of the radical species from the reduction of $Cp^{Me}{}_3Y(THF)$, **5**.

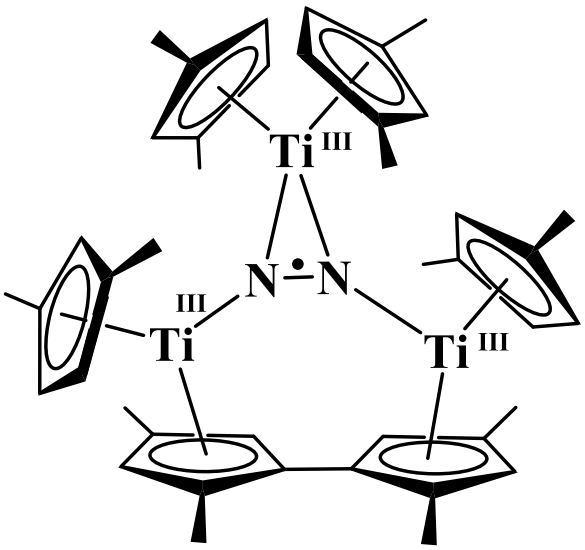

Figure 2.6. Diagram representation of the crystallographically-characterized complex of a trimetallic titanium complex reported by Chirik and et. al.[34]

It was previously reported that placement of a $Nd_2Fe_{14}B$ magnet on the outside of a crystallization vial may facilitate crystal formation of highly paramagnetic complexes.[35] In further attempts to obtain structural insights for the paramagnetic species, **5**, the analogous species was prepared with dysprosium as the rare-earth metal, since Dy^{3+} is highly paramagnetic (S = 5/2, L = 5, J = 15/2) and could be a good alternative for yttrium since both are similar in size.[36]

The reduction of $(C_5H_4Me)_3Dy(THF)$, **1-Dy**, using KC_8 in THF under dinitrogen also produced a brown-green solution. Unfortunately, attempts to obtain crystalline solid of the brown material for X-ray crystallography using a $Nd_2Fe_{14}B$ magnet were still unsuccessful. Nonetheless, removal of the solvent and subsequent extraction using toluene gave pale blue colored species that could be crystallized from the toluene solution at −35 °C and identified by X-ray crystallography as the dysprosium analog of **2-Y**, $[Cp^{Me}_2Y(THF)]_2(\mu\text{-}\eta^2\text{:}\eta^2\text{-}N_2)$, **2-Dy**, Figure 2.7, with a very similar 1.250(4) Å N−N distance consistent with an $(N{=}N)^{2-}$ bridge.

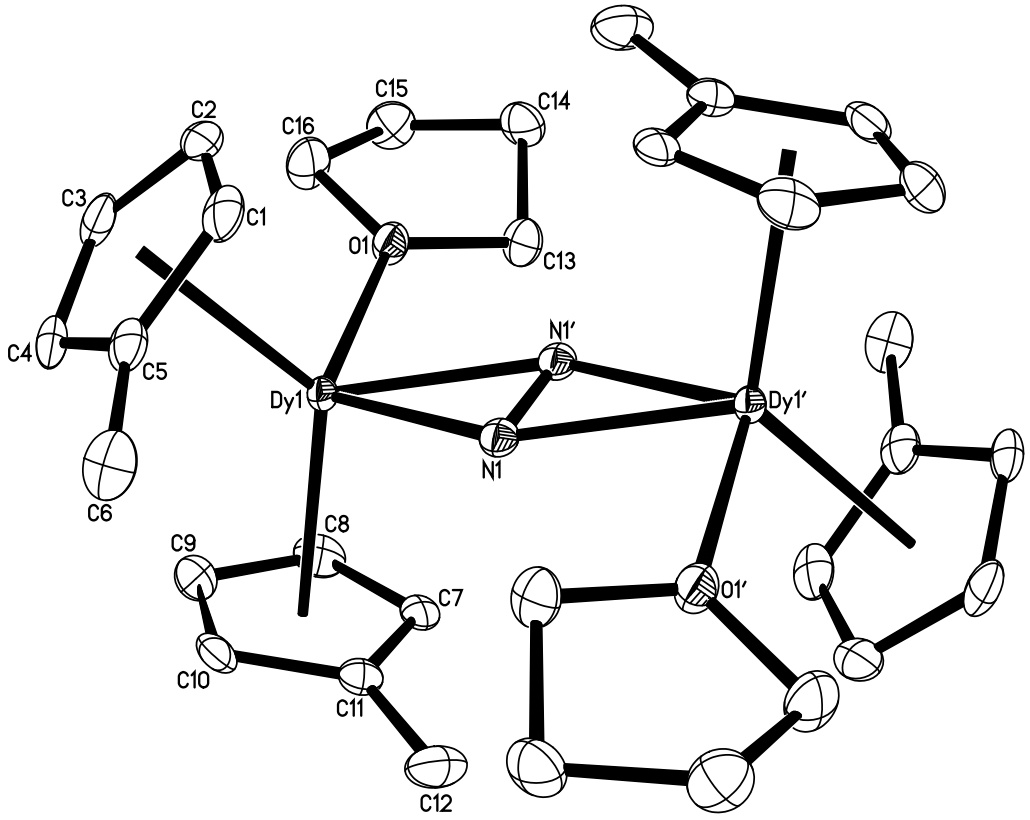

Figure 2.7. Thermal ellipsoid plot of $[Cp^{Me}_2Dy(THF)]_2(\mu\text{-}\eta^2\text{:}\eta^2\text{-}N_2)$, **2-Dy**, drawn at the 50% probability level. Hydrogen atoms are omitted for clarity.

The crystals of **2-Dy** were also analyzed using Raman spectroscopy, which consistently gave a peak at 1453 cm^{-1}, Figure 2.8. This Raman shift is very similar to the 1454 cm^{-1} of **2-Y**, which was as expected since dysprosium and yttrium are similar in size[36] and almost equally electropositive. Comparing the 1453 cm^{-1} Raman shift of **2-Dy** with the 1454 cm^{-1} Raman shift of another reduced dinitrogen complex with $(C_5Me_4H)^{1-}$ as ancillary ligands, $[Cp^{tet}_2Y(THF)]_2(\mu\text{-}\eta^2\text{:}\eta^2\text{-}N_2)$ ($Cp^{tet} = C_5Me_4H$),[28] which was measured by Dr. Megan E. Fieser, it appears that the additional methyl substituents on the cyclopentadienyl ligands did not result in a significant difference in dinitrogen activation.

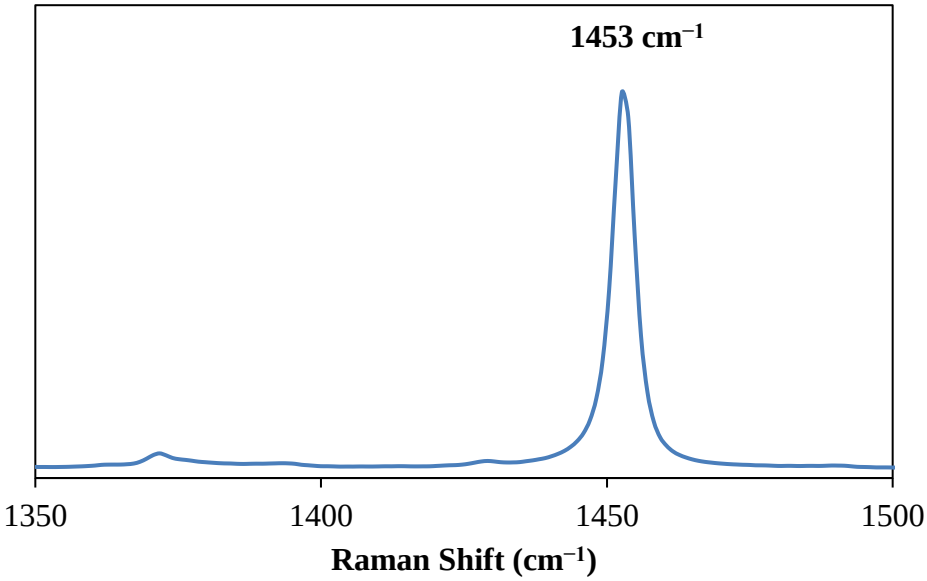

Figure 2.8. Raman spectrum of $[Cp^{Me}_2Dy(THF)]_2(\mu\text{-}\eta^2\text{:}\eta^2\text{-}N_2)$, **2-Dy** with $(N=N)^{2-}$ Raman shift at 1453 cm^{-1}.

Exposure of Dinitrogen to Freshly Generated Y^{2+}. In contrast to the reduction of $Cp^{Me}_3Y(THF)$ under dinitrogen, the exposure of dinitrogen to a freshly generated solution of the Y^{2+} species from the reduction of $Cp^{Me}_3Y(THF)$ with crypt using KC_8 in THF under argon at −78 °C, did not produce the $(N=N)^{2-}$ complex, $[Cp^{Me}_2Y(THF)]_2(\mu\text{-}\eta^2\text{:}\eta^2\text{-}N_2)$, **2-Y**, as determined by ^1H NMR spectroscopy. However, a color change from deep dark brown to orange-brown was observed to give an EPR active product, **7**, whose EPR spectrum is shown in Figure 2.9. This spectrum is different than that observed from the direct reduction of $Cp^{Me}_3Y(THF)$ under dinitrogen, **6-K**, Figure 2.3, described above.

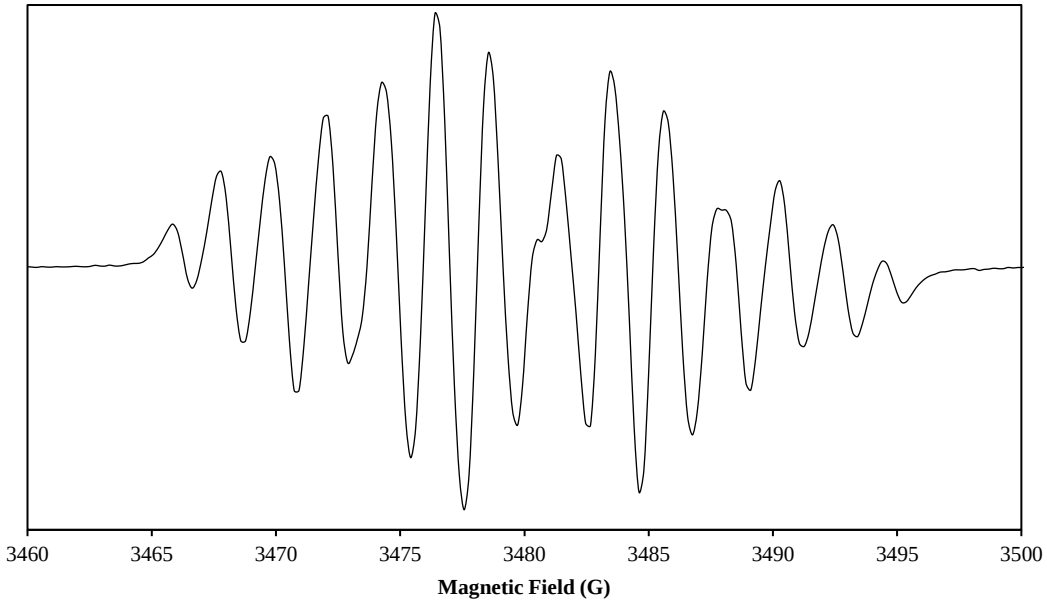

Figure 2.9. X-band EPR spectrum of the brown solution from the exposure of dinitrogen to a freshly generated solution of Y^{2+} species from the reduction of $Cp^{Me}_3Y(THF)$ with crypt using KC_8 in THF under argon −45 °C, **7**. The spectrum was collected at room temperature.

Simulation of the EPR spectrum of **7** was not successful due to the irregularity present in the spectrum between 3479 and 3482 G or around g = 2.001, which might have arisen from an electride species described in Chapter 1. However, this spectrum is similar to the yellow-orange solution obtained and analyzed by a previous Evans group member, Dr. Matthew R. Macdonald,[37] from the exposure of dinitrogen to the Y^{2+} complex, [K(crown)][Cp'_3Y] (crown = 18-crown-6), Figure 2.10. The spectrum shows an isotropic 16-line hyperfine pattern centered at g_{iso} = 2.005, and simulation parameters that best fit this spectrum suggest a radical delocalization within a three-nitrogen and three-yttrium atom core, "Y_3N_3". Unfortunately, no structural data could be obtained to definitively identify such species. This was also the case for **7**.

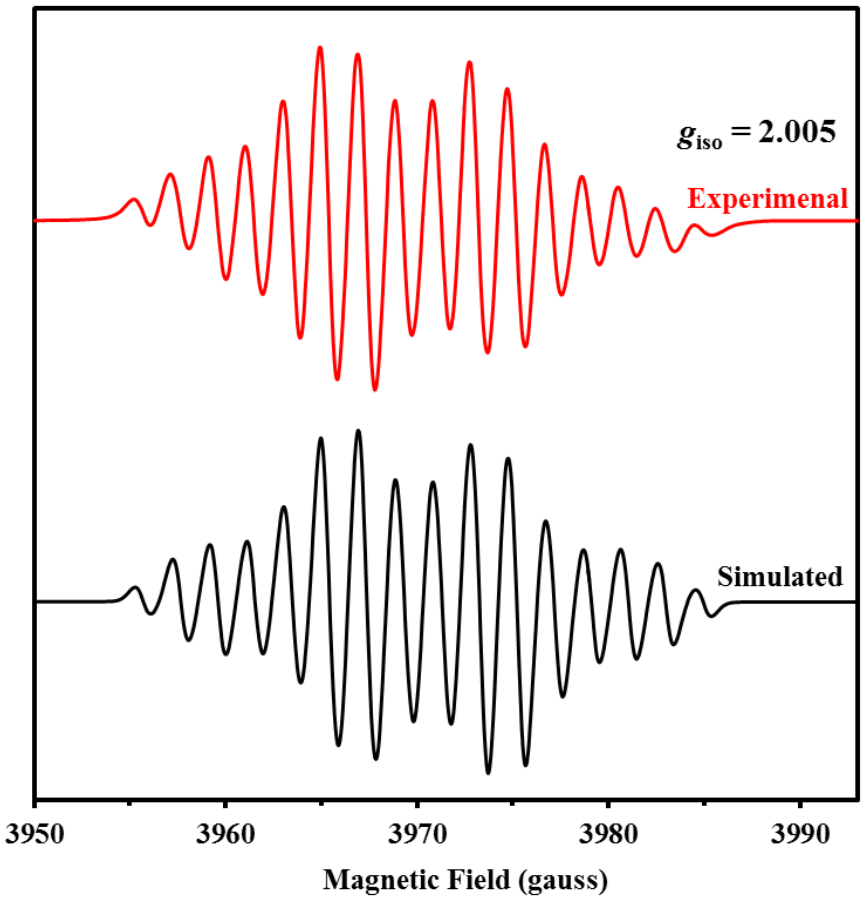

Figure 2.10. X-band EPR spectrum of the yellow-orange species produced in the reaction of [K(crown)][Cp′$_3$Y], with dinitrogen in Et_2O at −45 °C.[37]

Conclusion

The reduction of $Cp^{Me}_3Ln(THF)$ (Ln = Y, Dy), **1-Ln**, under dinitrogen produced pale-blue colored reduced dinitrogen complexes, $[Cp^{Me}_2Ln(THF)]_2(\mu\text{-}\eta^2\text{:}\eta^2\text{-}N_2)$, **2-Ln**, as characterized by X-ray crystallography and Raman spectroscopy. Both the crystal N−N distances and the Raman shifts indicate that the dinitrogen moieties in these complexes are the typical $(N{=}N)^{2-}$ bridging ligands found in other rare-earth metal dinitrogen complexes. Since it was found that the reduction of $Cp^{Me}_3Ln(THF)$ does not produce stable Ln^{2+} complexes, the isolation of **2-Ln** supports the generalization that systems that do not form stable Ln^{2+} complexes can form $(N{=}N)^{2-}$ complexes.

Besides the $(N=N)^{2-}$ complexes, the reduction of **1-Ln** under dinitrogen also generates brown byproducts, which were postulated to be radical-containing species. The EPR spectrum of the yttrium radical species was simulated using parameters consisting of a radical delocalized within a five-atom core, "Y_3N_2". In contrast, the exposure of dinitrogen to the Y^{2+} species from the reduction of $Cp^{Me}_3Y(THF)$ gave a product with a different EPR spectrum. Unfortunately, identification of any of these radical species was not successful.

Experimental

All manipulations and syntheses described below were conducted with the rigorous exclusion of air and water using standard Schlenk line and glovebox techniques under an argon or dinitrogen atmosphere. Solvents were sparged with UHP argon and dried by passage through columns containing Q-5 and molecular sieves prior to use. 2.2.2-Cryptand (crypt) was purchased from Merck and placed under vacuum (10^{-3} Torr) for 12 h before use. $^{15}N_2$ was purchased from Aldrich and used without further purification. The $Nd_2Fe_{14}B$ magnets used in the crystallizations were obtained from United Nuclear Scientific Equipment and Supplies. Deuterated NMR solvents were dried over NaK alloy, degassed by three freeze-pump-thaw cycles, and vacuum transferred before use. KC_8,[38] $Cp^{Me}_3Y(THF)$ (Cp^{Me} = C_5H_4Me), **1-Y**,[12] and $Cp_3Y(THF)$[39] were prepared according to the literature. ^1H NMR spectra were recorded on Bruker GN500 or CRYO500 MHz spectrometers (^{13}C NMR at 125 MHz) at 298 K unless otherwise stated and referenced internally to residual protio-solvent resonances. IR samples were prepared as KBr pellets on a Varian 1000 FT-IR system. Raman data were obtained from single crystals of samples in a custom-built quartz sample holder on a Renishaw inVia confocal Raman microscope. Elemental analyses were conducted on a Perkin-Elmer 2400 Series II CHNS elemental analyzer. Electron Paramagnetic

Resonance spectra were collected using X-band frequency (9.3 – 9.8 GHz) on a Bruker EMX spectrometer equipped with an ER041XG microwave bridge, and the magnetic field was calibrated with DPPH (g = 2.0036). EPR simulations were performed using P.E.S.T. WinSim developed by the National Institutes of Environmental Health Sciences or Easyspin.[40]

$Cp^{Me}_3Dy(THF)$, 1-Dy. Following a previously described procedure in Chapter 1 for $Cp^{Me}_3Y(THF)$,[30] a pale yellow THF (5 mL) solution of KCp^{Me} (500 mg, 4.23 mmol) was added to a THF (5 mL) slurry of $DyCl_3$ (379 mg, 1.41 mmol) and the cloudy yellow mixture was allowed to stir overnight. Pale yellow insoluble material was removed via centrifugation, and the yellow supernatant was filtered, dried under reduced pressure, and extracted using toluene. The extract was filtered and solvent was removed under reduced pressure to yield $Cp^{Me}_3Dy(THF)$ (279 mg, 78%) as a yellow powder. Colorless crystals were grown from toluene/hexane at −35 °C with a $Nd_2Fe_{14}B$ magnet attached to the outside of a scintillation vial. IR: 3086m, 2923s, 2862s, 2730w, 1623w, 1489w, 1454m, 1379w, 1339w, 1237w, 1164w, 1032s, 1011s, 932m, 830s, 769s, 613w cm^{-1}. Anal. Calcd for $C_{18}H_{21}Dy(OC_4H_8)_{0.3}$: C, 54.71; H, 5.60. Found: C, 54.69; H, 5.95.

$[Cp^{Me}_2Y(THF)]_2(\mu\text{-}\eta^2\text{:}\eta^2\text{-}N_2)$, 2-Y and its EPR active byproduct, 5-$^{14}N_2$. In a dinitrogen-filled glovebox, KC_8 (103 mg, 0.763 mmol) was tapped into a stirred THF (10 mL) solution of $Cp^{Me}_3Y(THF)$ (304 mg, 0.763 mmol). The mixture was allowed to stir for 2 h and then filtered to leave a brown-green solution. The solvent was removed under reduced pressure to produce green-yellow tacky solids which were extracted using toluene and then filtered to give a pale blue solution. Blue crystals of **2-Y** suitable for X-Ray diffraction were grown from the toluene solution at −35 °C (54 mg, 15%). ^{1}H NMR (C_6D_6): δ 5.73 (s, C_5H_4Me, 16H), 3.11 (m, C_4H_8O, 8H), 2.30 (s, C_5H_4Me, 12H), 1.39 (m, C_4H_8O, 8H). ^{1}H NMR (THF-d_8): δ 5.46 (m, C_5H_4Me, 8H), 5.39 (m, C_5H_4Me, 8H), 3.61 (m, C_4H_8O, 8H), 2.12 (s, C_5H_4Me, 12 H), 1.76 (m, C_4H_8O, 8H). ^{13}C

NMR (C_6D_6): δ 14.9 (C_5H_4*Me*), 25.4 (*C*$_4H_8O$), 72.1 (*C*$_4H_8O$), 109.1 (*C*$_5H_4$Me), 119.4 (*C*$_5H_4$Me). Raman N–N stretch: 1454 cm^{-1}. Anal. Calcd for $C_{32}H_{44}N_2O_2Y_2$: C, 57.66; H, 6.65; N, 4.20. Found: C, 57.79; H, 6.81; N, 4.00. The toluene insoluble material was washed with Et_2O to remove KCp^{Me} residue as well as other unidentified byproducts and then dissolved in THF to yield a brown EPR active solution, **5-$^{14}N_2$**.

Isotopologues of the species above, 2-Y($^{15}N_2$) and 5-$^{15}N_2$. The reaction was performed in a Schlenk flask equipped with an isolated side arm. In an argon-filled glovebox, KC_8 (60 mg, 0.44 mmol) was stored in the side arm of the flask and a THF (10 mL) solution of $Cp^{Me}_3Y(THF)$ (207 mg, 0.520 mmol) was placed at the bottom of the flask. The flask was brought out of the glovebox and connected to a Schlenk line. The THF solution was degassed by three freeze-pump-thaw cycles before $^{15}N_2$ was charged into the flask and KC_8 was tapped into the solution while stirred. The resulting black mixture was allowed to stir for one hour, transferred into a glovebox and filtered to yield a dark green solution, which was dried under reduced pressure to yield green tacky solids. The solids were washed with Et_2O and redissolved in THF to yield an orange EPR active solution, **5-$^{15}N_2$**. The Et_2O wash was left at −78 °C. Pale blue crystals of **2-Y($^{15}N_2$)** suitable for X-ray diffraction were grown from the Et_2O solution after several days. Raman N–N stretch: 1404 cm^{-1}.

[Cp$^{Me}_2$Dy(THF)]$_2$(μ-η^2:η^2-N$_2$), 2-Dy. In a nitrogen glovebox, KC_8 (37 mg, 0.275 mmol) was tapped into a stirred THF (10 mL) solution of $Cp^{Me}_3Dy(THF)$ (130 mg, 0.27 mmol). The mixture was stirred for 2 h and then filtered to leave a brown-green solution. The solvent was removed under reduced pressure to produce dark brown-green tacky solids that were extracted using toluene and filtered to give a green solution. Green crystals of **3-Dy** suitable for X-ray diffraction were grown from the toluene solution at −35 °C (21 mg, 19%).

EPR active product from the reaction of N_2 and the isolated $[Cp^{Me}{}_3Y]^-$, 7. In an argon-filled glovebox, one side of an H-tube flask was charged with 10 mL of THF, and the other side with $Cp^{Me}{}_3Y(THF)$ (71 mg, 0.22 mmol), cyrpt (82 mg, 0.22 mmol), KC_8 (35 mg, 0.26 mmol), and a stir bar. The H-tube flask was brought outside of the glovebox, connected to a Schlenk line, and evacuated to the solvent vapor pressure. Both sides of the H-tube flask were cooled to −78 °C, and then the THF was transferred onto the solid mixture while stirring. The solution was warmed up slightly until the mixture turned deep purple. Then, 1 atm of N_2 gas was added to the flask. The mixture was allowed to stir for 30 minutes and then filtered to the other side of the H-tube flask to yield a brown solution. The flask was brought into a nitrogen-filled glovebox, and the solution was filtered, concentrated to ~3 mL, and used for EPR measurement, **7**, Figure 2.9. The remaining solution was dried to a pale brown tacky solid. Multiple extractions with Et_2O yielded an faint yellow solution unidentifiable by ^1H NMR spectroscopy, confirming the absence of $[Cp^{Me}{}_2Y(THF)]_2(\mu\text{-}\eta^2\text{:}\eta^2\text{-}N_2)$, **2-Y**.

X-ray Data Collection, Structure Solution and Refinement for $[Cp^{Me}{}_2Y(THF)]_2(\mu\text{-}\eta^2\text{:}\eta^2\text{-}N_2)$, 2-Y. A blue crystal of approximate dimensions 0.148 x 0.184 x 0.273 mm was mounted on a glass fiber and transferred to a Bruker SMART APEX II diffractometer. The APEX2[41] program package was used to determine the unit-cell parameters and for data collection (15 sec/frame scan time for a sphere of diffraction data). The raw frame data was processed using SAINT[42] and SADABS[43] to yield the reflection data file. Subsequent calculations were carried out using the SHELXTL[44] program. The diffraction symmetry was 2/*m* and the systematic absences were consistent with the monoclinic space group $P2_1/n$ that was later determined to be correct. The structure was solved by direct methods and refined on F^2 by full-matrix least-squares techniques. The analytical scattering factors[45] for neutral atoms were used throughout the analysis.

Hydrogen atoms were located from a difference-Fourier map and refined (x,y,z and U_{iso}). The molecule was located about an inversion center. At convergence, wR2 = 0.0453 and Goof = 1.034 for 260 variables refined against 3825 data (0.73Å), R1 = 0.0193 for those 3517 data with I > 2.0σ(I).

X-ray Data Collection, Structure Solution and Refinement for $[Cp^{Me}_2Dy(THF)]_2(\mu\text{-}\eta^2\text{:}\eta^2\text{-}N_2)$, 2-Dy. A green crystal of approximate dimensions 0.169 x 0.199 x 0.265 mm was mounted on a glass fiber and transferred to a Bruker SMART APEX II diffractometer. The APEX2[41] program package and the CELL_NOW[46] were used to determine the unit-cell parameters. Data was collected using a 10 sec/frame scan time for a sphere of diffraction data. The raw frame data was processed using SAINT[42] and TWINABS[47] to yield the reflection data file (HKLF 5 format)[47]. Subsequent calculations were carried out using the SHELXTL[44] program. The diffraction symmetry was 2/*m* and the systematic absences were consistent with the monoclinic space group $P2_1/n$ that was later determined to be correct. The structure was solved by direct methods and refined on F^2 by full-matrix least-squares techniques. The analytical scattering factors[45] for neutral atoms were used throughout the analysis. Hydrogen atoms were included using a riding model. The molecule was located about an inversion center (Z = 2). At convergence, wR2 = 0.0403 and Goof = 1.036 for 175 variables refined against 3608 data (0.74Å), R1 = 0.0164 for those 3406 with I > 2.0σ(I). The structure was refined as a two-component twin, $BASF^5$ = 0.4066.

References

(1) Evans, W. J.; Allen, N. T.; Ziller, J. W. *J. Am. Chem. Soc.* **2001**, *123*, 7927-7928.

(2) Evans, W. J.; Allen, N. T.; Ziller, J. W. *Angew. Chem., Int. Ed.* **2002**, *41*, 359-361.

(3) Evans, W. J.; Lee, D. S. *Can. J. Chem.* **2005**, *83*, 375-384.

(4) Evans, W. J.; Lee, D. S.; Johnston, M. A.; Ziller, J. W. *Organometallics* **2005**, *24*, 6393-6397.

(5) Evans, W. J.; Lee, D. S.; Rego, D. B.; Perotti, J. M.; Kozimor, S. A.; Moore, E. K.; Ziller, J. W. *J. Am. Chem. Soc.* **2004**, *126*, 14574-14582.

(6) Evans, W. J.; Lee, D. S.; Lie, C.; Ziller, J. W. *Angew. Chem., Int. Ed.* **2004**, *43*, 5517-5519.

(7) Evans, W. J.; Lee, D. S.; Ziller, J. W. *J. Am. Chem. Soc.* **2004**, *126*, 454-455.

(8) MacDonald, M. R.; Bates, J. E.; Ziller, J. W.; Furche, F.; Evans, W. J. *J. Am. Chem. Soc.* **2013**, *135*, 9857-9868.

(9) MacDonald, M. R.; Bates, J. E.; Fieser, M. E.; Ziller, J. W.; Furche, F.; Evans, W. J. *J. Am. Chem. Soc.* **2012**, *134*, 8420-8423.

(10) Fieser, M. E.; MacDonald, M. R.; Krull, B. T.; Bates, J. E.; Ziller, J. W.; Furche, F.; Evans, W. J. *J. Am. Chem. Soc.* **2015**, *137*, 369-382.

(11) MacDonald, M. R.; Ziller, J. W.; Evans, W. J. *J. Am. Chem. Soc.* **2011**, *133*, 15914-15917.

(12) Corbey, J. F.; Woen, D. H.; Palumbo, C. T.; Ziller, J. W.; Evans, W. J. *Organometallics* **2015**, *34*, 3909-3921.

(13) Bazhenova, T. A.; Shilov, A. E. *Chem. Rev.* **1995**, *144*, 69-145.

(14) Hidai, M.; Mizobe, Y. *Chem. Rev.* **1995**, *95*, 1115-1133.

(15) Fryzuk, M. D.; Johnson, S. A. *Coord. Chem. Rev.* **2000**, *200-202*, 379-409.

(16) Cramer, C. J.; Tolman, W. B.; Theopold, K. H.; Rheingold, A. L. *Proc. Natl. Acad. Sci. U.S.A.* **2000**, *100*, 3635-3640.

(17) Shaver, M. P.; Fryzuk, M. D. *Adv. Synth. Catal.* **2003**, *345*, 1061-1076 and references therein.

(18) Gambarotta, S.; Scott, J. *Angew. Chem. Int. Ed.* **2004**, *43*, 5298-5308.

(19) MacKay, B. A.; Fryzuk, M. D. *Chem. Rev.* **2004**, *104*, 385-402 and references therein.

(20) Holland, P. L. *Dalton Trans.* **2010**, *39*, 5415-5425.

(21) Studt, F.; Morello, L.; Lehnert, N.; Fryzuk, M. D.; Tuczek, F. *Chem. Eur. J.* **2003**, *9*, 520-530.

(22) Evans, W. J.; Fang, M.; Zucchi, G.; Furche, F.; Ziller, J. W.; Hoekstra, R. M.; Zink, J. I. *J. Am. Chem. Soc.* **2009**, *131*, 11195–11202.

(23) Jaroschik, F.; Momin, A.; Nief, F.; Goff, X.-F. L.; Deacon, G. B.; Junk, P. C. *Angew. Chem., Int. Ed.* **2009**, *48*, 1117-1121.

(24) Mansell, S. M.; Kaltsoyannis, N.; Arnold, P. L. *J. Am. Chem. Soc.* **2011**, *133*, 9036-9051.

(25) Fang, M.; Farnaby, J. H.; Ziller, J. W.; Bates, J. E.; Furche, F.; Evans, W. J. *J. Am. Chem. Soc.* **2012**, *134*, 6064-6067.

(26) Mansell, S. M.; Farnaby, J. H.; Germeroth, A. I.; Arnold, P. L. *Organometallics* **2013**, *32*, 4214-4222.

(27) Fieser, M. E. *D. Phil.*, University of California, Irvine, 2015.

(28) Fieser, M. E.; Woen, D. H.; Corbey, J. F.; Mueller, T. J.; Ziller, J. W.; Evans, W. J. *Dalton Trans.* **2016**, *45*, 14634-14644.

(29) Schmiege, B. M.; Ziller, J. W.; Evans, W. J. *Inorg. Chem.* **2010**, *49*, 10506-10511.

(30) Mueller, T. J.; Fieser, M. E.; Ziller, J. W.; Evans, W. J. *Chem. Sci.* **2011**, *2*, 1992-1996.

(31) Evans, W. J.; Ulibarri, T. A.; Ziller, J. W. *J. Am. Chem. Soc.* **1988**, *110*, 6877-6879.

(32) Fang, M.; Bates, J. E.; Lorenz, S. E.; Lee, D. S.; Rego, D. B.; Ziller, J. W.; Furche, F.; Evans, W. J. *Inorg. Chem.* **2011**, *50*, 1459–1469.

(33) Fang, M.; Lee, D. S.; Ziller, J. W.; Doedens, R. J.; Bates, J. E.; Furche, F.; Evans, W. J. *J. Am. Chem. Soc.* **2011**, *133*, 3784-3787.

(34) Semproni, S. P.; Milsmann, C.; Chirik, P. J. *Organometallics* **2012**, *31*, 3672-3682.

(35) Meihaus, K. R.; Corbey, J. F.; Fang, M.; Ziller, J. W.; Long, J. R.; Evans, W. J. *Inorg. Chem.* **2014**, *53*, 3099-3107.

(36) Shannon, R. *Acta Crystallog., Sect. A* **1976**, *32*, 751-767.

(37) MacDonald, M. R. *Dissertation*, University of California, Irvine, 2013.

(38) Bergbreiter, D. E.; Killough, J. M. *J. Am. Chem. Soc.* **1978**, *100*, 2126-2134.

(39) Rogers, R. D.; Atwood, J. L.; Emad, A.; Sikora, D. J.; Rausch, M. D. *J. Organomet. Chem.* **1981**, *216*, 382-392.

(40) Stoll, S.; Schweiger, A. *J. Magn. Reson.* **2006**, *178*, 42-55.

(41) Bruker AXS, Inc., APEX2 Version 2014.11-0, Madison, WI, **2014**.

(42) Bruker AXS, Inc., SAINT Version 8.34a, Madison, WI, **2013**.

(43) Sheldrick, G. M.; SADABS, Version 2014/5, Bruker AXS, Inc., Madison, WI, **2014**.

(44) Sheldrick, G. M.; SHELXTL, Version 2014/7, Bruker AXS, Inc., Madison, WI, **2014**.

(45) *International Tables for Crystallography, Vol. C*, Kluwer Academic Publishers, Dordrecht, **1992**.

(46) Sheldrick, G. M.; CELL_NOW, Version 2008/4, Bruker AXS, Inc., Madison, WI, **2008**.

(47) Sheldrick, G. M.; TWINABS, Version 2012/1, Bruker AXS, Inc., Madison, WI, **2012**.

CHAPTER 3

Synthesis and Reactivity of +2 Ion Rare-Earth Metal Complexes with $(C_5Me_4H)^{1-}$ Ligands

Introduction

As described in Chapter 1, unlike the tris(monosilylcyclopentadienyl) ligand set, $(Cp'_3)^{3-}$,[1-4] the use of the tris(monomethylcyclopentadienyl) ligand set, $(Cp^{Me}_3)^{3-}$ ($Cp^{Me} = C_5H_4Me$), did not provide stable +2 ion rare-earth metal complexes. More specifically, the reduction of $Cp^{Me}_3Ln(THF)$ (Ln = La, Pr, Gd, Y) gave dark colored solutions with EPR spectra for Gd and Y that were consistent with Ln^{2+} species, presumably $[Cp^{Me}_3Ln]^{1-}$, that these reduction products were too reactive to isolate. Reactivity and decomposition studies of $[Cp^{Me}_3Ln]^{1-}$ suggested that the $(Cp^{Me}_3)^{3-}$ ligand environment was sterically under-saturated and provided an open coordination site that led to the observed high reactivity and low stability. In addition, it was reasoned, based on the EPR data and previous literature reports, that the alkyl substituents on the cyclopentadienyl ligands render these ligands more electron donating and unsuitable for stabilizing low oxidation states. Therefore, the isolation of stable "non-traditional" +2 ion complexes was postulated to depend both on steric and electron donor ability effects.

In efforts to further evaluate this postulation, it became of interest to explore the use of a ligand system comprised of bulkier cyclopentadienyl ligands. For this investigation, the tris(tetramethylcyclopentadienyl) ligand set, $(Cp^{tet}_3)^{3-}$ ($Cp^{tet} = C_5Me_4H$), was not initially considered a good candidate. Although the Cp^{tet} ligands are bulkier, they possess more alkyl substituents, which would presumably make them too electron donating to stabilize the +2 oxidation state. However, other results which will be discussed in Chapter 4, as well as results by

another group member in the Evans group, Austin J. Ryan, revealed that the use of a ligand system that was previously thought to be too electron donating, namely $[(NR_2)_3]^{3-}$ (R = $SiMe_3$), could actually provide isolable +2 rare-earth metal ion complexes. This inspired the exploration of $(Cp^{tet}_3)^{3-}$ as a ligand system for isolating +2 rare earth metal ion complexes even though it was thought to be too electron donating.

This study was initiated with the use of neodymium as the rare-earth metal center. Following the isolation and structural characterization of the Pu^{2+} ion complex, [K(crypt)][Cp″$_3$Pu] [crypt = 2.2.2-cryptand, Cp″ = $C_5H_3(SiMe_3)_2$],[5] it became of interest to expand the isolation of the +2 oxidation state to another transuranic metal, americium, with other cyclopentadienyl ligand sets. Neodymium was chosen as an appropriate surrogate for this investigation since the predicted nine-coordinate Nd^{2+} ionic radius of 1.35 Å is similar to the 1.31 Å of the predicted nine-coordinate Am^{2+} ionic radius.[6] The isolation of Nd^{2+} with the $(Cp'_3)^{3-}$ (Cp′ = $C_5H_4SiMe_3$) ligand set had been accomplished and reported previously by the Evans group,[4] and the use of the $(Cp''_3)^{3-}$ ligand set was already being explored by another Evans group member, Dr. Chad T. Palumbo. Therefore, as a contribution to this investigation, the use of $(Cp^{tet}_3)^{3-}$ was pursued.

Although neodymium has been considered as a "traditional" divalent metal, there had not been many reports of Nd^{2+} complexes in the literature because Nd^{2+} is among the most reducing ions of the "traditional" divalent ions. This Chapter describes the surprising results obtained from the reduction of Cp^{tet}_3Nd, which provided a stable Ln^{2+} complex with neodymium. Expansion of the use of the $(Cp^{tet}_3)^{3-}$ ligand set to obtain +2 ion complexes of the "non-traditional" divalent lanthanide, praseodymium, as well as yttrium is also described. In addition, reactivity studies with dinitrogen and $PhSiH_3$ are discussed.

Results and Discussion

Reduction of Cp^{tet}_3Nd. The reaction of Cp^{tet}_3Nd ($Cp^{tet} = C_5Me_4H$), **1-Nd**, with KC_8 in the presence of 2.2.2-cryptand (crypt) in THF under argon at −35 °C produced a deep dark green solution. The product could be crystallized from the THF solution by layer diffusion with Et_2O at −35 °C and it was identified by X-ray crystallography as the Nd^{2+} complex, $[K(crypt)][Cp^{tet}_3Nd]$, **2-Nd**, Figure 3.1. This complex crystallizes in the monoclinic space group $P2_1/c$ with one Et_2O solvent molecule in the lattice as well as another solvent molecule with mixed occupancy consisting of 0.47 Et_2O and 0.53 THF.

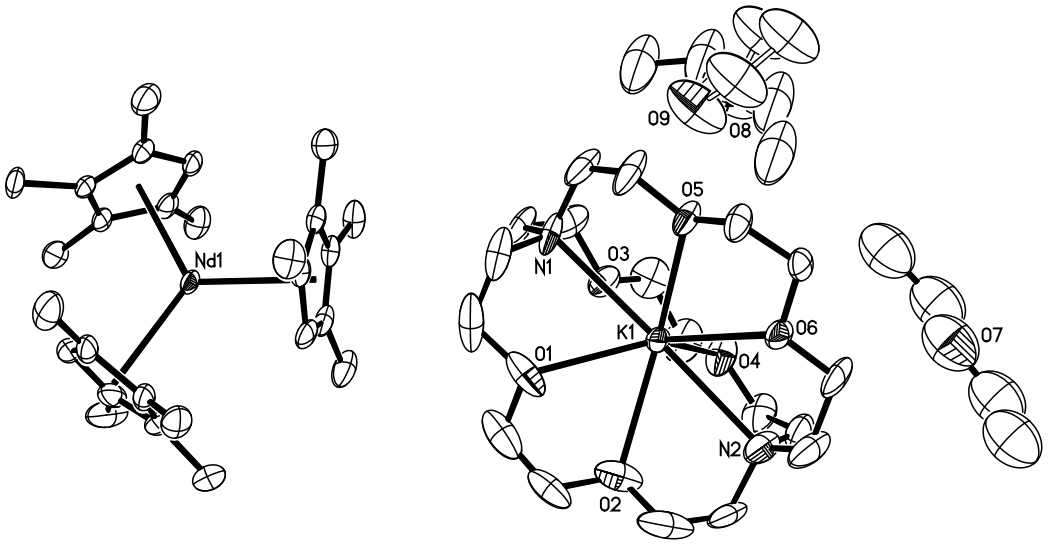

Figure 3.1. Thermal ellipsoid plot of $[K(crypt)][Cp^{tet}_3Nd]$, **2-Nd**, drawn at 50% probability level. Hydrogen atoms are omitted for clarity. Mixed solvents with 0.47 Et_2O and 0.53 THF partial occupancies are shown with labelled oxygen atoms, O8 and O9.

The Nd−ring centroid distances of **2-Nd** vary between 2.555-2.568 Å with an average of 2.563 Å. This is 0.045 Å longer than the 2.518 Å Nd−ring centroid distances of the Nd^{3+} precursor,

1-Nd.[7] Based on the data from the previously reported complexes with the tris(monosilylcyclopentadienyl) ligand set, $(Cp'_3)^{3-}$,[4] the small change in distances between the Nd^{3+} and Nd^{2+} complexes suggest that the added electron occupies the d_{z2} orbital.

The UV−visible−near-IR spectrum of **2-Nd** shows a strong absorption in the near-infrared region at λ_{max} = 812 nm with ε = 5600 $M^{-1}cm^{-1}$, Figure 3.2. This is different that the previously reported spectra of [K(crypt)][Cp'_3Nd], which absorbs strongly at λ_{max} = 420 and 483 nm in the visible region. However, the strong absorbance is still consistent with the assignment of $4f^n5d^1$ electron configuration since the Ln^{2+} metal complexes that were assigned $4f^{n+1}$ electron configurations, namely [K(crypt)][Cp'_3Ln] (Ln = Sm, Eu, Tm, and Yb), only showed weak absorptions. These findings provide another example in which Nd^{2+} could exhibit $4f^n5d^1$ rather than the previously found $4f^{n+1}$ electron configuration.

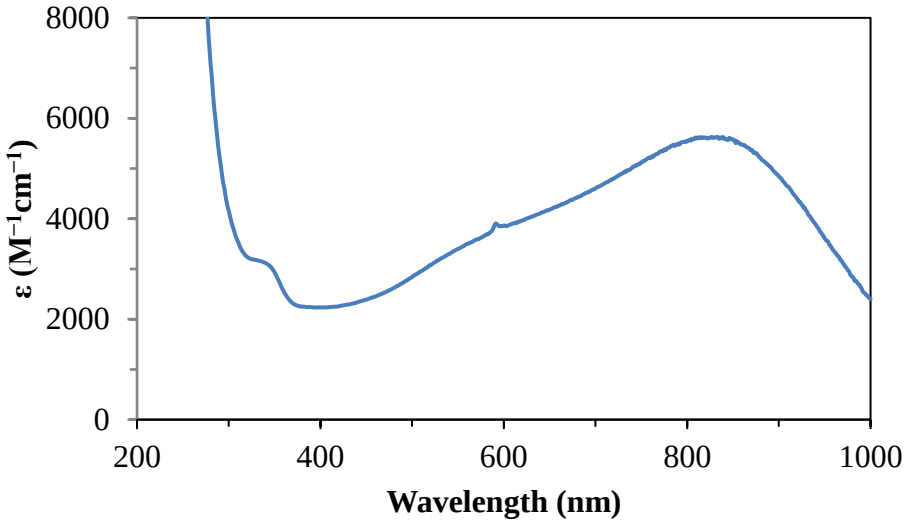

Figure 3.2. UV−visible−near-IR spectrum of a ~1 mM THF solution of [K(crypt)][Cp^{tet}_3Nd], **2-Nd**, (λ_{max} = 812 nm with ε = 5600 $M^{-1}cm^{-1}$). The sample showed negligible decomposition after 10 minutes of exposure to direct sunlight at room temperature, which signified the high stability of **2-Nd**.

Reduction of Cp^{tet}_3Pr. In order to determine whether the $(Cp^{tet}_3)^{3-}$ ligand set could also stabilize the +2 oxidation state of a "non-traditional" divalent lanthanide ion, the reduction of the praseodymium analog, Cp^{tet}_3Pr, **1-Pr**, was explored. Similar to the reduction of **2-Nd**, the reduction of **1-Pr** using KC_8 in the presence of crypt in THF under argon at −35 °C produced a deep dark blue solution. This product was also crystallized from the THF solution by layer diffusion with Et_2O to give an isomorphous structure of [K(crypt)][Cp^{tet}_3Pr], **2-Pr**., Figure 3.3.

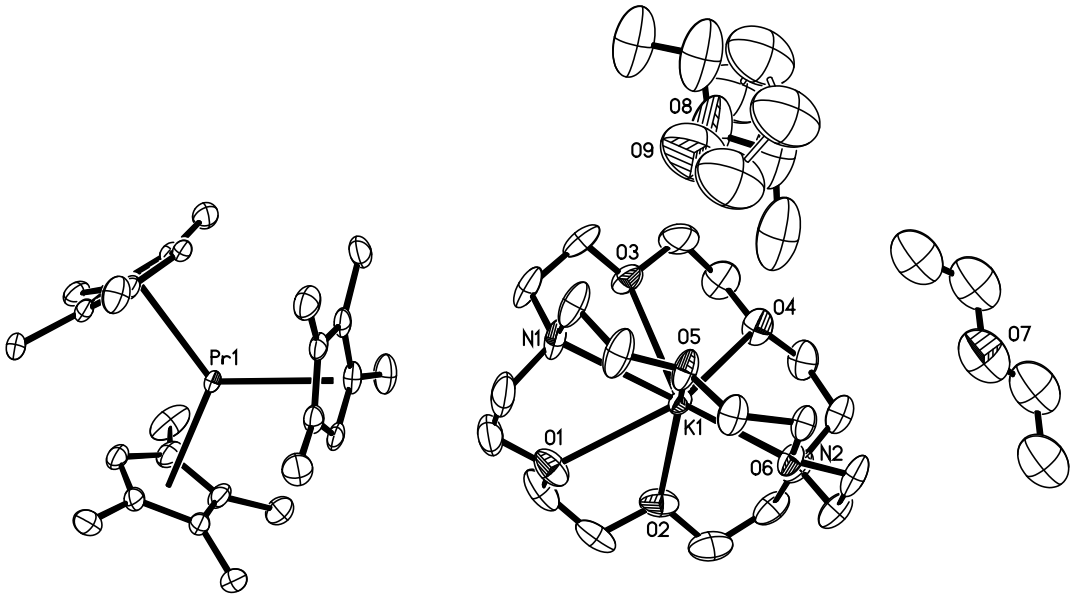

Figure 3.3. Thermal ellipsoid plot of [K(crypt)][Cp^{tet}_3Pr], **2-Pr**, drawn at 50% probability level. Hydrogen atoms are omitted for clarity. The partial mixed solvents are shown with labelled oxygen atoms, O8 and O9.

The Pr−ring centroid distances of **2-Pr** vary between 2.572-2.583 Å with an average of 2.578 Å. This is 0.046 Å longer than the distances observed in the Pr^{3+} precursor, **1-Pr**, and this

difference is similar to that observed in the case of neodymium. Again, this small change in metal−ring centroid distances is consistent with the assignment of a d_{z2} electron configuration, and the isolation of **2-Pr** suggest that methyl substituents do not make cyclopentadienyl rings too electron donating for isolating "non-traditional" divalent lanthanide ions.

The UV−visible−near-IR spectrum of **2-Pr** is similar to that of **2-Nd** and shows a strong absorption in the near-infrared region at λ_{max} = 845 nm with ε = 5200 $M^{-1}cm^{-1}$, Figure 3.4.

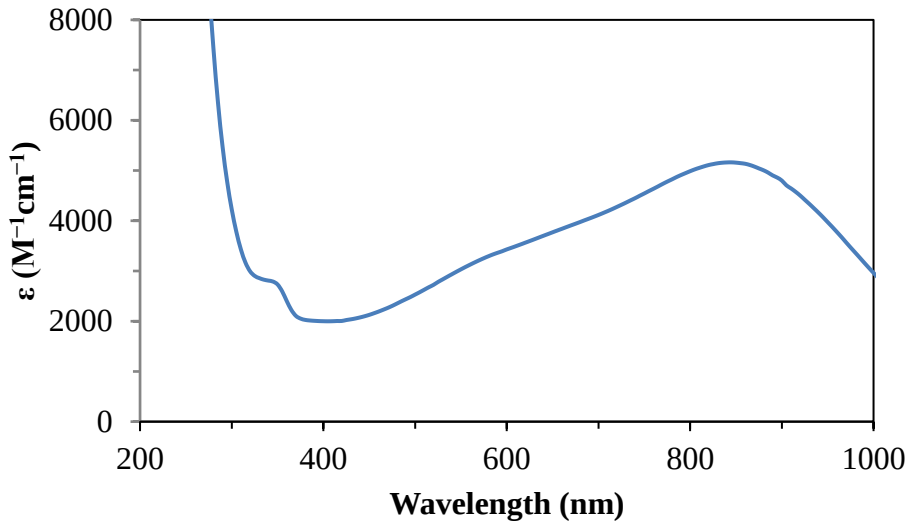

Figure 3.4. UV−visible−near-IR spectrum of a ~1 mM THF solution of [K(crypt)][Cp^{tet}_3Nd], **2-Nd**, (λ_{max} = 845 nm with ε = 5200 $M^{-1}cm^{-1}$).

Reduction of Cp^{tet}_3Y. For comparison with the results described in Chapter 1, the reduction of the yttrium analog, Cp^{tet}_3Y, **1-Y**, was explored. Similar to the reduction of $Cp_3Y(THF)$ (Cp = C_5H_5) and $Cp^{Me}_3Y(THF)$ (Cp^{Me} = C_5H_4Me) described in Chapter 1, the reduction of Cp^{tet}_3Y using KC_8 in the presence of crypt did not produce a stable +2 ion complex. The reduction produced a dark blue solution, **2-Y**, that decomposed to orange within minutes even at −35 °C. In order to obtain EPR spectroscopy data of the reduction product, the reaction was

performed on a small scale in an EPR tube at −78 °C. EPR spectroscopy measurements were performed on the sample and the data are presented in Figure 3.5.

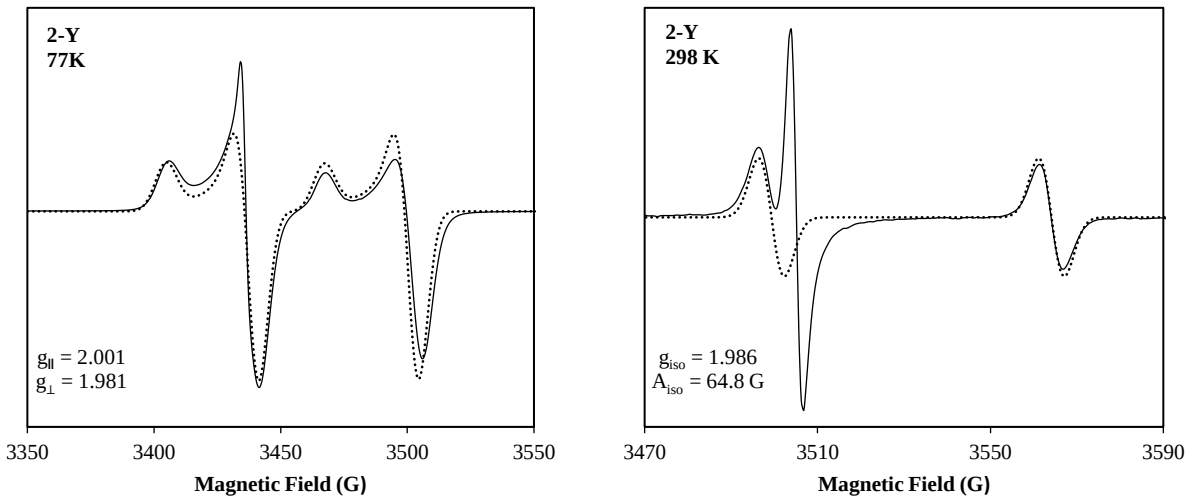

Figure 3.5. X-band EPR spectra of the reduction product of Cp^{tet}_3Y, **2-Y**, collected at 77 K (left) and 298 K (right). The simulated spectra (dotted lines) were generated with the exclusion of the extra feature attributed to an electride species already described in Chapter 1.

The EPR spectrum collected from the frozen solution at 77 K shows the expected axial signal with a two-line hyperfine pattern simulated to be around $g_{\parallel} = 2.001$ and $g_{\perp} = 1.981$ with an average hyperfine coupling constant of $A_{ave} = 62.8$ G. It is noticeable that there is an extra feature around g = 2.00 that is attributed to the presence of an electride species already described in Chapter 1. This extra feature was still present even when less than 1 equiv of crypt was used. It also consistently became more prominent in the room temperature spectrum possibly because the electride species was more stable than the Y^{2+} product at this temperature and only a small amount of the Y^{2+} species survived by the time the spectrum was collected. Nonetheless, the spectrum

was determined to be centered around g_{iso} = 1.986 with A = 64.8 G, based on the simulation. After the room temperature measurement was completed, the sample had already decomposed to pale orange/yellow.

Comparison of the room temperature hyperfine coupling constant of **2-Y** with those of other Y^{2+} species discussed in Chapter 1 is presented in Table 3.1. It appears that the coupling constant of **2-Y** still follows the trend that more alkyl substituents on cyclopentadienyl ligands lead to higher coupling constants. And as discussed in Chapter 1, this trend could be attributed to the generalization based on previous reports by Bercaw and Lappert that alkyl substituents render cyclopentadienyl ligands more electron donating, whereas silyl substituents have the opposite effect.[19,32]

Y^{3+} Precursors	**g_{iso}**	**A (G)**
a) Cp''_2YCp	1.990	34.6
b) Cp''_3Y	1.991	36.1
c) Cp''_2YCp^{Me}	1.990	36.4
d) Cp'_3Y	1.991	36.6
e) $Cp_3Y(THF)$	1.991	42.8
f) $Cp^{Me}_3Y(THF)$	1.990	46.9
g) Cp^{tet}_3Y	1.986	64.8

Table 3.1. Room temperature EPR spectra data of Y^{2+} complexes from the reduction of Y^{3+} complexes with varying ancillary ligands.

Although the $(Cp^{tet}_3)^{3-}$ ligand set appears to be more electron donating and should not be suitable for providing stable +2 rare-earth metal ion complexes, it allowed the isolation of stable

+2 ion complexes with the larger rare-earth metals, neodymium and praseodymium. This may indicate that electron donor ability effects could be less relevant than steric effects in stabilizing +2 rare-earth metal ions. It is possible that the $(Cp^{tet}_3)^{3-}$ ligand set is too sterically over-saturated in the case of the smaller rare-earth metal, yttrium, but suitable for the larger neodymium and praseodymium. Steric over-saturation has previously been attributed to lower stability in the case of the reduction of Cp''_3Y [$Cp'' = (C_5H_3(SiMe_3)_2]$, as described in Chapter 1. This also makes sense because the synthesis of Cp^{tet}_3Y was reported to be more difficult than Cp^{tet}_3Ln (Ln = Pr and Nd) due to steric over-saturation.[8]

Reactivity with Dinitrogen. It was previously reported that the reduction of several Cp^{tet}_3Ln complexes under dinitrogen yielded reduced dinitrogen complexes, $[Cp^{tet}_2Ln(THF)]_2[\mu\text{-}\eta^2\text{:}\eta^2\text{-}N_2]$ (Ln = La,[9] Ce,[10] Pr,[10] Nd,[9] Gd,[11] Dy[11]), through the general reaction, $LnA_3/M/N_2$ (A = Cp^{tet}, M = KC_8). As previously mentioned, the formation of the reduced dinitrogen complexes was thought to proceed through a Ln^{2+} intermediate. Therefore, the reaction of the Pr^{2+} complex, **2-Pr**, with dinitrogen was explored to determine if it would form a reduced dinitrogen species. However, exposure of dinitrogen to **2-Pr** in THF did not lead to apparent color change. Layer diffusion with Et_2O gave unidentifiable black solids as well as yellow mother liquor and yellow crystalline solids. The crystalline solids were identified by X-ray crystallography as the Pr^{3+} precursor, **1-Pr**.

This is another example showing that sometimes, the $LnA_3/M/N_2$ reaction does not generate the same product as the Ln^{2+}/N_2 reaction. A similar case was described in Chapter 2 in which the reduction of $Cp^{Me}_3Y(THF)$ under dinitrogen did not produce the same EPR active product as the reaction of $[Cp^{Me}_3Y]^{1-}$. A different scenario was reported from the reduction of $Y(NR_2)_3$ (R = $SiMe_3$) under dinitrogen, which produced the same reduced dinitrogen product,

$[(R_2N)_2Y(THF)]_2[\mu\text{-}\eta^2\text{:}\eta^2\text{-}N_2]$, as the reaction between freshly generated $[Y(NR_2)_3]^{1-}$.[12] However, in the case of the latter, no chelating agent, such as crypt or 18-crown-6, was present. Therefore, it is possible that the difference in reactivity was caused by the presence or absence of such chelating agent.

Reactivity with $PhSiH_3$. As described in Chapter 1, reactivity studies with $PhSiH_3$ is attractive since it has been shown to produce isolable hydride complexes with actinide and rare-earth metals.[13-14] In the case of Cp^{Me}_3Y, the reaction of the reduction product with $PhSiH_3$ also generated a rare Y−silyl complex, $[K(crypt)][Cp^{Me}_3Y(SiH_2Ph)]$. Therefore, the reaction of $[K(crypt)][Cp^{tet}_3Nd]$, **1-Nd**, with $PhSiH_3$ was pursued to study its reactivity.

The addition of excess $PhSiH_3$ to **1-Nd** in THF at −35 °C did not produce noticeable initial color change, but after layer diffusion with Et_2O over several days at −35 °C, pale-green crystalline solids were obtained. Identification of these solids by X-ray crystallography revealed that it was the Nd−silyl complex, $[K(crypt)][Cp^{tet}_3Nd(SiH_2Ph)]$, Figure 3.6. No examples of complexes with Nd−Si bonds were previously reported in the Cambridge Crystallographic Data Center. This complex crystallizes in the monoclinic space group $P2_1/c$ with no solvent molecules in the lattice.

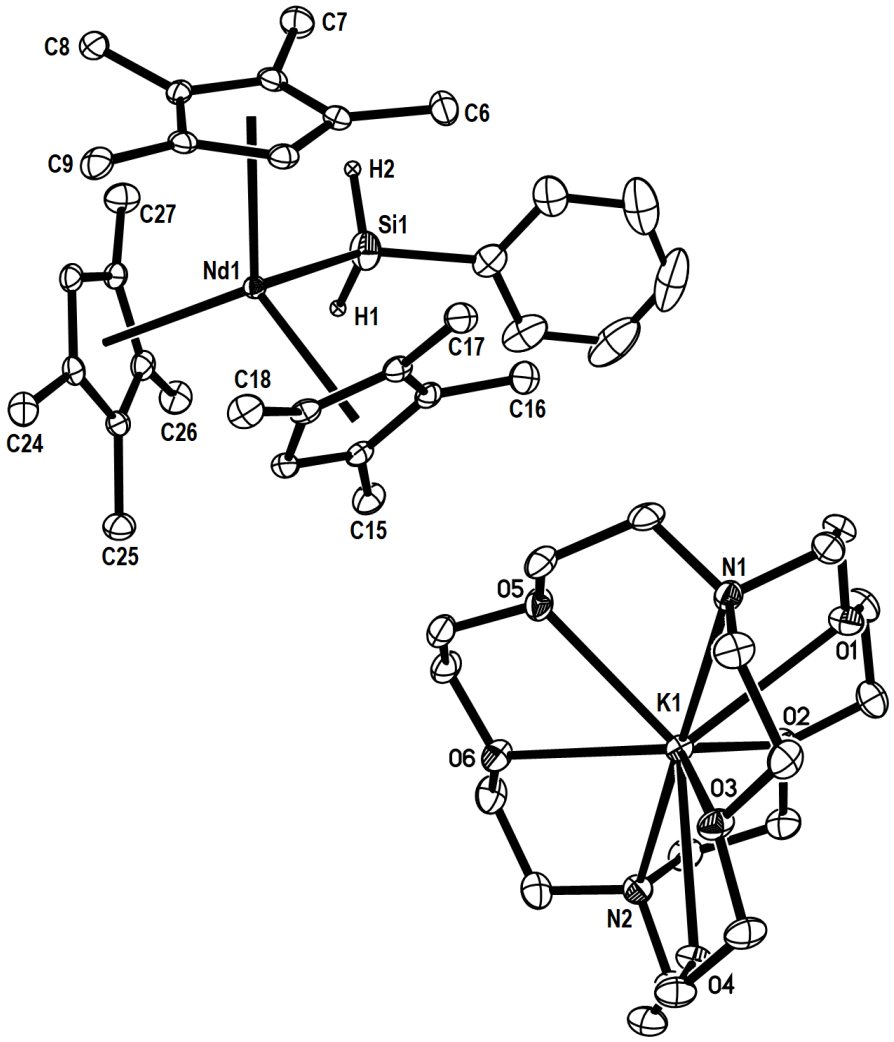

Figure 3.6. Thermal ellipsoid plot of [K(crypt)][Cp^{tet}_3Nd(SiH_2Ph)], **3-Nd**, drawn at 50% probability level. Hydrogen atoms, except H1 and H2, are omitted for clarity.

The formation of **3-Nd** was surprising since the $(Cp^{tet}_3)^{3-}$ ligand set is already quite sterically demanding, and the addition of an anionic ligand would be expected to lead to the loss of one of the cyclopentadienyl ligands. Since neutral Cp^y_2LnX (Cp^y = cyclopentadienyl ligand, X = anion) complexes are much more common, a neutral Cp^{tet}_2Nd(SiH_2Ph) product would be more reasonable to predict. Nonetheless, the fact that **3-Nd** was actually formed can be rationalized by the longer-than-expected metal−ligand distances observed in the crystal structure. The Nd−Si

bond distance of **3-Nd** is 3.148(8) Å, which is 0.194 Å longer than the 2.954 Å Y−Si bond distance in [K(crypt)][Cp^{Me}_3Y(SiH_2Ph)]. This difference is significantly larger than the 0.088 Å difference between the nine-coordinate Nd^{3+} vs Y^{3+}.[6] In addition, another rationalization can be derived from the long Nd−ring centroid distances of **3-Nd**, which vary between 2.596 and 2.630 Å with an average of 2.610 Å. This average distance is even longer than the nine-coordinate Nd^{2+} complex, **2-Nd**, by 0.047 Å, and is significantly longer than the nine-coordinate Nd^{3+} complex, **1-Nd**, by 0.092 Å.[7]

The fact that **3-Nd** has longer-than-expected metal ligand distances is similar to the case observed with the $(C_5Me_5)_3Ln$ complexes, which will be discussed in detail in Chapter 7. The cone angle of a $(C_5Me_5)^{1-}$ ligand was estimated to be 142° and three of these ligands would exceed 360°. In order for all the three ligands to fit around the metal center, the ligands had to be further away from the metal than in typical metal−cyclopentadienyl interactions, and that is what was observed in those $(C_5Me_5)_3Ln$ complexes. This seems to also be the case in **3-Nd** because the average Nd−centroid distance in **3-Nd** is in fact 0.027 Å longer than the 2.583 Å distances in $(C_5Me_5)_3Nd$.[15] However, this cannot be used as a direct comparison between the two since they have different coordination numbers.

Another feature that is similar between **3-Nd** and the $(C_5Me_5)_3Ln$ complexes is that the methyl substituents are displaced away from the metal centers above the plane of the cyclopentadienyl rings. Unlike in the case of the $(C_5Me_5)_3Ln$ complexes, which will be described in Chapter 7, the methyl displacements in **3-Nd** vary with no obvious trend, Table 3.2. The methyl displacements vary between 0.084-0.272 Å, and the average methyl displacements for each ring varies between 0.172-0.195 Å.

Table 3.2. Displacements of methyl substituents (Å) away from the cyclopentadienyl ring planes observed in [K(crypt)][$Cp^{tet}_3Nd(SiH_2Ph)$], **3-Nd**.

	Ring 1		Ring 2		Ring 3
C6	0.147	C15	0.084	C24	0.148
C7	0.182	C16	0.257	C25	0.271
C8	0.272	C17	0.221	C26	0.213
C9	0.147	C18	0.136	C27	0.108
Average	0.187		0.195		0.172

Conclusion

The reduction of Cp^{tet}_3Ln (Cp^{tet} = C_5Me_4H), **1-Ln**, complexes with the larger rare-earth metals, neodymium and praseodymium, produced stable +2 ion complexes, [K(crypt)][Cp^{tet}_3Ln] (Ln = Nd, Pr), **2-Ln**. However, the reduction of the smaller rare-earth metal analog with yttrium, Cp^{tet}_3Y, **1-Y**, did not provide a stable Y^{2+} complex. EPR spectroscopy studies of the reduction product of **1-Y** revealed that an Y^{2+} complex, **2-Y**, was in fact produced, but it was too unstable to be isolated and crystallographically analyzed. The hyperfine coupling constant in the EPR spectrum of **2-Y** is larger than those of any Y^{2+} species generated from other tris(cyclopentadienyl) yttrium complexes, Cp^x_3Y [Cp^x = $C_5H_3(SiMe_3)_2$, $C_5H_4SiMe_3$, C_5H_5, C_5H_4Me] and $Cp^xYCp^z_2$ [Cp^x = $C_5H_3(SiMe_3)_2$, Cp^z = C_5H_5, C_5H_4Me]. This is consistent with the postulation, based on previous reports by Bercaw and Lappert, that more alkyl substituents render the ligand more electron donating, which lead to more electron density near the metal.[19,32]

Reactivity studies of **2-Pr** with dinitrogen revealed that the Pr^{2+}/N_2 reaction does not produce the same reduced dinitrogen product from the direct $LnA_3/M/N_2$ (A = Cp^{tet}, M = KC_8)

reaction. This difference in reactivity is attributed to the presence of 2.2.2-cryptand (cryptand), which aids in the stabilization of the Pr^{2+} complex and may affect its reactivity.

Reactivity studies of **2-Nd** with $PhSiH_3$ generated the first crystallographically-characterized complex containing a Nd−Si bond, [K(crypt)][Cp^{tet}_3Nd(SiH_2Ph)], **3-Nd**. Surprisingly, this complex retained all three of the bulky $(Cp^{tet})^{1-}$ ligands which forming the Nd-Si bond. The result is a complex with bond distances longer than normal.

Experimental

All manipulations and syntheses described below were conducted with rigorous exclusion of air and water using standard Schlenk line and glovebox techniques under an argon or dinitrogen atmosphere. Solvents were sparged with UHP argon and dried by passage through columns containing Q-5 and molecular sieves prior to use. Deuterated NMR solvents were dried over NaK alloy, degassed by three freeze-pump-thaw cycles, and vacuum transferred before use. Methylcyclopentadiene were dried over molecular sieves and degassed by three freeze-pump-thaw cycles. 2.2.2-Cryptand (crypt) was purchased from Merck and dried under reduced pressure before use. KCp^{tet} (Cp^{tet} = C_5Me_4H),[12] anhydrous $LnCl_3$ (Ln = Pr, Nd, Y),[16] Cp^{tet}_3Ln (Ln= Pr[12], Nd,[14]) **1-Ln,** and KC_8[11] were synthesized via an adaptation of a literature procedure. ^{1}H NMR spectra were recorded on Bruker GN500 or CRYO500 MHz spectrometers (^{13}C NMR at 125 MHz) at 298 K unless otherwise stated and referenced internally to residual protio-solvent resonances. Electron paramagnetic resonance spectra were collected using a Bruker EMX spectrometer equipped with an ER041XG microwave bridge in THF at 298 K and 77 K unless otherwise specified. EPR simulations were performed using EasySpin.[17] UV−visible−near-IR measurements were conducted at 298 K in THF with a Jasco 670 UV−visible−near-IR Spectrophotometer. IR samples

were prepared as KBr pellets on a Varian 1000 FT-IR system. Elemental analyses were conducted on a Perkin-Elmer 2400 Series II CHNS elemental analyzer.

Cp^{tet}_3Y, 1-Y. A new direct method to synthesize this sterically over-saturated complex was used rather than the previously reported procedure.[13] In an argon-filled glovebox, THF (5 mL) was added to a mixture of YCl_3 (30 mg, 0.15 mmol) and KCp^{tet} (74 mg, 0.46 mmol). The mixture was stirred overnight. Subsequently, the THF solvent was removed under reduced pressure and toluene (10 mL) was added. The resulting yellow mixture was stirred while heating to a gentle boil for 5 min, and continued to stir at room temperature for 1 h. The mixture was centrifuged to remove pale yellow solids, and the yellow supernatant was filtered and dried under reduce pressure to yield yellow solid of **1-Y** (42 mg, 60%). ^{1}H NMR (ppm): 6.03 (s, 3H, $C_5Me_4\mathit{H}$), 2.03 (s, 18H, $C_5\mathit{Me}_4H$), 1.83 (s, 18H, $C_5\mathit{Me}_4H$). This NMR data is consistent with the previously reported data.[13]

Reduction of Cp^{tet}_3Y, 1-Y, to form a dark blue solution, 2-Y, for EPR measurements. In an argon-filled glovebox, **1-Y** (20 mg, 0.044 mmol) and crypt (16 mg, 0.043 mmol) was dissolved in THF (5 mL) to form a yellow solution. About 0.5 mL of this solution was transferred to a quartz EPR tube. KC_8 (10 mg, 0.074 mmol) was added to the top of the EPR tube while preventing it from coming in contact with **1-Y** solution. The tube was sealed and brought out of the glovebox. The solution was cooled to −78 °C using a dry ice/isopropanol bath, and the KC_8 was then tapped to the bottom of the tube to allow it to react with the cooled solution, yielding a deep dark blue solution. The EPR tube was transferred to a liquid nitrogen bath and the solution was kept frozen until it was inserted into the EPR spectrometer.

[K(crypt)][Cp^{tet}_3Pr], 2-Pr. 1-Pr (15 mg, 0.0274 mmol) and crypt (10g, 0.0274 mmol) were dissolved in THF (2 mL) and reacted with KC_8 (5 mg, 0.03 mmol) to form black crystalline

solid of **[K(crypt)][($C_5Me_4H)_3Pr$]**, **2-Pr**, (17 mg, 76%)**.** Black single crystals of **2-Pr** suitable for X-ray diffraction were obtained by layer diffusion of the concentrated THF solution with Et_2O at ¬35 °C. IR: 3077w, 2961m, 2882s, 2821s, 2702w, 1477m, 1445m, 1354m, 1296m, 1258m, 1134s, 1109vs, 1080s, 952s, 933m, 833w, 749m, 734w $cm^{¬1}$. UV−visible−near-IR (THF): 845 nm (5,100 M^{-1} cm^{-1}). Anal. Calcd for $C_{45}H_{75}KN_2O_6Pr$: C, 58.74; H, 8.22; N, 3.04. Found: C, 57.87; H, 7.95; N, 2.96.

[K(crypt)][Cp^{tet}_3Nd], 2-Nd. Similar to the preparation of **2-Pr**, **1-Nd** (40 mg, 0.079 mmol) and crypt (30 mg, 0.079 mmol) were dissolved in THF (2 mL) and reacted with KC_8 (13 mg, 0.095 mmol) to form black crystalline solid of **[K(crypt)][Cp^{tet}_3Nd]**, **2-Nd**, (33 mg, 45%)**.** Black single crystals of **2-Nd** suitable for X-ray diffraction were obtained by layer diffusion of the concentrated THF solution with Et_2O at ¬35 °C. IR: 3080w, 2962m, 2883s, 2822s, 2704w, 1477m, 1444m, 1354m, 1323w, 1296m, 1258m, 1238w, 1173w, 1134s, 1109vs, 1081s, 951s, 933m, 832w, 749m, 700w $cm^{¬1}$. UV−visible−near-IR (THF): 812 nm (5600 M^{-1} cm^{-1}). Anal. Calcd for $C_{45}H_{75}KN_2O_6Nd$: C, 58.53; H, 8.19; N, 3.03. Found: C, 57.96; H, 7.67; N, 3.29.

[K(crypt)][$Cp^{tet}_3Nd(SiH_2Ph)$], 3-Nd. In an argon-filled glovebox, **2-Nd (**22 mg, 0.024 mmol) was dissolved in THF (1 mL) to give a deep dark green solution. $PhSiH_3$ (excess) was added to the solution. No reaction was observed. The solution was layered with Et_2O and left at ¬35 °C. After several days, pale green-blue crystalline solids of [K(crypt)][$Cp^{tet}_3Nd(SiH_2Ph)$], **3-Nd**, suitable for X-ray diffraction were obtained (13 mg, 53%). IR: 3047w, 2961m, 2884s, 2853s, 2716 w, 1971m, 1576w, 1477m, 1444m, 1354s, 1327w, 1296m, 1258m, 1239w, 1173w, 1132s, 1105vs, 1078s, 1031 w, 952s, 933m, 921m, 833w, 791m, 757m, 708m, 609w, 563w, 525w $cm^{¬1}$.

X-ray Data Collection, Structure Solution and Refinement for [K(crypt)][Cp^{tet}_3Pr], 2-Pr. A black crystal of approximate dimensions 0.221 x 0.236 x 0.378 mm was mounted in a

cryoloop and transferred to a Bruker SMART APEX II diffractometer. The APEX2[18] program package was used to determine the unit-cell parameters and for data collection (30 sec/frame scan time for a sphere of diffraction data). The raw frame data was processed using SAINT[19] and SADABS[20] to yield the reflection data file. Subsequent calculations were carried out using the SHELXTL[21] program. The diffraction symmetry was 2/*m* and the systematic absences were consistent with the monoclinic space group $P2_1/c$ that was later determined to be correct. The structure was solved by dual space methods and refined on F^2 by full-matrix least-squares techniques. The analytical scattering factors[22] for neutral atoms were used throughout the analysis. Hydrogen atoms were included using a riding model. There were approximately 1.4 molecules of diethylether and 0.60 molecules of tetrahydrofuran solvents present. The partial mixed solvents (0.40 diethylether and 0.60 tetrahydrofuran) were included with partial site-occupancy-factors and geometric constraints. All solvents were refined with equivalent anisotropic thermal parameters. Least-squares analysis yielded wR2 = 0.1280 and Goof = 1.078 for 557 variables refined against 11753 data (0.80 Å), R1 = 0.0505 for those 9739 data with $I > 2.0\sigma(I)$.

X-ray Data Collection, Structure Solution and Refinement for [K(crypt)][Cp^{tet}_3Nd], 2-Nd. A black crystal of approximate dimensions 0.184 x 0.194 x 0.386 mm was mounted in a cryoloop and transferred to a Bruker SMART APEX II diffractometer. The APEX2[18] program package was used to determine the unit-cell parameters and for data collection (30 sec/frame scan time for a sphere of diffraction data). The raw frame data was processed using SAINT[19] and SADABS[20] to yield the reflection data file. Subsequent calculations were carried out using the SHELXTL[21] program. The diffraction symmetry was 2/*m* and the systematic absences were consistent with the monoclinic space group $P2_1/c$ that was later determined to be correct. The structure was solved by dual space methods and refined on F^2 by full-matrix least-squares

techniques. The analytical scattering factors[22] for neutral atoms were used throughout the analysis. Hydrogen atoms were included using a riding model. There were approximately 1.47 molecules of diethylether and 0.53 molecules of tetrahydrofuran solvents present. The partial mixed solvents (0.47 diethylether and 0.53 tetrahydrofuran) were included with partial site-occupancy-factors and geometric constraints. All solvents were refined with equivalent anisotropic thermal parameters. Least-squares analysis yielded wR2 = 0.1495 and Goof = 1.074 for 557 variables refined against 11752 data (0.80 Å), R1 = 0.0607 for those 9104 data with $I > 2.0\sigma(I)$.

X-ray Data Collection, Structure Solution and Refinement for [K(crypt)][$Cp^{tet}_3Nd(SiH_2Ph)$], 3-Nd. A blue crystal of approximate dimensions 0.112 x 0.249 x 0.377 mm was mounted in a cryoloop and transferred to a Bruker SMART APEX II diffractometer. The APEX2[18] program package was used to determine the unit-cell parameters and for data collection (10 sec/frame scan time for a sphere of diffraction data). The raw frame data was processed using SAINT[19] and SADABS[20] to yield the reflection data file. Subsequent calculations were carried out using the SHELXTL[21] program. The diffraction symmetry was 2/*m* and the systematic absences were consistent with the monoclinic space group $P2_1/c$ that was later determined to be correct. The structure was solved by dual space methods and refined on F^2 by full-matrix least-squares techniques. The analytical scattering factors[22] for neutral atoms were used throughout the analysis. Hydrogen atoms were located from a difference-Fourier map and refined (x,y,z and U_{iso}). Least-squares analysis yielded wR2 = 0.0620 and Goof = 1.024 for 877 variables refined against 11454 data (0.78 Å), R1 = 0.0280 for those 9403 data with $I > 2.0\sigma(I)$.

References

(1) MacDonald, M. R.; Ziller, J. W.; Evans, W. J. *J. Am. Chem. Soc.* **2011**, *133*, 15914-15917.

(2) MacDonald, M. R.; Bates, J. E.; Fieser, M. E.; Ziller, J. W.; Furche, F.; Evans, W. J. *J. Am. Chem. Soc.* **2012**, *134*, 8420-8423.

(3) MacDonald, M. R.; Bates, J. E.; Ziller, J. W.; Furche, F.; Evans, W. J. *J. Am. Chem. Soc.* **2013**, *135*, 9857-9868.

(4) Fieser, M. E.; MacDonald, M. R.; Krull, B. T.; Bates, J. E.; Ziller, J. W.; Furche, F.; Evans, W. J. *J. Am. Chem. Soc.* **2015**, *137*, 369-382.

(5) Windorff, C. J.; Chen, G. P.; Cross, J. N.; Evans, W. J.; Furche, F.; Gaunt, A. J.; Janicke, M. T.; Kozimor, S. A.; Scott, B. L. *J. Am. Chem. Soc.* **2017**, *139*, 3970-3973.

(6) Shannon, R. *Acta Crystallog., Sect. A* **1976**, *32*, 751-767.

(7) Windorff, C. J.; Dumas, M. T.; Ziller, J. W.; Gaunt, A. J.; Kozimor, S. A.; Evans, W. J. *Inorg. Chem.* **2017**, *56*, 11981-11989.

(8) Lorenz, S. E.; Schmiege, B. M.; Lee, D. S.; Ziller, J. W.; Evans, W. J. *Inorg. Chem.* **2010**, *49*, 6655-6663.

(9) Evans, W. J.; Lee, D. S.; Lie, C.; Ziller, J. W. *Angew. Chem., Int. Ed.* **2004**, *43*, 5517-5519.

(10) Evans, W. J.; Rego, D. B.; Ziller, J. W. *Inorg. Chem.* **2006**, *45*, 10790-10798.

(11) Fieser, M. E.; Woen, D. H.; Corbey, J. F.; Mueller, T. J.; Ziller, J. W.; Evans, W. J. *Dalton Trans.* **2016**, *45*, 14634-14644.

(12) Fang, M.; Lee, D. S.; Ziller, J. W.; Doedens, R. J.; Bates, J. E.; Furche, F.; Evans, W. J. *J. Am. Chem. Soc.* **2011**, *133*, 3784-3787.

(13) Windorff, C. J.; MacDonald, M. R.; Meihaus, K. R.; Ziller, J. W.; Long, J. R.; Evans, W. J. *Chem. Eur. J.* **2016**, *22*, 772-782.

(14) Pagano, J. K.; Dorhout, J. M.; Waterman, R.; Czerwinskic, K. R.; Kiplinger, J. L. *Chem. Commun.* **2015**, *51*, 17379-17381.

(15) Evans, W. J.; Seibel, C. A.; Ziller, J. W. *J. Am. Chem. Soc.* **1998**, *120*, 6745-6752.

(16) Meyer, G.; Ax, P. *Mater. Res. Bull.* **1982**, *17*, 1447-1455.

(17) Stoll, S.; Schweiger, A. J. *Magn. Reson.* **2006**, *178*, 42.

(18) Bruker AXS, Inc., APEX2 Version 2014.11-0, Madison, WI, **2014**.

(19) Bruker AXS, Inc., SAINT Version 8.34a, Madison, WI, **2013**.

(20) Sheldrick, G. M.; SADABS, Version 2014/5, Bruker AXS, Inc., Madison, WI, **2014**.

(21) Sheldrick, G. M.; SHELXTL, Version 2014/7, Bruker AXS, Inc., Madison, WI, **2014**.

(22) *International Tables for Crystallography, Vol. C*, Kluwer Academic Publishers, Dordrecht, **1992**.

CHAPTER 4

Solution Synthesis, Structure, and Physical Properties of a Sc^{2+} Complex, $\{Sc[N(SiMe_3)_2]_3\}^{1-}$

Introduction*

Scandium is attractive for theoretical studies since it has the lowest atomic number of any transition metal. However, its chemistry often lags behind the other transition metals due to the experimental difficulty of working with this small electropositive element.[1-12] The +3 oxidation state is predominant for Sc in molecular complexes in solution with only six examples reported in other oxidation states. These include one Sc^0 complex, $Sc(\eta^6\text{-}C_6H_3{}^tBu_3)_2$,[7 8] three Sc^{1+} complexes, $[\{\eta^5\text{-}P_3C_2{}^tBu_2)Sc\}_2(\mu\text{-}\eta^6\text{:}\eta^6\text{-}P_3C_3{}^tBu_3)]$,[9] $[Sc(\eta^5\text{-}P_3C_2{}^tBu_2)(\mu\text{-}\eta^2\text{:}\eta^5\text{-}P_3C_2{}^tBu_2)Sc(\eta^5\text{-}P_3C_2{}^tBu_2)]$,[10] and $(LMgBr)_2ScBr$ (L = $Et_2NCH_2CH_2NC(Me)CHC\text{-}(Me)NCH_2CH_2NEt_2$),[11] and two Sc^{2+} complexes, $Sc\{\eta^6\text{-}C_6H_3{}^tBu_3(\eta^6,\eta^1\text{-}{}^tBu_2[CMe_2CH_2]C_6H_3\}H$,[7] and $Sc(\eta^5\text{-}P_2C_3{}^tBu_3)_2$,[12] both of which were obtained via electron beam vaporization of Sc^0 into cryogenic matrices. Structural characterization was only possible on the Sc^0 and Sc^{1+} complexes; no reports of Sc^{2+} complexes characterized by X-ray diffraction are in the literature.

Following the isolation and structural characterization of +2 ion complexes of all the other rare-earth metals, *i.e.* Y and the lanthanides (except the radioactive Pm),[13-17] from the LnA_3/M reactions (Ln = rare-earth metal; A = anionic ligand; M = alkali metal) involving alkali metal reductions of tris(silylcyclopentadienyl) complexes, *i.e.* A = $C_5H_4SiMe_3$ and $C_5H_3(SiMe_3)_2$, eq 4.1, it was of interest to extend the series of the structurally-characterized complexes to the one

* Portions of this chapter have been published: Woen, D. H.; Chen, G. P.; Ziller, J. W.; Boyle, T. J.; Furche, F.; Evans, W. J. *Angew. Chem. Int. Ed.* **2017**, 56, 2050−2053; *Angew. Chem.* **2017**, 129, 2082–2085. DOI: 10.1002/ange.201611758.

remaining rare-earth metal ion which had not yet been identified crystallographically, Sc^{2+}. However, accessing the analogous "$Sc(C_5H_4SiMe_3)_3$" and "$Sc[C_5H_3(SiMe_3)_2]_3$" precursors could

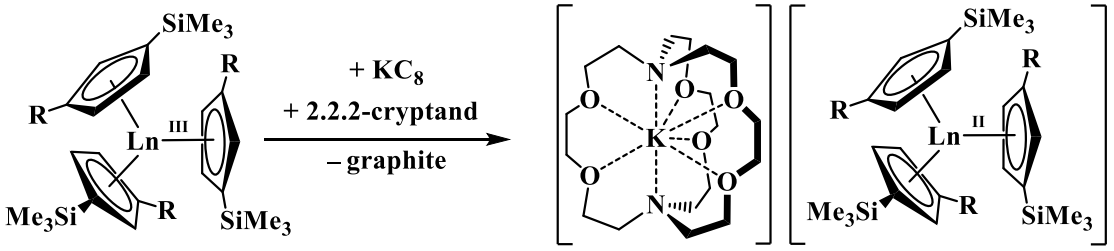

(4.1)

R = H, Ln = Y, La, Ce, Pr, Nd, Gd, Tb, Dy, Ho, Er, and Lu
R = $SiMe_3$, Ln = La and Ce

be problematic since the ionic size of Sc^{3+} is 0.107 Å smaller than that of Lu^{3+},[18] and the preparation of $Lu(C_5H_4SiMe_3)_3$ is already challenging due to steric crowding.[19] Moreover, the structure of the tris(cyclopentadienyl) Sc^{3+} complex, $[(\eta^5\text{-}C_5H_5)_2Sc(\mu\text{-}\eta^1\text{:}\eta^1\text{-}C_5H_5)]_n$,[20] suggests that "$Sc(C_5H_4SiMe_3)_3$" and "$Sc[C_5H_3(SiMe_3)_2]_3$" may not form the same trigonal coordination environment of all the examples in eq 4.1.

The bis(trimethylsilyl)amide complex, $Sc(NR_2)_3$ (R = $SiMe_3$),[21] **1**, was not initially considered as a precursor to Sc^{2+} since previous LnA_3/M reactions with A = NR_2 did not allow isolation of Ln^{2+} complexes. Instead, these $Ln(NR_2)_3$ reduction reactions generated reduced dinitrogen complexes containing $(N{=}N)^{2-}$, eq 4.2, and $(N_2)^{3-}$ moieties.[16-17,22-25] Although DFT

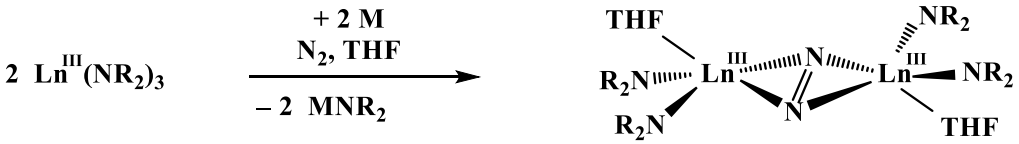

(4.2)

Ln = Nd, Gd, Tb, Dy, Ho, Er, Tm, Lu, Y
M = Na, K or KC_8

studies of $Y(NR_2)_3$ showed that both the LUMO of the trivalent complex, $Y(NR_2)_3$, and the HOMO of the reduced species, $[Y(NR_2)_3]^{1-}$, have primarily d_z^2 character,[26] only EPR data were obtainable

on a transient Y^{2+} species.[27] This chapter describes the surprising results obtained by examining the reduction of the scandium analog, **1**.

Results and Discussion

Reduction of $Sc(NR_2)_3$, **1**, with a potassium smear at −35 °C in Et_2O in the presence of 2.2.2-cryptand (crypt) and 18-crown-6 (crown) allowed the isolation of X-ray quality black crystals of [K(crypt)][$Sc(NR_2)_3$], **2-K(crypt)** (Figure 4.1), and [K(crown)][$Sc(NR_2)_3$], **2-K(crown)**, respectively, by diffusion of pentane into Et_2O solutions at −35 °C. Cesium reduction of **1** in the presence of crypt also forms a Sc^{2+} product, [Cs(crypt)][$Sc(NR_2)_3$], **2-Cs(crypt)**. These reactions are summarized in Scheme 4.1.

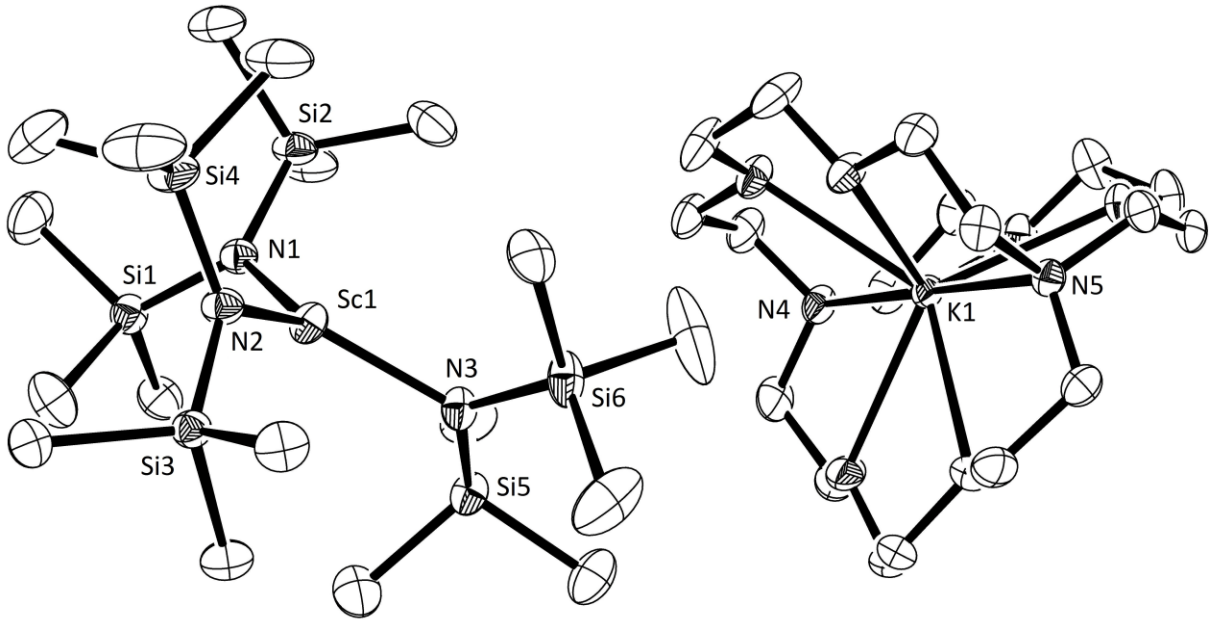

Figure 4.1. Thermal ellipsoid plot of **2-K(crypt)** drawn at 50% probability. Hydrogen atoms are omitted for clarity.

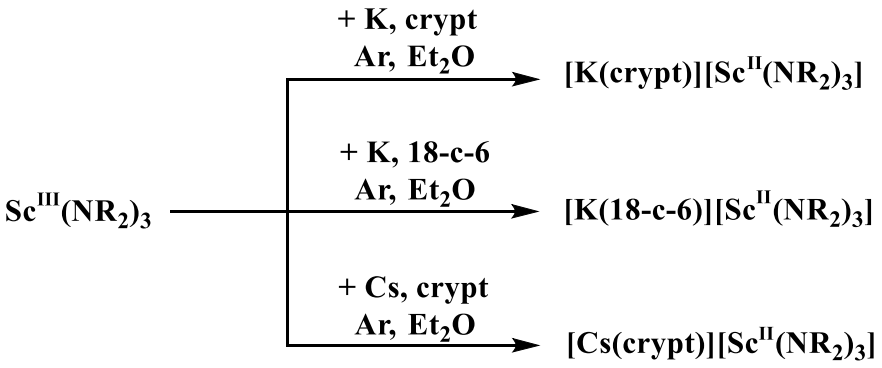

Scheme 4.1. Reduction reactions of **1**.

2-K(crypt) crystallizes in the triclinic space group $P\bar{1}$ with D_3 symmetry for the anion. Unfortunately, data from crystals of **2-K(crown)** were not good enough to discuss metrical parameters and **2-Cs(crypt)** gave a disordered structure. All of the structures of **2** are very different from the polymeric $[M(\mu\text{-}NR_2)_2Ln(\mu\text{-}NR_2)]_n$ structures of the traditional[15] Ln^{2+} rare-earth ions, $4f^6$ Sm^{2+} (M = Na, K),[28] $4f^7$ Eu^{2+} (M = Na),[29] and $4f^{14}$ Yb^{2+} (M = Na).[29]

EPR data of the three variants of **2** in *ca.* 1 mM Et_2O solutions gave identical spectra that confirmed the presence of Sc^{2+}. The room temperature EPR spectrum of **2-K(crypt)**, Figure 4.2, shows an isotropic signal with an eight-line hyperfine pattern at g_{iso} = 1.977 with A_{iso} = 214 G. This is consistent with an unpaired electron interacting with the 100% naturally abundant I = 7/2 ^{45}Sc isotope. The 77 K EPR spectrum shows an eight-line axial signal at $g_{\parallel}$ = 1.997 and $g_{\perp}$ = 1.964 with A_{ave} = 225 G. The EPR spectrum of $[Sc(\eta^5\text{-}P_2C_3{}^tBu_3)_2]$[12] has similar g-values, g_{iso} = 1.9823, $g_{\parallel}$ = 2.0098, and $g_{\perp}$ = 1.9273, but the coupling constants are significantly smaller: A_{iso} = 37.57 G, $A_{\parallel}$ = 29.9 G, and $A_{\perp}$ = 52.9 G.

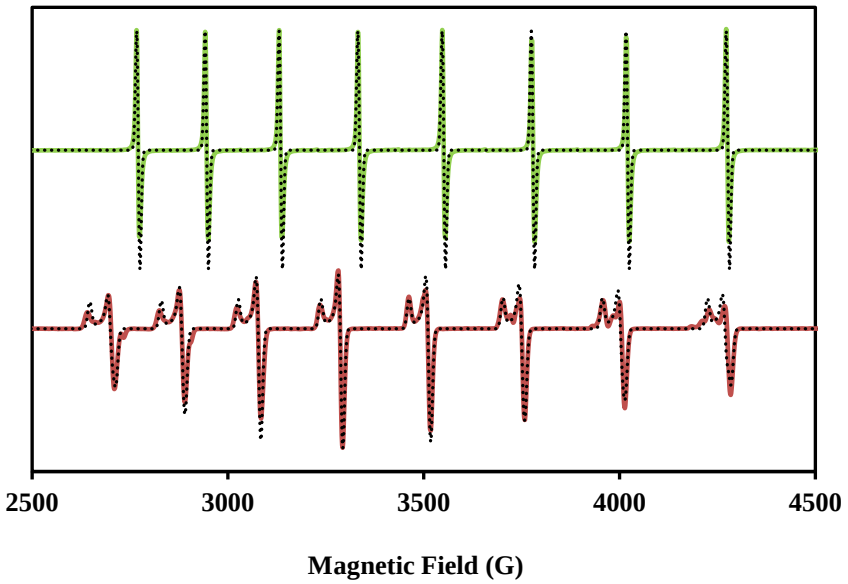

Figure 4.2. Experimental (solid) and simulated (dotted) X-band EPR spectra of **2-K(crypt)**, collected at room temperature (top) and 77 K (bottom).

In the structure of **2-K(crypt)**, the Sc^{2+} ion lies in the plane of the three nitrogen donor atoms. This differs from the pyramidal geometry previously described for the Sc^{3+} precursor, **1**,[21] and for the eight structurally-characterized examples of $Ln(NR_2)_3$,[30-36] that all have disordered pyramidal structures with the metal above and below the plane of the nitrogen atoms. However, structural comparison of **2-K(crypt)** and **1** was complicated by the fact that there was an apparent error in the metrical measurements of the latter and its cartesian coordinates were not available. Considering this, **1** was independently crystallized for new X-ray diffraction analyses. Crystals of **1** grown from solution gave metal disorder as previously described (**1a**, Figure 4.3),[21] but crystals grown by sublimation generated a structure with no disorder (**1b**, Figure 4.44) with the metal *ca.* 0.5 Å above the plane of the nitrogen atoms. The average Sc−N bond distance in **2-K(crypt)** is 0.08 Å larger than that in **1**. This is smaller than the 0.1-0.2 Å difference observed between $4f^{n+1}$

Ln^{2+} ions and $4f^n$ Ln^{3+} ions,[17] but larger than the *ca.* 0.03 Å difference between $4f^n5d^1$ Ln^{2+} ions in eq 1 and $4f^n$ Ln^{3+} ions.

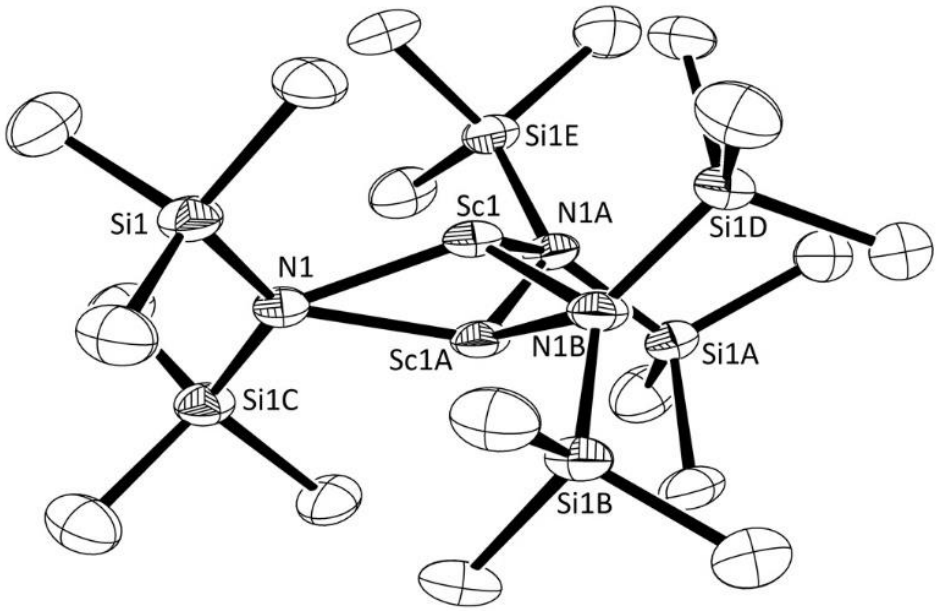

Figure 4.3. Thermal ellipsoid plot of **1a** drawn at 50% probability. Hydrogen atoms are omitted for clarity.

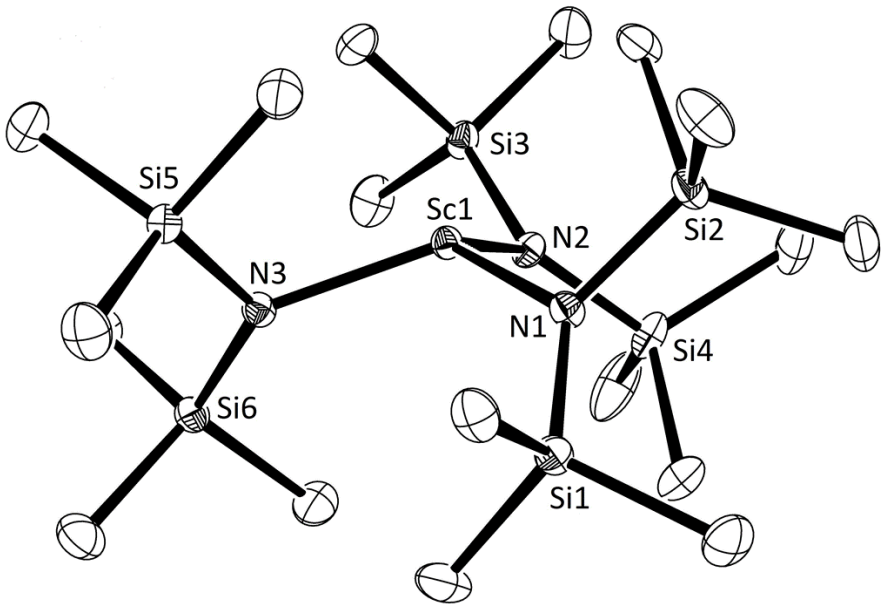

Figure 4.4. Thermal ellipsoid plot of **1b** drawn at 50% probability. Hydrogen atoms are omitted for clarity.

DFT geometry optimizations were performed by Guo P. Chen from the research group of Professor Filipp Furche on $Sc(NR_2)_3$ and $[Sc(NR_2)_3]^{1-}$ and the calculated structural parameters matched the pyramidal structure for **1** and the planar D_3 structure for the anion of **2**. The frontier molecular orbitals are similar to those of the Y analogs:[26] the LUMO of the Sc^{3+} precursor and the HOMO of the reduced Sc^{2+} product both have d_z^2 character (Figure 4.5). The $(3d_z^2)^1$ ground state for $[Sc(NR_2)_3]^{1-}$, is consistent with the experimental EPR data.

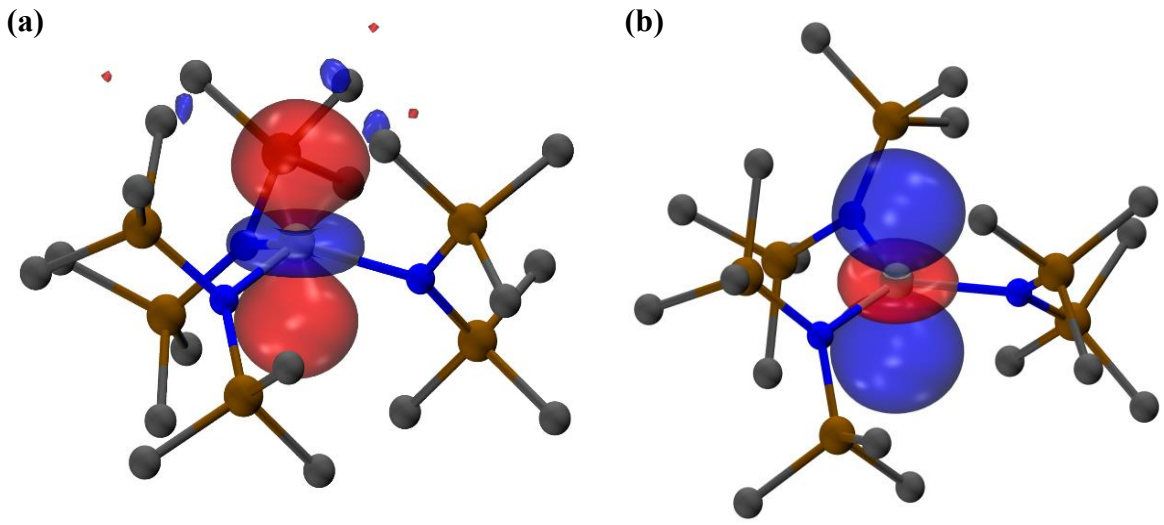

Figure 4.5. (a) LUMO of $Sc(NR_2)_3$ and (b) HOMO of $[Sc(NR_2)_3]^{1-}$ with contour value of 0.045. Hydrogen atoms are omitted for clarity.

The UV−visible spectra of each variant of **2** exhibit an intense absorption at 516 nm with ε = 4,000 $M^{-1}cm^{-1}$ similar to the spectra of the Ln^{2+} complexes shown in eq 4.1. Time-dependent density functional theory (TDDFT) calculations on $[Sc(NR_2)_3]^{1-}$ with D_3 symmetry gave a nearly quantitative reproduction of the experimental spectrum with the observed absorption band

attributed to electronic excitations at 499 nm, 478 nm, and 633 nm, in descending order of oscillator strength (Figure 4.6). These excitations correspond to transitions from the Sc-based HOMO ($27a_1$ α) to low-lying unoccupied orbitals of a_2 and e irreducible representations. The weak transition at 633 nm is predominantly d→d, while the more intense ones at 499 nm and 478 nm have significant d→ligand character. This assignment is consistent with previous studies on $[Cp'_3Ln]^{1-}$[14-15,37-38] showing strong absorptions due to transitions from the metal-based HOMO to ligand-based orbitals.

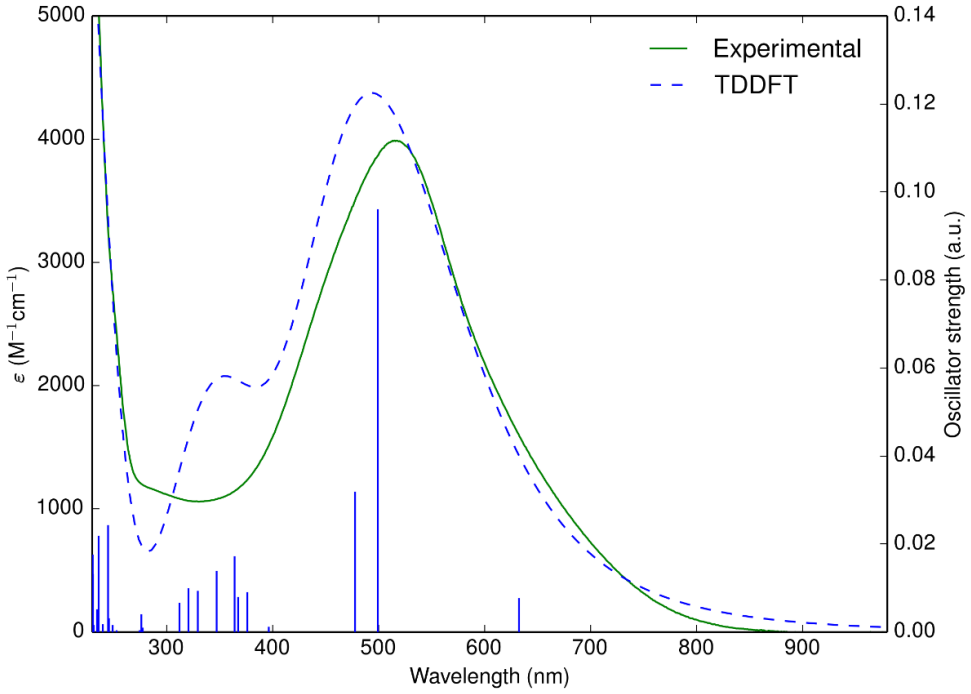

Figure 4.6. Experimental (solid) and simulated (dash) UV−visible spectra of $[K(crypt)][Sc(NR_2)_3]$, **2-K(crypt)**, in ~3 mM THF solution at room temperature. TDDFT excitations are shown as vertical lines.

The decomposition of **2-K(crypt)** was monitored by the decrease of the λ = 516 nm absorption at 2 h intervals with an initial ~3 mM concentration in THF. The plot of time vs

concentration, Figure 4.7, shows a ~28% decrease in concentration within 24 h. This demonstrates that **2-K(crypt)** is much more stable than [K(crypt)][$(C_5H_4SiMe_3)_3Lu$] since the latter shows 99% decomposition within 2 h. Determination of the rate constant of **2-K(crypt)** was complicated by the fact that it does not follow zero, first, or second-order decomposition rates. However, it was observed that when the sample was exposed to ambient light during the decomposition measurements, a faster decomposition of ~5% decrease within 4 h was observed.

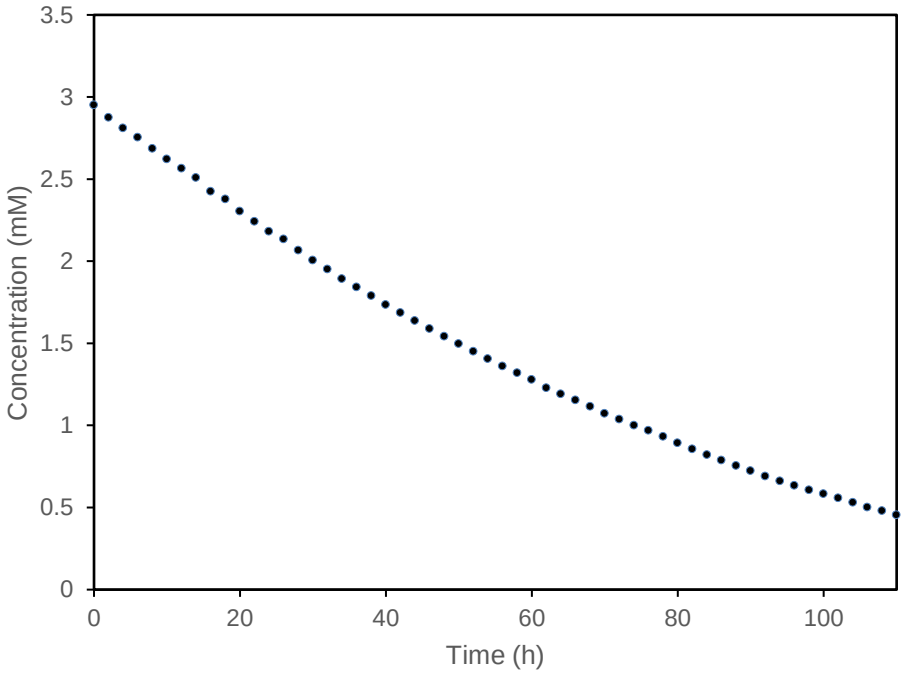

Figure 4.7. Decomposition plot of ~3 mM solution of [K(crypt)][$Sc(NR_2)_3$], **2-K(crypt)**, in THF at room temperature.

Since previous $Ln(NR_2)_3$ reductions under N_2 forms reduced dinitrogen complexes, eq 4.2, N_2 reduction studies with this scandium system were also pursued. Exposure of **2-K(crypt)** to N_2 by addition of THF/Et_2O to the crystalline solid inside an N_2 filled glovebox followed by cooling to −35 ºC consistently resulted in a dark maroon solution consistent with the Sc^{2+} species.

Performing reduction of the trivalent complex, **1**, in room temperature THF inside an N_2 glovebox also resulted in the formation of the Sc^{2+} complex. In fact, when no chelate, such as crypt or crown was used, the dark maroon solution of Sc^{2+} was still generated. This species is stable at room temperature for an extended period and only decomposed immediately to colorless when a nonpolar solvent like hexane was added. This suggests that the available THF molecules act as a stabilizing agent that binds K^{1+} in place of a chelate, but addition of hexane results in the dissociation of THF and the loss of the stabilizing effects. In comparison, this stabilization effect is not observed at all when Et_2O is used; the reduction in Et_2O under N_2 resulted in an unidentifiable pale-yellow solution that readily decomposed to colorless. A different scenario was observed when the reduction is performed under Ar since the dark maroon color can be generated in Et_2O without any chelating agent and is rather stable. This provided a hint that there was unique N_2 reactivity associated with the $[Sc(NR_2)_3]^{1-}$ system. This will be described further in Chapter 5.

Conclusion

A $Ln(NR_2)_3$ (R = $SiMe_3$) complex with the strongly donating amide ligands can be reduced to form isolable Ln^{2+} complexes in the case of the smallest rare-earth metal, scandium. This scandium system differs from its larger rare-earth metal analogs in that the Sc^{2+} complex, $[Sc(NR_2)_3]^{1-}$, **2**, does not readily react with N_2 to form an isolable $(N=N)^{2-}$ complex and can even be prepared under N_2. Previously, it was found that (a) strong field ligands like $(NR_2)^{1-}$ form $(N=N)^{2-}$ complexes in LnA_3/M reactions, but not isolable Ln^{2+} complexes, whereas (b) ligands like $[C_5H_4SiMe_3]^{1-}$ and $[C_5H_3(SiMe_3)_2]^{1-}$ give crystallographically-characterizable Ln^{2+} complexes, but not $(N=N)^{2-}$ complexes according to eq 3. This generalization clearly does not apply to scandium since the reduction of $Sc(NR_2)_3$, **1**, in THF under N_2 readily gave the Sc^{2+}

species, **2**, and the crypt complex, **2-K(crypt)**, has been shown to be very stable and does not reduce N_2.

Experimental

All manipulations and syntheses described below were conducted with rigorous exclusion of air and water using standard Schlenk line and glovebox techniques under an argon atmosphere. Solvents were sparged with UHP argon and dried by passage through columns containing Q-5 and molecular sieves prior to use. Deuterated NMR solvents were dried over NaK alloy, degassed by three freeze-pump-thaw cycles, and vacuum transferred before use. Potassium and cesium were purchased from Aldrich, washed with hexanes, and scraped to provide fresh surfaces before use. Potassium bis(trimethylsilyl)amide (KNR_2) was purchased from Aldrich, dissolved in toluene, centrifuged, decanted to remove tacky yellow insoluble material, and dried under reduced pressure before use. 2.2.2-Cryptand (crypt) was purchased from Merck and dried under reduced pressure before use. 18-Crown-6 (crown) was purchased from Aldrich and sublimed before use. ^{1}H NMR spectra were recorded on Bruker GN500 or CRYO500 MHz spectrometers (^{13}C NMR at 125 MHz) at 298 K referenced internally to residual protio-solvent resonances. EPR spectra were collected using a Bruker EMX spectrometer equipped with an ER041XG microwave bridge calibrated with DPPH. EPR simulations were performed as least-squares fits of the experimental spectra via the Nelder/Mead downhill simplex method using EasySpin.[39] Electronic absorption spectra were collected using a Varian Cary 50 Scan UV−visible spectrophotometer in THF at 298 K. IR samples were prepared as KBr pellets on a Jasco FT/IR-4700 - ATR-PRO ONE system. Elemental analyses were conducted on a Perkin-Elmer 2400 Series II CHNS elemental analyzer.

$Sc(NR_2)_3$, 1. Following previous literature procedures for the preparation of $Ln(NR_2)_3$ (R = $SiMe_3$) complexes,[40] $Sc(NR_2)_3$, **1**, was prepared by the reaction of $ScCl_3$ and KNR_2 in THF. Colorless single crystals of **1** suitable for X-ray diffraction were grown by slow evaporation of the Et_2O solution at room temperature overnight (**1a**) or by sublimation at 80 ºC under 10^{-3} torr over 2 days (**1b**). ^{1}H NMR (C_6D_6): δ 0.33 (s, Si*Me*$_3$, 54H). ^{13}C NMR (C_6D_6): δ 4.70 (Si*Me*$_3$). IR (cm^{-1}): 2952m, 2900w, 1248m, 951s, 835s, 779m, 756w, 674w, 663w, 629w, 613w. Anal. Calcd. for $C_{18}H_{54}N_3Si_6Sc$: C, 41.09; H, 10.35; N, 7.99. Found: C, 39.82; H, 10.52; N, 7.65. Low carbon values were obtained even after multiple analysis attempts using different batches of material that had been sublimed. This may be due to the high silicon content in **1**, as observed in other systems.[13]

[K(crypt)][$Sc(NR_2)_3$], 2-K(crypt). In a glovebox, a colorless solution of **1** (59 mg, 0.11 mmol) and crypt (39 mg, 0.10 mmol) in 5 mL of Et_2O was pre-chilled to −35 ºC and transferred to a scintillation vial containing a potassium smear and a glass stir bar. The reaction turned dark maroon after stirring for 5 min and was then stored at −35 ºC overnight. The solution was filtered, layered with pre-chilled hexane, and stored at −35 ºC. After 2 days, black/maroon solids formed and were separated from the mother liquor and dried under reduced pressure to yield [K(crypt)][$Sc(NR_2)_3$], **2-K(crypt)** (52 mg, 55%). Black single crystals of **2-K(crypt)** suitable for X-ray diffraction were grown from Et_2O/pentane at −35 ºC. IR (cm^{-1}): 2946m, 2884m, 2818w, 1478w, 1458w, 1445w, 1361m, 1354m, 1299w, 1261w, 1236m, 1135m, 1107s, 1079m, 987s, 952m, 934w, 869m, 831s, 775m, 752m, 701w, 663m, 611w. Anal. Calcd. for $C_{36}H_{90}KN_5O_6Si_6Sc$: C, 45.92; H, 9.63; N, 7.44. Found: C, 45.95; H, 9.56; N, 7.12.

[K(crown)][$Sc(NR_2)_3$], 2-K(crown). Similar to the preparation of **2-K(crypt)**, **1** (120 mg, 0.230 mmol) and crown (59 mg, 0.23 mmol) were reacted with a potassium smear to yield black/dark maroon solids of [K(crown)][$Sc(NR_2)_3$], **2-K(crown)**, (160 mg, 85%). Black single

crystals of **2-K(crown)** suitable for X-ray diffraction were grown from vapor diffusion of pentane into the Et_2O solution at −35 ºC. However, the collected data set provided connectivity only. IR (cm^{-1}): 2950m, 2898m, 1473w, 1457w, 1350m, 1285w, 1237s, 1110s, 985s, 965s, 870s, 833s, 777m, 754m, 700w, 663m, 610w. Anal. Calcd. for $C_{30}H_{78}KN_3O_6ScSi_6$: C, 43.44; H, 9.48; N, 5.07. Found: C, 43.82; H, 9.69; N, 4.96.

[Cs(crypt)][Sc(NR$_2$)$_3$], 2-Cs(crypt). Similar to the preparation of **2-K(crypt)**, **1** (105 mg, 0.199 mmol) and crypt (75 mg, 0.20 mmol) were reacted with a cesium smear to yield black/dark maroon solids of [Cs(crypt)][Sc(NR_2)$_3$], **2-Cs(crypt)**, (177 mg, 83%). Black single crystals of **2-Cs(crypt)** suitable for X-ray diffraction were grown from vapor diffusion of pentane into the Et_2O solution at −35 ºC. IR (cm^{-1}): 2954m, 2886m, 2816w, 1477w, 1460w, 1445w, 1352m, 1359m, 1298w, 1259m, 1236s, 1133m, 1107s, 1072m, 989s, 948s, 870s, 834s, 775w, 751w, 700w, 664m, 613w. Anal. Calcd. for $C_{36}H_{90}CsN_5O_6Si_6Sc$: C, 41.76; H, 8.76; N, 6.76. Found: C, 42.07; H, 8.68; N, 6.53.

X-ray Data Collection, Structure Solution, and Refinement for 1a. A colorless crystal of approximate dimensions 0.176 x 0.208 x 0.388 mm was mounted in a cryoloop and transferred to a Bruker SMART APEX II diffractometer. The APEX2[41] program package was used to determine the unit-cell parameters and for data collection (30 sec/frame scan time for a sphere of diffraction data). The raw frame data was processed using SAINT[42] and SADABS[43] to yield the reflection data file. Subsequent calculations were carried out using the SHELXTL[44] program. The centrosymmetric space group $P\bar{3}1c$ was assigned and later determined to be correct. The structure was solved by direct methods and refined on F^2 by full-matrix least-squares techniques. The analytical scattering factors[45] for neutral atoms were used throughout the analysis. The molecule was located on a site of 32 symmetry. Hydrogen atoms were included using a riding model. The

scandium atom was disordered and included with partial site-occupancy-factors. Least-squares analysis yielded wR2 = 0.2681 and Goof = 1.221 for 48 variables refined against 1309 data (0.80 Å), R1 = 0.1124 for those 1209 data with I > 2.0σ(I). There were several high residuals present in the final difference-Fourier map. It was not possible to determine the nature of the residuals although it was probable that diethyl ether and/or toluene solvents were present. The SQUEEZE[46] routine in the PLATON[47] program package was used to account for the electrons in the solvent accessible voids.

X-ray Data Collection, Structure Solution, and Refinement for 1b. A colorless crystal of approximate dimensions 0.118 x 0.233 x 0.281 mm was mounted in a cryoloop and transferred to a Bruker SMART APEX II diffractometer. The APEX2[41] program package and the CELL_NOW[48] were used to determine the unit-cell parameters. Data was collected using a 30 sec/frame scan time for a sphere of diffraction data. The raw frame data was processed using SAINT[42] and TWINABS[49] to yield the reflection data file (HKLF5 format)[49]. Subsequent calculations were carried out using the SHELXTL[44] program. The diffraction symmetry was 2/*m* and the systematic absences were consistent with the monoclinic space group $P2_1/c$ that was later determined to be correct. The structure was solved by direct methods and refined on F^2 by full-matrix least-squares techniques. The analytical scattering factors[45] for neutral atoms were used throughout the analysis. Hydrogen atoms were located form a difference-Fourier map and refined (x,y,z and U_{iso}). At convergence, wR2 = 0.0919 and Goof = 1.019 for 470 variables refined against 6613 data (0.80Å), R1 = 0.0378 for those 5381 with I > 2.0σ(I). The structure was refined as a two-component twin.

X-ray Data Collection, Structure Solution, and Refinement for 2-K(crypt). A black crystal of approximate dimensions 0.051 x 0.130 x 0.194 mm was mounted in a cryoloop and

transferred to a Bruker SMART APEX II diffractometer. The APEX2[41] program package was used to determine the unit-cell parameters and for data collection (60 sec/frame scan time for a sphere of diffraction data). The raw frame data was processed using SAINT[42] and SADABS[43] to yield the reflection data file. Subsequent calculations were carried out using the SHELXTL[44] program. There were no systematic absences nor any diffraction symmetry other than the Friedel condition. The centrosymmetric triclinic space group $P\bar{1}$ was assigned and later determined to be correct. The structure was solved by direct methods and refined on F^2 by full-matrix least-squares techniques. The analytical scattering factors[45] for neutral atoms were used throughout the analysis. Hydrogen atoms were included using a riding model. At convergence, wR2 = 0.1071 and Goof = 1.032 for 514 variables refined against 13641 data (0.75Å), R1 = 0.0401 for those 10885 data with $I > 2.0\sigma(I)$. There were several high residuals present in the final difference-Fourier map. It was not possible to determine the nature of the residuals although it was probable that diethylether or pentane solvent was present. The SQUEEZE[46] routine in the PLATON[47] program package was used to account for the electrons in the solvent accessible voids.

X-ray Data Collection, Structure Solution, and Refinement for 2-Cs(crypt). A black crystal of approximate dimensions 0.0.325 x 0.347 x 0.371 mm was mounted on a glass fiber and transferred to a Bruker SMART APEX II diffractometer. The APEX2[41] program package was used to determine the unit-cell parameters and for data collection (35 sec/frame scan time for a sphere of diffraction data). The raw frame data was processed using SAINT[42] and SADABS[43] to yield the reflection data file. Subsequent calculations were carried out using the SHELXTL[44] program. There were no systematic absences nor any diffraction symmetry other than the Friedel condition. The centrosymmetric triclinic space group $P\bar{1}$ was assigned and later determined to be correct. The structure was solved by direct methods and refined on F^2 by full-matrix least-squares

techniques. The analytical scattering factors[45] for neutral atoms were used throughout the analysis. Hydrogen atoms were included using a riding model. The scandium and several carbon atoms were disordered and included using multiple components with partial site-occupancy-factors. Least-squares analysis yielded wR2 = 0.3007 and Goof = 1.062 for 543 variables refined against 14072 data (0.73Å), R1 = 0.0875 for those 12390 data with $I > 2.0\sigma(I)$. There were several high residuals present in the final difference-Fourier map. It was not possible to determine the nature of the residuals although it was probable that diethylether and/or pentane solvent was present. The SQUEEZE[46] routine in the PLATON[47] program package was used to account for the electrons in the solvent accessible voids.

Computational Details

Density functional theory (DFT) calculations were performed by Guo P. Chen from the research group of Professor Filipp Furche using the hybrid meta- generalized gradient approximation (hybrid meta-GGA) functional TPSSh[50] with Grimme's D3 dispersion correction[51] and basis sets of triple-zeta plus polarization (def2-TZVP) quality.[52] Fine numerical grid of size m4[53] was used. The $Sc(NR_2)_3$ and $[Sc(NR_2)_3]^{1-}$ structures were optimized in C_1 and D_3 symmetry, respectively. The maximum norm of the Cartesian coordinate gradient was converged to $\leq 10^{-4}$ a.u. Vibrational normal mode analyses using numerical second derivatives were carried out to confirm that the optimized structures are minima on the nuclear potential energy surface. The electronic ground state of $Sc(NR_2)_3$ is closed-shell. For the spin-unrestricted calculation on the $^2A_1$ ground state of $[Sc(NR_2)_3]^{1-}$, the expectation value of $\hat{S}^2$ is 0.752, indicating negligible contamination. The structure of the monomeric unit of **6** was taken from the X-ray diffraction data without optimization. A single-point calculation was performed on the ^2A ground state, giving a $\hat{S}^2$ expectation value of 0.754. Solvent effects were included by the continuum solvation model

(COSMO)[54] with dielectric constant 7.52[55] and index of refraction 1.4050[56] of THF. All calculations were performed using TURBOMOLE 7.0 and 7.1.[57]

The UV−visible spectrum of $[Sc(NR_2)_3]^{1-}$ was simulated using time-dependent DFT (TDDFT) with the latest implementation of nonorthonormal Krylov subspace methods.[58] The gauge-invariant implementation of the TPSSh functional was employed.[59] def2-TZVP basis sets were used without diffuse functions because test calculations showed that a diffuse p function on Sc produced spurious unoccupied a_2 orbitals extending outside the COSMO cavity. def2-TZVP has been shown to provide accurate excitation energies in previous benchmark calculations.[60] Very fine numerical grid of size 5[53] was used in the TDDFT calculations. The absorption spectrum was simulated by superimposing Gaussian functions with an RMS width of 0.34 eV (Figure 4.6).

The excitation energies, oscillator strengths, and dominant orbital contributions of the lowest four electronic excitations of $[Sc(NR_2)_3]^{1-}$ are summarized in Table S8. The near-infrared excitation at 1221 nm lies outside of the experimental wavelength range and is not plotted. Pertinent orbitals are illustrated in Figures 4.8-4.11.

Table S8. Lowest electronic excitations of $[Sc(NR_2)_3]^{1-}$ computed using TPSSh functional and def2-TZVP basis sets. Oscillator strength are in length representation.

State	Wavelength (nm)	Oscillator Strength (10^{-2} a.u.)	Dominant contributions			Assignment
			occupied	unoccupied	% contribution	
1^2E	1221	0.005	$27a_1$ α	48e α	93.4	3d→3d
2^2E	633	0.75	$27a_1$ α	50e α	91.9	3d→3d
1^2A_2	499	9.59	$27a_1$ α	$25a_2$ α	98.9	3d→ligand/4p
3^2E	478	3.17	$27a_1$ α	49e α	98.8	3d→ligand

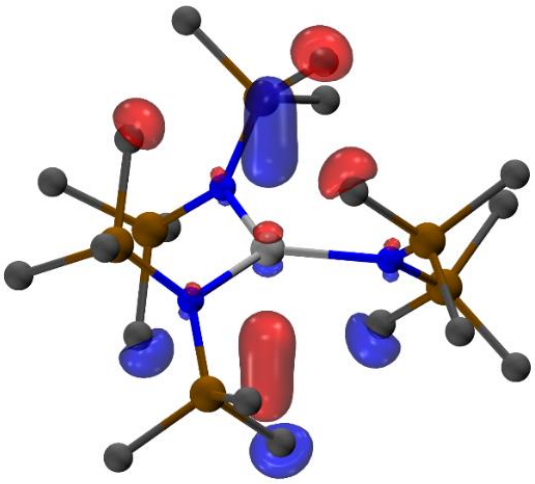

Figure 4.8. $25a_2$ α unoccupied orbital of $[Sc(NR_2)_3]^{1-}$ with a contour value of 0.045. Hydrogen atoms are omitted for clarity.

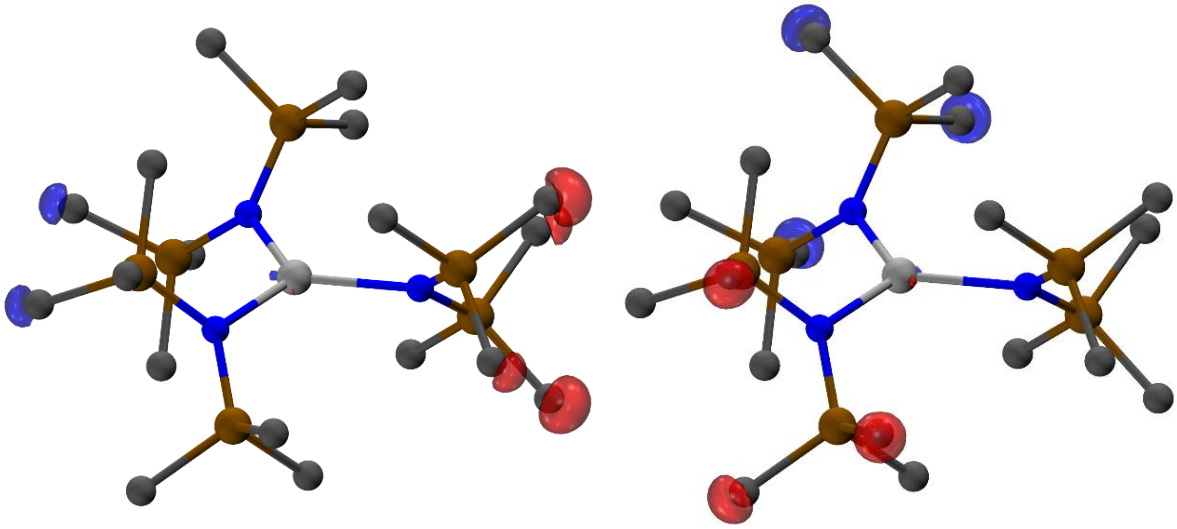

Figure 4.9. 49e α unoccupied orbitals of $[Sc(NR_2)_3]^{1-}$ with a contour value of 0.045. Hydrogen atoms are omitted for clarity.

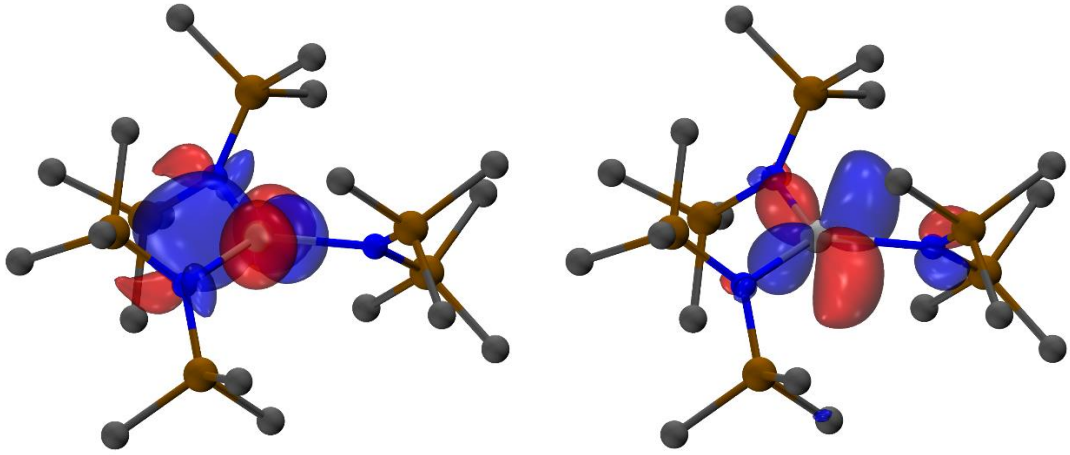

Figure 4.10. 50e α unoccupied orbitals of $[Sc(NR_2)_3]^{1-}$ with a contour value of 0.045. Hydrogen atoms are omitted for clarity.

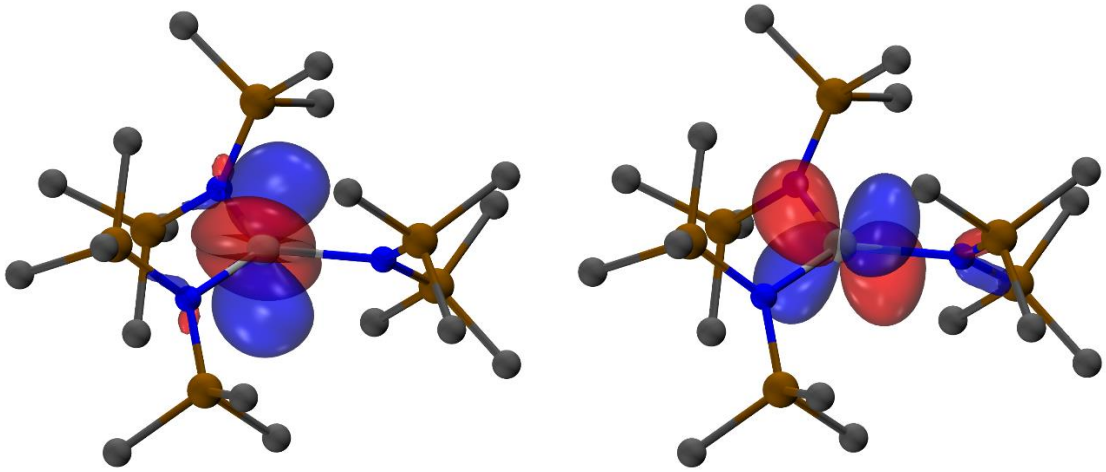

Figure 4.11. 48e α unoccupied orbitals of $[Sc(NR_2)_3]^{1-}$ with a contour value of 0.045. Hydrogen atoms are omitted for clarity.

References

(1) Burger, B. J.; Thompson, M. E.; Cotter, W. D.; Bercaw, J. E. *J. Am. Chem. Soc.* **1990**, *112*, 156-1577.

(2) Shapiro, P. J.; Schaefer, W. P.; Labinger, J. A.; Bercaw, J. E.; Cotter, W. D. *J. Am. Chem. Soc.* **1994**, *116*, 4623-4640.

(3) Sadow, A. D.; Tilley, T. D. *J. Am. Chem. Soc.* **2002**, *125*, 7971-7977.

(4) Sadow, A. D.; Tilley, T. D. *J. Am. Chem. Soc.* **2005**, *127*, 643-656.

(5) Barros, N.; Eisenstein, O.; Maron, L.; Tilley, T. D. *Organometallics* **2008**, *27*, 2252-2257.

(6) Demir, S.; Lorenz, S. E.; Fang, M.; Furche, F.; Meyer, G.; Ziller, J. W.; Evans, W. J. *J. Am. Chem. Soc.* **2010**, *132*, 11151-11158.

(7) Cloke, F. G. N.; Khan, K.; Perutz, R. N. *J. Chem. Soc., Chem. Commun.* **1991**, 1372-1373.

(8) Khan, K. D. *D. Phil.*, Univ of Sussex, 1992.

(9) Arnold, P. L.; Cloke, F. G. N.; Hitchcock, P. B.; Nixon, J. F. *J. Am. Chem. Soc.* **1996**, *118*, 7630-7631.

(10) Clentsmith, G. K. B.; Cloke, F. G. N.; Green, J. C.; Hanks, J.; Hitchcock, P. B.; Nixon, J. F. *Angew. Chem. Int. Ed.* **2003**, *42*, 1038-1041.

(11) Neculai, A. M.; Neculai, D.; Roesky, H. W.; Magull, J. *Organometallics* **2002**, *21*, 2590-2592.

(12) Polly L. Arnold; Cloke, F. G. N.; Nixon, J. F. *Chem. Commun.* **1998**, 797-798.

(13) Hitchcock, P. B.; Lappert, M. F.; Maron, L.; Protchenko, A. V. *Angew. Chem., Int. Ed.* **2008**, *47*, 1488-1491.

(14) MacDonald, M. R.; Bates, J. E.; Ziller, J. W.; Furche, F.; Evans, W. J. *J. Am. Chem. Soc.* **2013**, *135*, 9857-9868.

(15) Fieser, M. E.; MacDonald, M. R.; Krull, B. T.; Bates, J. E.; Ziller, J. W.; Furche, F.; Evans, W. J. *J. Am. Chem. Soc.* **2015**, *137*, 369-382.

(16) Evans, W. J. *Organometallics* **2016**, *35*, 3088-3100.

(17) Woen, D. H.; Evans, W. J. In *Handbook on the Physics and Chemistry of Rare Earths*; Bünzli, J.-C. G., Pecharsky, V. K., Eds.; Elsevier: Amsterdam, 2016; Vol. 50, p 337-394.

(18) Shannon, R. *Acta Crystallog., Sect. A* **1976**, *32*, 751-767.

(19) Peterson, J. K.; MacDonald, M. R.; Ziller, J. W.; Evans, W. J. *Organometallics* **2013**, *32*, 2625-2631.

(20) Atwood, J. L.; Smith, K. D. *J. Am. Chem. Soc.* **1973**, *95*, 1488-1491.

(21) Ghotra, J. S.; Hursthouse, M. B.; Welch, A. J. *J. Chem. Soc., Chem. Commun.* **1973**, 669-670.

(22) Evans, W. J.; Lee, D. S.; Ziller, J. W. *J. Am. Chem. Soc.* **2004**, *126*, 454-455.

(23) Evans, W. J.; Lee, D. S.; Rego, D. B.; Perotti, J. M.; Kozimor, S. A.; Moore, E. K.; Ziller, J. W. *J. Am. Chem. Soc.* **2004**, *126*, 14574-14582.

(24) Evans, W. J.; Rego, D. B.; Ziller, J. W. *Inorg. Chem.* **2006**, *45*, 10790-10798.

(25) Fang, M.; Bates, J. E.; Lorenz, S. E.; Lee, D. S.; Rego, D. B.; Ziller, J. W.; Furche, F.; Evans, W. J. *Inorg. Chem.* **2011**, *50*, 1459–1469.

(26) Fieser, M. E. *D. Phil.*, University of California, Irvine, 2015.

(27) Fang, M.; Lee, D. S.; Ziller, J. W.; Doedens, R. J.; Bates, J. E.; Furche, F.; Evans, W. J. *J. Am. Chem. Soc.* **2011**, *133*, 3784-3787.

(28) Evans, W. J.; Johnston, M. A.; Clark, R. D.; Anwander, R.; Ziller, J. W. *Polyhedron* **2001**, *20*, 2483-2490.

(29) Tilley, T. D.; Andersen, R. A.; Zalkin, A. *Inorg. Chem.* **1984**, *23*, 2271-2276.

(30) Rees, W. S. J.; Just, O.; VanDerveer, D. S. *J. Mater. Chem.* **1999**, *9*, 249-252.

(31) Herrmann, W. A.; Anwander, R.; Munck, F. C.; Scherer, W.; Dufaud, V.; Huber, N. W.; Artus, G. R. J. *Z. Naturforsch.* **1994**, *49*, 1789-1797.

(32) Westerhausen, M.; Hartmann, M.; Pfitzner, A.; Schwarz, W. *Z. Anorg. Allg. Chem.* **1995**, *621*, 837-850.

(33) Niemeyer, M. *Z. Anorg. Allg. Chem.* **2002**, *628*, 647-657.

(34) Brady, E. D.; Clark, D. L.; Gordon, J. C.; Hay, P. J.; Keogh, D. W.; Poli, R.; Scott, B. L.; Watkin, J. G. *Inorg. Chem.* **2003**, *42*, 6682-6690.

(35) Hitchcock, P. B.; Hulkes, A. G.; Lappert, M. F.; Li, Z. *Dalton Trans.* **2004**, 129-136.

(36) Scarela, G.; Wiemera, C.; Fanciullia, M.; Fedushkinb, I. L.; Fukinb, G. K.; Domrachevb, G. A.; Lebedinskiic, Y.; Zenkevichc, A.; Paviad, G. *Z. Anorg. Allg. Chem.* **2007**, *633*, 2097-2103.

(37) MacDonald, M. R.; Bates, J. E.; Fieser, M. E.; Ziller, J. W.; Furche, F.; Evans, W. J. *J. Am. Chem. Soc.* **2012**, *134*, 8420-8423.

(38) MacDonald, M. R.; Fieser, M. E.; Bates, J. E.; Ziller, J. W.; Furche, F.; Evans, W. J. *J. Am. Chem. Soc.* **2013**, *135*, 13310-13313.

(39) Stoll, S.; Schweiger, A. J. *Magn. Reson.* **2006**, *178*, 42.

(40) Edelmann, F. T. In *Synthetic Methods of Organometallics and Inorganic Chemistry*; Herrmann, W. A., Ed.; Thieme Verlag Stuttgart: New York, 1997; Vol. 6, p 37-40.

(41) Bruker AXS, Inc., APEX2 Version 2014.11-0, Madison, WI, **2014**.

(42) Bruker AXS, Inc., SAINT Version 8.34a, Madison, WI, **2013**.

(43) Sheldrick, G. M.; SADABS, Version 2014/5, Bruker AXS, Inc., Madison, WI, **2014**.

(44) Sheldrick, G. M.; SHELXTL, Version 2014/7, Bruker AXS, Inc., Madison, WI, **2014**.

(45) *International Tables for Crystallography, Vol. C*, Kluwer Academic Publishers, Dordrecht, **1992**.

(46) Spek, A. L. *Acta Cryst.* **2015**, *C17*, 9-19.

(47) Spek, A. L. *Acta Cryst.* **2009**, *D65*, 148-155.

(48) Sheldrick, G. M.; CELL_NOW, Version 2008/4, Bruker AXS, Inc., Madison, WI, **2008**.

(49) Sheldrick, G. M.; TWINABS, Version 2012/1, Bruker AXS, Inc., Madison, WI, **2012**.

(50) Staroverov, V. N.; Scuseria, G. E.; Tao, J.; Perdew, J. P. *J. Chem. Phys.* **2003**, *119*, 12129.

(51) Grimme, S. *J. Comput. Chem.* **2006**, *27*, 1787-1799.

(52) Weigend, F.; Ahlrichs, R. *Phys. Chem. Chem. Phys.* **2005**, *7*, 3297-3305.

(53) Treutler, O.; Ahlrichs, R. *J. Chem. Phys.* **1995**, *102*, 346.

(54) Klamt, A.; Schüürmann, G. *J. Chem. Soc., Perkin Trans. 2* **1993**, 799-805.

(55) In *CRC Handbook of Chemistry and Physics*; Lide, D. R., Ed.; CRC Press: Boca Raton, FL, 2008; Vol. 88, p 136-136.

(56) In *CRC Handbook of Chemistry and Physics*; Lide, D. R., Ed.; CRC Press: Boca Raton, FL, 2008; Vol. 88, p 474-474.

(57) Furche, F.; Ahlrichs, R.; Hättig, C.; Klopper, W.; Sierka, M.; Weigend, F. *WIREs Comput Mol Sci* **2014**, *4*, 91-100.

(58) Furche, F.; Krull, B. T.; Nguyen, B. D.; Kwon, J. *J. Chem. Phys.* **2016**, *144*, 174105.

(59) Bates, J. E.; Furche, F. *J. Chem. Phys.* **2012**, *137*, 164105.

(60) Send, R.; Kühn, M.; Furche, F. *J. Chem. Theory Comput.* **2011**, *7*, 2376-2386.

CHAPTER 5

End-on Bridging Dinitrogen Complex of Scandium

Introduction*

The reduction of the Ln^{3+} bis(trimethylsilylamide) complexes, $Ln(NR_2)_3$ (R = $SiMe_3$), under dinitrogen at room temperature reliably provided side-on bridging dinitrogen complexes across the rare-earth metal series with crystal structures of $[(R_2N)_2Ln(THF)]_2[\mu\text{-}\eta^2\text{:}\eta^2\text{-}N_2]$, eq 5.1.[1-2] It was postulated that these reactions proceeded through a transient Ln^{2+} intermediate

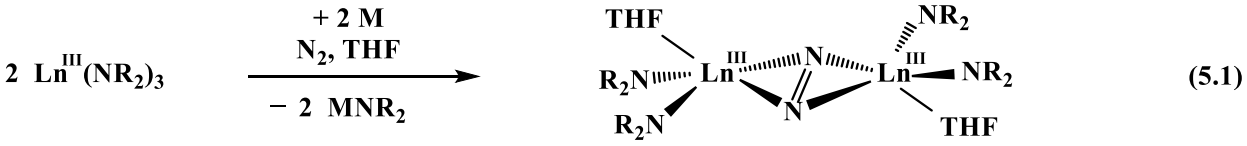

followed by the loss of one $(NR_2)^{1-}$ ligand per metal, and finally, the formation of a neutral bimetallic complex bridged by an $(N{=}N)^{2-}$ moiety in a planar side-on bridging mode. The $(\mu\text{-}\eta^2\text{:}\eta^2\text{-}N_2)^{2-}$ structural motif had been a hallmark of rare-earth metal dinitrogen chemistry since its first discovery in 1988 with $[(C_5Me_5)_2Sm]_2[\mu\text{-}\eta^2\text{:}\eta^2\text{-}N_2]$.[3] Since then, over 40 side-on bridging dinitrogen rare earth metal complexes had been reported in the Cambridge Structural Database (CSD)[1-2,4-21] and no other dinitrogen binding mode had been observed with these metals.

For scandium, a reduced dinitrogen complex having this side-on bridging motif, $[(C_5Me_4H)_2Sc]_2[\mu\text{-}\eta^2\text{:}\eta^2\text{-}N_2]$, was reported in 2010 by the Evans group from the reduction of the heteroleptic Sc^{3+} complex, $(C_5Me_4H)_2Sc(\mu\text{-}\eta^1\text{-}Ph)BPh_3$, under dinitrogen, eq 5.2. This reaction

* Portions of this chapter have been published: Woen, D. H.; Chen, G. P.; Ziller, J. W.; Boyle, T. J.; Furche, F.; Evans, W. J. *J. Am. Chem. Soc.* **2017**, *139*, 14861–14864. DOI: 10.1021/jacs.7b08456

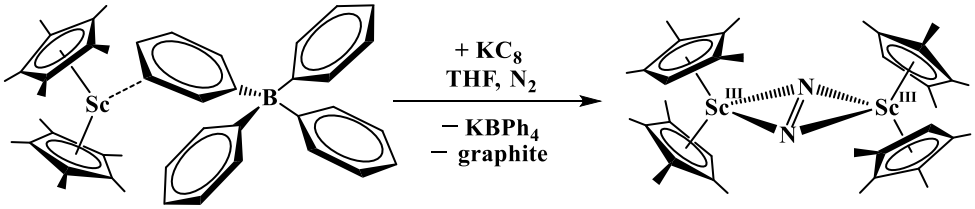

(5.2)

to form dinitrogen complexes with $(C_5Me_4H)^{1-}$ ancillary ligands was also achievable with other rare earth metals, and similarly, proceeded through the loss of an anionic ligand, $(BPh_4)^{1-}$. Since it had been established that the reduction of $Ln(NR_2)_3$ readily formed side-on bridging dinitrogen complexes and that scandium could form this side-on bridging motif with another ligand system, it was expected that the reduction of $Sc(NR_2)_3$ would form the side-on bridging dinitrogen complex, $[(R_2N)_2Sc(THF)]_2[\mu\text{-}\eta^2\text{:}\eta^2\text{-}N_2]$.

However, as described in Chapter 4, the reduction of $Sc(NR_2)_3$ under dinitrogen at room temperature consistently generated a dark maroon species identified as the Sc^{2+} complex, $[Sc(NR_2)_3]^{1-}$, **1**. Exposure of the isolated Sc^{2+} complex, $[K(crypt)][Sc(NR_2)_3]$ (crypt = 2.2.2-cryptand), **1-crypt**, to dinitrogen also did not produce the expected $(N{=}N)^{2-}$ complex. This lack of apparent reactivity was associated with the high stability of the Sc^{2+} complex. This Chapter describes further examination of this system using other reduction conditions, which lead to the isolation of a reduced dinitrogen complex with a unique end-on bridging motif rather than the conventional side-on structure.

Results and Discussion

In the absence of ambient light and at −35 °C, the reduction of $Sc(NR_2)_3$ in Et_2O using K smear in the presence of crypt under dinitrogen generates orange crystals which, were identified by X-ray crystallography as $\{K(crypt)\}_2\{[(NR_2)_3Sc]_2[\mu\text{-}\eta^1\text{:}\eta^1\text{-}N_2]\}$, **2-crypt**, Figure 5.1, Scheme 5.1. The **2-crypt** complex is the first rare-earth metal complex that contains an end-on bridging

dinitrogen ligand and was isolated in 35% yield. Each Sc^{3+} ion retains all three of the anionic amide ligands from the starting material. Hence, the complex is isolated as a dianion with two K^+ countercations. In contrast, the $Ln(NR_2)_3$/K reaction, eq 5.1, involves loss of one amide ligand per

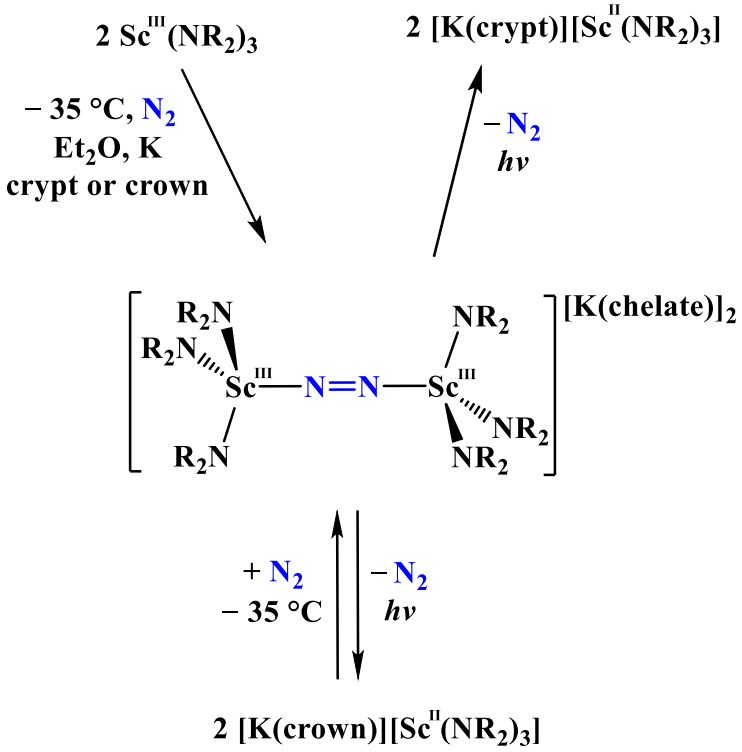

Scheme 5.1. Scandium dinitrogen reactivity (chelate = crypt or crown).

metal center to generate KNR_2 as a co-product while forming the neutral side-on product, $[(R_2N)_2Ln(THF)]_2[\mu\text{-}\eta^2\text{:}\eta^2\text{-}N_2]$.[1-2] The tris(amide) dianion motif of **2-crypt** has been previously observed in the oxalate complexes, $\{K_2(crown)_3\}\{[(R_2N)_3Sc]_2(\mu\text{-}C_2O_4\text{-}\kappa^1O\text{:}\kappa^1O'')\}$[22] and $[(X_3Ti)_2(\mu\text{-}C_2O_4\text{-}\kappa^1O\text{:}\kappa^1O'')]$ [X = N(ᵗBu)(3,5-dimethylanilide)].[23]

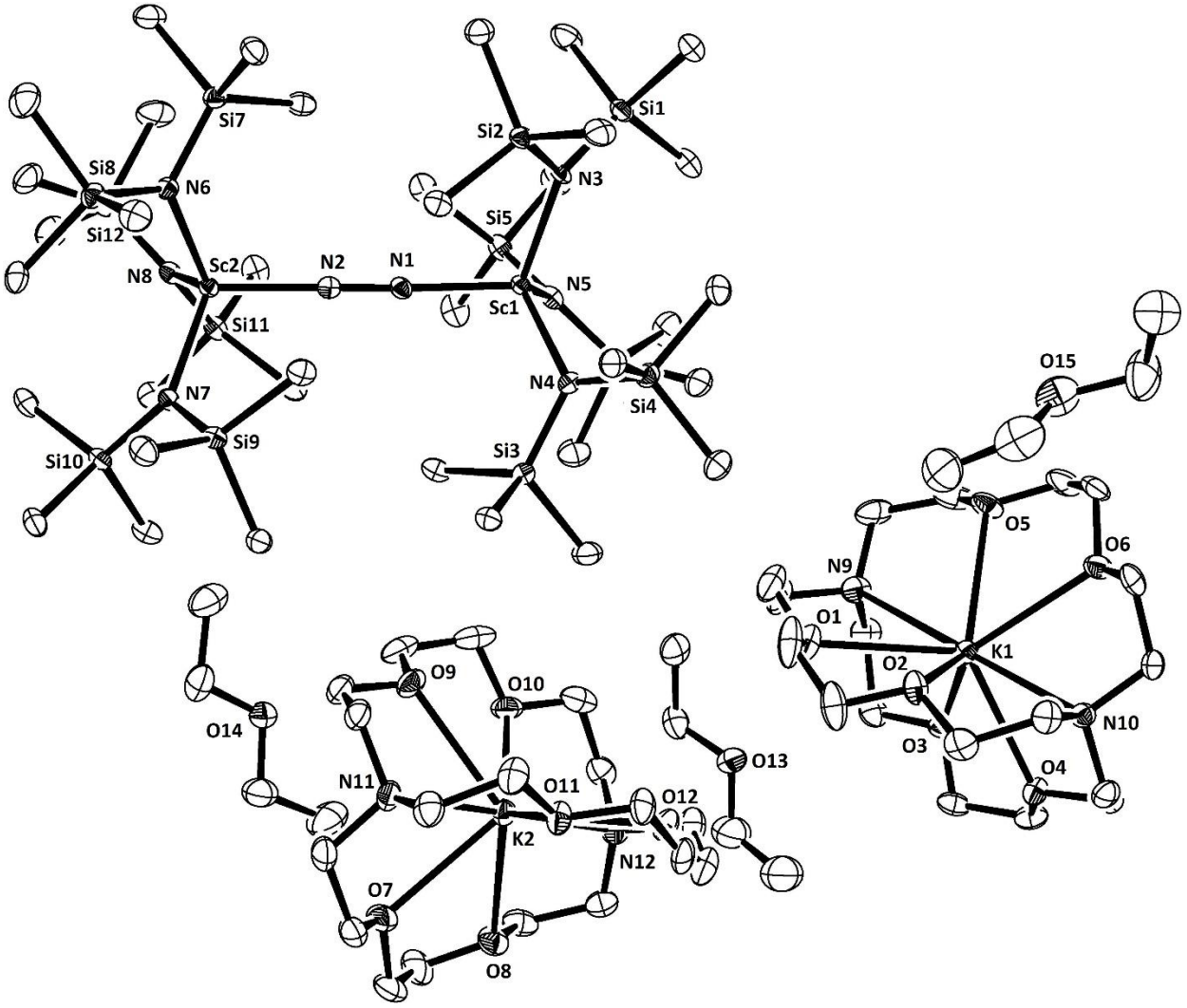

Figure 5.1. Thermal ellipsoid plot of $\{K(crypt)\}_2\{[(NR_2)_3Sc]_2[\mu\text{-}\eta^1\text{:}\eta^1\text{-}N_2]\}$, **2-crypt**, drawn at 50% probability. Hydrogen atoms are omitted for clarity.

The 1.221(3) Å N(1)–N(2) distance in **2-crypt** is in the double bond range[24] consistent with an $(N=N)^{2-}$ ligand and can be compared to the 1.258(3)-1.305(6) Å range in $[(R_2N)_2Ln(THF)]_2[\mu_2\text{-}\eta^2\text{:}\eta^2\text{-}N_2]$ complexes of eq 5.1.[1-2] The only previously-reported dinitrogen complex of Sc, the side-on complex, $[(C_5Me_4H)_2Sc]_2[\mu\text{-}\eta^2\text{:}\eta^2\text{-}N_2]$, **3**,[20] eq 5.2, has a 1.239(3) Å N–N bond length and 2.2161(1)-2.220(1) Å Sc–N(N_2) distances. The 2.032(3) Å and 2.030(3) Å Sc–N(N_2) distances

are noticeably shorter than the 2.143(2)-2.161(2) Å Sc–N(NR_2) distances, which suggests a stronger interaction between the metal centers and the bridging $(N=N)^{2-}$ ligand than with the terminal NR_2 ligands. In comparison, the Sc–N(NR_2) distances in the Sc^{3+} precursor, $Sc(NR_2)_3$, are 2.048(2)-2.057(2) Å.[25]

Density functional theory (DFT) calculations by Guo P. Chen from the research group of Professor Filipp Furche on the dianion $\{[(R_2N)_3Sc]_2[\mu\text{-}\eta^1\text{:}\eta^1\text{-}N_2]\}^{2-}$, **2**, reproduced the experimentally observed structure of **2-crypt** with an N–N distance of 1.202 Å. The calculations indicate a triplet ($^3A_2$) ground state in D_3 symmetry with two unpaired electrons in the HOMOs consisting of two degenerate orbitals that are mainly N_2 π^* in character, but have Sc–N_2–Sc π bonding components, Figure 5.2. The ^{1}H NMR and ^{13}C NMR spectra show no resonances for the Si*Me*$_3$ groups, which is consistent with the paramagnetism of the complex. The measured magnetic moment (Evans method[26-27]), $\mu_{eff} = 2.3\ \mu_B$, is larger than the spin-only value of $\mu_{eff} = 1.73\ \mu_B$ for one unpaired electron and smaller than the $\mu_{eff} = 2.83\ \mu_B$ for two unpaired electrons. Triplet $(N_2)^{2-}$ moieties are known in end-on dinitrogen complexes of transition metals such as in the dimolybdenum complex, $[(Ar[^tBu]N)_3Mo]_2(\mu\text{-}\eta^1\text{:}\eta^1\text{-}N_2)$, **3**,[28] and the diiron complex, $L^{Me}FeNNFeL^{Me}$ (L^{Me} = β-diketiminate with R = CH_3), **4**,[29] Figure

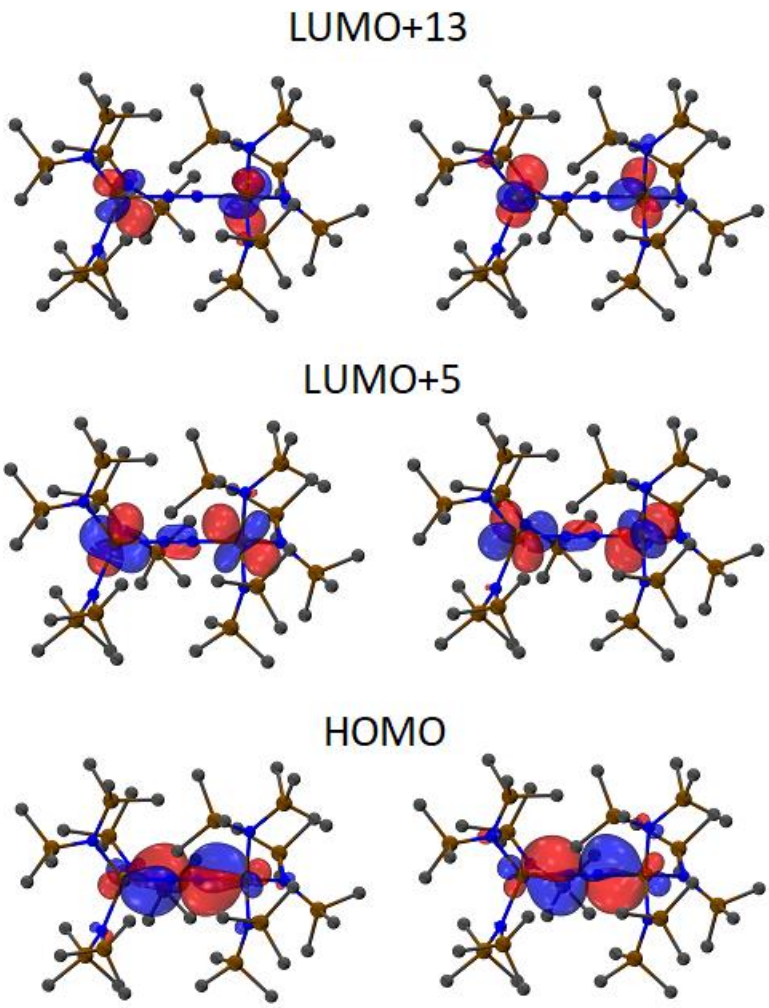

Figure 5.2. HOMO, LUMO+5, and LUMO+13 of $\{[(NR_2)_3Sc]_2[\mu\text{-}\eta^1\text{:}\eta^1\text{-}N_2]\}^{2-}$, **2**, with a contour value of 0.045. Hydrogen atoms are omitted for clarity.

The UV−visible spectrum of **2-crypt** exhibits an intense absorption at 406 nm (14,000 M^{-1} cm^{-1}), Figure 3. Time-dependent DFT (TD-DFT) calculations attribute this absorption to electronic excitations at 364 nm and 408 nm, Figure 5.3. Both of these contain large contributions due to transitions from the degenerate Sc–N_2–Sc π bonding orbitals (96e α, HOMO) to the Sc–N_2–Sc π anti-bonding orbitals (99e α, LUMO+5) and two degenerate orbitals that are of Sc d character (104e α, LUMO+13).

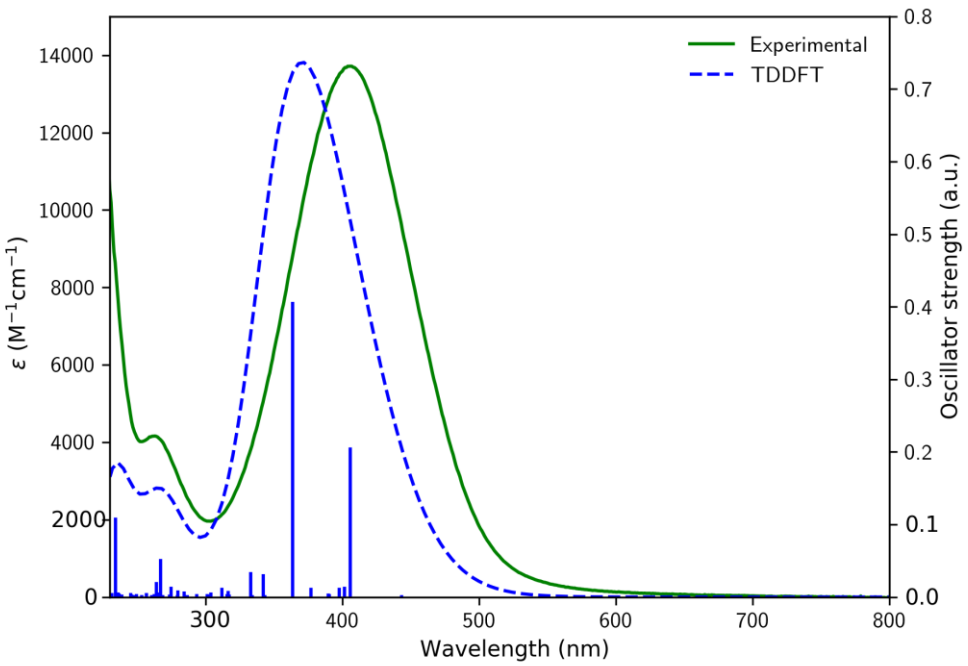

Figure 5.3. Experimental (green solid-line) and TDDFT calculated (blue dashed-line) UV−visible spectra of $\{K(crypt)\}_2\{[(NR_2)_3Sc]_2[\mu\text{-}\eta^1\text{:}\eta^1\text{-}N_2]\}$, **2-crypt**, collected from a ca. 1 mM THF solution.

Brief exposure of **2-crypt** to UV light (365 nm), even at −78 °C, results in the loss of N_2, Scheme 5.1, to form the dark maroon $3d^1$ Sc^{2+} complex, **1-crypt**, described in Chapter 4, Figure 5.4. Such conversion is not commonly observed in rare-earth metal dinitrogen chemistry: with the exception of Sm^{3+} dinitrogen complexes,[1,8] once an $(N{=}N)^{2-}$ complex of a Ln^{3+} ion is formed, e.g. as in eq 5.1 and 5.2, it does not revert to Ln^{2+} and N_2. This photo-conversion is consistent with the TD-DFT calculations, which show that the transitions populate Sc–N_2–Sc anti-bonding orbitals and Sc 3d orbitals. In contrast, $[(C_5Me_4H)_2Sc]_2[\mu\text{-}\eta^2\text{:}\eta^2\text{-}N_2]$,[20] synthesized by the reduction of $(C_5Me_4H)_2Sc(\mu\text{-}\eta^1\text{-}Ph)BPh_3$ under dinitrogen, has only weak absorptions in its UV−visible spectrum at 592 nm (ε = 60 M^{-1} cm^{-1}) and 447 nm (ε = 200 M^{-1} cm^{-1}) and does not

form a Sc^{2+} complex photochemically. Complexes $[(Ar[^tBu]N)_3Mo]_2(\mu\text{-}\eta^1\text{:}\eta^1\text{-}N_2)$, **3**,[28] and $L^{Me}FeNNFeL^{Me}$, **4**,[29] described above, also extrude dinitrogen upon photolysis.[28-29]

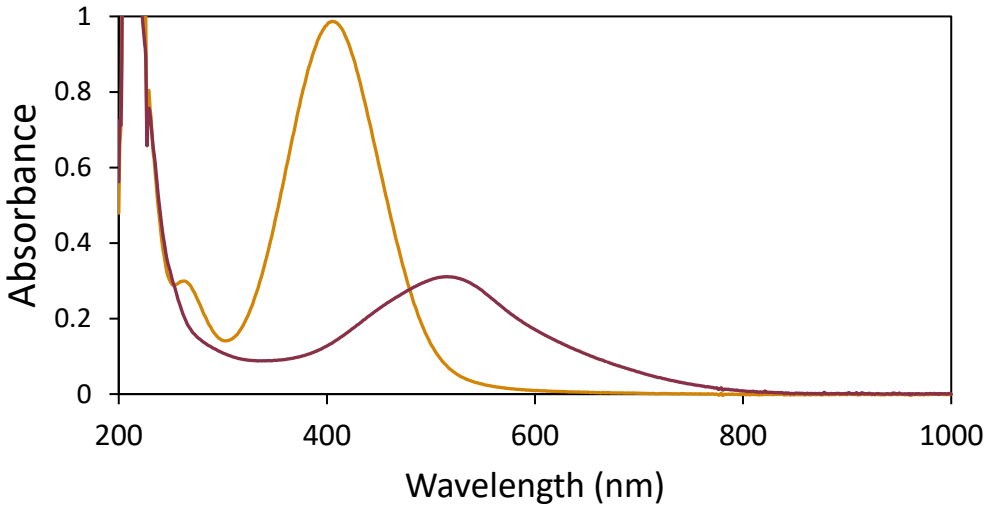

Figure 5.4. UV−visible spectra of **2-crypt** (orange, λ_{max} = 406 nm) and its decomposition product after exposure to UV light (maroon, λ_{max} = 516 nm), which is consistent with that of the previously reported **1-crypt**.[2]

The light sensitivity of **2-crypt** was also observed during Raman measurements. A Raman spectrum of **2-crypt** could not be obtained due to sample decomposition using the 532 nm laser previously used to analyze over 20 other rare-earth metal dinitrogen complexes.[21] However, the use of a lower-energy 785 nm laser provided a Raman scattering signal at 1644 cm^{-1} for **2-crypt**, Figure 5.5. The DFT calculated value of 1676 cm^{-1} matches the experimental value at the level previously observed for rare-earth metal dinitrogen complexes.[21] This stretching frequency is noticeably higher than the 1413-1473 cm^{-1} range observed for the side-on dinitrogen bridged complexes of rare-earth metals, which indicates a lower degree of dinitrogen activation. DFT calculations were also carried out on the hypothetical neutral side-on bound dinitrogen complex

with two amide ligands per metal, i.e. $[(R_2N)_2Sc(THF)]_2[\mu\text{-}\eta^2\text{:}\eta^2\text{-}N_2]$, and the dianionic side-on analog of **2**, $\{[(R_2N)_3Sc]_2[\mu\text{-}\eta^2\text{:}\eta^2\text{-}N_2]\}^{2-}$. The calculations suggest that the N-N stretching frequencies should be below 1550 cm^{-1} for these side-on complexes, Table 5.1.

Table 5.1. Structural parameters of $\{[(NR_2)_3Sc]_2[\mu\text{-}\eta^1\text{:}\eta^1\text{-}N_2]\}^{2-}$, **2**, and the side-on complexes $\{[(NR_2)_3Sc]_2[\mu\text{-}\eta^2\text{:}\eta^2\text{-}N_2]\}^{2-}$ and $[(NR_2)_2Sc(THF)]_2[\mu\text{-}\eta^2\text{:}\eta^2\text{-}N_2]$. Bond distances are reported in Å, while the N-N stretching frequencies are reported as wavenumbers in cm^{-1}.

Compound	Method	N-N distance	Average Sc-N(N_2) distance	Average Sc-N(NR_2) distance	N-N stretching frequency
$\{[(NR_2)_3Sc]_2[\mu\text{-}\eta^1\text{:}\eta^1\text{-}N_2]\}^{2-}$	Expt. (**2-crypt**)	1.221	2.031	2.150	1644
	TPSS/def2-SV(P)	1.207	2.044	2.160	1724
	TPSS/def2-TZVP	1.202	2.045	2.160	1676
$\{[(NR_2)_3Sc]_2[\mu\text{-}\eta^2\text{:}\eta^2\text{-}N_2]\}^{2-}$	TPSS/def2-SV(P)	1.240	2.229	2.195	1542
$[(NR_2)_2Sc(THF)]_2[\mu\text{-}\eta^2\text{:}\eta^2\text{-}N_2]$	TPSS/def2-SV(P)	1.245	2.182	2.079	1520

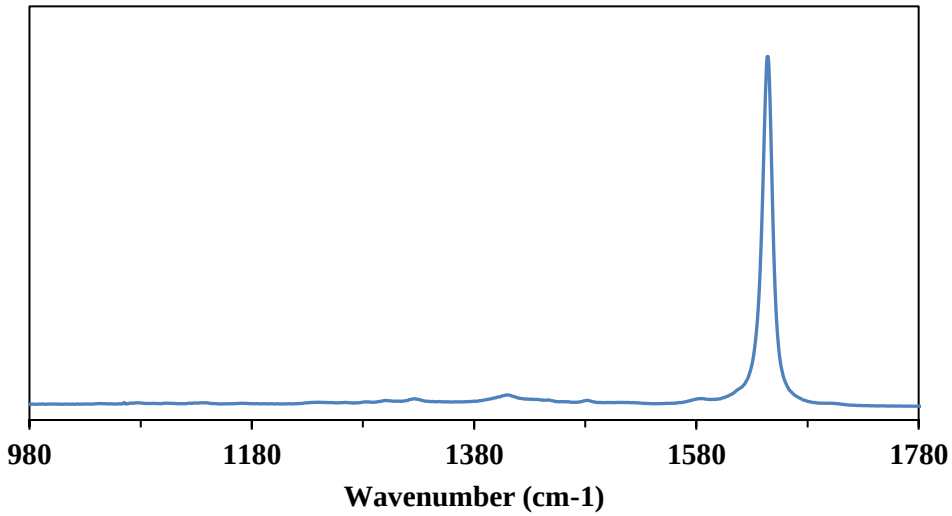

Figure 5.5. Raman Spectrum of $\{K(crypt)\}_2\{[(NR_2)_3Sc]_2[\mu\text{-}\eta^1\text{:}\eta^1\text{-}N_2]\}$, **2-crypt**.

These calculations also reveal that the hypothetical $\{[(R_2N)_3Sc]_2[\mu\text{-}\eta^2\text{:}\eta^2\text{-}N_2]\}^{2-}$ is 12 kcal/mol higher in energy than **2**. The preference for the end-on binding motif is likely caused by the steric constraint of the three ancillary ligands. The influence of ancillary ligand size on the binding mode of $(N{=}N)^{2-}$ has previously been observed with cyclopentadienyl Ti and Zr complexes. The pair $[(C_5Me_4H)_2Ti]_2[\mu\text{-}\eta^1\text{:}\eta^1\text{-}N_2]$[30] and $[(C_5Me_3H_2)_2Ti]_2[\mu\text{-}\eta^2\text{:}\eta^2\text{-}N_2]$.[31-32] as well as $[(C_5Me_5)_2Zr]_2[\mu\text{-}\eta^1\text{:}\eta^1\text{-}N_2]$[33] and $[(C_5Me_4H)_2Zr]_2[\mu\text{-}\eta^2\text{:}\eta^2\text{-}N_2]$[34] illustrate this point. The small size and high Lewis acidity of Sc^{3+} could be responsible for the retainment of all three ancillary anionic amide ligands per metal. This ligand environment is sterically more crowded than the bis(amide)(THF) coordination in $[(R_2N)_2Ln(THF)]_2[\mu_2\text{-}\eta^2\text{:}\eta^2\text{-}N_2]$ and an end-on structure results in **2-crypt**.

Multiple attempts to demonstrate that isolated **1-crypt** reduces N_2 to form **2-crypt** to establish the reversibility of the cycle of the dinitrogen binding were unsuccessful. However, reduction of dinitrogen by a Sc^{2+} amide complex was achievable with the 18-crown-6 (crown) variant, $[K(crown)][Sc(NR_2)_3]$, **1-crown**. A dark maroon Et_2O solution of **1-crown** in the presence of N_2 at −35 °C produces orange crystals by Et_2O/hexane diffusion. X-ray diffraction revealed that these are the crown analog of **2-crypt**, namely, $\{K(crown)\}_2\{[(NR_2)_3Sc]_2[\mu\text{-}\eta^1\text{:}\eta^1\text{-}N_2]\}$, **2-crown**, Figure 5.6, Scheme 5.1. This complex can also be synthesized following the procedure for **2-crypt**, and the Raman, Figure 5.7, as well as the UV−visible spectrum, Figure 5.8, are identical to those of **2-crypt**. In addition, **2-crown** can be converted to the Sc^{2+} complex, **1-crown**,[25] by exposure to UV light. This demonstrates the reversibility of the dinitrogen binding with this Sc^{3+}/Sc^{2+} system, Scheme 5.1.

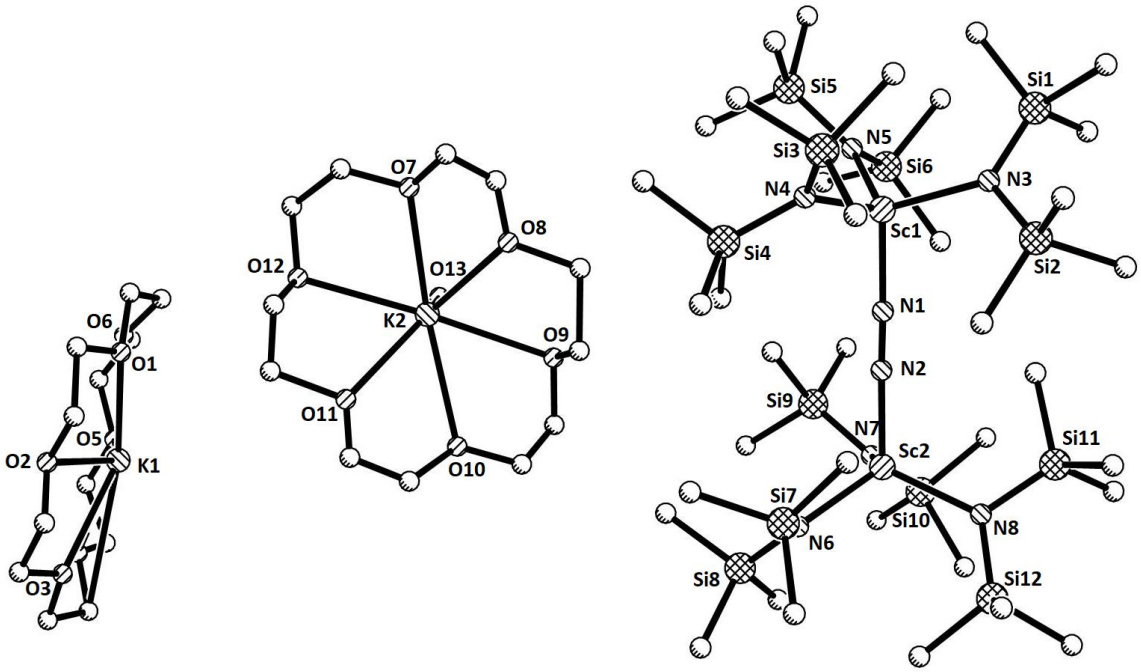

Figure 5.6. Ball and stick representation of $\{K(crown)\}_2\{[(NR_2)_3Sc]_2[\mu\text{-}\eta^1\text{:}\eta^1\text{-}N_2]\}$,**2-crown**. Hydrogen atoms are omitted for clarity.

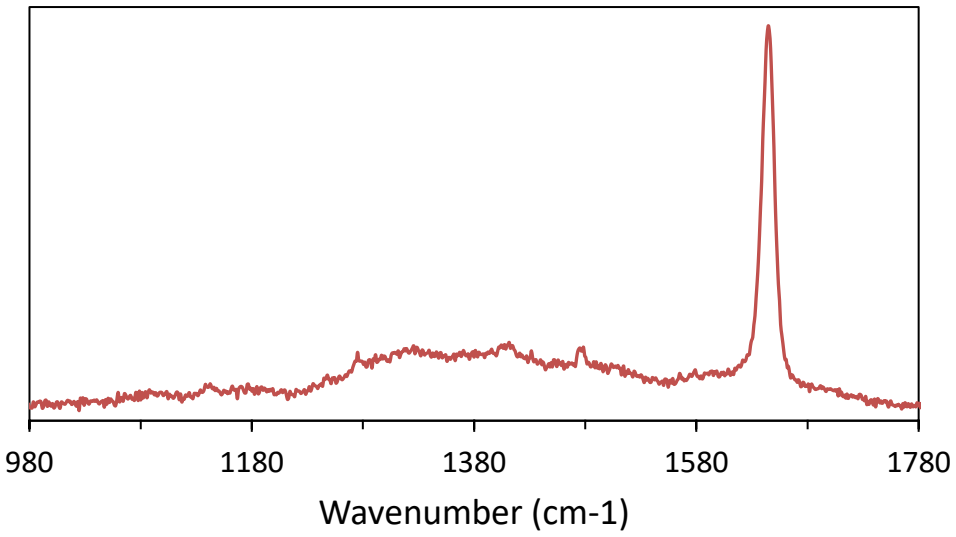

Figure 5.7. Raman Spectrum of $\{K(crown)\}_2\{[(NR_2)_3Sc]_2[\mu\text{-}\eta^1\text{:}\eta^1\text{-}N_2]\}$,**2-crown** (brown).

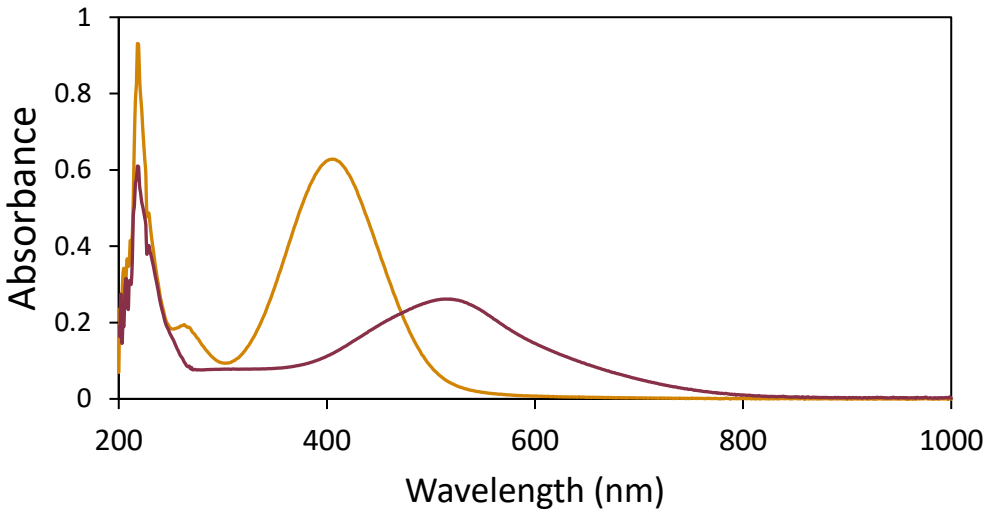

Figure 5.8. UV−visible spectra of $\{K(crown)\}_2\{[(NR_2)_3Sc]_2[\mu\text{-}\eta^1\text{:}\eta^1\text{-}N_2]\}$, **2-crown** (green, λ_{max} = 406 nm) and its decomposition product after exposure to UV light (green, λ_{max} = 516 nm), which is consistent with that of the previously reported 1-crown.[2]

Conclusion

The first Ln−N=N−Ln moiety has been isolated as the dianion, $\{[(NR_2)_3Sc]_2[\mu\text{-}\eta^1\text{:}\eta^1\text{-}N_2]\}^{2-}$, **2**, which contains three anionic ancillary amide ligands per metal. This contrasts with almost 30 years of finding exclusively neutral side-on dinitrogen complexes, $[A_2Ln(THF)_x]_2[\mu\text{-}\eta^2\text{:}\eta^2\text{-}N_2]$, which have only two anionic ancillary ligands per metal. The end-on dinitrogen complex, **2**, is also unusual in that it can photolytically convert to a Sc^{2+} complex, $[Sc(NR_2)_3]^{1-}$.

These results support a new mechanistic option for the formation of the previously isolated rare-earth metal dinitrogen complexes including the possible interconversion of the two types of bridging modes, Scheme 5.2. It is conceivable that end-on complexes are initially formed during

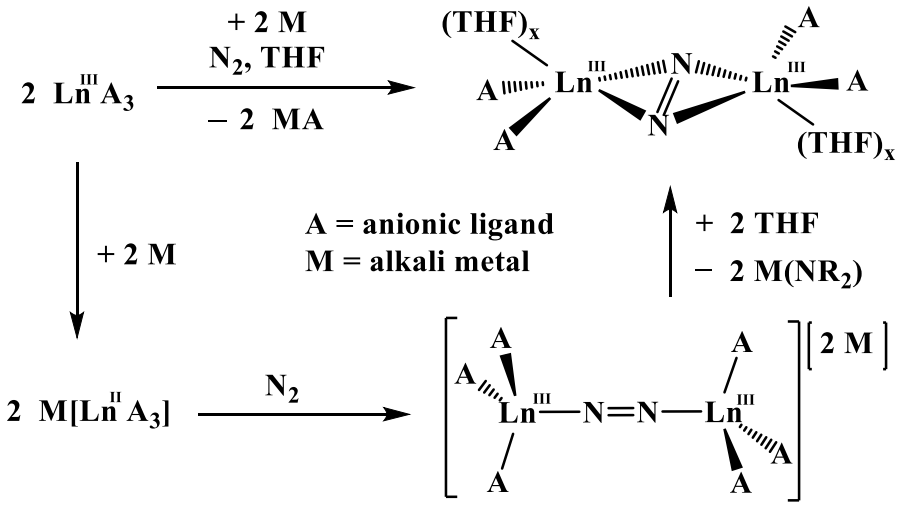

Scheme 5.2. Mechanistic option for the formation of the previously isolated rare-earth metal dinitrogen complexes, $[(R_2N)_2Ln(THF)]_2[\mu_2\text{-}\eta^2\text{:}\eta^2\text{-}N_2]$.

reductions involving $Ln(NR_2)_3$ complexes and those intermediates subsequently lose an amide ligand and convert to the side-on bound products. The loss of the amide may be more facile when K chelates like crypt and crown are not present to stabilize the end-on dianionic complex. In addition, the small size and high Lewis acidity of Sc may aid in retaining the three amide ligands per metal. Furthermore, the retainment of the three amide ligands might be a contributing factor as to why the formation of the dinitrogen complex was only observed when the reaction was performed at low temperature. This is understandable since the complexation of three molecules (two $[(ScNR_2)_3]^{1-}$ and one N_2) into one molecule is entropically more favorable at low temperature. The choice of chelates also appears to be crucial for reduction of dinitrogen by isolated Sc^{2+} complexes since **1-crypt** does not accomplish this reduction, but **1-crown** does.

Experimental

All manipulations and syntheses described below were conducted with rigorous exclusion of air and water using standard Schlenk line and glovebox techniques under a nitrogen atmosphere. Solvents were sparged with UHP argon and dried by passage through columns containing Q-5 and molecular sieves prior to use. THF-d_8 (Cambridge Isotope Laboratories) was dried over NaK alloy, degassed by three freeze-pump-thaw cycles, and vacuum transferred before use. Potassium was purchased from Aldrich, washed with hexanes, and scraped to provide a fresh surface before use. 2.2.2-Cryptand (crypt) was purchased from Merck and dried under reduced pressure before use. 18-Crown-6 (crown) was purchased from Aldrich and sublimed before used. $Sc(NR_2)_3$ (R = $SiMe_3$),[1,2] [K(crypt)][$Sc(NR_2)_3$], **1-crypt**,[2] and [K(crown)][$Sc(NR_2)_3$], **1-crown**,[2] were prepared following the literature procedures. ^{1}H NMR spectra were recorded on a Bruker CRYO500 MHz spectrometer at 298 K and referenced internally to THF-d_8 resonances. UV−visible spectra were collected using a Varian Cary 50 Scan UV−visible spectrophotometer in THF at 298 K. The UV−visible samples were limited from exposure to ambient light during transfer and showed negligible decomposition from each measurement. IR samples were prepared as KBr pellets and analyzed on a Jasco FT/IR-4700 - ATR-PRO ONE system. Raman spectra were collected on a Renishaw InVia Raman microscope using a 785 nm laser source. Elemental analyses were conducted on a Perkin-Elmer 2400 Series II CHNS elemental analyzer.

{K(crypt)}$_2${[$(R_2N)_3Sc]_2$[μ-η^1:η^1-N_2]}, 2-crypt. $Sc(NR_2)_3$ (81 mg, 0.15 mmol) and crypt (58 mg, 0.15 mmol) were dissolved in 10 mL of Et_2O and chilled in a −35 °C freezer. After a few hours, the colorless solution was quickly transferred into a vial that had been smeared with potassium (excess) and pre-chilled at −35 °C. The solution quickly started to turn orange/brown and the vial was then immediately placed in a −35 °C freezer. After 24 h, orange crystals of

{K(crypt)}$_2${[(R$_2$N)$_3$Sc]$_2$[μ-η^1:η^1-N$_2$]}, **2-crypt**, suitable for X-ray diffraction were obtained. Both the orange crystals and colorless mother liquor were transferred to another vial using a pipette. The mother liquor was decanted and the crystals were washed with cold Et$_2$O (3x). Subsequent drying under reduced pressure yielded orange solids of **2-crypt** (51 mg, 35%). UV−visible (THF): 264 nm (4,000 M^{-1} cm^{-1}), 406 nm (14,000 M^{-1} cm^{-1}). ^{1}H NMR (THF-d_8): δ 3.60 (OC*H*$_2$C*H*$_2$O), 3.55 (NCH$_2$C*H*$_2$O), 2.57 (br, 12H, NC*H*$_2$CH$_2$O). No accurate interpretation of the OC*H*$_2$C*H*$_2$O and NCH$_2$C*H*$_2$O resonances could be derived due to overlap with a THF-d_8 resonance. The Si*Me*$_3$ resonance is not observable within a ± 200 ppm window due to the paramagnetism of the complex. ^{13}C NMR (THF-d_8): δ 71.76 (O*C*H$_2$*C*H$_2$O), 68.91 (NCH$_2$*C*H$_2$O), 55.15 (s, 12H, N*C*H$_2$CH$_2$O). The Si*Me*$_3$ resonance is not observable within a ± 300 ppm window due to the paramagnetism of the complex. μ_{eff}: 2.3 μ_B. IR: 2963s, 2893m, 2826w, 1478w, 1445w, 1357w, 1297w, 1258s, 1185s, 1135m, 1109m, 1076m, 939vs, 848vs, 778m, 754m, 708w, 672w, 611m, 584m cm^{-1}. Raman: 1644 cm^{-1}. Anal. Calcd for C$_{72}$H$_{180}$K$_2$N$_{12}$O$_{12}$Sc$_2$Si$_{12}$: C, 45.24; H, 9.49; N, 8.79. Found: C, 45.04; H, 9.62; N, 8.48.

Conversion of 2-crypt to 1-crypt using UV light. A crystalline powder of **2-crypt** (5.5 mg, 0.72 mmol) was dissolved in 4 mL of THF to give an orange solution. 1 mL of this solution was transferred into a sealable quartz UV−visible cuvette (b = 1 mm). The cuvette was brought out of the glovebox with limited exposure to ambient light. An initial UV−visible measurement was performed on the sample to confirm its identity and a second subsequent measurement showed negligible decomposition. The sample was then cooled to −78 °C using an acetone/dry ice bath and exposed to a mercury lamp (365 nm) for 1 min, causing a color change from orange to maroon. Subsequent UV−visible measurement on the maroon sample revealed a strong absorption at λ_{max} = 516 nm, consistent with that of the Sc^{2+} complex, **1-crypt**.[2] The observed intensity of this

absorption is less than the previously reported possibly due to partial decomposition of the Sc^{2+} product within the brief exposure to UV light. The solution was brought into a glovebox and transferred into an EPR tube. EPR measurements produced the expected eight-line hyperfine pattern previously observed for **1-crypt**.[2]

Attempts to synthesize 2-crypt from 1-crypt. The Sc^{2+} complex, **1-crypt**, (25 mg, 0.013 mmol) was dissolved in 1 mL of Et_2O. Vapor diffusion with pentane at −35 °C over several days did not yield the desired orange crystals of the dinitrogen complex, **2-crypt**, rather, dark maroon crystals was obtained and identified as **1-crypt**. Crystallization by layer diffusion of the Et_2O solution with pentane even at −35 °C and a similar attempt using THF rather than Et_2O still yielded **1-crypt**.

{K(crown)}$_2${[(R$_2$N)$_3$Sc]$_2$[μ-η^1:η^1-N$_2$]}, 2-crown. As described for **2-crypt**, a 5 mL Et_2O solution of $Sc(NR_2)_3$ (33 mg, 0.064 mmol) and crown (17 mg, 0.064 mmol) was reacted with a potassium smear at −35 °C to yield orange solids of {K(crown)}$_2${[(R$_2$N)$_3$Sc]$_2$[μ-η^1:η^1-N$_2$]}, **2-crown** (28 mg, 52%). UV−visible (THF): 264 nm (4,000 M^{-1} cm^{-1}), 406 nm (14,000 M^{-1} cm^{-1}). IR: 2946s, 2897s, 1473w, 1455w, 1434w, 1353m, 1285w, 1240s, 1184w, 1109vs, 936vs, 867s, 828vs, 779m, 755m, 709w, 765m, 612w cm^{-1}. ^{1}H NMR (THF-d_8): δ 3.61 (s, 24H, OC_2H_4O). The SiMe_3 resonance is not observable within a ± 200 ppm window due to the paramagnetism of the complex. ^{13}C NMR (THF-d_8): δ 71.63 (OCH_2CH_2O). The SiMe_3 resonance is not observable within a ± 300 ppm window due to the paramagnetism of the complex. μ_{eff}: 2.4 μ_B. Raman: 1644 cm^{-1}. Anal. Calcd for $C_{60}H_{156}K_2N_8O_{12}Sc_2Si_{12}\cdot C_4H_{10}O$: C, 43.65; H, 9.50; N, 6.36. Found: C, 43.46; H, 9.39; N, 5.91.

Synthesis of 2-crown from 1-crown. In a nitrogen-filled glovebox, **1-crown** (59 mg, 0.071 mmol) was dissolved in 1 mL of pre-chilled Et_2O (−35 °C) and set up for a vapor diffusion

with prechilled pentane (−35 °C). After 24 h, orange crystals of **2-crown**, (31 mg, 52%) suitable for X-ray diffraction were obtained. The acquired data were insufficient for metrical discussions. Raman: 1644 cm^{-1}.

Conversion of 2-crown to 1-crown using UV light. Similar to the conversion of **2-crypt** to **1-crypt**, crystalline powder of **2-crown** (3.0 mg, 0.45 mmol) was dissolved in 4 mL of THF and analyzed by UV−visible spectroscopy before and after photolysis, which revealed the conversion to form **1-crown**.[2]

Evans Method for Magnetic Susceptibility Measurements. Samples were prepared by dissolving crystalline powder of **2-crypt** (9.0 mg) or **2-crown** (10.3 mg) in 0.5 mL of THF-d_8. The samples were transferred into an NMR tube containing a capillary tube filled with pure THF-d_8. ^{1}H NMR spectra of the samples were collected to give $\Delta\nu$ = 50 Hz (**2-crypt**) and $\Delta\nu$ = 65 Hz (**2-crown**), which translate to μ_{eff} = 2.3 μ_B and μ_{eff} = 2.4 μ_B, respectively.

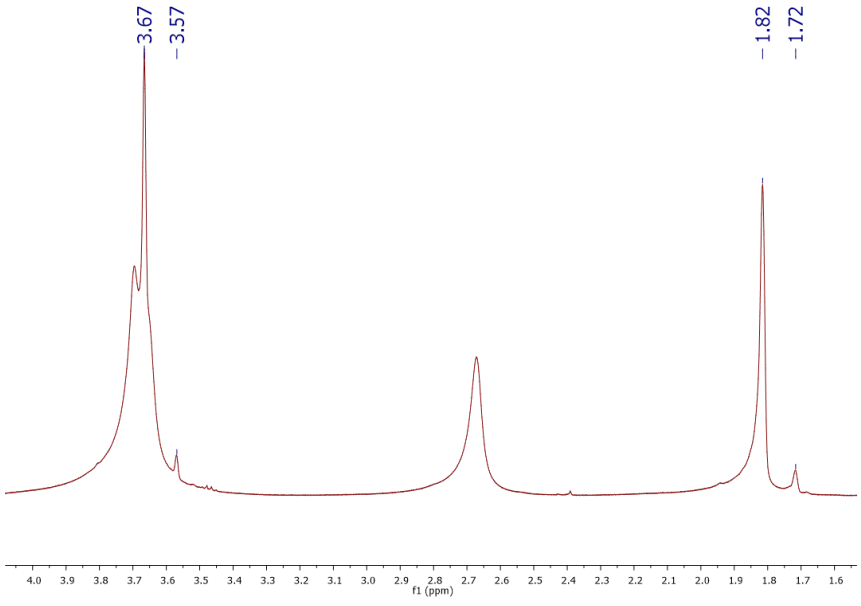

Figure 5.9. ^{1}H NMR spectrum of a 9.4 mM solution of {K(crypt)}$_2${[(NR$_2$)$_3$Sc]$_2$[μ-η^1:η^1-N$_2$]}, **2-crypt**, with an isolated inner THF-d_8 standard for Evans method measurement. (ν = 500 MGHz, $\Delta\nu$ = 50 Hz, μ_{eff} = 2.3 μ_B)

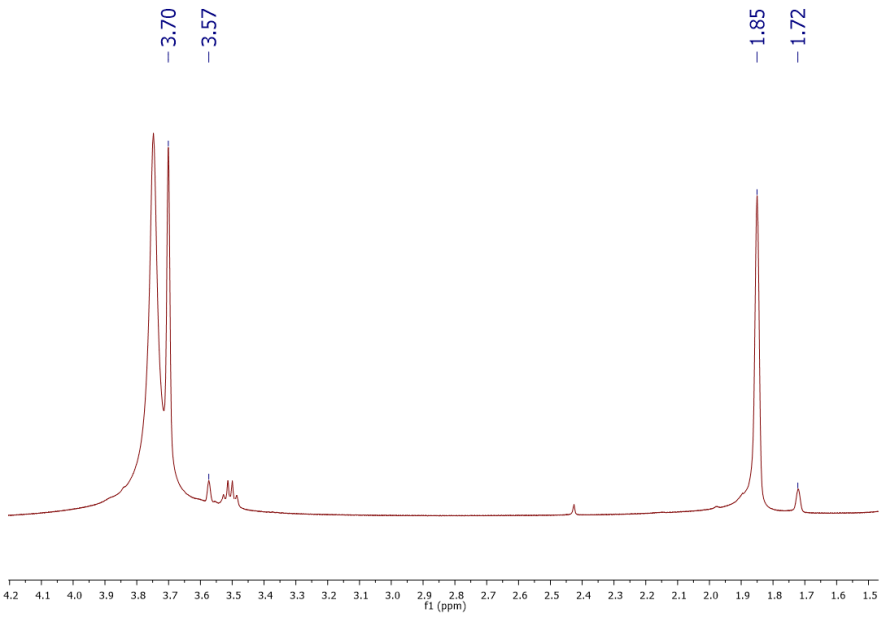

Figure 5.10. ^{1}H NMR spectrum of a 13.0 mM solution of {K(crown)}$_2${[(NR$_2$)$_3$Sc]$_2$[μ-η^1:η^1-N$_2$]}, **2-crown**, with an isolated inner THF-d_8 standard for Evans method measurement. (ν = 500 MGHz, $\Delta\nu$ = 65 Hz, μ_{eff} = 2.4 μ_B)

X-ray Data Collection, Structure Solution and Refinement for 2-crypt. An orange crystal of approximate dimensions 0.124 x 0.162 x 0.246 mm was mounted in a cryoloop and transferred to a Bruker SMART APEX II diffractometer. The APEX2[35] program package was used to determine the unit-cell parameters and for data collection (120 sec/frame scan time for a sphere of diffraction data). The raw frame data was processed using SAINT[36] and SADABS[37] to yield the reflection data file. Subsequent calculations were carried out using the SHELXTL[38] program. There were no systematic absences nor any diffraction symmetry other than the Friedel condition. The centrosymmetric triclinic space group $P\bar{1}$ was assigned and later determined to be correct. The structure was solved by direct methods and refined on F^2 by full-matrix least-squares techniques. The analytical scattering factors[39] for neutral atoms were used throughout the analysis.

Hydrogen atoms were included using a riding model. There were three molecules of diethylether solvent present. At convergence, wR2 = 0.1229 and Goof = 0.99 for 1186 variables refined against 25220 data (0.80Å), R1 = 0.0564 for those 15401 data with I > 2.0σ(I).

Computational Details

Ground-state DFT calculations were carried out by Guo P. Chen from the research group of Professor Filipp Furche using the TPSS[40] meta-generalized-gradient-approximation (meta-GGA) functional with Grimme's D3 dispersion correction.[41-42] Two different basis sets (def2-SV(P)[43] and def2-TZVP[44]) were used for $\{[(R_2N)_3Sc]_2[\mu\text{-}\eta^1\text{:}\eta^1\text{-}N_2]\}^{2-}$, **2**; The differences in the optimized bond distances are within 0.01 Å. Density grid m4 or larger[45] was employed. The structure of **2** was optimized in D_3 symmetry with convergence criterion for maximum norm of Cartesian energy gradient set to 10^{-4} a.u. Spin-unrestricted calculations suggest a triplet ($^3A_2$) ground state with a squared total spin expectation value of 2.003, which indicates negligible spin contamination. For comparison, hypothetical side-on complexes $\{[(R_2N)_3Sc]_2[\mu\text{-}\eta^2\text{:}\eta^2\text{-}N_2]\}^{2-}$ and $[(R_2N)_2Sc(THF)]_2[\mu\text{-}\eta^2\text{:}\eta^2\text{-}N_2]$ were optimized in C_2 and C_i symmetries, respectively, using def2-SV(P) basis set. For the anionic complexes, the COSMO continuum solvation model[46] was employed to account for the THF solvent using dielectric constant of 7.52[47] and refractive index of 1.4050.[48] The COSMO cavity was constructed using atomic radii of 1.300 Å, 2.000 Å, 1.830 Å, 2.200 Å, and 2.223 Å for H, C, N, Si, and Sc, respectively, and solvent radius of 3.18 Å. Structure optimization of the neutral complex $[(R_2N)_2Sc(THF)]_2[\mu\text{-}\eta^2\text{:}\eta^2\text{-}N_2]$ was performed in gas phase due to numerical instability of optimization with COMSO. Vibrational normal mode analyses were performed to confirm that the optimized structures are minima on the respective ground-state potential energy surfaces. Hessians were determined numerically for COSMO

calculations and analytically[49] for gas-phase calculations. The computed vibrational frequencies were scaled by 0.98 to account for anharmonicity.[50] Structural parameters of both **2** and the side-on complexes are summarized in Table 5.1. The ground-state energy difference between **2** and $\{[(R_2N)_3Sc]_2[\mu\text{-}\eta^2\text{:}\eta^2\text{-}N_2]\}^{2-}$ was obtained from single-point calculations using the def2-TZVP basis set based on structures optimized using the def2-SV(P) basis set.

The UV−visible spectrum of **2** was simulated using time-dependent DFT (TD-DFT) and nonorthonormal Krylov subspace method[51] with 25 and 40 exited states in A_1 and E irreducible representations, respectively. The calculation was performed using PBE0 functional[52-53] and def2-SVPD basis set[54] based on the structure optimized using the def2-TZVP basis set. The simulated spectrum was obtained by superimposing Gaussian functions with an RMS width of 0.25 eV (Figure 3). All calculations were performed using Turbomole 7.0 and 7.1.[55]

The excitation energies, oscillator strengths, and dominant orbital contributions of the electronic excitations of **2** at 364 nm and 406 nm are summarized in Table 5.2. Pertinent orbitals are illustrated in Figure 5.2.

Table 5.2. Electronic excitations of $\{[(NR_2)_3Sc]_2[\mu\text{-}\eta^1\text{:}\eta^1\text{-}N_2]\}^{2-}$, **2**, with significant intensity. Oscillator strengths are in length representation. Transitions with contributions larger than 10% are listed.

State	Wavelength (nm)	Oscillator Strength (a.u.)	Dominant contributions			Assignment
			occupied	unoccupied	contribution	
1^3A_1	406	0.203	96e α	99e α	53.4%	Sc-N_2-Sc π → Sc-N_2-Sc π*
			96e α	104e α	11.1%	Sc-N_2-Sc π →Sc d
4^3A_1	364	0.404	96e α	99e α	35.7%	Sc-N_2-Sc π → Sc-N_2-Sc π*
			96e α	104e α	28.0%	Sc-N_2-Sc π →Sc d
			96e α	103e α	19.9%	Sc-N_2-Sc π →Sc d

References

(1) Evans, W. J.; Lee, D. S.; Rego, D. B.; Perotti, J. M.; Kozimor, S. A.; Moore, E. K.; Ziller, J. W. *J. Am. Chem. Soc.* **2004**, *126*, 14574-14582.

(2) Evans, W. J.; Lee, D. S.; Ziller, J. W. *J. Am. Chem. Soc.* **2004**, *126*, 454-455.

(3) Evans, W. J.; Ulibarri, T. A.; Ziller, J. W. *J. Am. Chem. Soc.* **1988**, *110*, 6877-6879.

(4) Evans, W. J.; Lee, D. S.; Lie, C.; Ziller, J. W. *Angew. Chem., Int. Ed.* **2004**, *43*, 5517-5519.

(5) Campazzi, E.; Solari, E.; Floriani, C.; Scopelliti, R. *Chem. Commun.* **1998**, 2603-2604.

(6) Guan, J.; Dubé, T.; Gambarotta, S.; Yap, G. P. A. *Organometallics* **2000**, *19*, 4820-4827.

(7) Evans, W. J.; Rego, D. B.; Ziller, J. W. *Inorg. Chem.* **2006**, *45*, 10790-10798.

(8) Jaroschik, F.; Momin, A.; Nief, F.; Goff, X.-F. L.; Deacon, G. B.; Junk, P. C. *Angew. Chem., Int. Ed.* **2009**, *48*, 1117-1121.

(9) Evans, W. J.; Zucchi, G.; Ziller, J. W. *J. Am. Chem. Soc.* **2003**, *125*, 10-11.

(10) Evans, W. J.; Allen, N. T.; Ziller, J. W. *Angew. Chem. Int. Ed.* **2002**, *41*, 359-361.

(11) Evans, W. J.; Fang, M.; Zucchi, G.; Furche, F.; Ziller, J. W.; Hoekstra, R. M.; Zink, J. I. *J. Am. Chem. Soc.* **2009**, *131*, 11195–11202.

(12) Evans, W. J.; Allen, N. T.; Ziller, J. W. *J. Am. Chem. Soc.* **2001**, *123*, 7927-7928.

(13) Cheng, J.; Takats, J.; Ferguson, M. J.; McDonald, R. *J. Am. Chem. Soc.* **2008**, *130*, 1544-1545.

(14) Schmiege, B. M.; Ziller, J. W.; Evans, W. J. *Inorg. Chem.* **2010**, *49*, 10506-10511.

(15) Evans, W. J.; Lee, D. S.; Johnston, M. A.; Ziller, J. W. *Organometallics* **2005**, *24*, 6393-6397.

(16) Mueller, T. J.; Fieser, M. E.; Ziller, J. W.; Evans, W. J. *Chem. Sci.* **2011**, *2*, 1992-1996.

(17) Lorenz, S. E.; Schmiege, B. M.; Lee, D. S.; Ziller, J. W.; Evans, W. J. *Inorg. Chem.* **2010**, *49*, 6655-6663.

(18) Corbey, J. F.; Farnaby, J. H.; Bates, J. E.; Ziller, J. W.; Furche, F.; Evans, W. J. *Inorg. Chem.* **2012**, *51*, 7867-7874.

(19) MacDonald, M. R.; Ziller, J. W.; Evans, W. J. *J. Am. Chem. Soc.* **2011**, *133*, 15914-15917.

(20) Demir, S.; Lorenz, S. E.; Fang, M.; Furche, F.; Meyer, G.; Ziller, J. W.; Evans, W. J. *J. Am. Chem. Soc.* **2010**, *132*, 11151-11158.

(21) Fieser, M. E.; Woen, D. H.; Corbey, J. F.; Mueller, T. J.; Ziller, J. W.; Evans, W. J. *Dalton Trans.* **2016**, *45*, 14634-14644.

(22) Fang, M.; Farnaby, J. H.; Ziller, J. W.; Bates, J. E.; Furche, F.; Evans, W. J. *J. Am. Chem. Soc.* **2012**, *134*, 6064-6067.

(23) Paparo, A.; Silvia, J. S.; Kefalidis, C. E.; Spaniol, T. P.; Maron, L.; Okuda, J.; Cummins, C. C. *Angew. Chem. Int. Ed.* **2015**, *54*, 9115-9119.

(24) Holland, P. L. *Dalton Trans.* **2010**, *39*, 5415-5425.

(25) Woen, D. H.; Chen, G. P.; Ziller, J. W.; Boyle, T. J.; Furche, F.; Evans, W. J. *Angew. Chem. Int. Ed.* **2017**, *56*, 2050-2053.

(26) Evans, D. F. *J. Chem. Soc.* **1959**, 2003-2005.

(27) Evans, D. F.; Fazakerley, G. V.; Phillips, R. F. *J. Chem. Soc. (A)* **1971**, 1931-1934.

(28) Curley, J. J.; Cook, T. R.; Reece, S. Y.; Müller, P.; Cummins, C. C. *J. Am. Chem. Soc.* **2008**, *130*, 9394-9405.

(29) Smith, J. M.; Sadique, A. R.; Cundari, T. R.; Rodgers, K. R.; Lukat-Rodgers, G.; Lachicotte, R. J.; Flaschenriem, C. J.; Vela, J.; Holland, P. L. *J. Am. Chem. Soc.* **2006**, *128*, 756-769.

(30) de Wolf, J. M.; Blaauw, R.; Meetsma, A.; Teuben, J. H.; Gyepes, R.; Varga, V.; Mach, K.; Veldman, N.; Spek, A. L. *Organometallics* **1996**, *15*, 4977-4983.

(31) Hanna, T. E.; Bernskoetter, W. H.; Bouwkamp, M. W.; Lobkovsky, E.; Chirik, P. J. *Organometallics* **2007**, *26*, 2431-2438.

(32) Semproni, S. P.; Milsmann, C.; Chirik, P. J. *Organometallics* **2012**, *31*, 3672-3682.

(33) Manriquez, J. M.; Bercaw, J. E. *J. Am. Chem. Soc.* **1974**, *96*, 6229-6230.

(34) Pool, J. A.; Chirik, P. J. *Can. J. Chem.* **2005**, 286-295.

(35) Bruker AXS, Inc., APEX2 Version 2014.11-0, Madison, WI, **2014**.

(36) Bruker AXS, Inc., SAINT Version 8.34a, Madison, WI, **2013**.

(37) Sheldrick, G. M.; SADABS, Version 2014/5, Bruker AXS, Inc., Madison, WI, **2014**.

(38) Sheldrick, G. M.; SHELXTL, Version 2014/7, Bruker AXS, Inc., Madison, WI, **2014**.

(39) *International Tables for Crystallography, Vol. C*, Kluwer Academic Publishers, Dordrecht, **1992**.

(40) Tao, J.; Perdew, J.; Staroverov, V.; Scuseria, G. *Phys. Rev. Lett.* **2003**, *91*, 146401.

(41) Grimme, S. *J. Comput. Chem.* **2006**, *27*, 1787-1799.

(42) Grimme, S.; Antony, J.; Ehrlich, S.; Krieg, H. *J. Chem. Phys.* **2010**, *132*, 154104.

(43) Schäfer, A.; Horn, H.; Ahlrichs, R. *J. Chem. Phys.* **1992**, *97*, 2571-2577.

(44) Weigend, F.; Ahlrichs, R. *Phys. Chem. Chem. Phys.* **2005**, *7*, 3297-3305.

(45) Treutler, O.; Ahlrichs, R. *J. Chem. Phys.* **1995**, *102*, 346.

(46) Klamt, A.; Schüürmann, G. *J. Chem. Soc., Perkin Trans.* **1993**, 799-805.

(47) In *CRC Handbook of Chemistry and Physics*; Lide, D. R., Ed.; CRC Press: Boca Raton, FL, 2008; Vol. 88, p 136.

(48) In *CRC Handbook of Chemistry and Physics*; Lide, D. R., Ed.; CRC Press: Boca Raton, FL, 2008; Vol. 88, p 474.

(49) Deglmann, P.; May, K.; Furche, F.; Ahlrichs, R. *Chem. Phys. Lett.* **2004**, *384*, 103-107.

(50) Kashinski, D. O.; Chase, G. M.; Nelson, R. G.; Di Nallo, O. E.; Scales, A. N.; VanderLey, D. L.; Byrd, E. F. C. *J. Phys. Chem. A* **2017**, *121*, 2265-2273.

(51) Furche, F.; Krull, B. T.; Nguyen, B. D.; Kwon, J. *J. Chem. Phys.* **2016**, *144*, 174105.

(52) Perdew, J. P.; Ernzerhof, M.; Burke, K. *J. Chem. Phys.* **1996**, *105*, 9982-9985.

(53) Adamo, C.; Barone, V. *J. Chem. Phys.* **1999**, *110*, 6158-6170.

(54) Rappoport, D.; Furche, F. *J. Chem. Phys.* **2010**, *133*, 134105.

(55) Furche, F.; Ahlrichs, R.; Hättig, C.; Klopper, W.; Sierka, M.; Weigend, F. *Wiley Interdisciplinary Reviews: Computational Molecular Science***2014**, *4*, 91-100.

CHAPTER 6

Reactivity of $\{Sc[N(SiMe_3)_2]_3\}^{1-}$ with Carbon Monoxide, Carbon Dioxide, and Acetonitrile

Introduction*

It was previously reported by the Evans group that the highly unstable Y^{2+} species generated from the reduction of $Y(NR_2)_3$ (R = $SiMe_3$), presumably "$[Y(NR_2)]^{1-}$" as indicated by EPR spectroscopy, showed high reactivity with dinitrogen to form a side-on bridging dinitrogen complex, $[(R_2N)_2Y(THF)]_2[\mu\text{-}\eta^2\text{:}\eta^2\text{-}N_2]$, **1**, Scheme 6.1.[1] Further reactivity studies of this Y^{2+} complex with carbon monoxide as well as carbon dioxide revealed that it can reduce both substrates to form $(CO)^{1-}$ and $(CO_2)^{1-}$ complexes as extended polymers in $\{[(\mu\text{-}CO)(R_2N)_3Y(\mu\text{-}OC)][K_2(crown)_2]\}_n$ (crown = 18-crown-6), **2**, and $\{[(\mu\text{-}CO_2)(R_2N)_3Y(\mu\text{-}CO_2)][K_2(crown)_2]\}_n$, **3**, respectively, Scheme 6.1.[2] These complexes were just the second isolated crystallographically-characterizable molecular examples containing the singly reduced forms of these substrates, i.e. $(CO)^{1-}$ and $(CO_2)^{1-}$, following previous reports by Meyer et. al. of $[L_1U(\mu\text{-}\eta^1\text{-}CO)UL_1]$[3] ($L_1$ = 1,4,7-tris(3,5-di-*tert*-butyl-2-hydroxybenzylate)-1,4,7-triazacyclononane) and $[L_2U(\eta^1\text{-}CO_2)]$ (L_2 = 1,4,7-tris(3-adamantyl-5-^{t}Bu-2-hydroxybenzyl)1,4,7-triazacyclononane).[4]

In addition to the formation of the $(CO)^{1-}$ complex, **2**, the reaction of "$[Y(NR_2)]^{1-}$" with carbon monoxide also showed a two-electron coupling reaction of $(CO)^{1-}$ to form a bridging ynediolate product, $\{[K(crown)]_2(crown)\}[(R_2N)_3Y]_2(\mu\text{-}OC{\equiv}CO)]$, **4**, Scheme 6.1.[2] Unlike the bridging dinitrogen complex, **1**, this bridging ynediolate complex retained all three of the anionic

* Portions of this chapter have been published: Woen, D. H.; Chen, G. P.; Ziller, J. W.; Boyle, T. J.; Furche, F.; Evans, W. J. *Angew. Chem. Int. Ed.* **2017**, 56, 2050−2053; *Angew. Chem.* **2017**, 129, 2082–2085. DOI: 10.1002/ange.201611758.

amide ligands per metal and was isolated as a dianion. The retainment of the three amide ligands was also shown in the formation of **2** and **3**. This indicates one obvious difference in reactivity of the Y^{2+} system with dinitrogen vs CO and CO_2.

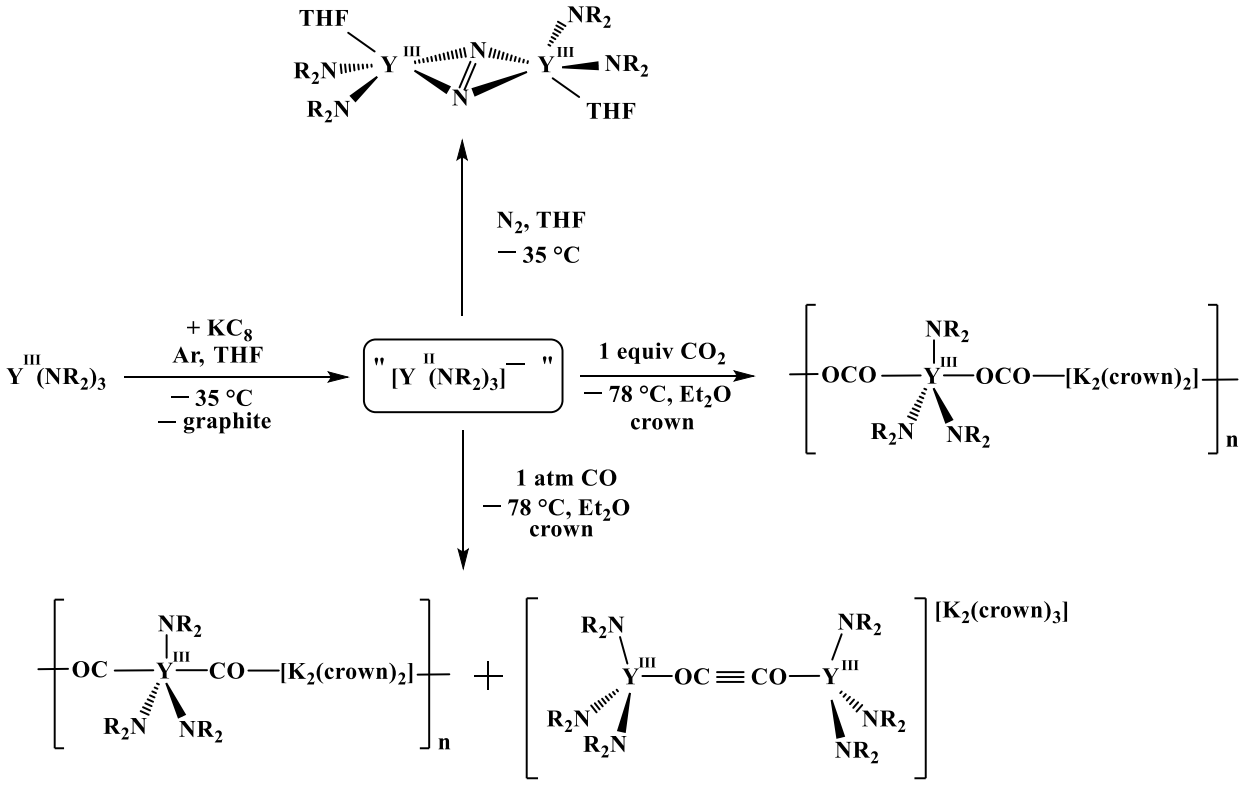

Scheme 6.1. Reactivity of an Y^{2+} species generated from the reduction of $Y(NR_2)_3$.

As described in Chapters 4 and 5, the reduction of the scandium analog, $Sc(NR_2)_3$, gave an isolable Sc^{2+} complex, $[Sc(NR_2)]^{1-}$, **5**, that was relatively inert towards dinitrogen since it only reacted under specific photolytic conditions to form a reduced dinitrogen complex, $\{[(R_2N)_3Sc]_2[\mu\text{-}\eta^1\text{:}\eta^1\text{-}N_2]\}^{2-}$.[5] Complex **5** differs from the yttrium analog since the yttrium species was highly unstable and readily reacted with dinitrogen.[1] In addition, the dinitrogen reduction reactivity of **5** resulted in a different structure with an end-on bridging reduced dinitrogen ligand, ($\mu\text{-}\eta^1\text{:}\eta^1\text{-}N_2$), rather than the ($\mu\text{-}\eta^2\text{:}\eta^2\text{-}N_2$) ligand in the yttrium analog.

Since the Y^{2+} species also showed interesting reactivity with carbon monoxide and carbon dioxide, it became of interest to explore the reactivity of the Sc^{2+} complex with these substrates for comparison with the yttrium analog. This Chapter describes the reaction of **5** with carbon monoxide as well as carbon dioxide. In addition, an acetonitrile reaction similar to the carbon dioxide reduction is also described.

Results and Discussion

Carbon Monoxide Reduction Reactivity. The addition of carbon monoxide (1 atm) to a dark maroon Et_2O solution of a crystalline sample of [K(crypt)][$Sc(NR_2)_3$] (crypt = 2.2.2-cryptand, R = $SiMe_3$), **5-crypt**, at −78 °C results in a color change to red/orange. The orange color of the solution reverts to dark maroon within a few minutes when the CO atmosphere is removed via vacuum at −78 °C. Attempts to isolate and identify the orange species by X-ray crystallography have been unsuccessful. UV−visible measurement of this orange species revealed a broad absorption at λ_{max} = 370 nm, Figure 6.1, which is significantly higher in energy compared to that of the Sc^{2+} precursor, **5-crypt** (λ_{max} = 516 nm), and only slightly higher than that of the reduced dinitrogen complex described in Chapter 5, $\{K(crypt)\}_2\{[(R_2N)_3Sc]_2[\mu\text{-}\eta^1\text{:}\eta^1\text{-}N_2]\}$ (λ_{max} = 406 nm). Based on these UV−visible data, it is possible that the addition of carbon monoxide to **5-crypt** results in the binding and reduction of carbon monoxide to form a bimetallic $(CO)^{2-}$ product, "[K(crypt)][$(R_2N)_3Sc(\mu\text{-}\eta^1\text{:}\eta^1\text{-}CO)$]", which would be structurally similar to the end-on bridging dinitrogen complex, $\{K(crypt)\}_2\{[(R_2N)_3Sc]_2[\mu\text{-}\eta^1\text{:}\eta^1\text{-}N_2]\}$. The $(CO)^{2-}$ moiety would be isoelectronic to the $(N_2)^{2-}$ bridge.

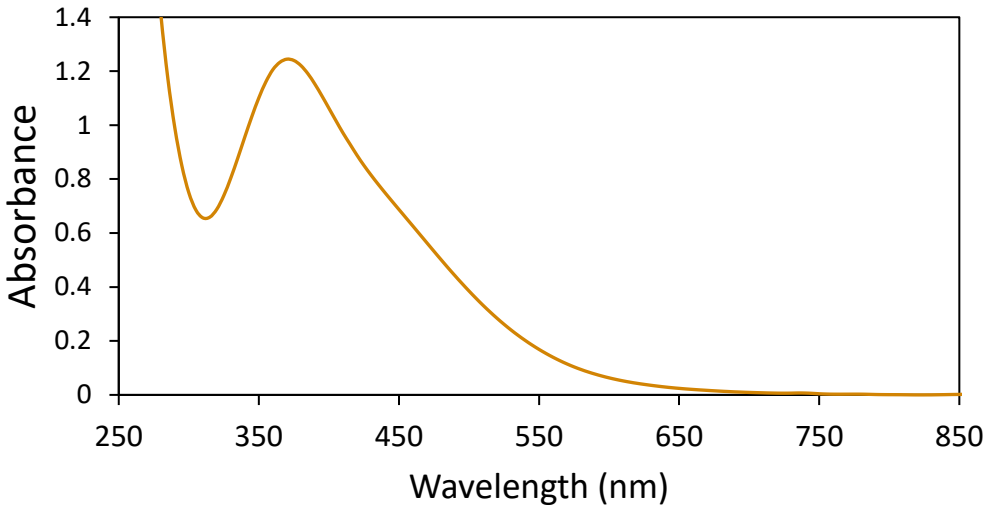

Figure 6.1. UV−visible spectrum of the reaction product of [K(crypt)][Sc(NR$_2$)$_3$, **5-crypt**, with carbon monoxide.

Carbon Dioxide Reduction Reactivity. Addition of carbon dioxide (1 atm) to the crown version of [Sc(NR$_2$)$_3$]$^{1-}$, [K(crown)][Sc(NR$_2$)$_3$], **5-K(crown),** prepared *in situ* immediately forms the colorless bridging oxalate complex, {K$_2$(crown)$_3$}{[(R$_2$N)$_3$Sc]$_2$(μ-C$_2$O$_4$-κ^1O:κ^1O")}, **6** (Figure 6.2). This oxalate complex is isolated as a dianion with three (NR$_2$)$^{1-}$ ligands per Sc rather than as a neutral [(R$_2$N)$_2$Sc]$_2$(μ-C$_2$O$_4$) product. In this sense, **6** is similar to the yttrium complexes **2**, **3**, and **4** [2] as well as the bridging oxalate complex of titanium, [(TiX$_3$)$_2$(μ-C$_2$O$_4$-κ^1O:κ^1O")] (X = N-^{t}Bu-3,5-dimethylanilide).[6] The bridged dication of **6**, [K$_2$(crown)$_3$]$^{2+}$ (Figure 6.3), has been reported previously in the literature.[2,7-10]

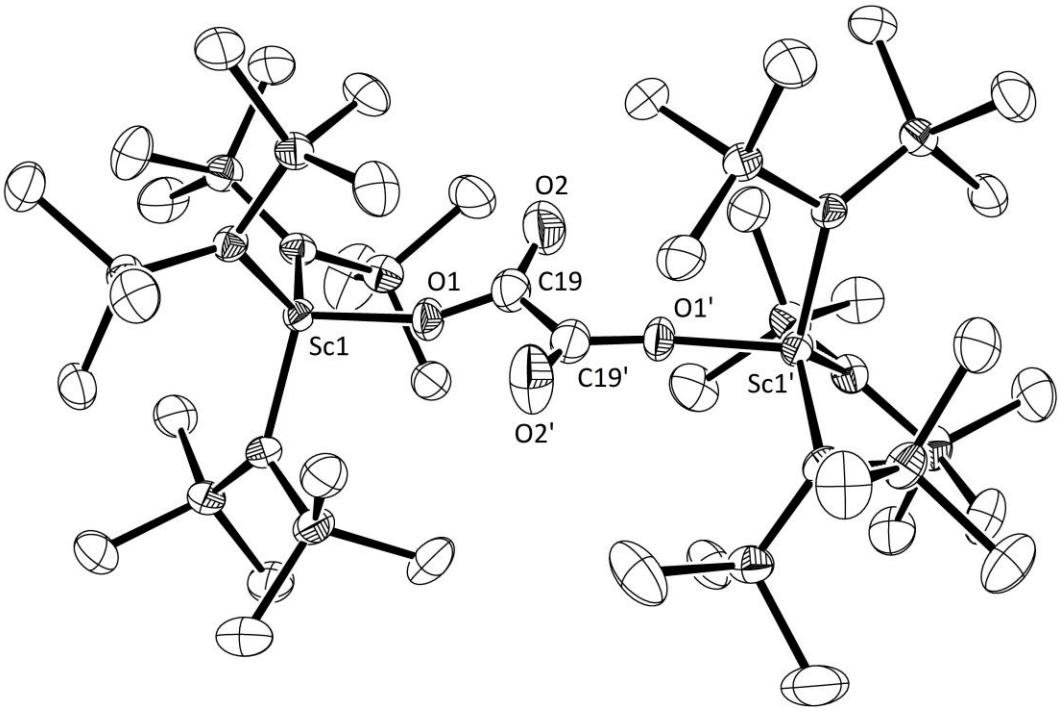

Figure 6.2. Thermal ellipsoid plot of the dianion of $\{K_2(crown)_3\}\{[(R_2N)_3Sc]_2(\mu\text{-}C_2O_4\text{-}\kappa^1O{:}\kappa^1O'')\}$, **6**, drawn at 50% probability level. Hydrogen atoms, co-crystallized Et_2O, and the $[K_2(crown)_3]^{2+}$ countercation are omitted for clarity.

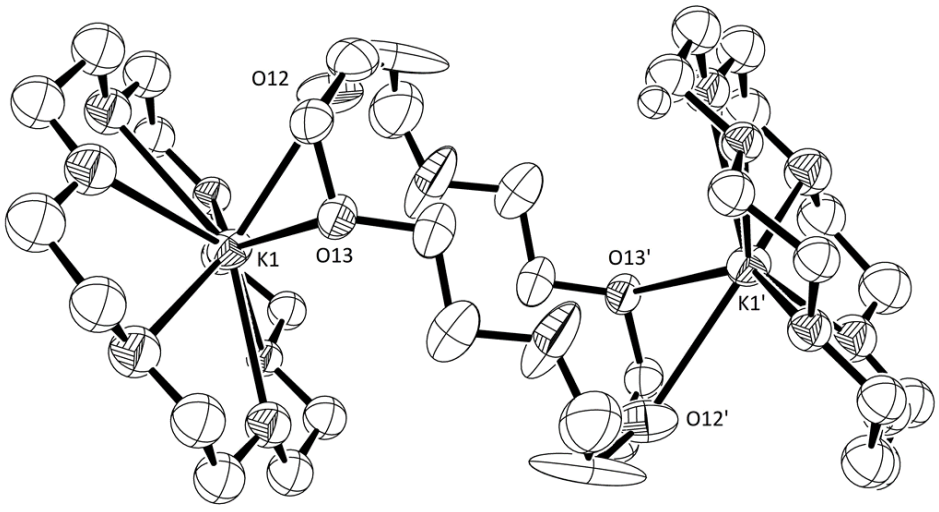

Figure 6.3. Thermal ellipsoid plot of the countercation of **6** drawn at 50% probability level. Hydrogen atoms and disordered atoms are omitted for clarity.

Complex **6** crystallizes in the monoclinic space group *C*2/c as a dimer with a two-fold rotational axis, which results in only one unique Sc atom per dimer. The Sc−N(amide) distances in this four-coordinate Sc^{3+} complex range from 2.108(3)-2.116(3) Å, which are noticeably longer than the 2.048(2)-2.057(2) Å distances in the three coordinate Sc^{3+} complex, $Sc(NR_2)_3$, but similar to the 2.116(2)-2.137(1) Å distances in the three coordinate Sc^{2+} complex, $[Sc(NR_2)_3]^{1-}$. The longer Sc−N(amide) distances of the Sc^{3+} complex, **6**, compared those in $Sc(NR_2)_3$ are consistent with the increase in coordination number.[11] The O1−C19 distance of 1.294(4) in **6** is slightly shorter than typical C−O single bonds, and the O2−C19 distance of 1.214(5) Å is slightly shorter than typical C=O double bonds. This is consistent with reports of other bridging oxalate complexes in the literature.[4,6,12-14] The monohapto binding of the bridging oxalate has been observed with other transition metal bridging oxalate complexes, but it is different than the dihapto binding observed in the only previously isolated bridging oxalate complex of a rare-earth metal, $[(C_5Me_5)_2Sm]_2[\mu\text{-}\kappa^2,\kappa^2\text{-}C_2O_4]$.[12] This is likely due to the smaller open coordination site caused by the retainment of the three ionic ligands in **6**.

When the CO_2 reaction was repeated to get full characterization of **6**, the FT-IR spectrum of the crude product indicated the presence of another CO_2-derived product. Subsequently, crystals of $[(R_2N)_3Sc(\mu\text{-}OCO\text{-}\kappa^1O{:}\kappa^1O')K(crown)]_n$, **7** (Figure 6.4), were isolated from the mixture. Again, this Sc^{3+} ion retains the three amide ligands. Like **2** and **3**, this $(CO_2)^{1-}$ complex is polymeric, but the repeating units are connected by a linkage between a $[K(crown)]^{1+}$ unit and a methyl group of a $(NR_2)^{1-}$ ligand. The 2.089(2)-2.107(2) Å Sc−N(amide) distances are similar to those in complex **6**. The 1.183(3) and 1.186(3) Å C−O bond distances in **7** are similar to those in **3**: 1.183(4) and 1.198(4) Å.[2] DFT analysis by Guo P. Chen in the group of Professor Filipp Furche indicated that the unpaired electron was delocalized over several atoms (Figure 6.5). Other

than **3** and **7**, only one other $(CO_2)^{1-}$ complex has been reported: the U^{4+} compound, {[(^{Ad}ArO)$_3$tacn]U(CO_2)}, where (^{Ad}ArOH)$_3$tacn = 1,4,7- tris(3-adamantyl-5-^{t}Bu-2-hydroxybenzyl)1,4,7-triazacyclononane.[4] The CO_2 reduction reactivity of **5-crown** is summarized in Scheme 6.2.

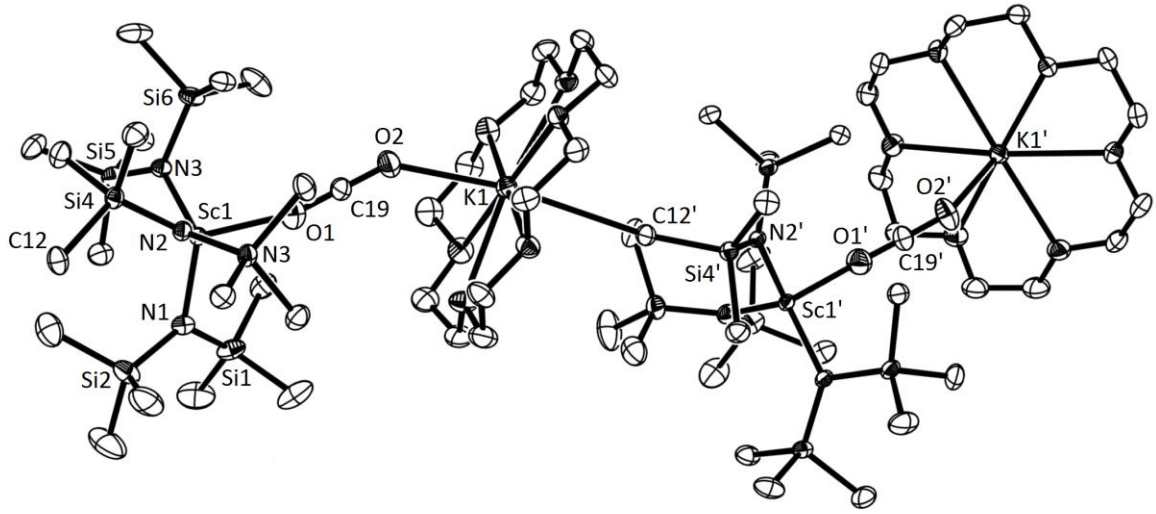

Figure 6.4. Thermal ellipsoid plot of two repeating units of [(R_2N)$_3$Sc(μ-OCO-κ^1O:κ^1O')K(crown)]$_n$, **7**, drawn at the 50% probability level. Hydrogen atoms are omitted for clarity.

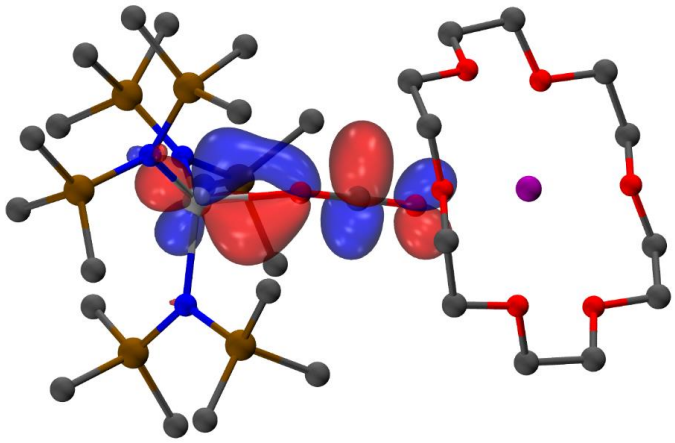

Figure 6.5. HOMO of monomeric unit of **6** with a contour value of 0.06. Hydrogen atoms are omitted for clarity.

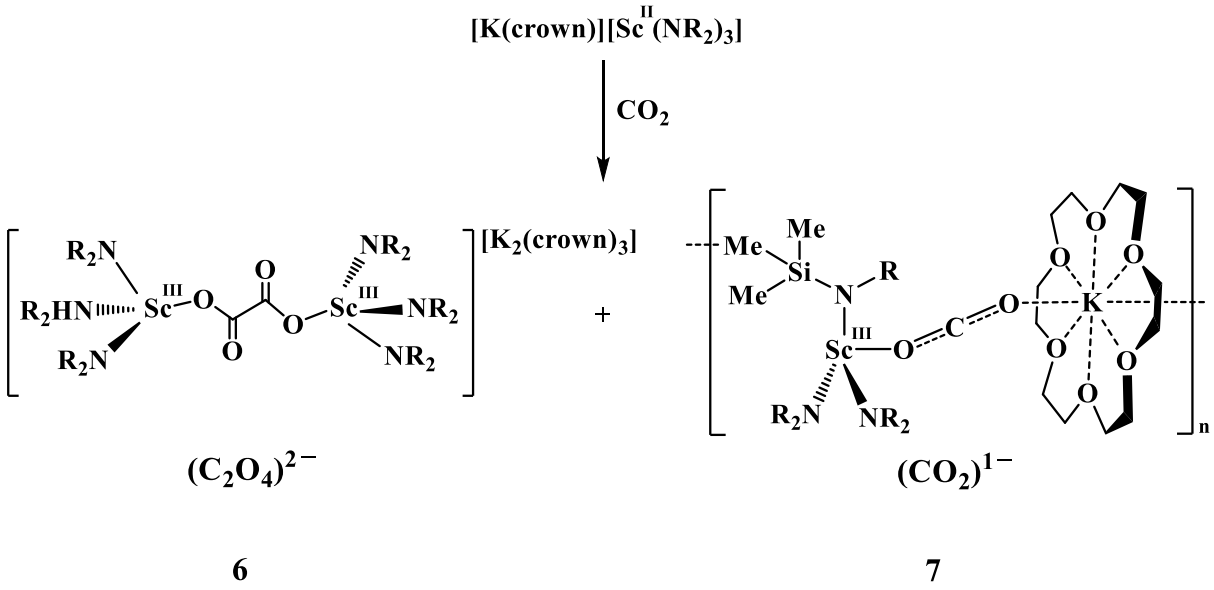

Scheme 6.2. Reaction of **5-crown** with CO_2.

The FT-IR data of the **6**/**7** mixture are consistent with the structures (Figures 6.6 and 6.7). An absorption at 1671 cm^{-1} is within the 1556-1710 cm^{-1} range observed in bridging oxalate complexes[6 14 15-19] and a band at 2228 cm^{-1} is similar to the 2210 cm^{-1} of $\{[(\mu\text{-}CO_2)(R_2N)_3Y(\mu\text{-}CO_2)][K_2(crown)_2]\}_n$, **3**. The reaction of **5-crown** with $^{13}CO_2$ gives a product mixture in which these absorptions shift to 1625 cm^{-1} and 2170 cm^{-1}. The $^{12}C/^{13}C$ isotopic ratios of 1.0283 and 1.0272, respectively, are as expected.[4,6,12-14]

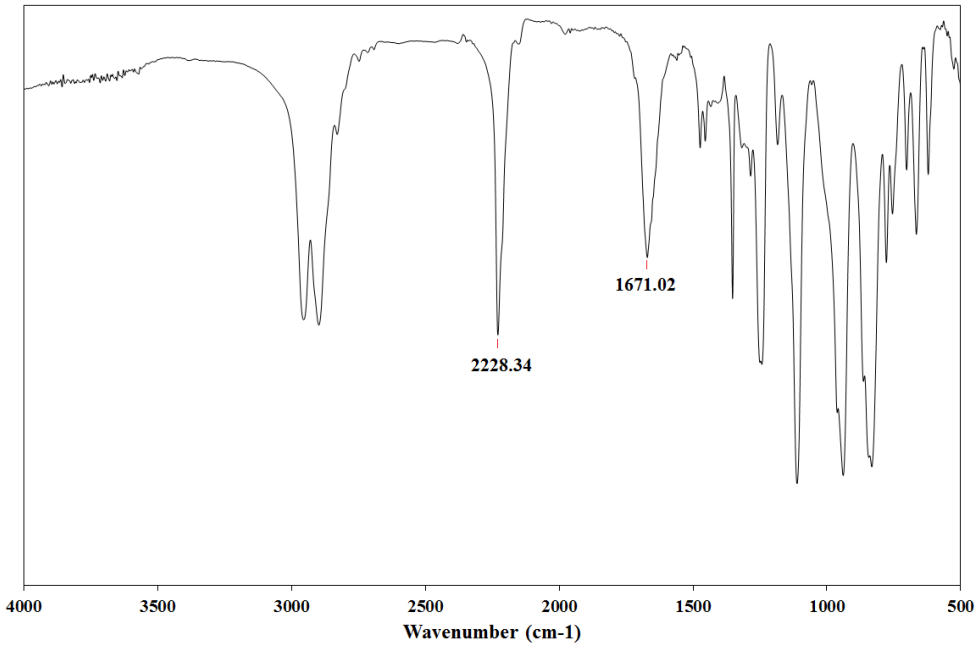

Figure 6.6. FT-IR spectrum of the reaction product of [K(crown)][Sc(NR$_2$)$_3$], **5-crown**, with $^{12}CO_2$.

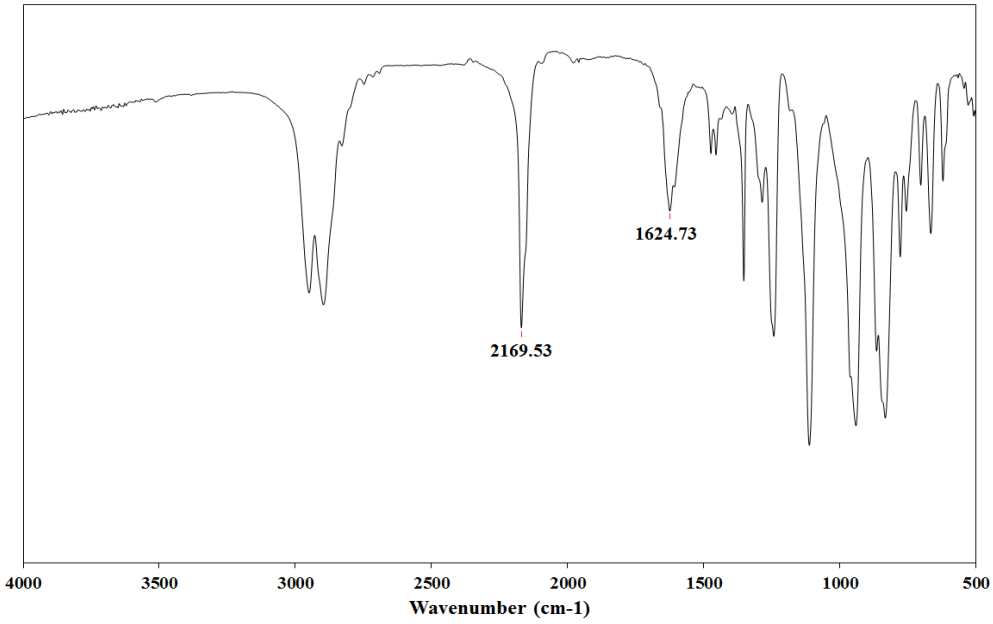

Figure 6.7. FT-IR spectrum of the reaction product of [K(crown)][Sc(NR$_2$)$_3$], **5-crown**, with $^{13}CO_2$.

Acetonitrile Reduction Reactivity. Addition of acetonitrile to crystalline solids of [K(crypt)][Sc(NR_2)$_3$], **5-crypt**, resulted in the dissolution of the solids and the irreversible formation of a pale blue-green solution. Cooling the solution to −35 ºC overnight resulted in the formation of green crystalline solids identified by X-ray crystallography as the bridging butane-2,3-diimino(2-)-N,N' complex, [K(crypt)]$_2${[(R_2N)$_3$Sc]$_2$[μ-N(Me)CC(Me)N]}, **8** (Figure 6.8). This complex crystallizes in the triclinic space group $P\bar{1}$ with two unequal complex units in its crystalline lattice, totaling to two {[(R_2N)$_3$Sc]$_2$[μ-N(Me)CC(Me)N]}$^{2-}$ dianions and four [K(crypt)]$^+$ cations per unit cell. One of the dianionic units has a disorder on the bridging moiety (Figure 6.8), whereas the other dianionic unit has no disorder (Figure 6.9).

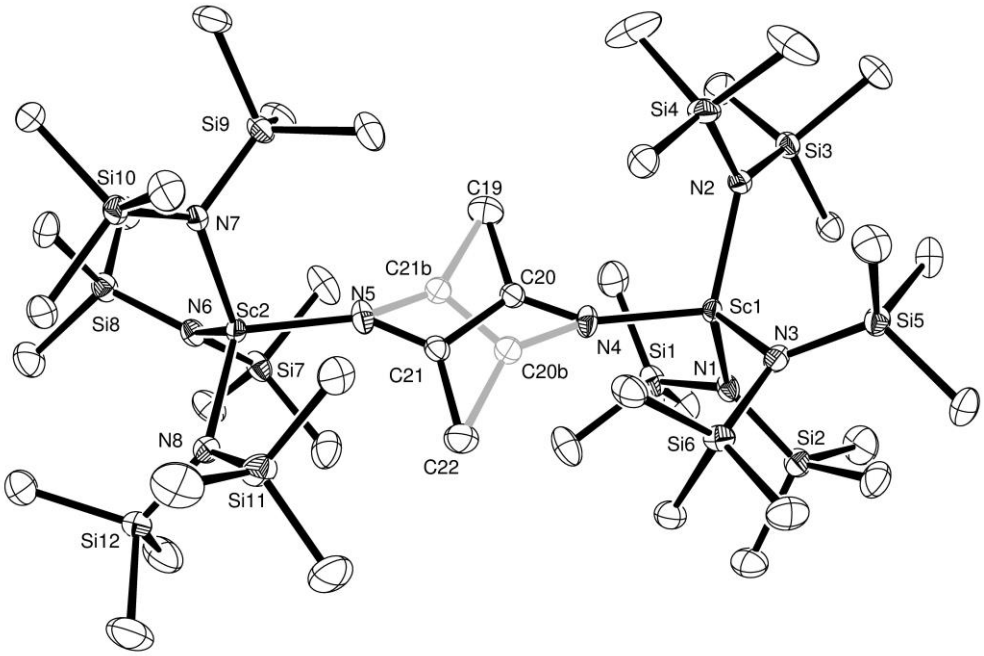

Figure 6.8. Thermal ellipsoid plots of one of the dianionic units with disorder in the crystal lattice of [K(crypt)]$_2${[(R_2N)$_3$Sc]$_2$[μ-N(Me)CC(Me)N]}, **8**, drawn at 50% probability. The disorder of C20 and C21 are drawn in gray and the corresponding atoms are labeled as C20b and C21b,

respectively. The other $\{[(R_2N)_3Sc]_2[\mu\text{-}N(Me)CC(Me)N]\}^{2-}$ dianion unit, four $[K(crypt)]^+$ cations, and hydrogen atoms are omitted for clarity.

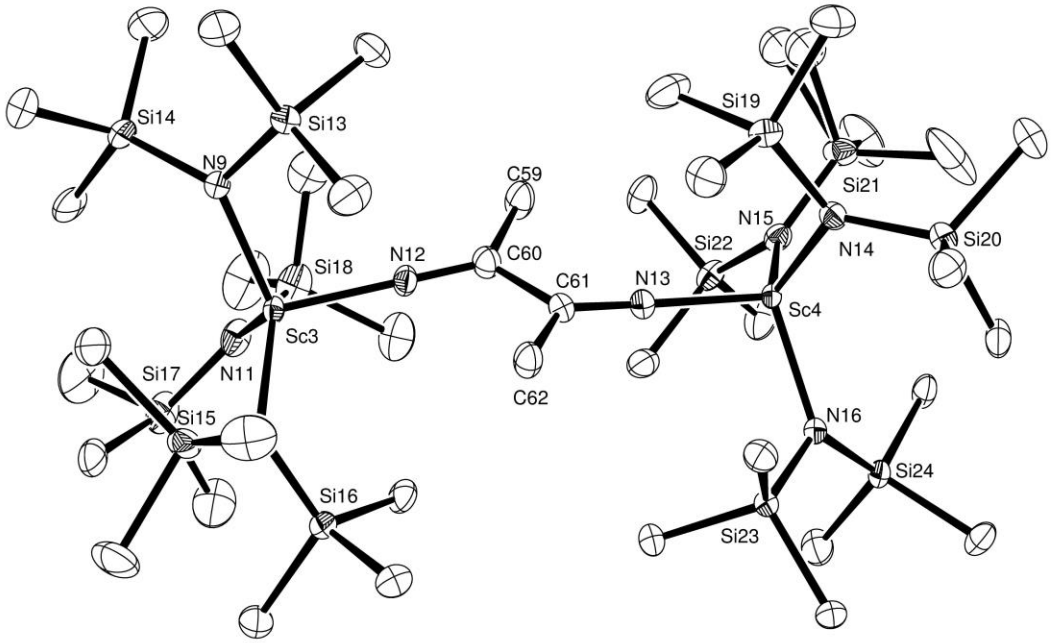

Figure 6.9. Thermal ellipsoid plots of one of the dianionic units without disorder in the crystal lattice of $[K(crypt)]_2\{[(R_2N)_3Sc]_2[\mu\text{-}N(Me)CC(Me)N]\}$, **8**, drawn at 50% probability. The other $\{[(R_2N)_3Sc]_2[\mu\text{-}N(Me)CC(Me)N]\}^{2-}$ dianion unit, four $[K(crypt)]^+$ cations, and hydrogen atoms are omitted for clarity.

Looking at the unit with no disorder, the Sc−N(amide) distances range from 2.133(2)-2.156(2) Å and are consistent with those of the other four-coordinate Sc^{3+} complexes, **6** and **7**. The 1.267(3) Å N12−C60 and 1.261(3) Å N13−C61 distances are consistent with N=C double bonds and the C−C distances of 1.522(4)-1.549(4) Å between adjacent carbons of the butane moiety (C59-C62) are consistent with C−C single bonds. These distances are similar to those of other bridging butane-2,3-diimino-(2-)-N:N' transition metal complexes.[20-22]

The formation of this bridging complex to some extent is similar to the formation of the bridging oxalate complex, $\{K_2(crown)_3\}\{[(R_2N)_3Sc]_2(\mu\text{-}C_2O_4\text{-}\kappa^1O\text{:}\kappa^1O'')\}$, **6**It was previously postulated by Cummins et. al. that the formation of bridging oxalate, as in the case of the titanium complex, $[(TiX_3)_2(\mu\text{-}C_2O_4\text{-}\kappa^1O\text{:}\kappa^1O'')]$ (X = N-^{t}Bu-3,5-dimethylanilide), proceeds through the formation of a metallocarbene bridging $(CO_2)^{2-}$ species, $[(TiX_3)_2(\mu\text{-}CO_2\text{-}\kappa^2C,O\text{:}kO')]$, that attacks another free carbon dioxide molecule to form the bridging $(C_2O_4)^{2-}$ moiety.[6] It is possible that the formation of **8** also proceeds through a similar mechanism.

Conclusion

The reaction of $[Sc(NR_2)_3]^{1-}$ with carbon monoxide at low temperature resulted in a reversible color change from dark maroon to orange, indicating the formation of an activated form of carbon monoxide. The reversibility of this reaction is similar to the reversible binding of dinitrogen described in Chapter 5, except that the reverse reaction with carbon monoxide results under reduced pressure, whereas the reverse reaction with dinitrogen results from exposure to UV-light. It is postulated that the reaction with carbon monoxide forms a product analogous to the $\{[(R_2N)_3Sc]_2[\mu\text{-}\eta^1\text{:}\eta^1\text{-}N_2]\}^{1-}$ described in Chapter 5, namely $\{[(R_2N)_3Sc]_2[\mu\text{-}\eta^1\text{:}\eta^1\text{-}CO]\}^{1-}$.

In contrast, the reaction of $[Sc(NR_2)_3]^{1-}$ with carbon dioxide results in an irreversible color change to form two identifiable products, the bridging oxalate complex, $\{K_2(crown)_3\}\{[(R_2N)_3Sc]_2(\mu\text{-}C_2O_4\text{-}\kappa^1O\text{:}\kappa^1O'')\}$, **6**, as well as the polymeric $(CO_2)^{1-}$ complex, $[(R_2N)_3Sc(\mu\text{-}OCO\text{-}\kappa^1O\text{:}\kappa^1O')K(crown)]_n$, **7**. Complex **6** seems to result from the two electron coupling of $(CO_2)^{1-}$ to form the $(C_2O_4)^{2-}$ moiety. A similar coupling reaction was observed with acetonitrile to form the butane-2,3-diimino-(2-)-N:N' bridging moiety in

$[K(crypt)]_2\{[(R_2N)_3Sc]_2[\mu\text{-}N(Me)CC(Me)N]\}$, **8**. Similar acetonitrile coupling reactions have been reported with other d-block metals. [20-24]

Reactivity studies with the Sc^{2+} complex, $[Sc(NR_2)_3]^{1-}$ have resulted in several crystallographically identifiably products, notably with dinitrogen, carbon dioxide, and acetonitrile. In all these products, each metal center retains all three of the amide ligands. It appears that this scandium system is a good fit for exploring one-electron/coupling reactivity for +2 rare-earth metal ion complexes.

Experimental

All manipulations and syntheses described below were conducted with rigorous exclusion of air and water using standard Schlenk line and glovebox techniques under an argon atmosphere. Solvents were sparged with UHP argon and dried by passage through columns containing Q-5 and molecular sieves prior to use. Deuterated NMR solvents were dried over NaK alloy, degassed by three freeze-pump-thaw cycles, and vacuum transferred before use. Potassium was purchased from Aldrich, washed with hexanes, and scraped to provide fresh surfaces before use. CO and CO_2 were purchased from Airgas and used without further purification. $^{13}CO_2$ was purchased from Aldrich and used without further purification. 2.2.2-Cryptand (crypt) was purchased from Merck and dried under reduced pressure before use. 18-Crown-6 (crown) was purchased from Aldrich and sublimed before use. $Sc(NR_2)_3$, $[K(crypt)][Sc(NR_2)_3]$, and $[K(crown)][Sc(NR_2)_3]$ were prepared following previous procedures described in Chapter 4. ^1H NMR spectra were recorded on Bruker GN500 or CRYO500 MHz spectrometers (^{13}C NMR at 125 MHz) at 298 K referenced internally to residual protio-solvent resonances. IR samples were prepared as KBr pellets on a

Jasco FT/IR-4700 - ATR-PRO ONE system. Elemental analyses were conducted on a Perkin-Elmer 2400 Series II CHNS elemental analyzer.

Reaction of [K(crypt)][Sc(NR$_2$)$_3$], 5-crypt, with carbon monoxide. In a glovebox, [K(crypt)][Sc(NR$_2$)$_3$] (35 mg, mmol) was dissolved in 5 mL of Et$_2$O to produce a dark maroon solution. This solution was transferred to a Schlenk flask. The vessel was sealed using a Teflon stopper, brought out of the glovebox, and connected to a Schlenk line. The solution was cooled to −78 ºC using an isopropanol/dry ice bath and evacuated briefly to remove argon. Then, 1 atm of carbon monoxide was added to the vessel resulting in a color change from dark maroon to orange. When reduced pressure was introduced to remove excess carbon monoxide in the vessel, the orange color slowly reverted to the dark maroon color. Addition of more carbon monoxide (1 atm) resulted in the conversion to the orange color again.

Reaction of [K(crypt)][Sc(NR$_2$)$_3$], 5-crypt, with carbon monoxide and UV−Visible Measurement. In a glovebox, [K(crypt)][Sc(NR$_2$)$_3$] (25 mg, 0.026 mmol) was dissolved in 5 mL of Et$_2$O to produce a dark maroon solution. 0.5 mL of the solution was transferred to a 1 cm cuvette that has a side arm fitted with a ground glass stopcock, then the solution was diluted to 3 mL with additional Et$_2$O. The cuvette was sealed, brought out of the glovebox, and cooled to −78 ºC using an isopropanol/dry ice bath. The vessel was briefly evacuated to remove argon. Then, 1 atm of carbon monoxide was added to the vessel resulting in a color change from dark maroon to orange. UV−Visible (Et$_2$O): λ_{max} = 370 nm.

[K$_2$(crown)$_3$]{[(R$_2$N)$_3$Sc]$_2$(μ-C$_2$O$_4$-κ^1O:κ^1O")}, 6. In a glovebox, Sc(NR$_2$)$_3$ (112 mg, 0.213 mmol) was dissolved in 10 mL of Et$_2$O and transferred to a scintillation vial containing potassium smear and a Teflon stir bar. The mixture was stirred for 30 min and the resulting dark maroon solution was filtered into a side-arm Schlenk flask before crown (53 mg, 0.20 mmol) was

added. The flask was sealed, brought out of the glovebox, and the solution was frozen using a liquid N_2 bath before attaching the flask to a vacuum line. The flask was evacuated under reduced pressure and then excess CO_2 was added to the frozen solution at 77 K. The solution was thawed using a room temperature water bath while being continuously swirled and it quickly turned colorless. The vessel was briefly evacuated and then returned to a glovebox. The solution was filtered and concentrated to ~5 mL. Single crystals of $[K_2(crown)_3]\{[(R_2N)_3Sc]_2(\mu\text{-}C_2O_4\text{-}\kappa^1O\text{:}\kappa^1O'')\}$, **6**, suitable for X-ray diffraction were grown from slow vapor diffusion of pentane into the concentrated Et_2O solution at −35 ºC.

Reaction of [K(crown)][Sc(NR$_2$)$_3$], 5-crown, with CO$_2$ and isolation of [(R$_2$N)$_3$Sc(μ-OCO-κ^1O:κ^1O')K(crown)]$_n$, 7. In a glovebox, a side-arm Schlenk flask was charged with **5-crown** (50 mg, 0.060 mmol) in 10 mL Et_2O. The flask was sealed, brought out of the glovebox, and the solution was frozen using a liquid N_2 bath before attaching the flask to a vacuum line. The flask was evacuated and excess CO_2 was added to the frozen solution at 77 K. The solution was thawed using a room temperature water bath while being continuously swirled and quickly turned colorless. The vessel was briefly evacuated to remove excess CO_2 and then returned to a glovebox. The solution was filtered, and the solvent was removed under reduced pressure to yield a colorless oil. When hexane (5 mL) was added and the vial swirled for a few seconds, a white precipitate formed. The solvent was decanted, and the solids were dried under reduced pressure. ^{1}H NMR (C_6D_6): δ 0.71 (s, Si*Me*$_3$), 3.21 (s, O*CH*$_2$*CH*$_2$O). ^{13}C NMR (C_6D_6): δ 177.70 (*C*$_2$O$_4$), 122.20 (t, coordinated *C*$_6$D$_6$), 70.31 (crown), 7.32 (Si*Me*$_3$). The 177.70 ppm shift is observable only when $^{13}CO_2$ was used and is similar to those of oxalic acid (163.2 ppm in DMSO-d$_6$)[14] and $[(TiX_3)_2(\mu\text{-}C_2O_4\text{-}\kappa^1O\text{:}\kappa^1O'')]$ (X = N-^{t}Bu-3,5-dimethylanilide) (162.8 ppm in chloroform-d$_1$). Therefore, the obtained NMR data were attributed to arise from an oxalate complex similar to **3** with a slight

variation of the cation. IR of sample prepared using $^{12}CO_2$ (cm^{-1}): 2953m, 2895m, 2228m, 1671m, 1472w, 1453w, 1353m, 1285w, 1248m, 1185w, 1112s, 939s, 833s, 779m, 756m, 703w, 667m, 623w. IR of sample prepared using $^{13}CO_2$ (cm^{-1}): 2951m, 2898m, 2169m, 1625m, 1475w, 1455w, 1353m, 1285w, 1242m, 1112s, 941s, 833s, 778m, 756m, 703w, 666m, 622w. The white precipitate was re-dissolved in Et_2O (2 mL) and colorless single crystals of $[(R_2N)_3Sc(\mu\text{-OCO-}\kappa^1O{:}\kappa^1O')K(crown)]_n$, **7**, suitable for X-ray diffraction were grown from slow vapor diffusion of pentane into the Et_2O solution at −35 ºC. These crystals were obtained along with non-crystalline white solids. This complex was not observable by NMR spectroscopy presumably due to its paramagnetism.

$[K(crypt)]_2\{[(R_2N)_3Sc]_2[\mu\text{-N(Me)CC(Me)N}]\}$, 8. In a glovebox, acetonitrile (1 mL) was added to crystalline solids of **5-crypt** (20 mg, 0.021 mM), resulting in the dissolution of the dark maroon solids to form a pale blue-green solution and some pale yellow insolubles. The was filtered and stored a −35 ºC. Pale green crystals of $[K(crypt)]_2\{[(R_2N)_3Sc]_2[\mu\text{-N(Me)CC(Me)N}]\}$, **8**, (8 mg, 39%) suitable for X-ray diffraction were grown from the solution after 24 h. IR (cm^{-1}): 2959s, 2890s, 2820m, 2616w, 2074m, 1698m, 1644m, 1478m, 1446m, 1360s, 1298m, 1239vs, 1107vs, 951vs, 867vs, 831vs, 777s, 755m, 704m, 664s, 614m, 562w, 525w. Anal. Calcd. for $C_{76}H_{186}N_{12}Si_{12}Sc_2K_2O_{12}$: C, 46.44; H, 9.54; N, 8.55. Found: C, 45.03; H, 10.32; N, 8.54.

X-ray Data Collection, Structure Solution, and Refinement for 6. A colorless crystal of approximate dimensions 0.274 x 0.391 x 0.579 mm was mounted on a glass fiber and transferred to a Bruker SMART APEX II diffractometer. The APEX2[25] program package was used to determine the unit-cell parameters and for data collection (15 sec/frame scan time for a sphere of diffraction data). The raw frame data was processed using SAINT[26] and SADABS[27] to yield the reflection data file. Subsequent calculations were carried out using the SHELXTL[28] program. The

diffraction symmetry was 2/*m* and the systematic absences were consistent with the monoclinic space groups *Cc* and *C*2/*c*. It was later determined that space group *C*2/*c* was correct. The structure was solved by direct methods and refined on F^2 by full-matrix least-squares techniques. The analytical scattering factors[29] for neutral atoms were used throughout the analysis. Hydrogen atoms were included using a riding model. The molecule was a dimer and was located about a two-fold rotation axis. There was one molecule of diethylether present per dimeric formula-unit which was located on a two-fold rotation axis. The $K_2(crown)_3$ unit was located about an inversion center. Several atoms were disordered and included using multiple components with partial site-occupancy-factors. The disordered crown defined by atoms O(6A)-C(31B) was refined using the SAME command[28]. Least-squares analysis yielded wR2 = 0.1878 and Goof = 1.024 for 556 variables refined against 11658 data (0.82Å), R1 = 0.0690 for those 9579 data with $I > 2.0\sigma(I)$. There were high residuals present in the final difference-Fourier map. It was not possible to determine the nature of the residuals although it was probable that additional diethylether solvent was present. The SQUEEZE[30] routine in the PLATON[31] program package was used to account for the electrons in the solvent accessible voids.

X-ray Data Collection, Structure Solution, and Refinement for 7. A colorless crystal of approximate dimensions 0.190 x 0.273 x 0.357 mm was mounted on a glass fiber and transferred to a Bruker SMART APEX II diffractometer. The APEX2[25] program package was used to determine the unit-cell parameters and for data collection (20 sec/frame scan time for a sphere of diffraction data). The raw frame data was processed using SAINT[26] and SADABS[27] to yield the reflection data file. Subsequent calculations were carried out using the SHELXTL[28] program. The diffraction symmetry was 2/*m* and the systematic absences were consistent with the monoclinic space group $P2_1/n$ that was later determined to be correct. The structure was solved by direct

methods and refined on F^2 by full-matrix least-squares techniques. The analytical scattering factors[29] for neutral atoms were used throughout the analysis. Hydrogen atoms were included using a riding model. The complex repeated through the interaction of K(1) with C(12). At convergence, wR2 = 0.1137 and Goof = 1.028 for 469 variables refined against 11856 data (0.76Å), R1 = 0.0429 for those 8775 data with $I > 2.0\sigma(I)$.

X-ray Data Collection, Structure Solution, and Refinement for 8. A green crystal of approximate dimensions 0.224 x 0.258 x 0.381 mm was mounted in a cryoloop and transferred to a Bruker SMART APEX II diffractometer. The APEX2[25] program package was used to determine the unit-cell parameters and for data collection (60 sec/frame scan time for a sphere of diffraction data). The raw frame data was processed using SAINT[26] and SADABS[27] to yield the reflection data file. Subsequent calculations were carried out using the SHELXTL[28] program. There were no systematic absences nor any diffraction symmetry other than the Friedel condition. The centrosymmetric triclinic space group $P\bar{1}$ was assigned and later determined to be correct. The structure was solved by dual space methods and refined on F^2 by full-matrix least-squares techniques. The analytical scattering factors[5] for neutral atoms were used throughout the analysis. Hydrogen atoms were included using a riding model. There were two molecules of the formula-unit present. Atoms C(20), C(21) and C(70) were disordered and included using multiple components with partial site-occupancy-factors. Least-squares analysis yielded wR2 = 0.1460 and Goof = 1.027 for 2171 variables refined against 53433 data (0.75 Å), R1 = 0.0571 for those 38310 data with $I > 2.0\sigma(I)$

References

(1) Fang, M.; Lee, D. S.; Ziller, J. W.; Doedens, R. J.; Bates, J. E.; Furche, F.; Evans, W. J. *J. Am. Chem. Soc.* **2011**, *133*, 3784-3787.

(2) Fang, M.; Farnaby, J. H.; Ziller, J. W.; Bates, J. E.; Furche, F.; Evans, W. J. *J. Am. Chem. Soc.* **2012**, *134*, 6064-6067.

(3) Castro-Rodriguez, I.; Meyer, K. *J. Am. Chem. Soc.* **2005**, *127*, 11242-11243.

(4) Castro-Rodriguez, I.; Nakai, H.; Zakharov, L. N.; Rheingold, A. L.; Meyer, K. *Science* **2004**, *305*, 1757-1759.

(5) Woen, D. H.; Chen, G. P.; Ziller, J. W.; Boyle, T. J.; Furche, F.; Evans, W. J. *J. Am. Chem. Soc.* **2017**, *139*, 14861-14864.

(6) Paparo, A.; Silvia, J. S.; Kefalidis, C. E.; Spaniol, T. P.; Maron, L.; Okuda, J.; Cummins, C. C. *Angew. Chem. Int. Ed.* **2015**, *54*, 9115-9119.

(7) Budzichowski, T. A.; Chisholm, M. H.; Folting, K.; Huffman, J. C.; Streib, W. E. *J. Am. Chem. Soc.* **1995**, *117*, 7428-7440.

(8) Uhl, W.; Jasper, B.; Lawerenz, A.; Marschner, C.; Fischer, J. *Z. Anorg. Allg. Chem.* **2007**, *633*, 2321-2325.

(9) Gaderbauer, W.; Balatoni, I.; Wagner, H.; Baumgartner, J.; Marschner, C. *Dalton Trans.* **2009**, *39*, 1598-1603.

(10) Lin, C.-Y.; Fettinger, J. C.; Chilton, N. F.; Formanuik, A.; Grandjean, F.; Long, G. J.; Power, P. P. *Chem. Commun.* **2015**, *51*, 1375-1378.

(11) Shannon, R. *Acta Crystallog., Sect. A* **1976**, *32*, 751-767.

(12) Evans, W. J.; Seibel, C. A.; Ziller, J. W. *Inorg. Chem.* **1998**, *37*, 770-776.

(13) Meyer, K.; Bart, S. C. In *Advances in Inorganic Chemistry*; Eldik, R. v., Ed.; Academic Press: Amsterdam, 2008; Vol. 60, p 1-28.

(14) Pokharel, U. R.; Fronczek, F. R.; Maverick, A. W. *Nat. Commun.* **2014**, *5*, 5883.

(15) Govindarajan, S.; Patil, K. C.; Poojary, M. D.; Monohar, H. *Inorg. Chim. Acta* **1986**, *120*, 103-107.

(16) Evans, W. J.; Seibel, C. A.; Ziller, J. W. *Inorg. Chem.* **1998**, *37*, 770-776.

(17) Kim, J. C.; Cho, J.; Lough, A. J. *Inorg. Chim. Acta* **2001**, *317*, 252-258.

(18) Das, N.; Ghosh, A.; Arif, A. M.; Stang, P. J. *Inorg. Chem.* **2005**, *44*, 7130-7137.

(19) Arias, A.; Forniés, J.; Fortuño, C.; Martín, A. *Inorg. Chim. Acta* **2013**, *407*, 189-196.

(20) Yue, Y.-F.; Gao, E.-Q.; Fang, C.-J.; Zheng, T.; Liang, J.; Yan, C.-H. *CrystEngComm* **2008**, *10*, 614-622.

(21) Burford, R. J.; Piers, W. E.; Parvez, M. *Eur. J. Inorg. Chem.* **2013**, 3826-3830.

(22) Segerer, U.; Blaurock, S.; Sieler, J.; Hey-Hawkins, E. *Organometallics* **1999**, *18*, 28382842.

(23) Young, C. G.; Philipp, C. C.; White, P. S.; Templeton, J. L. *Inorg. Chem.* **1995**, *34*, 6412-6414.

(24) Tsai, Y.-C.; Johnson, M. J. A.; Mindiola, D. J.; Cummins, C. C. *J. Am. Chem. Soc.* **1999**, *121*, 10426-10427.

(25) Bruker AXS, Inc., APEX2 Version 2014.11-0, Madison, WI, **2014**.

(26) Bruker AXS, Inc., SAINT Version 8.34a, Madison, WI, **2013**.

(27) Sheldrick, G. M.; SADABS, Version 2014/5, Bruker AXS, Inc., Madison, WI, **2014**.

(28) Sheldrick, G. M.; SHELXTL, Version 2014/7, Bruker AXS, Inc., Madison, WI, **2014**.

(29) *International Tables for Crystallography, Vol. C*, Kluwer Academic Publishers, Dordrecht, **1992**.

(30) Spek, A. L. *Acta Cryst.* **2015**, *C17*, 9-19.

(31) Spek, A. L. *Acta Cryst.* **2009**, *D65*, 148-155.

CHAPTER 7

Tris(pentamethylcyclopentadienyl) Complexes of the Late Lanthanides, Tb, Dy, Ho, and Er: Solution and Mechanochemical Syntheses and Structural Comparisons

Introduction*

For decades, tris(pentamethylcyclopentadienyl) metal complexes, $(C_5Me_5)_3M$, were thought to be too sterically crowded to exist[1] since the cone angle of a $(C_5Me_5)^{1-}$ ligand was estimated to be 142° and three of these ligands would exceed 360°.[2] The discovery of $(C_5Me_5)_3Sm$, eq 7.1, was surprising since this showed that C_5Me_5 rings can have a 120° cone

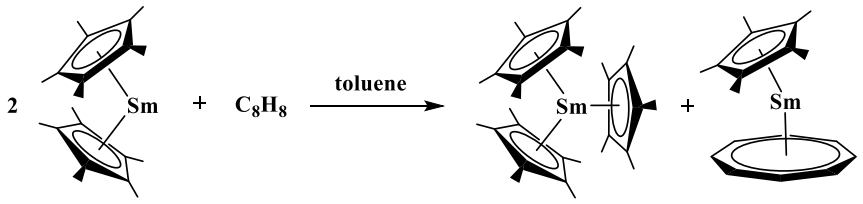

(7.1)

angle.[3] This smaller cone angle was possible since the rings in $(C_5Me_5)_3Sm$ were much further from the metal with Sm–C bond distances approximately 0.1 Å greater than those previously observed for pentamethylcyclopentadienyl Sm^{3+} complexes.[4]

Associated with these long distances was unusual pentamethylcyclopentadienyl reactivity. Since the $(C_5Me_5)^{1-}$ ligands were bound at distances longer than typically found in samarium pentamethylcyclopentadienyl complexes, they were not sufficiently stabilized by the Sm^{3+} ion. As a result, one of the rings in $(C_5Me_5)_3Sm$ can react as a one electron reductant, leading to redox activity that has been termed sterically induced reduction, SIR.[5-7] It was also found that

* Portions of this chapter have been published: Woen, D. H.; Kotyk C. M.; Mueller, T. J.; Ziller, J. W.; Evans, W. J. *Organometallics* **2017**, *in press*. DOI: 10.1021/acs.organomet.7b00385.

$(C_5Me_5)_3Sm$ could react like an alkyl complex, effectively as $(\eta^5\text{-}C_5Me_5)_2Sm(\eta^1\text{-}C_5Me_5)$. Hence, $(C_5Me_5)_3Sm$ ring-opens THF to make $(C_5Me_5)_2Sm[O(CH_2)_4(C_5Me_5)](THF)$ and displays alkyl-like reactivity with other substrates such as H_2, CO, and PhCN.[7]

The original synthesis of $(C_5Me_5)_3Sm$ relied on the fact that the Sm^{2+} complex, $(C_5Me_5)_2Sm$,[8-9] was isolable and highly reactive. $(C_5Me_5)_2Eu$[9] and $(C_5Me_5)_2Yb$[10] were not reducing enough to generate $(C_5Me_5)_3Ln$ complexes and $(C_5Me_5)_2Ln$ complexes were not known for any other lanthanides. However, new methods were subsequently found to synthesize $(C_5Me_5)_3Ln$ complexes from Ln^{3+} precursors. $(C_5Me_5)_3Ln$ complexes of La,[11] Ce,[7] Pr,[7] Nd,[12] and Gd,[13] as well as $(C_5Me_5)_3U$[14] were synthesized by reacting KC_5Me_5 with the cationic metallocenes, $(C_5Me_5)_2M(\mu\text{-}Ph)_2BPh_2$, that had labile tetraphenylborate counteranions, eq 7.2. These $(C_5Me_5)_3M$ complexes also exhibited alkyl reactivity and SIR and they ring-opened THF.

M = La, Ce, Pr, Nd, Gd, U

(7.2)

Attempts to isolate an analogous complex with the smaller metal, yttrium, gave the phenyl and benzyl products, $(C_5Me_5)_2Y(C_6H_5)$ and $(C_5Me_5)_2Y(CH_2C_6H_5)$, when the reactions were conducted in benzene and toluene, respectively, eq 7.3.[13] Subsequently, an arene-free method

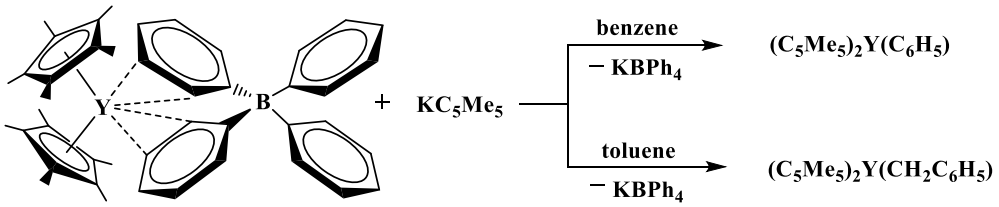

(7.3)

was utilized to synthesize $(C_5Me_5)_3Y$ from $[(C_5Me_5)_2Y(\mu\text{-}H)]_2$ and 1,2,3,4-tetramethylfulvene (TMF) in methylcyclohexane (MCH), eq 7.4. Once isolated, it was confirmed that $(C_5Me_5)_3Y$

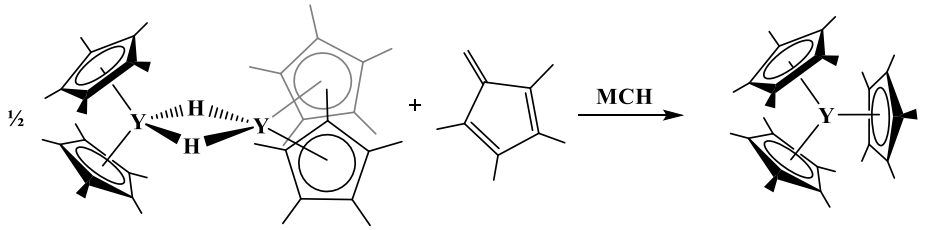

(7.4)

was capable of metalating both benzene and toluene. These reactions that formally generate a stronger hydrocarbon acid (C_5Me_5H) from weaker ones (benzene or toluene) are possible due to the steric crowding in $(C_5Me_5)_3Y$.[9] Attempts to synthesize the analog of the smallest lanthanide, $(C_5Me_5)_3Lu$, using the arene-free method gave only products of C–H bond activation of the reactants, namely a vinyl complex and a tuckover product, eq 7.5.[15]

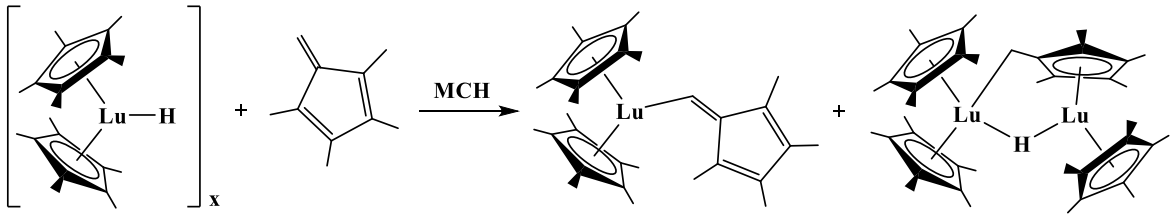

(7.5)

Synthesis of the other members of the $(C_5Me_5)_3Ln$ series, Ln = Tb, Dy, Ho, and Er are complicated by the large paramagnetism of the Ln^{3+} ions. Synthetic intermediates cannot be characterized by NMR spectroscopy and definitive characterization requires X-ray crystallography. In addition, it was expected that the complexes with the smaller metals would be more reactive. It was unknown exactly how much steric crowding was necessary to activate the arene metalation reactivity since $(C_5Me_5)_3Y$ metalates arenes, but $(C_5Me_5)_3Gd$ does not. The crossover point could occur with metals of any intermediate size.

This Chapter describes the syntheses of the Tb, Dy, Ho, and Er members of the series including mechanochemistry as a new solvent-free method for generating $(C_5Me_5)_3Ln$ complexes. Mechanochemistry, the harnessing of mechanical energy through grinding and friction by ball-milling or simple mortar and pestle methods, has been applied in many different fields for a variety

of useful chemical transformations.[16-19] Recently, there has been a growing interest in the use of mechanochemistry to simplify the synthesis of highly reactive organometallic complexes that would not be obtainable by solvent-based methods.[20-21] Subsequently, a previous Evans group member, Dr. Christopher M. Kotyk, initiated the implementation of mechanochemistry in the Evans group. It is demonstrated herein that this technique is applicable to air-sensitive cyclopentadienyl lanthanide chemistry and that it can be used to avoid the arene metalation reactivity shown in eq 7.3. The isolation of these new examples of the $(C_5Me_5)_3Ln$ series also allows structural comparisons to be made with the smaller metals in the lanthanide series. Previously, comparisons between adjacent metals could only be made for the larger metals, La-Sm.[22]

Results and Discussion

Synthetic Precursors. The cationic metallocene complexes, $(C_5Me_5)_2Ln(\mu\text{-}Ph)_2BPh_2$, utilized as precursors in this study were synthesized as previously reported for the Sm[12] and Y[13] analogs. The reaction of $LnCl_3$ with two equiv of KC_5Me_5 affords the ate-salt complexes, $(C_5Me_5)_2Ln(\mu\text{-}Cl_2)K(THF)_x$, which are then treated with allylmagnesiumchloride to form the allyl complexes, $(C_5Me_5)_2Ln(\eta^3\text{-}C_3H_5)$. The allyl complexes react with $[HNEt_3][BPh_4]$ to form $(C_5Me_5)_2Ln(\mu\text{-}Ph)_2BPh_2$. The structures were confirmed by X-ray diffraction (Figure 7.1 and Figure 7.2).

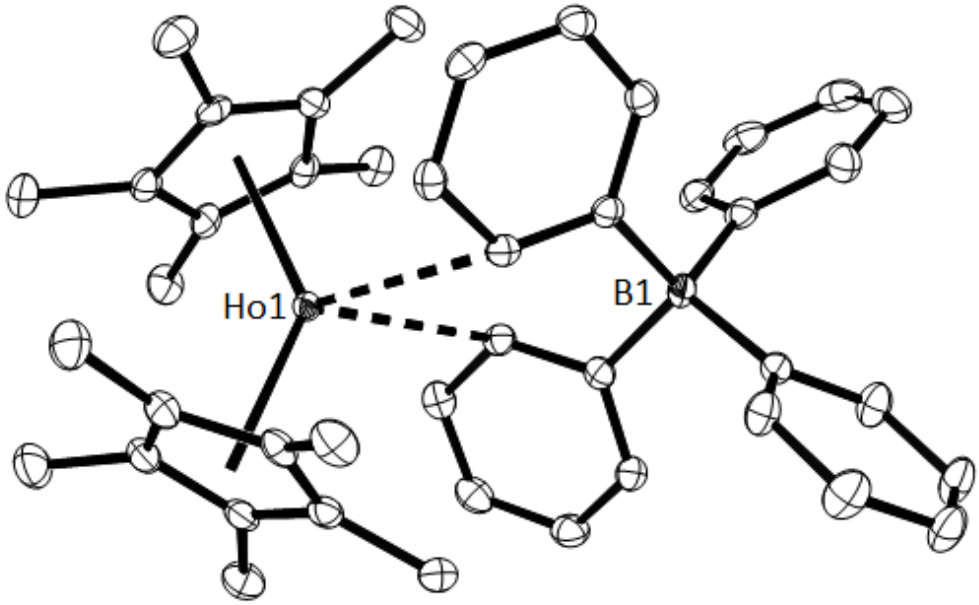

Figure 7.1. Thermal ellipsoid plots of $(C_5Me_5)_2Ho(\mu\text{-}Ph)_2BPh_2$ drawn at the 50% probability level. Hydrogen atoms are omitted for clarity.

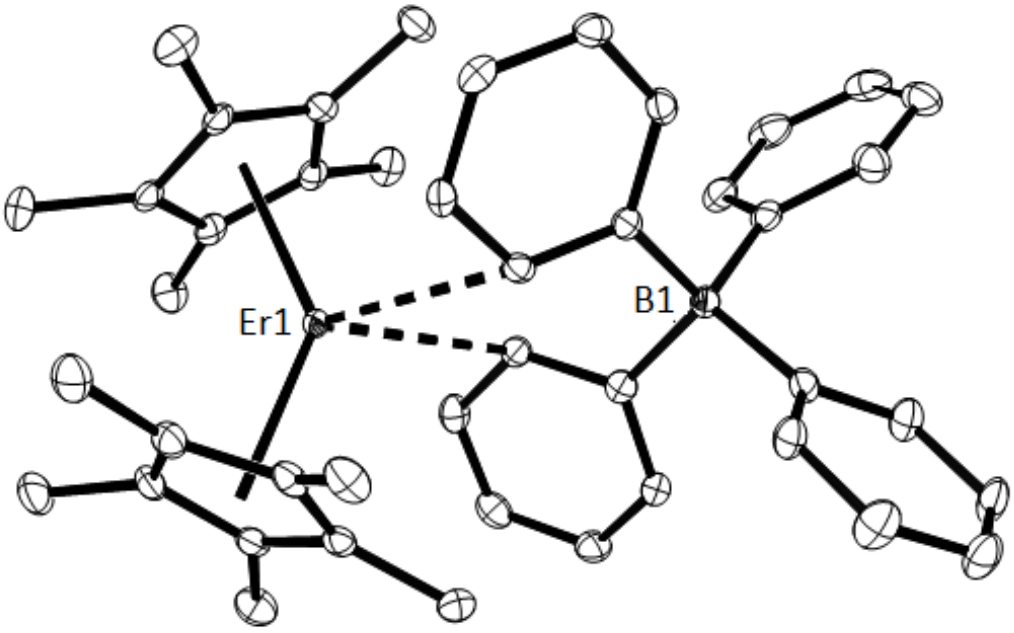

Figure 7.2. Thermal ellipsoid plots of $(C_5Me_5)_2Er(\mu\text{-}Ph)_2BPh_2$ drawn at the 50% probability level. Hydrogen atoms are omitted for clarity.

$(C_5Me_5)_3Tb$. In a reaction analogous to eq 7.2, pale yellow $(C_5Me_5)_2Tb(\mu\text{-}Ph)_2BPh_2$ reacts with KC_5Me_5 in benzene over two days to form a red-orange product that crystallizes from toluene over several days and was identified as $(C_5Me_5)_3Tb$ by X-ray crystallography, Figure 7.3. Since the synthesis involves extended exposure of the product both to benzene and toluene, it is apparent that $(C_5Me_5)_3Tb$ is not reactive toward benzene or toluene in contrast to $(C_5Me_5)_3Y$, eq 7.3.

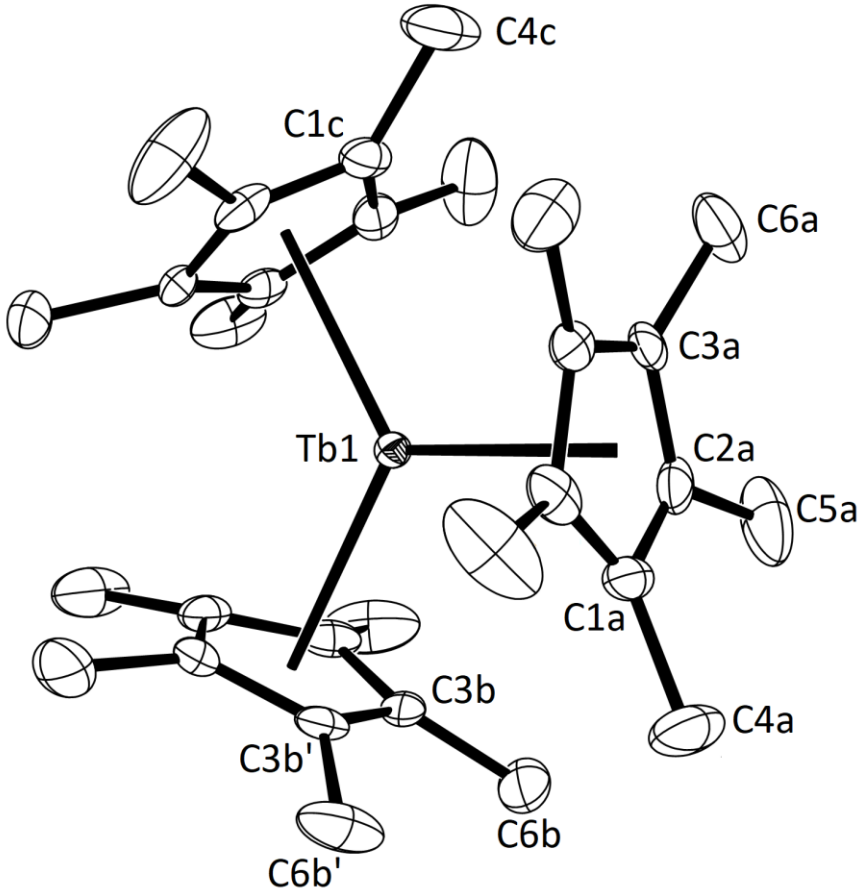

Figure 7.3. Thermal ellipsoid plot of $(C_5Me_5)_3Tb$ drawn at the 50% probability level. Hydrogen atoms are omitted for clarity.

$(C_5Me_5)_3Dy$. For the smaller metal, Dy, multiple efforts to synthesize the presumably more sterically crowded complex from $(C_5Me_5)_2Dy(\mu\text{-}Ph)_2BPh_2$ using the method for the Tb

analog, gave only pale orange products that failed to crystallize and were unidentifiable. Hence, a previous group member, Dr. Thomas J. Mueller, used the arene-free method analogous to eq 7.4 to synthesize this complex. $[(C_5Me_5)_2Dy(\mu\text{-}H)]_2$ and 1,2,3,4-tetramethylfulvene react immediately in methylcyclohexane to form a dark red-orange solution. Removal of the solvent produced a red tacky solid that was washed with cold pentane and recrystallized from methylcyclohexane to form red-orange single crystals suitable for X-ray diffraction. The product was identified as $(C_5Me_5)_3Dy$ and has a structure (Figure 7.4) isomorphous to that of $(C_5Me_5)_3Tb$ (Figure 7.3).

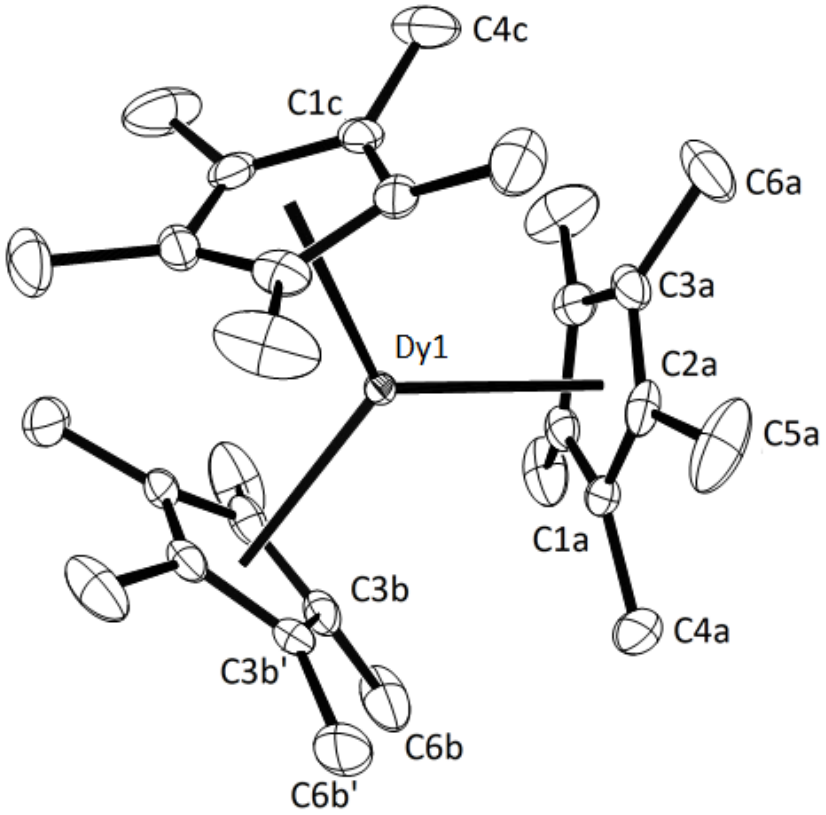

Figure 7.4. Thermal ellipsoid plot of $(C_5Me_5)_3Dy$ drawn at the 50% probability level. Hydrogen atoms are omitted for clarity.

Mechanochemical Synthesis of $(C_5Me_5)_3Ln$. $(C_5Me_5)_3Y$ was chosen as the first target of mechanochemical synthesis since it was previously synthesized via eq 7.4[13] and since the

diamagnetism of Y^{3+} allows facile identification of the product by ^1H NMR spectroscopy. Milling a colorless mixture of $(C_5Me_5)_2Y(\mu\text{-}Ph)_2BPh_2$ and KC_5Me_5 using stainless steel balls in a BMT-20-S tube powered by an Ultra-Turrax Tube Drive for 40 minutes produced a pale orange mixture. This mixture was extracted into hexane to produce a red-orange solution, and removal of solvent from the extract gave an orange powder with a ^1H NMR spectrum consistent with that of the previously reported $(C_5Me_5)_3Y$.[13] Single crystals of this complex were obtained from a concentrated pentane solution at −35 °C and their identity was confirmed by X-ray crystallography.

The mechanochemical method was applied to the synthesis of the lanthanide metal analogs Tb, Dy, Ho, and Er, eq 7.6. In each case, red-orange crystalline products were collected

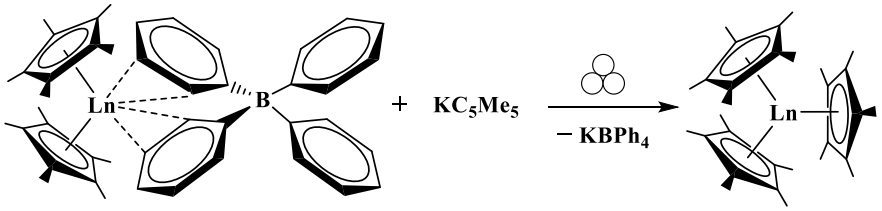

(7.6)

by crystallization at −35 °C from the hexane extract. Each product was characterized by X-ray crystallography and identified as $(C_5Me_5)_3Ln$ (Figures 7.3-7.6).

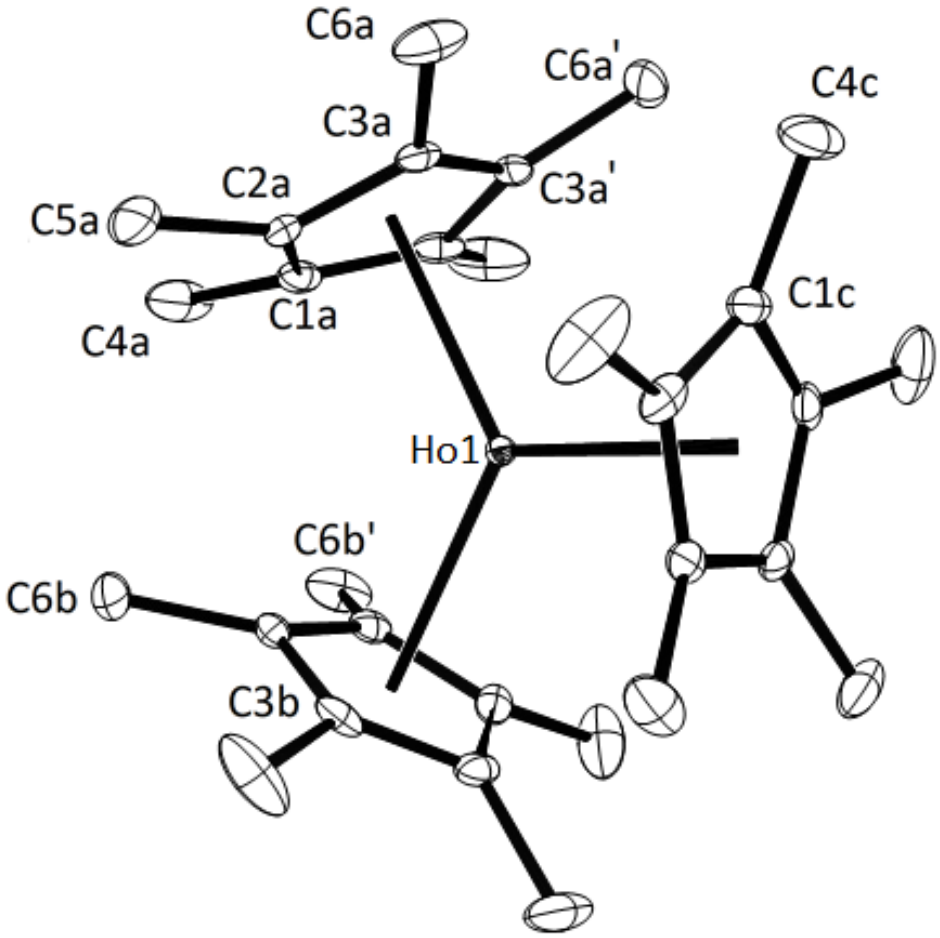

Figure 7.5. Thermal ellipsoid plots of $(C_5Me_5)_3Ho$ drawn at the 50% probability level. Hydrogen atoms are omitted for clarity.

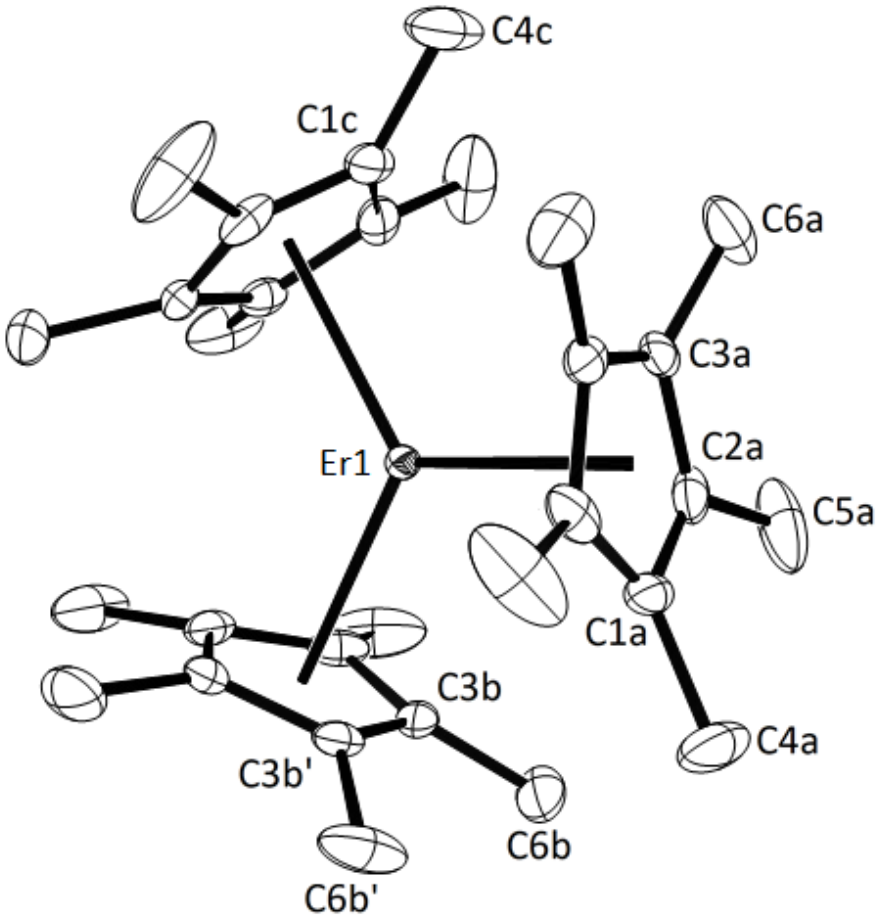

Figure 7.6. Thermal ellipsoid plots of $(C_5Me_5)_3Er$ drawn at the 50% probability level. Hydrogen atoms are omitted for clarity.

Structural Comparisons. The four new complexes, $(C_5Me_5)_3Ln$ (Ln = Tb, Dy, Ho, Er), are isomorphous with all the previously reported $(C_5Me_5)_3Ln$ complexes: they all crystallize in the hexagonal space group $P6_3/m$ with similar unit cells. Due to their high symmetry, $(C_5Me_5)_3Ln$ complexes only have three unique ring carbon atoms, C1, C2, and C3, and three unique methyl carbon atoms, C4, C5, C6, as labeled in Figures 7.3-7.6. The C1−C4 vector is a unique (ring carbon)−(methyl carbon) vector in each ring. The rings are oriented so that this vector lies in a plane that is perpendicular to and bisects the C3−C3' (ring carbon)−(ring carbon) bond of the next

ring. This staggers the steric bulk to the greatest extent. All three methyl groups are displaced away from the cyclopentadienyl plane as is typical for rare-earth metal complexes with $(C_5Me_5)^{1-}$ ligands.[22] However, in the sterically crowded $(C_5Me_5)_3Ln$ complexes, there is one methyl group, C4, that is displaced much further out of the plane than normal. With the exception of thorium complexes,[23-24] it has been observed that when this displacement is greater than 0.48 Å, the complex exhibits unusual $(C_5Me_5)^{1-}$ reactivity like that shown in Schemes 1 and 2.[22]

Studies on the previously reported complexes with Ln = La, Ce, Pr, Nd, and Sm revealed that there is a trend of increasing methyl displacement out of the average ring plane with decreasing metal 9-coordinate ionic radii,[25] as shown in Table 7.1, entries a-e.[22] This trend continues with Gd, since $(C_5Me_5)_3Gd$, entry f, has an even greater out of plane displacement of 0.55 Å. However, this seems to be a maximum for C4, since none of the smaller metals, Ln = Tb, Dy, Y, and Er, Table 7.1, entries g-k, have larger maximum displacements. There is a gradual increase of methyl displacements for C5 and C6 for the entire series as the metal size decreases. The overall displacements are variable enough that the sum of the displacements for Y, Ho, and Er are all the same (1.14 Å) and are numerically only 0.01 Å more than the sum for Dy, Tb, and Gd, 1.13 Å).

Table 7.1. Nine-coordinate ionic radii (Å), displacements (Å) for the three unique methyl substituents (C4-C6) from the average ring plane of the $(C_5Me_5)^{1-}$ ligand, the metal-centroid-C(ring) angles (°), and the deviation of the ring planes from being perpendicular to the ring centroid-metal vector, θ (°).

		Methyl Displacement			**Ln−Cnt−C(ring)**			**Deviation**
	Ln Ionic Radius[25]	**C4**	**C5**	**C6**	**C1**	**C2**	**C3**	θ
a. $(C_5Me_5)_3La$[11]	1.216	0.50	0.16	0.31	93.8	89.8	88.4	3.0
b. $(C_5Me_5)_3Ce$[7]	1.196	0.50	0.17	0.32	93.9	89.8	88.3	3.1
c. $(C_5Me_5)_3Pr$[7]	1.179	0.52	0.17	0.33	94.0	89.8	88.2	3.2
d. $(C_5Me_5)_3Nd$[12]	1.163	0.52	0.17	0.34	94.1	89.8	88.2	3.3
e. $(C_5Me_5)_3Sm$[3]	1.132	0.52	0.18	0.36	94.7	89.9	87.8	3.8
f. $(C_5Me_5)_3Gd$[13]	1.107	0.55	0.18	0.36	94.9	89.7	87.9	3.9
g. $(C_5Me_5)_3Tb$	1.095	0.55	0.19	0.37	95.0	89.8	87.7	4.0
h. $(C_5Me_5)_3Dy$	1.083	0.54	0.19	0.38	95.5	90.0	87.2	4.5
i. $(C_5Me_5)_3Y$[13]	1.075	0.55	0.19	0.39	95.7	90.0	87.1	4.7
j. $(C_5Me_5)_3Ho$	1.072	0.54	0.19	0.39	95.6	90.0	87.1	4.6
k. $(C_5Me_5)_3Er$	1.062	0.54	0.20	0.40	96.1	90.1	86.9	5.1

Isolation of the $(C_5Me_5)_3Ln$ complexes of the smaller metals has provided the means to clearly identify another trend in these structures. There is an increase in tilting of the $(C_5Me_5)^{1-}$ ring away from the metal center as the ionic radius of the metal decreases. This is illustrated in the ball-and-stick models of $(C_5Me_5)_3La$ and $(C_5Me_5)_3Er$, Figure 7.7, which shows that the tilt is larger for the smaller metal.

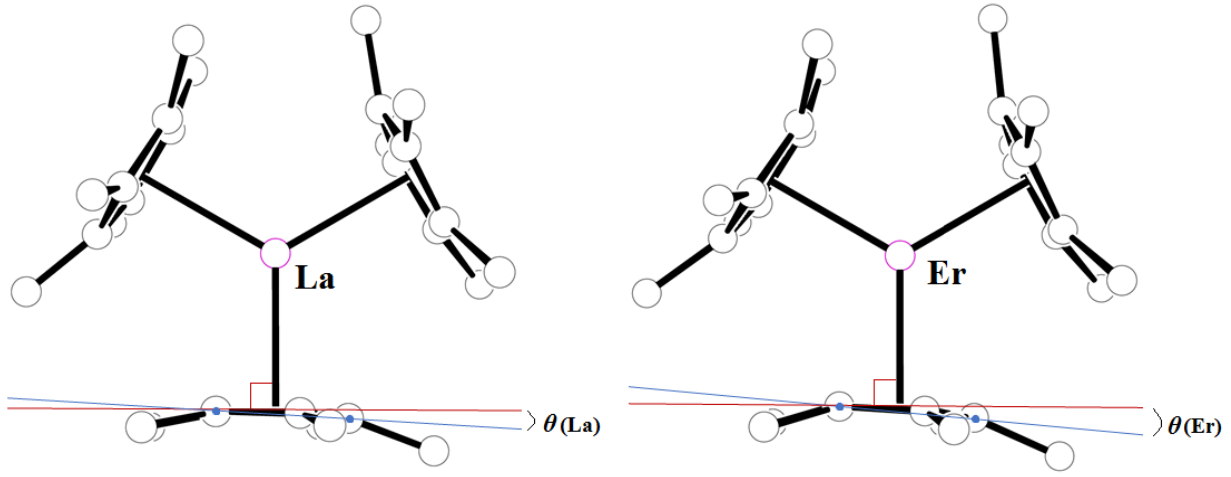

Figure 7.7. Depiction of the increase in the $(C_5Me_5)^{1-}$ ring tilting between $(C_5Me_5)_3La$ and $(C_5Me_5)_3Er$, in which $\theta(La) < \theta(Er)$.

The angular data in Table 7.1 show that with smaller metals, the Ln−(centroid)−C1 angle increases beyond 90° and the Ln−(centroid)−C3 angle decreases below 90° while the Ln−(ring centroid)−C2 angle stays close to 90°. This occurs with the larger metals also, but the effect is not as great, as shown in Figure 7.8. $(C_5Me_5)_3Er$ has the greatest deviation of rings from being perpendicular to the ring centroid-metal vector.

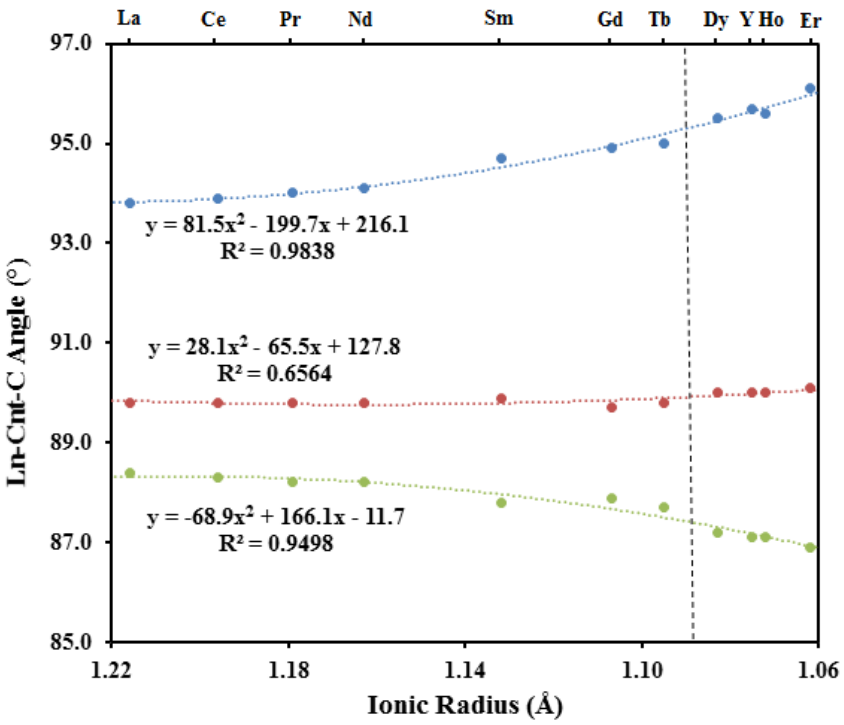

Figure 7.8. Plots of nine-coordinate ionic radii vs. Ln−Cnt−C angles showing an increase in Ln−Cnt−C1 angles (top) and a decrease in Ln−Cnt−C3 angles (bottom) with decreasing ionic radii while Ln−Cnt−C2 angles stay almost constant (middle). The perpendicular line drawn between Tb and Dy indicates the crossover point at which C−H bond activation of benzene and toluene occurs.

Since it was found that $(C_5Me_5)_3Tb$ can be prepared in aromatic solvents but not $(C_5Me_5)_3Dy$, a line can be drawn between Ln = Tb and Dy to signify the crossover point in ionic radii at which C−H bond activation of benzene or toluene is observed. Hence, the degree of deviation of the ring planes from their expected perpendicularity to the metal center provides a more subtle factor to evaluate arene C−H bond activation reactivity than methyl displacement. The possibility of an increased tilt in the more reactive complexes of the smaller metals, as demonstrated in the solid state data, may be related to the enhanced reactivity in solution. If this

tilted structure can be accessed in solution as it is in the solid state, it may facilitate interaction with the arene. It could also lead to an η^5 to η^1 transformation that would form a reactive Ln−C single bond that could effect the C−H bond activation by sigma bond metathesis.[26]

Since dispersion forces can be used to explain the stability of sterically bulky complexes, the possibility that dispersion forces are stabilizing the $(C_5Me_5)_3Ln$ complexes has been suggested.[27] The closest intramolecular C−C contacts decrease with decreasing size of the metal and increased steric crowding: (in Å) La, 3.40; Ce, 3.38; Pr, 3.37; Nd, 3.36; Sm, 3.34; Gd, 3.34; Tb 3.33; Dy, 3.32; Ho, 3.32; Er, 3.32. Although these are all within the 3.4 Å sum of the van der Waals radii of two carbon atoms,[28] the closer intramolecular contact are associated with the more reactive complexes. Hence, it is possible that all compounds in the series are stabilized by this effect, but it does not obviate the C−H bond activation reactivity of the more crowded complexes.

Conclusion

The sterically crowded complexes $(C_5Me_5)_3Ln$ (Ln = Tb, Dy, Ho, and Er) were synthesized for the first time and characterized by X-ray crystallography. These complexes, as well as the yttrium analog, could be synthesized by a solvent-free mechanochemical method that avoids the problem that the more crowded complexes react with arene solvents, benzene and toluene, by C−H bond activation. Structural comparison of the new complexes as well as the previously isolated larger metal analogs (Ln = La, Ce, Pr, Nd, Sm and Gd) revealed that the gradual increase in the C4 methyl displacements, which is correlated to the unusual pentamethylcyclopentadienyl reactivity of the complexes, appears to reach a maximum of 0.55 Å at Gd. Consequently, this metric does not constitute a structural feature that identifies the onset of arene C−H bond activation reactivity that occurs with more crowded complexes of the smaller metals. However, the structures

of the complexes of the smaller metals revealed another trend involving the tilt of the $(C_5Me_5)^{1-}$ rings away from the metal center. This increases as the ionic radius of the metal gets smaller and provides a metric for the crossover in arene C−H bond activation reactivity that starts at dysprosium.

Experimental Details

All manipulations and syntheses described below were conducted with the rigorous exclusion of air and water using standard Schlenk line and glovebox techniques under an argon or dinitrogen atmosphere. Solvents were sparged with UHP argon and dried by passage through columns containing Q-5 and molecular sieves prior to use. Deuterated NMR solvents were dried over NaK alloy, degassed by three freeze-pump-thaw cycles, and vacuum transferred before use. Allylmagnesiumchloride and dioxane were purchased from Aldrich and used without further purification. $[HNEt_3][BPh_4]$,[29] $K(C_5Me_5)$,[30] $(C_5Me_5)_2Ln(\mu\text{-}Ph)_2BPh_2$ (Ln = Tb, Dy,[31-32] Y[13]), $[(C_5Me_5)_2Dy(\mu\text{-}H)]_2$,[33] and 1,2,3,4-tetramethylfulvene (TMF)[34] were prepared according to literature procedures. ^1H NMR spectra were recorded on Bruker GN500 or CRYO500 MHz spectrometers at 298 K unless otherwise stated and referenced internally to residual protio-solvent resonances. IR samples were prepared as KBr pellets on a Varian 1000 FT-IR system. Elemental analyses were conducted on a Perkin-Elmer 2400 Series II CHNS elemental analyzer. Disperser milling was performed with an Ultra-Turrax Tube Drive and BMT-20-S tubes, both purchased from IKA.

$(C_5Me_5)_3Tb$. In an argon-filled glovebox free of coordinating solvents, benzene (15 mL) was added to $(C_5Me_5)_2Tb(\mu\text{-}Ph)_2BPh_2$ (212 mg, 0.284 mmol) and KC_5Me_5 (54 mg, 0.31 mmol), and the pale yellow mixture was stirred for two days. The resulting orange mixture was

centrifuged to yield a dark red-orange solution. Toluene (5 mL) was added to the supernatant, and the solution was dried under reduced pressure to produce red-orange solids (134 mg, 83%). The solids were dissolved in hot toluene (2 mL) and left at ambient temperature. Red-orange crystals of $(C_5Me_5)_3Tb$ suitable for X-ray diffraction were grown from the toluene solution at ambient temperature after 24 h. IR: 2964m, 2903s, 2856s, 2718w, 2348w, 1436m, 1381m, 1364m, 1248w, 1147w, 1048w, 1013w, 955w, 804w, 604w cm^{-1}. Anal. Calcd for $C_{30}H_{45}Tb$: C, 63.82; H, 8.03. Found: C, 63.86; H, 8.33.

Mechanochemical Synthesis of $(C_5Me_5)_3Tb$. In an argon-filled glovebox free of coordinating and aromatic solvents, a BMT-20-S tube was charged with $(C_5Me_5)_2Tb(\mu\text{-}Ph)_2BPh_2$ (200 mg, 0.267 mmol), KC_5Me_5 (50 mg, 0.29 mmol) and 40 stainless-steel balls (6 mm). The faint yellow mixture was milled for 40 minutes using an Ultra-Turrax Tube Drive (max speed setting), after which, a pale orange mixture was obtained. Hexane (10 mL) was added to the mixture, followed by centrifugation to produce a dark red-orange solution which was collected in a vial and left at −35 °C. Red-orange single crystals of $(C_5Me_5)_3Tb$ (88 mg, 29%) were obtained after several days, as confirmed by X-ray diffraction.

$(C_5Me_5)_3Dy$. $[(C_5Me_5)_2Dy(\mu\text{-}H)]_2$ (458 mg, 1.05 mmol) was dissolved in methylcyclohexane (10 mL) and TMF (1.15 mL of a 0.50 M in hexane solution, 0.580 mmol) was added to the stirred yellow solution. After 20 h, the solvent of the dark red-orange solution was removed under reduced pressure to yield an oily red product. This was washed with cold pentane (ca. 2 mL) and the resulting material was dried under reduced pressure to yield $(C_5Me_5)_3Dy$ as an orange solid (190 mg, 58%). Red-orange X-ray quality crystals of $(C_5Me_5)_3Dy$ were grown from methylcyclohexane at 25 °C. IR: 2954s, 2908s, 2858s, 2723m, 2360w, 2241w, 2105m, 1492m,

1440s, 1301s, 1366m, 1063w, 1021m, 951w, 804w, 729w, 676w, 657w, 616w, 600w, 551w cm^{-1}. Anal. Calcd for $C_{30}H_{45}Dy$: C, 63.42; H, 7.98. Found: C, 63.32; H, 7.93.

Mechanochemical synthesis of $(C_5Me_5)_3Dy$. Similar to the mechanochemical procedure for $(C_5Me_5)_3Tb$, $(C_5Me_5)_2Dy(\mu\text{-}Ph)_2BPh_2$ (164 mg, 0.182 mmol) and KC_5Me_5 (42 mg, 0.24 mmol) were reacted to yield red-orange crystals of $(C_5Me_5)_3Dy$ (36 mg, 35%), as confirmed by X-ray diffraction.

Mechanochemical synthesis of $(C_5Me_5)_3Y$. Similar to the mechanochemical procedure for $(C_5Me_5)_3Tb$, $(C_5Me_5)_2Y(\mu\text{-}Ph)_2BPh_2$ (208 mg, 0.306 mmol) and KC_5Me_5 (64 mg, 0.37 mmol) were reacted to yield red-orange crystals of $(C_5Me_5)_3Y$ (28 mg, 18%), as confirmed by ^1H NMR spectroscopy (methylcyclohexane-d_{14}) and X-ray diffraction.[13]

$(C_5Me_5)_2Ho(\mu\text{-}Cl_2)K(THF)_x$. In an argon-filled glovebox, KC_5Me_5 (4.00 g, 22.9 mmol) was slowly added to a stirred slurry of $HoCl_3$ (2.11 g, 7.78 mmol) in THF (100 mL) and the reaction was allowed to stir for 2 d. The resulting pink mixture was centrifuged, filtered, and the solvent was removed under reduced pressure. Washing with toluene and subsequent drying yielded $(C_5Me_5)_2Ho(\mu\text{-}Cl_2)K(THF)_x$ as a pink solid (4.50 g, 99.5%, with x = 0.5). IR: 2965s, 2904s, 2859s, 2722w, 1489w, 1434m, 1377m, 1246w, 1131w, 1104w, 1053m, 967w, 912w, 826w, 803w, 740w, 620w cm^{-1}. Anal. Calcd for $C_{20}H_{30}Cl_2HoK\bullet(THF)_{0.5}$: C, 45.26; H, 5.87. Found: C, 45.44; H, 5.95.

$(C_5Me_5)_2Ho(\eta^3\text{-}C_3H_5)$. In an argon-filled glovebox, allylmagnesiumchloride (3.9 mL of a 2.0 M THF solution) was added to a stirring pink slurry of $(C_5Me_5)_2Ho(\mu\text{-}Cl_2)K(THF)_{0.5}$ (4.50 g, 7.74 mmol) in toluene (50 mL) to produce an immediate color change to orange. The reaction was allowed to stir for 4 h and then volatiles were removed under reduced pressure. Hexane (100 mL) and dioxane (2 mL) were added and the orange mixture was allowed to stir. After 12 h, the mixture

was centrifuged and the solvent was removed under reduced pressure to yield $(C_5Me_5)_2Ho(\eta^3\text{-}C_3H_5)$ as an orange powder (1.91 g, 52%). IR: 3063m, 2965s, 2906s, 2859s, 2726w, 1539s, 1486m, 1449s, 1437s, 1379s, 1310w, 1244m, 1023m, 778vs, 677s, 596w cm^{-1}. Anal. Calcd for $C_{23}H_{35}Ho$: C, 57.98; H, 7.40. Found: C, 58.31; H, 7.47.

$(C_5Me_5)_2Ho(\mu\text{-}Ph)_2BPh_2$. In an argon-filled glovebox free of coordinating solvents, $(C_5Me_5)_2Ho(\eta^3\text{-}C_3H_5)$ (750 mg, 1.57 mmol) was dissolved in toluene (5 mL) and added to a stirred slurry of $[HNEt_3][BPh_4]$ (663 mg, 1.57 mmol) in toluene (15 mL). The reaction was allowed to stir for 48 h and resulted in a color change to yellow. The mixture was washed with toluene and hexane to yield $(C_5Me_5)_2Ho(\mu\text{-}Ph)_2BPh_2$ as a pale yellow solid (1.12 g, 79%). Pale yellow single crystals of $(C_5Me_5)_2Ho(\mu\text{-}Ph)_2BPh_2$ suitable for X-ray diffraction were grown from vapor diffusion of pentane into a benzene solution of the pale yellow solid at ambient temperature. IR: 3054s, 2999s, 2984s, 2907s, 2861s, 1695s, 1579m, 1474s, 1428s, 1383s, 1263m, 1178w, 1152w, 1134w, 1062m, 1030m, 967w, 929w, 875w, 846m, 754s, 742vs, 735vs, 704vs, 626w, 610m, 592m cm^{-1}. Anal. Calcd for $C_{44}H_{50}BHo$: C, 70.03; H, 6.68. Found: C, 68.43; H, 6.48. Low carbon and hydrogen values were obtained even after multiple analysis attempts using different batches of samples. The found C/H ratio, $C_{44}H_{49.6}$, is consistent with the formula and suggests incomplete combustion occurs with this compound.

$(C_5Me_5)_3Ho$. Similar to the mechanochemical procedure for $(C_5Me_5)_3Tb$, $(C_5Me_5)_2Ho(\mu\text{-}Ph)_2BPh_2$ (200 mg, 0.22 mmol) and KC_5Me_5 (47 mg, 0.27 mmol) were reacted to yield red-orange crystals of $(C_5Me_5)_3Ho$ (31 mg, 24%) suitable for X-ray diffraction. IR: 2971m, 2904s, 2854s, 2719w, 1435m, 1381m, 1364m, 1054m, 1016w, 948w, 804w, 676w, 616w, 601m cm^{-1}. Anal. Calcd for $C_{30}H_{45}Ho$: C, 63.15; H, 7.95. Found: C, 61.43; H, 7.80. As in the previous example,

incomplete combustion was observed, but the found C/H ratio, $C_{30}H_{45.4}$, is close to the calculated value.

$(C_5Me_5)_2Er(\mu\text{-}Cl_2)K(THF)_x$. Similar to the procedure for $(C_5Me_5)_2Ho(\mu\text{-}Cl_2)K(THF)_x$, $ErCl_3$ (2.07 g, 7.56 mmol) and KC_5Me_5 (2.40 g, 13.7 mmol) were reacted to yield $(C_5Me_5)_2Er(\mu\text{-}Cl_2)K(THF)_x$ as a pink solid (2.79 g, 70%, with x = 0.5). IR: 2970s, 2933s, 2900s, 2864s, 2721w, 1490w, 1433m, 1389w, 1375m, 1292w, 1245w, 1179w, 1137w, 1053s, 1023m, 952w, 913m, 899m, 802w, 731w, 661w, 593w cm^{-1}. Anal. Calcd for $C_{20}H_{30}Cl_2ErK\bullet(THF)_{0.5}$: C, 45.26; H, 5.87. Found: C, 45.31; H, 5.98.

$(C_5Me_5)_2Er(\eta^3\text{-}C_3H_5)$. Similar to the procedure for $(C_5Me_5)_2Ho(\eta^3\text{-}C_3H_5)$, allylmagnesiumchloride (2.0 mL of a 2.0 M THF solution) and $(C_5Me_5)_2Er(\mu\text{-}Cl_2)K(THF)_{0.5}$ (2.48 g, 4.25 mmol) were reacted to yield $(C_5Me_5)_2Er(\eta^3\text{-}C_3H_5)$ as an orange powder (1.68 g, 83%). IR: 3689w, 3065m, 2964s, 2907s, 2857s, 2727m, 2537w, 1537s, 1489m, 1453m, 1437m, 1378s, 1312w, 1244m, 1163w, 1059w, 1023s, 948w, 913w, 779vs, 710m, 680s, 630m, 617m, 596s cm^{-1}. Anal. Calcd for $C_{23}H_{35}Er$: C, 57.70; H, 7.37. Found: C, 57.93; H, 7.50.

$(C_5Me_5)_2Er(\mu\text{-}Ph)_2BPh_2$. Similar to the procedure for $(C_5Me_5)_2Ho(\mu\text{-}Ph)_2BPh_2$, $(C_5Me_5)_2Er(\eta^3\text{-}C_3H_5)$ (501 mg, 1.05 mmol) and $[HNEt_3][BPh_4]$ (441 mg, 1.04 mmol) in toluene (15 mL) were reacted to yield $(C_5Me_5)_2Er(\mu\text{-}Ph)_2BPh_2$ as a pink solid (792 mg, 90%). Pale pink single crystals of $(C_5Me_5)_2Er(\mu\text{-}Ph)_2BPh_2$ suitable for X-ray diffraction were grown from vapor diffusion of pentane into a benzene solution of the pink solid at ambient temperature. IR: 3047m, 2986m, 2944m, 2898m, 2860m, 1603w, 1578w, 1479m, 1429m, 1380w, 1272w, 1243w, 1157m, 1066w, 1029m, 960w, 923w, 874w, 847m, 743s, 735s, 717s, 703s, 625w, 613m, 603s, 593w cm^{-1}. Anal. Calcd for $C_{44}H_{50}BEr$: C, 69.82; H, 6.66. Found: C, 68.61; H, 6.50. As observed for the

holmium analog above, incomplete combustion was observed, but the found C/H ratio, $C_{44}H_{49.7}$, is close to the calculated value.

$(C_5Me_5)_3Er$. Similar to the mechanochemical procedure for $(C_5Me_5)_2Er(\mu\text{-}Ph)_2BPh_2$ (99 mg, 0.11 mmol) and KC_5Me_5 (21 mg, 0.12 mmol) were reacted to yield red-orange crystals of $(C_5Me_5)_3Er$ (23 mg, 37%) suitable for X-ray diffraction. IR: 2965m, 2900s, 2853s, 2818w, 2437w, 2347w, 2237w, 2143w, 2052w, 1990w, 1958w, 1886w, 1434s, 1380s, 1364s, 1247m, 1146m, 1050w, 1012m, 953w, 803w, 662w, 615w cm^{-1}. Anal. Calcd for $C_{30}H_{45}Er$: C, 62.89; H, 7.92. Found: C, 62.67; H, 7.65.

X-ray Data Collection, Structure Solution and Refinement for $(C_5Me_5)_2Ho(\mu\text{-}Ph)_2BPh_2$. A yellow crystal of approximate dimensions 0.206 x 0.216 x 0.368 mm was mounted in a cryoloop and transferred to a Bruker SMART APEX II diffractometer. The APEX2[35] program package was used to determine the unit-cell parameters and for data collection (10 sec/frame scan time for a sphere of diffraction data). The raw frame data was processed using SAINT[36] and SADABS[37] to yield the reflection data file. Subsequent calculations were carried out using the SHELXTL[38] program. The diffraction symmetry was 2/*m* and the systematic absences were consistent with the monoclinic space group $P2_1/n$ that was later determined to be correct.

The structure was solved by using the coordinates of the erbium analogue and refined on F^2 by full-matrix least-squares techniques. The analytical scattering factors[39] for neutral atoms were used throughout the analysis. Hydrogen atoms were located from a difference-Fourier map and refined (x,y,z and U_{iso}). There was one-half molecule of benzene solvent present per formula-unit. The solvent was located about an inversion center. At convergence, wR2 = 0.0647 and Goof = 1.057 for 654 variables refined against 9319 data (0.74Å), R1 = 0.0253 for those 8151 data with $I > 2.0\sigma(I)$.

X-ray Data Collection, Structure Solution and Refinement for $(C_5Me_5)_2Er(\mu\text{-}Ph)_2BPh_2$. A pink crystal of approximate dimensions 0.154 x 0.259 x 0.260 mm was mounted in a cryoloop and transferred to a Bruker SMART APEX II diffractometer. The APEX2[35] program package was used to determine the unit-cell parameters and for data collection (10 sec/frame scan time for a sphere of diffraction data). The raw frame data was processed using SAINT[36] and SADABS[37] to yield the reflection data file. Subsequent calculations were carried out using the SHELXTL[38] program. The diffraction symmetry was 2/*m* and the systematic absences were consistent with the monoclinic space group $P2_1/n$ that was later determined to be correct.

The structure was solved by dual space methods and refined on F^2 by full-matrix least-squares techniques. The analytical scattering factors[39] for neutral atoms were used throughout the analysis. Hydrogen atoms were located from a difference-Fourier map and refined (x,y,z and U_{iso}). There was one-half molecule of benzene solvent present per formula-unit. The solvent was located about an inversion center. At convergence, wR2 = 0.0661 and Goof = 1.060 for 654 variables refined against 9318 data (0.74Å), R1 = 0.0252 for those 8276 data with $I > 2.0\sigma(I)$.

X-ray Data Collection, Structure Solution and Refinement for $(C_5Me_5)_3Tb$. A red crystal of approximate dimensions 0.264 x 0.286 x 0.316 mm was mounted on a glass fiber and transferred to a Bruker SMART APEX II diffractometer. The APEX2[35] program package was used to determine the unit-cell parameters and for data collection (10 sec/frame scan time for a sphere of diffraction data). The raw frame data was processed using SAINT[36] and SADABS[37] to yield the reflection data file. Subsequent calculations were carried out using the SHELXTL[38] program. The systematic absences were consistent with the hexagonal space groups $P6_3$, $P6_3/m$ and $P6_322$. The centrosymmetric space group $P6_3/m$ was assigned and later determined to be correct.

The structure was solved by direct methods and refined on F^2 by full-matrix least-squares techniques. The analytical scattering factors[39] for neutral atoms were used throughout the analysis. Hydrogen atoms were included using a riding model. The molecule was located on a site of $\bar{3}$ symmetry (Z = 2). At convergence, wR2 = 0.0484 and Goof = 1.220 for 54 variables refined against 1162 data (0.74 Å), R1 = 0.0212 for those 1149 data with I > 2.0σ(I).

X-ray Data Collection, Structure Solution and Refinement for $(C_5Me_5)_3Dy$. An orange crystal of approximate dimensions 0.08 x 0.08 x 0.20 mm was mounted on a glass fiber and transferred to a Bruker SMART APEX II diffractometer. The APEX2[40] program package was used to determine the unit-cell parameters and for data collection (30 sec/frame scan time for a sphere of diffraction data). The raw frame data was processed using SAINT[41] and SADABS[42] to yield the reflection data file. Subsequent calculations were carried out using the SHELXTL[43] program. The systematic absences were consistent with the hexagonal space group $P6_3/m$ which was known to be correct based on the structure of the previously determined samarium analogue.[3]

The structure was solved by direct methods and refined on F^2 by full-matrix least-squares techniques. The analytical scattering factors[39] for neutral atoms were used throughout the analysis. Hydrogen atoms were included using a riding model. The molecule was located on a site of $3/m$ symmetry. At convergence, wR2 = 0.0374 and Goof = 1.089 for 54 variables refined against 1122 data (0.74 Å), R1 = 0.0149 for those 1047 data with I > 2.0σ(I).

X-ray Data Collection, Structure Solution and Refinement for $(C_5Me_5)_3Ho$. An orange crystal of approximate dimensions 0.061 x 0.095 x 0.309 mm was mounted in a cryoloop and transferred to a Bruker SMART APEX II diffractometer. The APEX2[35] program package was used to determine the unit-cell parameters and for data collection (15 sec/frame scan time for a sphere of diffraction data). The raw frame data was processed using SAINT[36] and SADABS[37]to

yield the reflection data file. Subsequent calculations were carried out using the SHELXTL[38] program package. The systematic absences were consistent with the hexagonal space groups $P6_3$, $P6_3/m$ and $P6_322$. The centrosymmetric space group $P6_3/m$ was assigned and later determined to be correct.

The structure was solved using the coordinates of the samarium analogue[3] and refined on F^2 by full-matrix least-squares techniques. The analytical scattering factors[39] for neutral atoms were used throughout the analysis. Hydrogen atoms were included using a riding model. At convergence, wR2 = 0.0393 and Goof = 1.141 for 54 variables refined against 1009 data (0.78Å), R1 = 0.0157 for those 949 data with $I > 2.0\sigma(I)$.

X-ray Data Collection, Structure Solution and Refinement for $(C_5Me_5)_3Er$. An orange crystal of approximate dimensions 0.125 x 0.141 x 0.358 mm was mounted on a glass fiber and transferred to a Bruker SMART APEX II diffractometer. The APEX2[35] program package was used to determine the unit-cell parameters and for data collection (10 sec/frame scan time for a sphere of diffraction data). The raw frame data was processed using SAINT[36] and SADABS[37] to yield the reflection data file. The systematic absences were consistent with the hexagonal space groups $P6_3$ and $P6_3/m$ and $P6_322$. The centrosymmetric space group $P6_3/m$ was assigned and later determined to be correct.

The structure was solved using the coordinates of the samarium analog[3] and refined on F^2 by full-matrix least-squares techniques. The analytical scattering factors[39] for neutral atoms were used throughout the analysis. The molecule was located on a site of $\bar{6}$ symmetry. Hydrogen atoms were included using a riding model. At convergence, wR2 = 0.0449 and Goof = 1.168 for 54 variables refined against 1209 data (0.73Å), R1 = 0.0185 for those 1175 data with $I > 2.0\sigma(I)$.

Table 7.2. Crystal Data and Structure Refinement Parameters for $(C_5Me_5)_2Ho(\mu\text{-}Ph)_2BPh_2$ (Ln = Ho, Er).

	$(C_5Me_5)_2Ho(\mu\text{-}Ph)_2BPh_2$	$(C_5Me_5)_2Er(\mu\text{-}Ph)_2BPh_2$
Empirical formula	$C_{44}H_{50}BHo \bullet \frac{1}{2}(C_6H_6)$	$C_{44}H_{50}BEr \bullet \frac{1}{2}(C_6H_6)$
Formula weight	793.63	795.96
Temperature (K)	133(2) K	133(2) K
Space group	$P2_1/n$	$P2_1/n$
a (Å)	14.2122(10)	14.2060(9)
b (Å)	14.8656(10)	14.8698(9)
c (Å)	18.4059(12)	18.4105(11)
α (°)	90	90
β (°)	103.2789(8)	103.4922(7)
γ (°)	90	90
Volume (Å^3)	3784.7(4)	3781.7(4)
Z	4	4
ρ_{calcd} (Mg/m^3)	1.393	1.398
μ (mm^{-1})	2.122	2.251
$R1^a$	0.0253	0.0252
$wR2^b$	0.0647	0.0661

$^aR1 = \Sigma||F_o|-|F_c|| / \Sigma|F_o|$. $^bwR2 = [\Sigma[w(F_o^2-F_c^2)^2] / \Sigma[w(F_o^2)^2]]^{1/2}$

Table 7.3. Crystal Data and Structure Refinement Parameters for $(C_5Me_5)_3Ln$ (Ln = Tb, Dy, Ho, Er).

	$(C_5Me_5)_3Tb$	$(C_5Me_5)_3Dy$	$(C_5Me_5)_3Ho$	$(C_5Me_5)_3Er$
Empirical formula	$C_{30}H_{45}Tb$	$C_{30}H_{45}Dy$	$C_{30}H_{45}Ho$	$C_{30}H_{45}Er$
Formula weight	564.58	568.16	570.59	572.92
Temperature (K)	133(2) K	143(2) K	133(2) K	88(2) K
Space group	$P6_3/m$	$P6_3/m$	$P6_3/m$	$P6_3/m$
a (Å)	9.9241(5)	9.9048(6)	9.8973(6)	9.8908(4)
b (Å)	9.9241(5)	9.9048(6)	9.8973(6)	9.8908(4)
c (Å)	15.4960(8)	15.5090(9)	15.5227(9)	15.5392(7)
α (°)	90	90	90	90
β (°)	90	90	90	90
γ (°)	120	120	120	120
Volume ($Å^3$)	1321.70(15)	1317.67(14)	1316.83(18)	1316.49(12)
Z	2	2	2	2
ρ_{calcd} (Mg/m^3)	1.419	1.432	1.439	1.445
μ (mm^{-1})	2.689	2.849	3.018	3.201
$R1^a$	0.0212	0.0149	0.0157	0.0185
$wR2^b$	0.0484	0.0374	0.0393	0.0449

$^aR1 = \Sigma||F_o|-|F_c|| / \Sigma|F_o|$. $^bwR2 = [\Sigma[w(F_o^2-F_c^2)^2] / \Sigma[w(F_o^2)^2]]^{1/2}$

References

(1) Tilley, T. D.; Andersen, R. A. *Inorg. Chem.* **1980**, *20*, 3267-3270.

(2) Davies, C. E.; Gardiner, I. M.; Green, J. C.; Green, M. L. H.; Hazel, N. J.; Grebenik, P. D.; Mtetwa, V. S. B.; Prout, K. *J. Chem. Soc. Dalton Trans.* **1985**, 669-683.

(3) Evans, W. J.; Gonzales, S. L.; Ziller, J. W. *J. Am. Chem. Soc.* **1991**, *113*, 7423-7424.

(4) Evans, W. J.; Ulibarri, T. A. *J. Am. Chem. Soc.* **1987**, *109*, 4292-4297.

(5) Evans, W. J. *J. Organomet. Chem.* **2002**, *647*, 2-11.

(6) Evans, W. J.; Forrestal, K. J.; Ziller, J. W. *J. Am. Chem. Soc.* **1998**, *120*, 9273-9282.

(7) Evans, W. J.; Perotti, J. M.; Kozimor, S. A.; Champagne, T. M.; Davis, B. L.; Nyce, G. W.; Fujimoto, C. H.; Clark, R. D.; Johnston, M. A.; Ziller, J. W. *Organometallics* **2005**, *24*, 3916-3931.

(8) Evans, W. J.; Hughes, L. A.; Hanusa, T. P. *J. Am. Chem. Soc.* **1984**, *106*, 4270-4272.

(9) Evans, W. J.; Hughes, L. A.; Hanusa, T. P. *Organometallics* **1986**, *5*.

(10) Schultz, M.; Burns, C. J.; Schwartz, D. J.; Andersen, R. A. *Organometallics* **2000**, *19*, 781-789.

(11) Evans, W. J.; Davis, B. L.; Ziller, J. W. *Inorg. Chem.* **2001**, *40*, 6341-6348.

(12) Evans, W. J.; Seibel, C. A.; Ziller, J. W. *J. Am. Chem. Soc.* **1998**, *120*, 6745-6752.

(13) Evans, W. J.; Davis, B. L.; Champagne, T. M.; Ziller, J. W. *Proc. Natl. Acad. Sci. U.S.A.* **2006**, *103*, 12678-12683.

(14) Evans, W. J.; Nyce, G. W.; Forrestal, K. J.; Ziller, J. W. *Organometallics* **2002**, *21*, 1050-1055.

(15) Evans, W. J.; Champagne, T. M.; Ziller, J. W. *J. Am. Chem. Soc.* **2006**, *128*, 14270-14271.

(16) Larsen, M. B.; Boydston, A. J. *Macromol. Chem. Phys.* **2016**, *217*, 354-364.

(17) James, S. L.; Adams, C. J.; Bolm, C.; Braga, D.; Collier, P.; Friščić, T.; Grepioni, F.; Harris, K. D. M.; Hyett, G.; Jones, W.; Krebs, A.; Mack, J.; Maini, L.; Orpen, A. G.; Parkin, I. P.; Shearouse, W. C.; Steed, J. W.; Waddell, D. C. *Chem. Soc. Rev.* **2016**, *41*, 413-447.

(18) Takacs, L. *Chem. Soc. Rev.* **2013**, *42*, 7649-7659.

(19) Rightmire, N. R.; Hanusa, T. P. *Dalton Trans.* **2016**, *45*, 2352-2362.

(20) Rightmire, N. R.; Hanusa, T. P.; Rheingold, A. L. *Organometallics* **2014**, *33*, 5952-5955.

(21) X.Shi, Y.; Xu, K.; Clegg, J. K.; Ganguly, R.; Hirao, H.; Friščić, T.; Garcia, F. *Angew. Chem. Int. Ed.* **2016**, *55*, 12736-12740.

(22) Evans, W. J.; Kozimor, S. A.; Ziller, J. W. *Inorg. Chem.* **2005**, *44*, 7960-7969.

(23) Evans, W. J.; Nyce, G. W.; Ziller, J. W. *Organometallics* **2001**, *20*, 5489-5491.

(24) Langeslay, R.; Chen, G. P.; Windorff, C. J.; Chan, A. K.; Ziller, J. W.; Furche, F.; Evans, W. J. *J. Am. Chem. Soc.* **2017**, *139*, 3387-3398.

(25) Shannon, R. *Acta Crystallog., Sect. A* **1976**, *32*, 751-767.

(26) Demir, S.; Mueller, T. J.; Ziller, J. W.; Evans, W. J. *Angew. Chem. Int. Ed.* **2011**, *50*, 515-518.

(27) Liptrot, D. J.; Power, P. P. *Nat. Rev. Chem.* **2017**, *1*, 0004.

(28) Bondi, A. *J. Phys. Chem.* **1964**, *68*, 441-551.

(29) Berthet, J.-C.; Villiers, C.; Le Maréchal, J.-F.; Delavaux-Nicot, B.; Lance, M.; Nierlich, M.; Vigner, J.; Ephritikhine, M. *J. Organomet. Chem.* **1992**, *440*, 53-65.

(30) Evans, W. J.; Kozimor, S. A.; Ziller, J. W.; Kaltsoyannis, N. *J. Am. Chem. Soc.* **2004**, *126*, 14533-14547.

(31) Evans, W. J.; Mueller, T. J.; Ziller, J. W. *Unpublished results* **2011**.

(32) Demir, S.; Zadrozny, J. M.; Nippe, M.; Long, J. R. *J. Am. Chem. Soc.* **2012**, *134*, 18546-18549.

(33) Liu, S.-S.; Gao, S.; Ziller, J. W.; Evans, W. J. *Dalton Trans.* **2014**, *43*, 15526-15531.

(34) Jutzi, P.; Heidemann, T.; Neumann, B.; Stammler, H. G. *Synthesis* **1992**, 1096-1098.

(35) Bruker AXS, Inc., APEX2 Version 2014.11-0, Madison, WI, **2014**.

(36) Bruker AXS, Inc., SAINT Version 8.34a, Madison, WI, **2013**.

(37) Sheldrick, G. M.; SADABS, Version 2014/5, Bruker AXS, Inc., Madison, WI, **2014**.

(38) Sheldrick, G. M.; SHELXTL, Version 2014/7, Bruker AXS, Inc., Madison, WI, **2014**.

(39) *International Tables for Crystallography, Vol. C*, Kluwer Academic Publishers, Dordrecht, **1992**.

(40) APEX2 Version 2010.9-1, Bruker AXS, Inc.; Madison, WI **2010**.

(41) SAINT Version 7.68a, Bruker AXS, Inc.; Madison, WI **2009**.

(42) Sheldrick, G. M. SADABS, Version 2008/1, Bruker AXS, Inc.; Madison, WI **2008**.

(43) Sheldrick, G. M. SHELXTL, Version 2008/3, Bruker AXS, Inc.; Madison, WI **2008**.

EPILOGUE

Collectively, in addition to the results already reported in the literature, the results obtained from the projects described in this dissertation appear to suggest that the synthesis and reactivity of +2 ion rare-earth metal complexes can be influenced by three aspects. These include: 1) electron donor strength of the ancillary ligands, 2) steric saturation of the ligand systems, and 3) choice of alkali metal chelating agents.

Although donor strengths of the ancillary ligands affect the reduction potentials of the metal complexes, it appears that there is no clear correlation between the donor strengths of the ligands and the stability of the generated +2 ion complexes. Previous reduction potential studies by Parkin and Bercaw et al.[1] and Lappert et al.[2] clearly showed that alkyl substituents on cyclopentadienyl ligands make the ligands more electron donating, whereas silyl substituents have the opposite effect. As described in Chapter 3, however, the isolation of stable +2 ion complexes was not only achievable with the use of the less electron donating monosilyl-substituted cyclopentadienyl ligand system, $(Cp')_3^{3-}$ ($Cp' = C_5H_4SiMe_3$),[3-6] but also with the use of the more electron donating tetramethyl-substituted cyclopentadienyl ligand system, $(Cp^{tet})_3^{3-}$ ($Cp^{tet} = C_5Me_4H$). Moreover, as described in Chapter 1, the use of the monomethyl-substituted cyclopentadienyl ligand system, $(Cp^{Me})_3^{3-}$ ($Cp^{Me} = C_5H_4Me$), which should be less electron donating than $(Cp^{tet})_3^{3-}$, only gave highly unstable +2 ion complexes.[7]

The stability of the +2 ion complexes appears to be better correlated to the steric saturation of the ligand systems. For example, the use the sterically demanding ligand system, $(Cp^{tet})_3^{3-}$, allowed the isolation of stable +2 ion complexes only with the larger metals, Pr and Nd, but not with the smaller metal, Y. A similar case was observed in the use of another sterically demanding system, $(Cp'')_3^{3-}$ [$Cp'' = C_5H_3(SiMe_3)$], which was found by Lappert to form a stable +2 ion

complex with the larger metal, La,[8] but as was found by Dr. Chad T. Palumbo, did not form stable +2 ion complexes with the smaller metals, Gd and Y.[7] As described in Chapter 1, in the case of $(Cp^{Me})_3^{3-}$, the generated +2 ion complexes were found to be unstable with both the larger metals, La and Pr, as well as the smaller metals, Gd and Y. This could be attributed to the small steric footprint of the $(Cp^{Me})^{1-}$ ligands that lead to steric under-saturation and inability of the ligands to provide steric protection.

The choice of chelating agents appears to also affect the stability of the +2 ion complexes in certain cases. For example, as was observed by Dr. Matthew R. Macdonald, the use of 2.2.2-cryptand (crypt) provided better stability to the +2 ion Cp′ complexes with Y, Ho, and Er than with the use of 18-crown-6 (crown).[3] In addition, these +2 ion complexes are not stable enough to be crystallized without the use of a chelating agent to encapsulate the K^+ cation and prevent it from abstracting the ancillary ligands of the metal.

In terms of reactivity, donor strength and choice of chelating agents seem to play a role in certain cases. The reduction of dinitrogen to form $(N=N)^{2-}$ complexes was only observed from the reduction of +3 ion complexes with the more electron donating ligand systems, $(NR_2)_3^{3-}$ (R = $SiMe_3$),[9-10] $(Cp^{tet})_3^{3-}$,[11-15] and $(Cp^{Me})_3^{3-}$,[15] but not with the less electron donating systems, $(C_5H_5)_3^{3-}$, $(Cp')_3^{3-}$ and $(Cp'')_3^{3-}$.[6] In the case of $(Cp^{tet})_3^{3-}$ and $(Cp^{Me})_3^{3-}$, the formation of the $(N=N)^{2-}$ complexes were only observed when the reduction reactions were performed in the absence of a chelating agent.[11-15] Therefore, it is possible that the open coordination site on the K^+ countercation also plays a role in the formation of these $(N=N)^{2-}$ complexes. This seems to also be the case in the reduction of dinitrogen by the Sc^{2+} complex, $[Sc(NR_2)_3]^{1-}$, which only proceeded when crown was used and not when crypt was used, as described in Chapter 5.[16]

In conclusion, at this point in the development of this chemistry, the stability of the +2 complexes and the reductive reactivity appears to involve a delicate balance of steric and electronic effects of the ligands as well as the nature of the reductant/chelate combination.

References

(1) Zachmanoglou, C. E.; Docrat, A.; Bridgewater, B. M.; Parkin, G.; Brandow, C. G.; Bercaw, J. E.; Jardine, C. N.; Lyall, M.; Green, J. C.; Keister, a. J. B. *J. Am. Chem. Soc.* **2002**, *124*, 9525-9546.

(2) Cassani, M. C.; Duncalf, D. J.; Lappert, M. F. *J. Am. Chem. Soc.* **1998**, *120*, 12958-12959.

(3) MacDonald, M. R.; Bates, J. E.; Ziller, J. W.; Furche, F.; Evans, W. J. *J. Am. Chem. Soc.* **2013**, *135*, 9857-9868.

(4) MacDonald, M. R.; Bates, J. E.; Fieser, M. E.; Ziller, J. W.; Furche, F.; Evans, W. J. *J. Am. Chem. Soc.* **2012**, *134*, 8420-8423.

(5) Fieser, M. E.; MacDonald, M. R.; Krull, B. T.; Bates, J. E.; Ziller, J. W.; Furche, F.; Evans, W. J. *J. Am. Chem. Soc.* **2015**, *137*, 369-382.

(6) MacDonald, M. R.; Ziller, J. W.; Evans, W. J. *J. Am. Chem. Soc.* **2011**, *133*, 15914-15917.

(7) Corbey, J. F.; Woen, D. H.; Palumbo, C. T.; Ziller, J. W.; Evans, W. J. *Organometallics* **2015**, *34*, 3909-3921.

(8) Hitchcock, P. B.; Lappert, M. F.; Maron, L.; Protchenko, A. V. *Angew. Chem., Int. Ed.* **2008**, *47*, 1488-1491.

(9) Evans, W. J.; Lee, D. S.; Rego, D. B.; Perotti, J. M.; Kozimor, S. A.; Moore, E. K.; Ziller, J. W. *J. Am. Chem. Soc.* **2004**, *126*, 14574-14582.

(10) Evans, W. J.; Lee, D. S.; Ziller, J. W. *J. Am. Chem. Soc.* **2004**, *126*, 454-455.

(11) Evans, W. J.; Rego, D. B.; Ziller, J. W. *Inorg. Chem.* **2006**, *45*, 10790-10798.

(12) Evans, W. J.; Lee, D. S.; Johnston, M. A.; Ziller, J. W. *Organometallics* **2005**, *24*, 6393-6397.

(13) Evans, W. J.; Lee, D. S.; Lie, C.; Ziller, J. W. *Angew. Chem., Int. Ed.* **2004**, *43*, 5517-5519.

(14) Lorenz, S. E.; Schmiege, B. M.; Lee, D. S.; Ziller, J. W.; Evans, W. J. *Inorg. Chem.* **2010**, *49*, 6655-6663.

(15) Fieser, M. E.; Woen, D. H.; Corbey, J. F.; Mueller, T. J.; Ziller, J. W.; Evans, W. J. *Dalton Trans.* **2016**, *45*, 14634-14644.

(16) Woen, D. H.; Chen, G. P.; Ziller, J. W.; Boyle, T. J.; Furche, F.; Evans, W. J. *J. Am. Chem. Soc.* **2017**, *139*, 14861-14864.

APPENDIX A

Attempts to synthesize $(C_5Me_5)_3Ln$ complexes with Ln = Tm, Yb, Lu

Introduction

As described in Chapter 7, the sterically over-saturated rare-earth metal complexes, $(C_5Me_5)_3Ln$ (Ln = Tb, Dy, Ho, Er, and Y), **1-Ln**, were successfully synthesized using mechanochemistry. Specifically, the cationic metal precursors, $(C_5Me_5)_2Ln(\mu\text{-}Ph)_2BPh_2$, were reacted in the solid state with $K(C_5Me_5)$ by ball-milling using stainless steel balls in a disperser tube.[1] This synthetic approach was advantageous since it avoided the need for the reaction to be performed in aromatic solvents, such as benzene or toluene, which have previously been shown to react with the **1-Ln** of the smaller metal, yttrium, to form phenyl or benzyl complexes, eq 1. Hence, it became of interest to further utilize this synthetic approach in attempts to isolate the analogous complexes with the smaller lanthanide metals, Ln = Tm, Yb, and Lu.

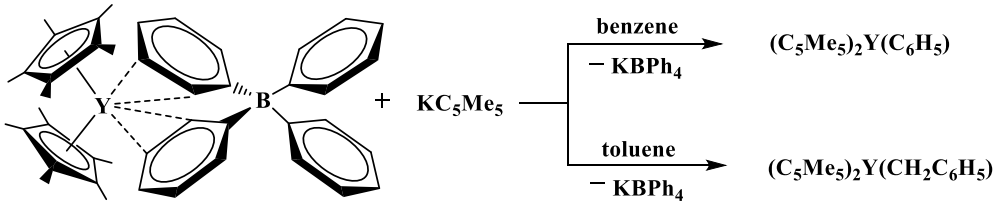

(1)

Results and Discussion

For ytterbium, attempts to synthesize the cationic precursor by the same literature procedure[2-3] described in Chapter 7 through the reaction of the allyl complex, $(C_5Me_5)_2Yb(\eta^3\text{-}C_3H_5)$, **2**, Figure A.1, with $HNEt_3BPh_4$ resulted in a reduction reaction to yield the +2 ion complex, $(C_5Me_5)Yb(\mu\text{-}Ph)_2BPh_2$, **3**, eq 2, Figure A.2, as identified by X-ray crystallography.

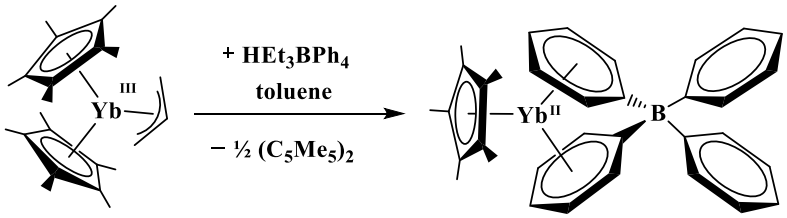

(2)

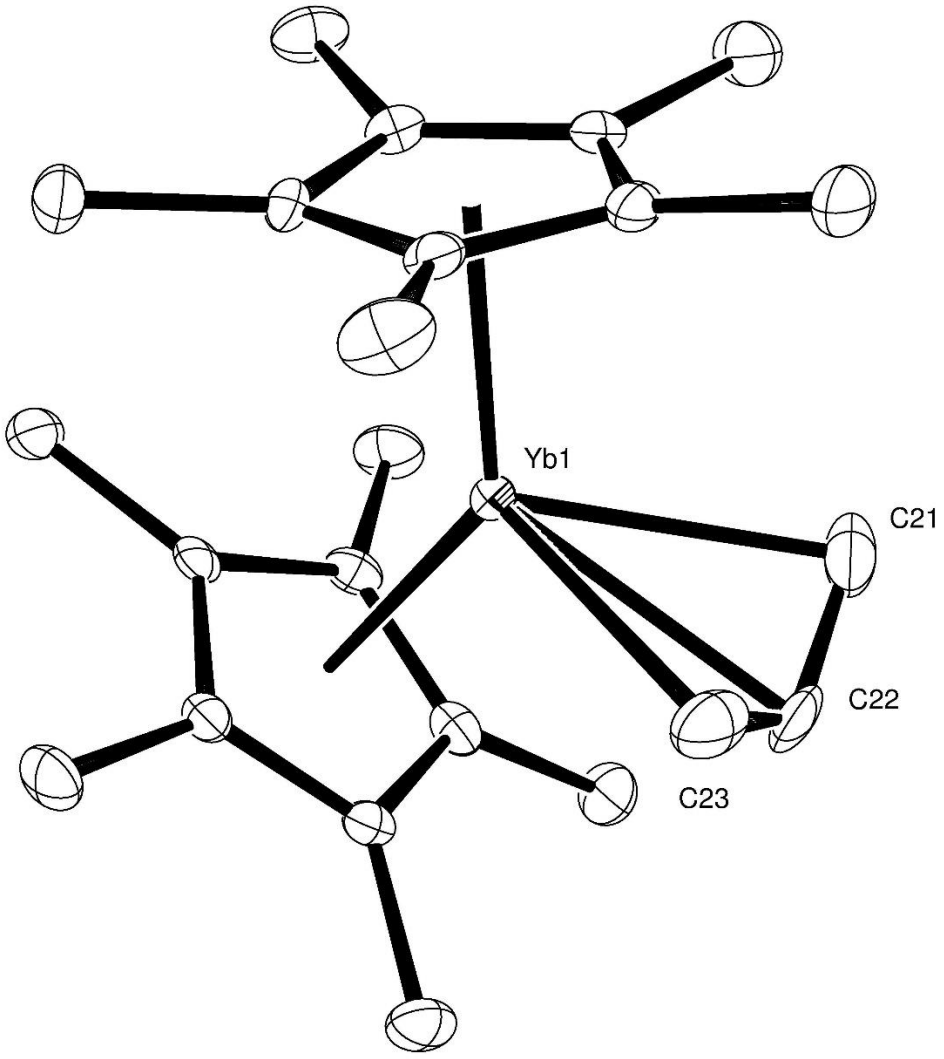

Figure A.1. Thermal ellipsoid plot of $(C_5Me_5)_2Yb(\eta^3\text{-}C_3H_5)$, **2**, drawn at 50% probability level. Hydrogen atoms are omitted for clarity.

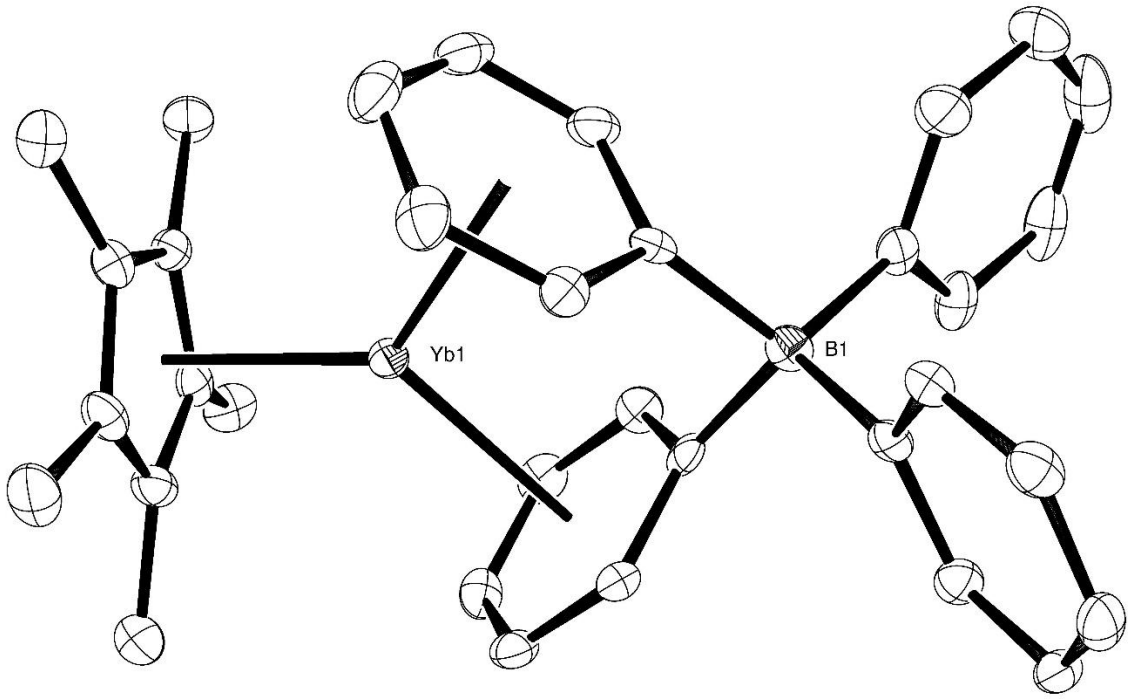

Figure A.2. Thermal ellipsoid plot of $(C_5Me_5)Yb(\mu\text{-}Ph)_2BPh_2$, **3**. Hydrogen atoms, another $(C_5Me_5)Yb(\mu\text{-}Ph)_2BPh_2$ unit, and two toluene molecules are omitted for clarity.

The crystals of **3** were obtained from a concentrated toluene solution at −35 °C. Previously, the same structure had also been reported in the literature with crystallization from a concentrated benzene solution of the sample.[4] In each structure, the crystal lattice contains molecules of the solvent in which it was crystallized from. Hence, each structure has a different unit cell than the other. Nonetheless, both had the monoclinic space group, $P2_1/n$.

The fact that the Yb^{3+} ion in the precursor, **2**, was reduced to an Yb^{2+} ion in the product, **3**, renders the use of mechanochemistry to synthesize the sterically crowded complex, **1-Ln**, with ytterbium infeasible. However, it is curious that, although the reduction of Yb^{3+} is typically facile, the reduction reaction occurred by the addition of an acid, $HNEt_3BPh_4$. It is possible that the metal

complex was reduced by one of the $(C_5Me_5)^{1-}$ ligands, which dimerizes to form ½ equiv of $(C_5Me_5)_2$, eq 2.

For thulium and lutetium, the cationic metal precursors, $(C_5Me_5)_2Ln(\mu\text{-}Ph)_2BPh_2$, **4-Ln**, were successfully prepared following the same literature procedure for the other rare-earth metal analogs,[2-3] as described in Chapter 7. Milling these cationic complexes with $K(C_5Me_5)$ both gave dark orange material identified by X-ray crystallography as the tuck-over bridging hydride species, $(C_5Me_5)_2Ln(\mu\text{-}H)(\mu\text{-}\eta^1\text{:}\eta^5\text{-}CH_2C_5Me_4)Ln(C_5Me_5)$ (Ln = Tm, Lu), **5-Ln**, eq 3. In the case of

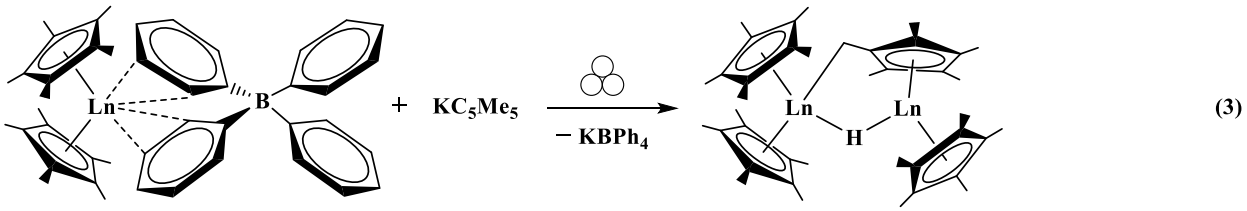

Ln = Tm, Lu

lutetium, **5-Lu**, Figure A.3, the crystals were grown from a concentrated methylcyclohexane solution at −35 °C and the complex crystallized in the monoclinic space group, $P2_1/n$. This space group is different than the triclinic space group, $P\bar{1}$, of the previously reported structure of the same complex with Ln = Lu,[5] as well as with Ln = Sm[6] and the mixed La/Lu.[7] This difference is likely caused by the presence of a methylcyclohexane molecule in the lattice of the crystals grown from methylcyclohexane. There are no solvent molecules in the previously reported structures.[5-7] In the case of thulium, **5-Tm**, the crystals were grown from pentane and were found to be isomorphous to those in the previous reports with no solvent molecules in the lattice. The whole data set of the Tm complex was not collected once the structure was identified.

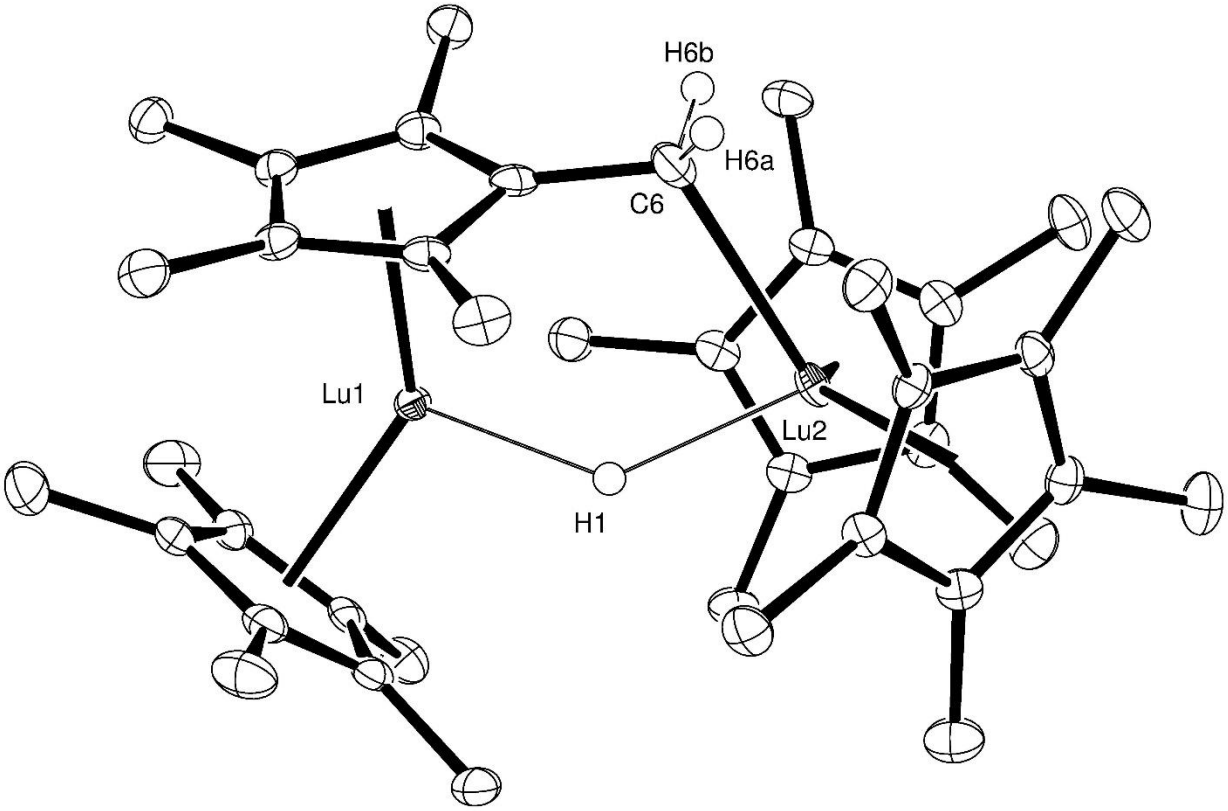

Figure A.3. Thermal ellipsoid plot of $(C_5Me_5)_2Lu(\mu\text{-}H)(\mu\text{-}\eta^1\text{:}\eta^5\text{-}CH_2C_5Me_4)Lu(C_5Me_5)$, **5-Lu**, drawn at 50% probability level. A methylcyclohexane molecule and hydrogen atoms, except H1, H6a and H6b, are omitted for clarity.

The tuckover hydride complexes, **5-Ln**, had previously been generated from the decomposition of the bridging hydride complex, $[(C_5Me_5)_2Ln]_2(\mu\text{-}H)_2$, through the loss of H_2.[5-8] Since no hydrides are present in the cationic precursor, **4-Ln**, it is possible that the formation of **5-Ln** could proceed through the C−H bond activation of one $(C_5Me_5)^{1-}$ ligand by two 1 e^- transfers from two other $(C_5Me_5)^{1-}$ ligands through the reduction of two metal centers. It is possible that the desired **1-Ln** product were actually generated, but only transiently. This product could decompose through an electron transfer from a $(C_5Me_5)^{1-}$ from each metal and the formation of

$(C_5Me_5)_2$, Scheme 1, similar to the reduction observed from the conversion of **2** to **3**, discussed above.

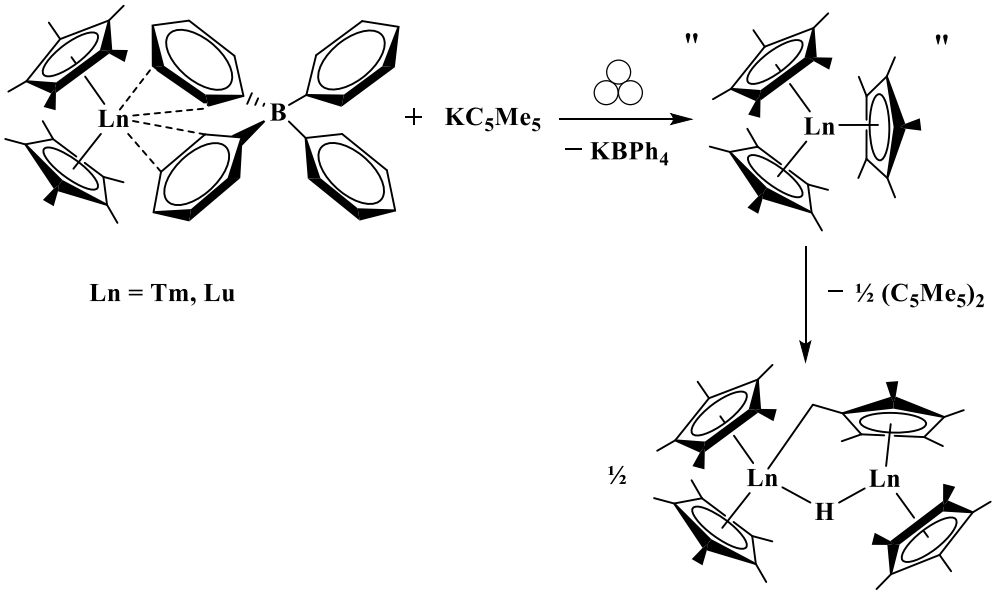

Scheme 1. Possible mechanism in the formation of a tuckover hydride species.

During the previous course of studying the mechanochemical synthesis of the structurally characterized complexes, $(C_5Me_5)_3Ln$ (Ln = Ho and Er), **1-Ln**, the tuckover hydride complexes, $(C_5Me_5)_2Ln(\mu\text{-}H)(\mu\text{-}h^1\text{:}\eta^5\text{-}CH_2C_5Me_4)Ln(C_5Me_5)$, **5-Ln**, were occasionally obtained as dark red-orange material. In the case of erbium, X-ray crystallographic data of the tuckover hydride complex, **5-Er**, was obtained. The formation of these tuckover hydride complexes was not understood, but it is possible that they are the decomposition products of the sterically over-saturated complexes, **1-Ln**, similar to the second step proposed in Scheme 1.

Conclusion

Attempts to synthesize the sterically over-saturated complexes, $(C_5Me_5)_3Ln$, **1-Ln**, with the smaller lanthanide metals, Tm, Yb, and Lu, using mechanochemistry have not been successful.

For ytterbium, attempts to prepare the cationic precursor led to the reduction of the metal and formation of the Yb^{2+} complex, $(C_5Me_5)Yb(\mu\text{-}Ph)_2BPh_2$, **3**. This metal reduction is postulated to originate from the release of an electron from a $(C_5Me_5)^{1-}$ ligand, which subsequently couples to form $(C_5Me_5)_2$. For thulium and lutetium, the reaction of the cationic precursors, $(C_5Me_5)_2Ln(\mu\text{-}Ph)_2BPh_2$, **4-Ln**, with $K(C_5Me_5)$ by ball-milling led to the formation of the tuckover hydride complexes, $(C_5Me_5)_2Ln(\mu\text{-}H)(\mu\text{-}\eta^1\text{:}\eta^5\text{-}CH_2C_5Me_4)Ln(C_5Me_5)$, **5-Ln**. The formation of the analogous tuckover hydride complexes was occasionally observed in the synthesis of **1-Ln** (Ln = Ho, Er). It is possible that it is a decomposition reaction from a similar release of electron from a $(C_5Me_5)^{1-}$ ligand that is postulated in the case of ytterbium. This can easily be tested by performing mass spectroscopy analysis of the samples to identify the presence of $(C_5Me_5)_2$.

Experimental

All manipulations and syntheses described below were conducted with the rigorous exclusion of air and water using standard Schlenk line and glovebox techniques under an argon or dinitrogen atmosphere. Solvents were sparged with UHP argon and dried by passage through columns containing Q-5 and molecular sieves prior to use. Deuterated NMR solvents were dried over NaK alloy, degassed by three freeze-pump-thaw cycles, and vacuum transferred before use. Allylmagnesiumchloride and dioxane were purchased from Aldrich and used without further purification. $[HNEt_3][BPh_4]$,[9] $K(C_5Me_5)$,[10] and $(C_5Me_5)_2Ln(\mu\text{-}Ph)_2BPh_2$ (Ln = Tm,[2] Lu[11]) were prepared according to literature procedures. Disperser milling was performed with an Ultra-Turrax Tube Drive and BMT-20-S tubes, both purchased from IKA.

$(C_5Me_5)_2Yb(\mu\text{-}Cl_2)K(THF)_{0.5}$. In a nitrogen-filled glovebox, KC_5Me_5 (4.00 g, 22.9 mmol) was slowly added to a stirred colorless slurry of $YbCl_3$ (2.17 g, 7.78 mmol) in THF (100

mL). The reaction mixture initially turned deep blue then slowly changed color to dark maroon. After 2 d, the solution mixture was concentrated to 40 mL and centrifuged to remove insoluble material. The dark supernatant was filtered and dried under reduced pressure to give a dark maroon solid. This solid was washed using toluene (3x) and hexane (3x) over a glass filter frit, then collected and dried under reduced pressure to give the ate-salt complex, $(C_5Me_5)_2Yb(\mu\text{-}Cl_2)K(THF)_{1.5}$, (3.56 g, 78%).

$(C_5Me_5)_2Yb(\eta^3\text{-}C_3H_5)$, 2. In a nitrogen-filled glovebox, allylmagnesiumchloride (3.0 mL of a 2.0 M THF solution) was added to a stirring maroon slurry of $(C_5Me_5)_2Yb(\mu\text{-}Cl_2)K(THF)_{0.5}$ (3.56 g, 6.0 mmol) in toluene (50 mL). No obvious color change was observed. The reaction was allowed to stir for 4 h and then volatiles were removed under reduced pressure to yield a mixture of brown and white solids. Hexane (40 mL) and dioxane (1 mL) were added and the mixture was allowed to stir. After 4 h, the mixture was centrifuged, and the solvent was removed under reduced pressure to yield $(C_5Me_5)_2Ho(\eta^3\text{-}C_3H_5)$, **2**, as black crystalline solids. The solids were dried further under reduced pressure at 45 °C over three days to give black crystalline solids of **2** (1.20 g, 41%). Black single crystals of **2** suitable for X-ray diffraction were grown from a concentrated hexane solution at −30 °C.

$(C_5Me_5)Yb(\mu\text{-}Ph)_2BPh_2$, 3. In an argon-filled glovebox free of coordinating solvents, $HNEt_3BPh_4$ (44 mg, 1.0 mmol) was slowly added to a stirring solution of $(C_5Me_5)_2Yb(\eta^3\text{-}C_3H_5)$ (500 mg, 1.03 mmol) in toluene (15 mL). The solution mixture immediately changed color from deep brown to blue and then slowly turned dark brown-green over time. The mixture was centrifuged to remove black insoluble material. Black single crystals of $(C_5Me_5)Yb(\mu\text{-}Ph)_2BPh_2$, **3**, suitable for X-ray diffraction were grown from the toluene solution by pentane layer diffusion

at −30 °C. ^{1}H NMR (C_6D_6): δ 7.65 (s, B*Ph*$_4$), 7.13 (m, B*Ph*$_4$), 7.05 (m, B*Ph*$_4$), 1.67 (s, C_5*Me*$_5$) ppm.

($C_5Me_5)_2Lu(\mu$-H)(μ-h^1:η^5-$CH_2C_5Me_4)Lu(C_5Me_5)$, 5-Lu. In an argon-filled glovebox free of coordinating and aromatic solvents, a BMT-20-S tube was charged with $(C_5Me_5)_2Lu(\mu$-$Ph)_2BPh_2$ (340 mg, 0.46 mmol), KC_5Me_5 (135 mg, 0.78 mmol) and 40 stainless-steel balls (6 mm). The colorless mixture was milled for 40 minutes using an Ultra-Turrax Tube Drive (max speed setting), after which, a pale orange mixture was obtained. Hexane (10 mL) was added to the mixture, followed by centrifugation to produce a dark red-orange solution which was collected in a vial. The solvent was removed under reduced pressure to give a dark orange oil. The oil was dissolved in minimal amount of methylcyclohexane and left at −35 °C. Orange single crystals of $(C_5Me_5)_2Lu(\mu$-H)(μ-h^1:η^5-$CH_2C_5Me_4)Lu(C_5Me_5)$, **5-Lu**, were obtained after several days, as confirmed by X-ray diffraction.

($C_5Me_5)_2Tm$ (μ-H)(μ-h^1:η^5-$CH_2C_5Me_4)Tm(C_5Me_5)$, 5-Tm. Similar to the procedure for **5-Lu**, in an argon-filled glovebox free of coordinating and aromatic solvents, $(C_5Me_5)_2Tm(\mu$-$Ph)_2BPh_2$ (200 mg, 0.264 mmol) and KC_5Me_5 (46 mg, 0.264 mmol) were milled, extracted, and dried to give an orange oil. Pentane (2 mL) was added to the oil, and the resulting orange solution was filtered and stored at −35 °C. Dark orange single crystals of $(C_5Me_5)_2Tm$ (μ-H)(μ-h^1:η^5-$CH_2C_5Me_4)Tm(C_5Me_5)$, **5-Tm**, were obtained after several days, as confirmed by matching unit cell using X-ray diffraction.

References

(1) Woen, D. H.; Kotyk, C. M.; Mueller, T. J.; Ziller, J. W.; Evans, W. J. *Organometallics* **2017**, *in press*.

(2) Evans, W. J.; Seibel, C. A.; Ziller, J. W. *J. Am. Chem. Soc.* **1998**, *120*, 6745-6752.

(3) Evans, W. J.; Davis, B. L.; Champagne, T. M.; Ziller, J. W. *Proc. Natl. Acad. Sci. U.S.A.* **2006**, *103*, 12678-12683.

(4) Evans, W. J.; Champagne, T. M.; Ziller, J. W. *Organometallics* **2007**, *26*, 1204-1211.

(5) Evans, W. J.; Champagne, T. M.; Ziller, J. W. *J. Am. Chem. Soc.* **2006**, *128*, 14270-14271.

(6) Evans, W. J.; Ulibarri, T. A.; Ziller, J. W. *Organometallics* **1991**, *10*, 134-142.

(7) Fieser, M. E.; Mueller, T. J.; Bates, J. E.; Ziller, J. W.; Furche, F.; Evans, W. J. *Organometallics* **2014**, *33*, 3882-3890.

(8) Evans, W. J.; Perotti, J. M.; Ziller, J. W. *Inorg. Chem.* **2005**, *44*, 5820-5825.

(9) Berthet, J.-C.; Villiers, C.; Le Maréchal, J.-F.; Delavaux-Nicot, B.; Lance, M.; Nierlich, M.; Vigner, J.; Ephritikhine, M. *J. Organomet. Chem.* **1992**, *440*, 53-65.

(10) Evans, W. J.; Kozimor, S. A.; Ziller, J. W.; Kaltsoyannis, N. *J. Am. Chem. Soc.* **2004**, *126*, 14533-14547.

(11) Schmiege, B. M.; Ziller, J. W.; Evans, W. J. *Inorg. Chem.* **2010**, *49*, 10506-10511.

APPENDIX B

A Bridging $(N_2)^{3-}$ Radical Complex of Yttrium and Its Reactivity with Nitric Oxide

Introduction

It was previously reported that the reaction of nitric oxide with the radical $(N_2)^{3-}$ bridged complex, $\{K(THF)_6\}\{[(R_2N)_2Y(THF)]_2[\mu\text{-}\eta^2\text{:}\eta^2\text{-}N_2]\}$ (R = $SiMe_3$),[1] resulted in the exchange of the bridging ligand with nitric oxide and the formation of a radical $(NO)^{2-}$ bridged complex, $\{[(R_2N)_2Y(THF)]_2[\mu\text{-}\eta^2\text{:}\eta^2\text{-}N_2]\}$.[2] This was the first and is still the only example of an $(NO)^{2-}$ radical species ever reported in the literature. Therefore, it became of interest to find other examples of this rare species. This Appendix section describes the synthesis of an $(N_2)^{3-}$ bridge yttrium complex with $(C_5Me_4H)^{1-}$ ancillary ligands and preliminary reactivity studies with nitric oxide.

Results and Discussion

The reduction of the previously reported bridging $(N{=}N)^{2-}$ complex, $[Cp^{tet}{}_2Y(THF)]_2[\mu\text{-}\eta^2\text{:}\eta^2\text{-}N_2]$ (Cp^{tet} = C_5Me_4H),[3] in the presence of 2.2.2-cryptand (crypt) yielded a color change from green-blue to dark orange. Crystallization of the product by vapor diffusion with pentane gave orange crystals identified by X-ray crystallography as the $(N_2)^{3-}$ complex, $\{(THF)K(crypt)\}\{[(Cp^{tet}{}_2Y(THF)]_2[\mu\text{-}\eta^2\text{:}\eta^2\text{-}N_2]$, **1**, Figure B.1. EPR spectroscopy analysis of a room temperature solution of this compound in THF gave a spectrum with a 15-line hyperfine pattern, Figure B.2, consistent with an unpaired electron interaction with two ^{89}Y (I = ½) and two ^{14}N (I = 1) nuclei.

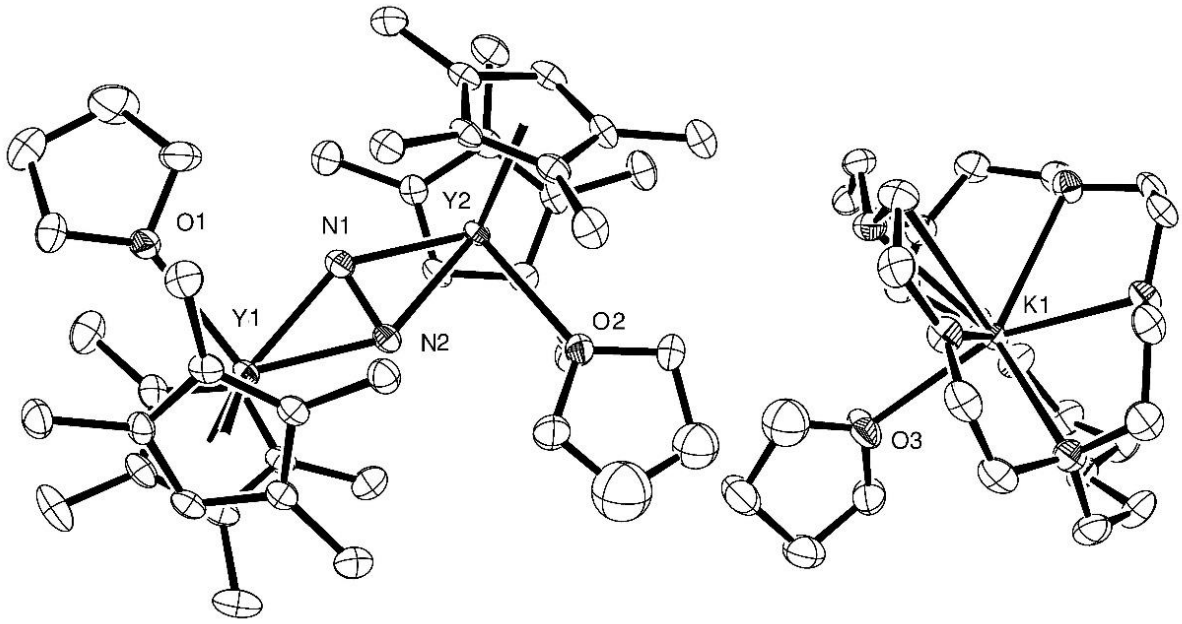

Figure B.1. Thermal ellipsoid plot of {(THF)K(crypt)}{[(Cp$^{tet}_2$Y(THF)]$_2$[μ-η^2:η^2-N$_2$], **1**, drawn at 50% probability level. Hydrogen atoms are omitted for clarity.

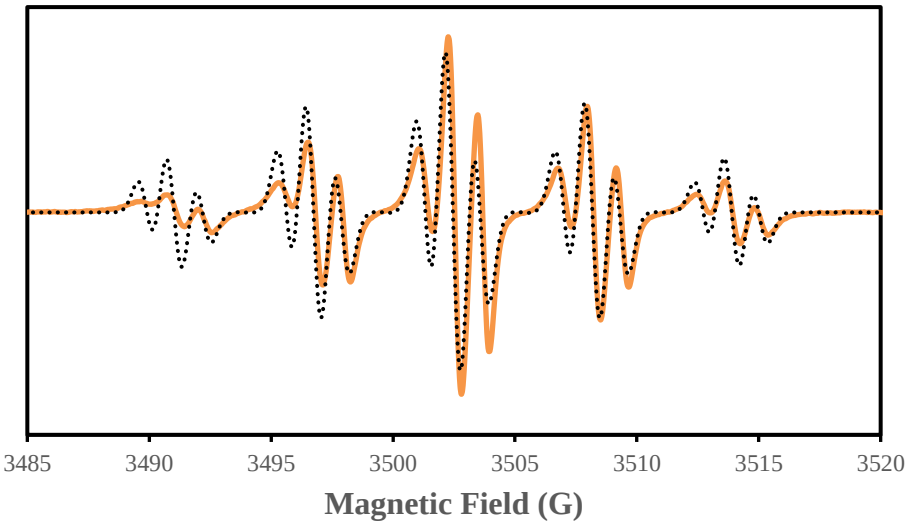

Figure B.2. Experimental (orange, solid) and simulated (black, dotted) EPR spectra of {(THF)K(crypt)}{[(Cp$^{tet}_2$Y(THF)]$_2$[μ-η^2:η^2-N$_2$], **1**. Simulated parameters: g_{iso} = 2.003, A_{iso}(^{14}N) = 5.8 G, A_{iso}(^{89}Y) = 1.2 G.

Addition of a slight excess (1.1 equiv) of nitric oxide to a THF solution of **1** at −78 °C resulted in a color change from dark orange to a pale yellow-green solution. EPR analysis of the sample shows a multi-line hyperfine pattern centered at g = 2.002, Figure B.3. This spectrum has a similar feature compared to that of the previously reported radical $(NO)^{2-}$ bridged yttrium complex, $\{K(THF)_6\}\{[(R_2N)_2Y(THF)]_2[\mu\text{-}\eta^2\text{:}\eta^2\text{-}N_2]\}$ (R = $SiMe_3$), Figure B.4, indicating the possibility that a similar $(NO)^{2-}$ radical species was obtained. However, attempts to obtain crystals of this product have not been successful.

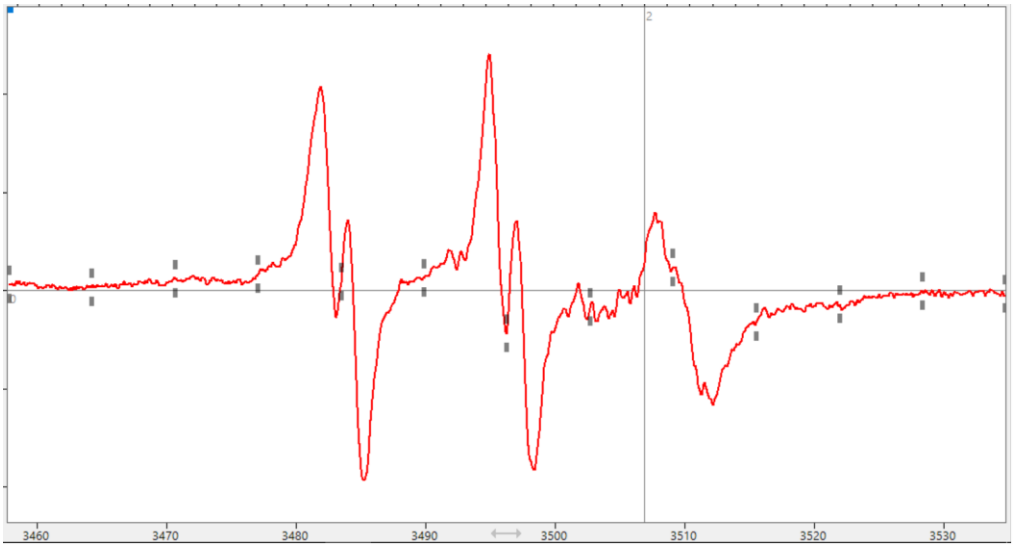

Figure B.3. X-band EPR spectrum of the reaction of nitric oxide and $\{(THF)K(crypt)\}\{[(Cp^{tet}{}_2Y(THF)]_2[\mu\text{-}\eta^2\text{:}\eta^2\text{-}N_2]$, **1**, collected in THF at 298 K.

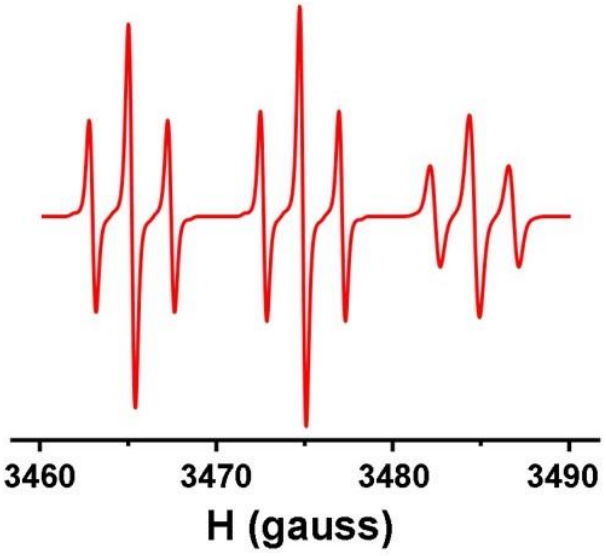

Figure B.4. X-band EPR spectrum of the previously reported radical $(NO)^{2-}$ bridged yttrium complex, $\{K(THF)_6\}\{[(R_2N)_2Y(THF)]_2[\mu\text{-}\eta^2\text{:}\eta^2\text{-}N_2]\}$ (R = $SiMe_3$).

Experimental

All manipulations and syntheses described below were conducted with rigorous exclusion of air and water using standard Schlenk line and glovebox techniques under an argon or dinitrogen atmosphere. Solvents were sparged with UHP argon and dried by passage through columns containing Q-5 and molecular sieves prior to use. 2.2.2-Cryptand (crypt) was purchased from Merck and dried under reduced pressure before use. $[Cp^{tet}_2Y(THF)]_2[\mu\text{-}\eta^2\text{:}\eta^2\text{-}N_2]$ (Cp^{tet} = C_5Me_4H)[3] and KC_8[4] were synthesized via an adaptation of the literature procedures. Electron paramagnetic resonance spectra were collected using a Bruker EMX spectrometer equipped with an ER041XG microwave bridge in THF at 298 K and 77 K unless otherwise specified. EPR simulations were performed using EasySpin.[5]

$\{(THF)K(crypt)\}\{[(Cp^{tet}_2Y(THF)]_2[\mu\text{-}\eta^2\text{:}\eta^2\text{-}N_2]$, 1. In a nitrogen-filled glovebox, KC_8 (6 mg, 0.05 mmol) was added to a stirring THF solution (10 mL) of $[Cp^{tet}_2Y(THF)]_2[\mu\text{-}\eta^2\text{:}\eta^2\text{-}N_2]$ (32

mg, 0.046 mmol), which resulted in a color change from pale yellow-green to black. The mixture was filtered to remove graphite and yielded a dark orange solution. The solution was concentrated to ~ 1 mL and set for vapor diffusion with Et_2O and pentane. Single crystals of {(THF)K(crypt)}{[$(Cp^{tet}{}_2Y(THF)]_2[\mu$-$\eta^2$:$\eta^2$-$N_2$], **1**, suitable for X-ray diffraction was grown after several days at −35 °C.

Reaction of nitric oxide and 1. In a nitrogen-filled glovebox, a Schlenk flask equipped with a side-arm was charged with a dark orange solution of **1** (24 mg, 0.019 mmol) in 20 mL of THF. The flask was sealed, brought out of the glovebox, connected to a Schlenk line, and cooled to −78 °C using an isopropanol/dry ice bath. Subsequently, nitric oxide was added to the vessel while stirring vigorously. The solution immediately changed color from dark orange to pale yellow-green. The vessel was brought into a glovebox, the solution was concentrated to ~0.5 mL and analyzed by EPR spectroscopy to give the spectrum shown in Figure B.3.

References

(1) Fang, M.; Bates, J. E.; Lorenz, S. E.; Lee, D. S.; Rego, D. B.; Ziller, J. W.; Furche, F.; Evans, W. J. *Inorg. Chem.* **2011**, *50*, 1459–1469.

(2) Evans, W. J.; Fang, M.; Bates, J. E.; Furche, F.; Ziller, J. W.; Kiesz, M. D.; Zink, J. I. *Nat. Chem.* **2010**, *2*, 644-647.

(3) Lorenz, S. E.; Schmiege, B. M.; Lee, D. S.; Ziller, J. W.; Evans, W. J. *Inorg. Chem.* **2010**, *49*, 6655-6663.

(4) Bergbreiter, D. E.; Killough, J. M. *J. Am. Chem. Soc.* **1978**, *100*, 2126-2134.

(5) Stoll, S.; Schweiger, A. J. *Magn. Reson.* **2006**, *178*, 42.

APPENDIX C

List of Crystal Structures, Cell Parameters, and UCI X-ray Codes

Code	Formula	a (Å)	b (Å)	c (Å)	α (Å)	β (Å)	γ (Å)	Volume (Å)
dhw4	$C_p^{Me}{}_3Y(THF)$	9.3	12.6	16.3	90	90	90	1899
dhw6	$C_p^{Me}{}_{33}Gd(THF)$	17.7	25.8	16.5	90	90	90	7519
dhw9	$[Cp^{Me}{}_2Y(THF)]_2[\mu\text{-}\eta^2\text{:}\eta^2\text{-}N_2]$	11.9	10.0	12.7	90	95.8	90	1510
dhw12	$Y(Cp^{Me})Cl_2(THF)_3$	14.9	10.5	13.0	90	90	90	2032
dhw14	$(Cp^{Me}{}_2Y)_2(\mu\text{-}Cl)_2$	21.8	7.0	16.3	90	109.7	90	2347
dhw15	$[Cp^{Me}{}_2Dy(THF)]_2(\mu\text{-}\eta^2\text{:}\eta^2\text{-}N_2)$	11.9	10.0	12.8	90	95.8	90	1514
dhw16	$(C_5Me_5)_3Tb$	9.9	9.9	15.5	90	90	120	1322
dhw18	$(C_5Me_5)_3Er$	9.9	9.9	15.5	90	90	120	1317
dhw19	$[K(crypt)][Cp^{Me}{}_3YSiH_2Ph]$	11.9	10.0	12.7	90	95.8	90	1513.95
dhw20	$[K(crypt)][Cp^{Me}{}_3YSiH_2Ph]$	11.6	27.4	14.5	90	91.1	90	4598
dhw21	$[K(crypt)][Cp^{Me}{}_3Y)_2(\mu\text{-}H)]$	14.9	21.8	32.4	90	95.8	90	10529
dhw22	$[(C_5Me_5)_2Dy(THF)(NH_3)][BPh_4]$	11.8	22.5	15.4	90	91.8	90	4077

dhw23	$(C_5Me_5)_2Lu(\mu\text{-}H)(\mu\text{-}h^1\text{:}\eta^5\text{-}CH_2C_5Me_4)Lu(C_5Me_5)$	10.0	27.2	15.8	90	100.0	90	4193
dhw25	$[K(crypt)][(Cl)Sc(NR_2)_3]$	11.8	14.1	19.7	102.7	103.3	93.5	3100
dhw26	$[K(crypt)][Sc(NR_2)_3]$	11.5	15.6	16.7	84.1	78.5	88.8	2895
dhw27	$(C_5Me_5)_2Yb(Et_2O)$	18.2	8.5	15.1	90	90	90	2333
dhw28	$[K(crown)][Sc(NR_2)_3]$	15.4	17.8	21.7	90	93.9	90	5960
dhw29	$\{K(crown)\}\{(R_2N)_2Sc[CH_2Si(Me_2)NSiMe_3]\}$	12.6	20.1	19.1	90	91.1	90	4828
dhw30	$[K_2(crown)_3]\{[(R_2N)_3Sc]_2(\mu\text{-}C_2O_4\text{-}\kappa^1O\text{:}\kappa^1O')\}$	27.6	17.9	25.8	90	105.6	90	12282
dhw31	$[Cs(crypt)][Sc(NR_2)_3]$	11.5	15.5	16.7	84.5	77.6	89.7	2892
dhw33	$(C_5Me_5)_2Er(\mu\text{-}H)(\mu\text{-}h^1\text{:}\eta^5\text{-}CH_2C_5Me_4)Er(C_5Me_5)$	10.5	13.7	15.1	114.1	90.7	100.1	1933
dhw34	$\{Sc(NSiMe_3)_3][OCO][K(crown)]\}_n$	18.2	11.4	25.7	90	110.2	90	4999
dhw35	$Sc(NR_2)_3$ (sub)	8.4	21.-	18.4	90	93.4	90	3230
dhw36	$[K(crypt)][Yb(NR_2)_3]$	11.7	15.7	16.8	96.2	104.7	90.2	2963
dhw37	$Yb(NR_2)_3$	28.2	8.4	28.1	90	98.9	90	6555
dhw38	$[K(crypt)]_2\{[(R_2N)_3Sc]_2[\mu\text{-}N(Me)CC(Me)N]\}$	16.5	25.1	30.4	111.5	95.1	98.5	11402
dhw39	$Sc(NR_2)_3$ (sol)	16.2	16.2	8.4	90	90	120	1899

dhw41	{K(crown)}{$(R_2N)_2$Sc-$[CH_2Si(Me_2)NSiMe_3]$}	11.0	19.8	12.2	90	114.4	90	
dhw42	[K(crypt)][$Sc(NR_2)_3$	11.5	15.6	16.6	83.3)	77.8	87.9	2911
dhw44	[Rb(crypt)][$Sc(NR_2)_3$	11.5	15.6	16.6	83.2	77.9	87.7	2911
dhw45	{K(crown)}$_2${$[(R_2N)_3Sc]_2[\mu$-η^1:η^1-$N_2]$}	15.6	17.4	24.5	85.5	83.4	67.5	6093
dhw46	$[(C_5Me_5)_2Dy][\mu$-OTf$]_2$[K(toluene)]	16.2	13.0	20.3	90	110.5	90	4280.4
dhw47	$[(C_5Me_5)_2Er][BPh_4]$	14.2	14.9	18.4	90	103.5	90	3782
dhw48	$[(C_5Me_5)_3Ho$	9.9	9.9	15.5	90	90	90	1317
dhw49	{K(crown)}$_2${$[(R_2N)_3Sc]_2[\mu$-η^1:η^1-$N_2]$}	23.9	19.2	24.3	90	107.7	90	11110
dhw50	{K(crypt)}$_2${$[(R_2N)_3Sc]_2[\mu$-η^1:η^1-$N_2]$}	15.2	20.5	21.1	75.1	79.4	78.1	6135
dhw51	$[(C_5Me_5)Yb][BPh_4]$	9.6	42.9	15.8	75.1	93.5	78.1	6507
dhw52	{(THF)K(crypt)}{$[(Cp^{tet}{}_2Y(THF)]_2[\mu$-$\eta^2$:$\eta^2$-$N_2]$	10.8	17.2	18.3	94.2	92.8	92.1	3369
dhw53	[K(crypt)][$Cp^{tet}{}_3Nd$]	16.7	24.7	13.9	90	91.6	90	5730
dhw54	[K(crypt)][$Cp^{tet}{}_3Pr$]	16.7	24.7	13.9	90	91.6	90	5736
dhw55	$[(C_5Me_5)_2H][BPh_4]$	14.2	14.9	18.4	90	103.3	90	3785
dhw56	[K(crypt)][$Cp^{tet}{}_3UCl$]	10.3	16.0	17.3	90	101.3	90	2845

dhw57	$(C_5Me_5)_2Yb(\eta^3\text{-}C_3H_5)$	22.5	22.5	8.4	90	90	90	4255
dhw58	$[(C_5Me_5)_2Er][BPh_4]$	11.2	27.9	13.2	90	97.9	90	4092
dhw59	$[K(crypt)]_2[(Cp^{Me}{}_3Pr)_2(\mu\text{-}OC_3H_6CH_2)]$	13.9	21.4	14.8	90	96.1	90	4373
dhw60	$[K(crypt)]_2[(Cp^{Me}{}_3Pr)_2(\mu\text{-}OC_3H_6CH_2)]$	13.9	21.4	14.8	90	96.1	90	4372
dhw61	$[K(crypt)]_2[(Cp^{Me}{}_3La)_2(\mu\text{-}OC_3H_6CH_2)]$	14.0	21.4	14.8	90	96.0	90	4402
dhw62	$[K(crypt)]_2[Cp^{tet}{}_3Nd(SiH_2Ph)]$	17.2	15.0	20.2	90	91.7	90	5191

Abbreviations

crypt = 2.2.2-cryptand

crown = 18-crown-6

$Cp^{Me} = C_5H_4Me$

$Cp^{tet} = C_5Me_4H$

$R = SiMe_3$